SCHOOL OF
CIVIL ENGINEERING

INDIANA
DEPARTMENT OF TRANSPORTATION

JOINT HIGHWAY RESEARCH PROJECT

FHWA/IN/JHRP-96/3
Final Report

ANAYLSIS AND LOAD TESTING OF TWO STEEL THROUGH TRUSS BRIDGES IN INDIANA

Brian J. Malone
Mark A. Heffron
Julio A. Ramirez
Donald W. White

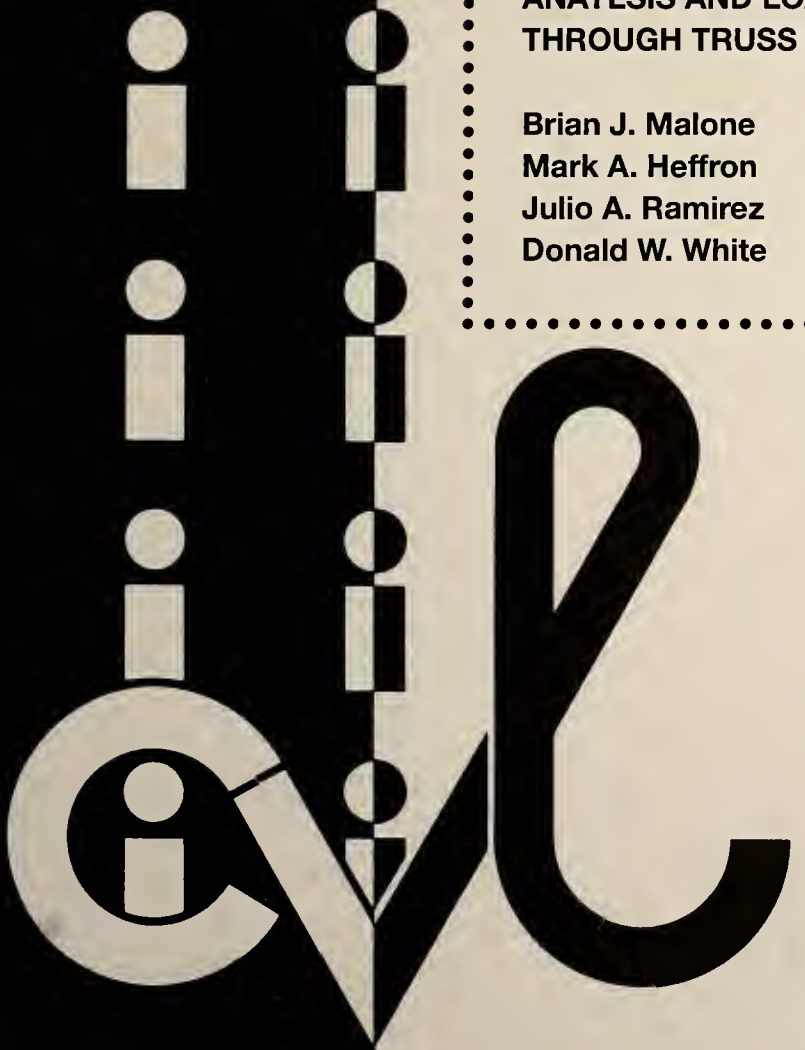

PURDUE UNIVERSITY

Final Report

ANALYSIS AND LOAD TESTING OF TWO STEEL THROUGH TRUSS BRIDGES IN INDIANA:

BRIDGE STRUCTURE NO. 58-14-3244
AND
BRIDGE STRUCTURE NO. 46-11-1316

Brian J. Malone
Mark A. Heffron
Julio A. Ramirez
Donald W. White

Purdue University

Joint Highway Research Project

Project No: HPR-2100
File No: 7-4-35

Conducted in Cooperation with the

Indiana Department of Transportation

and

Federal Highway Administration

Purdue University
West Lafayette, IN 47907
September 11, 1996

ACKNOWLEDGMENTS

Thanks are extended to the advisory committee members, Joe Torkos, Brett Safewright, Wesley Billups, Larry O'Donnell, Firooz Zandi, and Jaffar Golkhajeh. Appreciation is expressed to the Federal Highway Administration and the Indiana Department of Transportation through the Joint Highway Research Project for providing the funding for this study.

TECHNICAL REPORT STANDARD TITLE PAGE

1. Report No.	2. Government Accession No.	3. Recipient's Catalog No.
FHWA/IN/JHRP-96/3		

4. Title and Subtitle	5. Report Date
Analysis and Load Testing of Two Steel Through Truss Bridges in Indiana	September 11, 1996
	6. Performing Organization Code

7. Author(s)	8. Performing Organization Report No.
Brian J. Malone, Mark A. Heffron, Julio A. Ramirez, Donald W. White	FHWA/IN/JHRP-96/3

9. Performing Organization Name and Address	10. Work Unit No.
Joint Highway Research Project Civil Engineering Building Purdue University West Lafayette, Indiana 47907-1284	11. Contract or Grant No. HPR-2100

12. Sponsoring Agency Name and Address	13. Type of Report and Period Covered
Indiana Department of Transportation State Office Building 1000 North Senate Avenue Indianapolis, IN 46204	Final Report Executive Summary November 1, 1993- May 1, 1996
	14. Sponsoring Agency Code

15. Supplementary Notes

16. Abstract

Results of the load tests of two steel through truss bridges were used to evaluate the assumptions used by BARS for the rating of this type of bridge. Based on the results from this study it is recommended that the Indiana Department of Transportation use the load distribution factors in the 1994 LRFD Specifications in the rating of these bridges. This will imply replacing the load distribution factors currently used in BARS.

The implementation of the new distribution factors will result in a less conservative rating of the longitudinal beams in this type of bridge. The increase in the allowed moments for the girders may lead to the truss members controlling the rating of the bridge. The experimental results from this study show that the current methods and assumptions adequately predict the capacities of the truss members.

17. Key Words	18. Distribution Statement
structural performance, deflections,truss, bridge, load test, rating	No restrictions. This document is available to the public through the National Technical Information Service, Virginia, 22161

19. Security Classif. (of this report)	20. Security Classif. (of this page)	21. No. of Pages	22. Price
Unclassified	Unclassified	224	

Form DOT F 1700.7 (8-69)

Analysis and Load Testing of Two Steel Through Truss Bridges in Indiana

Implementation Report

Results of the load tests of two steel through truss bridges were used to evaluate the assumptions used by BARS for the rating of this type of bridge. Based on the results from this study it is recommended that the Indiana Department of Transportation use the load distribution factors in the 1994 LRFD Specifications in the rating of these bridges. This will imply replacing the load distribution factors currently used in BARS.

The implementation of the new distribution factors will result in a less conservative rating of the longitudinal beams in this type of bridge. The increase in the allowed moments for the girders may lead to the truss members controlling the rating of the bridge. The experimental results from this study show that the current methods and assumptions adequately predict the capacities of the truss members.

TABLE OF CONTENTS

LIST OF TABLES

LIST OF FIGURES

CHAPTER 1 - INTRODUCTION

1.1 Motivation for Study

In recent years, higher truck loads have required that many older bridges sustain loads in excess of those assumed during bridge design. There is concern that this increase in "demand" will accelerate the rate of deterioration in highway bridges. Future gross vehicle weights are expected to escalate, and knowledge of the actual behavior of bridges under these increasing loads is critical.

During a recent study [24], a representative sample of 148 highway bridges was rated using Bridge Analysis and Rating System (BARS), for a sample of 25 overloaded vehicles. In the sample, Steel Through Truss bridges were identified as a weak link in terms of load carrying capacity. In addition, the critical component causing these low ratings was observed to be the longitudinal stringer floor members rather than the main load-carrying trusses.

1.2 Objective

The main objectives of the study described in this report were to: (1) evaluate the behavior of two steel through truss bridges under controlled loading, and (2) assess the assumptions made by BARS in rating this bridge type for overload vehicles using the information obtained during the field testing.

Because the effect of increasing loads on the long-term life of the structure is the main concern when a structure is rated for permitting, load testing was limited to the allowable stress range as specified in BARS [3]. It is known that as-built bridge structures often possess considerable reserve capacity. During this study, the reserve capacity of bridge structures was identified. This report contains a description of reserve capacity and results of a study of the effects of modifying the assumptions used by BARS on the evaluation of the load capacity of bridge structures No. 46-11-1316 and No. 58-14-3244. Furthermore, the validity of extrapolating these findings to bridges that could not be inspected or instrumented prior to rating will be assessed.

1.3 Scope

The scope of the study described in this report consisted of three tasks. The first task was to survey previous research related to field testing of truss bridges. The second task was the field testing of the two bridges. The performance of the truss and floor members was investigated by analyzing the following information:

1) strains measured in five longitudinal stringers across the deck,
2) strains measured in three locations along one transverse floor beam,
3) strains measured in the vertical, diagonal, top chord, and bottom chord members of the truss,

4) deflections measured at the midspan of one bottom chord and five longitudinal stringers (SR46 only), and

5) overall truss deflection measured at the span centerline.

The effects of impact loading are not evaluated, because only a static load tests were performed. The third task was to compare the analyses of the truss bridges with the experimental results obtained during the second task. Special emphasis was given to the evaluations of the following rating assumptions made by BARS:

1) truss joints provide no moment restraint to individual axial members,

2) live loads are distributed throughout the deck as assumed in the 1992 AASHTO provisions,

3) floor members act noncompositely with the concrete slab, and

4) longitudinal stringers and transverse floor beams are simple span members.

The proposed implementation of revised AASHTO 1992 distribution factors [2] described in Chapter 7 is the culmination of the third task.

CHAPTER 2 - BACKGROUND AND LITERATURE REVIEW

Previous research in the area of bridge field testing includes common instrumentation and load testing procedures as well as investigations of the correlation between experimental and predicted behavior. In the following section, field testing procedures and previously observed behavior relevant to the present study will be discussed.

2.1 Field Testing Techniques

2.1.1 Instrumentation

Static diagnostic load tests are performed to determine the response characteristics of a bridge for use in analytical rating calculations. These characteristics include strains, deflections, and other responses of structural components, which can be used in analytical calculations to evaluate bridge behavior. Instrumentation for load tests may vary from ordinary levels and dial gages, to strain gages, deflection transducers, and automatic data acquisition systems. This instrumentation should be installed at critical locations, as determined from preliminary analysis, to measure strains, displacements, rotations, and crack widths. Enough instrumentation should be installed to obtain quantities and data required for used in analytical evaluation of the bridge and calibration of rating procedures.

Instrumentation may consist of manually read instruments (surveying equipment) and automatically read instruments (electrical strain gages, linear variable differential transducers

(LVDT), and computerized data acquisition systems). Electronic instrumentation has the advantage of being able to control and monitor load tests from remote locations. Instrumentation for field tests consists primarily of deflection measuring devices and strain measuring devices.

Deflection measurements can be made by optical, mechanical, or electrical instruments. Optical devices include standard surveying instruments (precision levels, transits, and lasers) which measure vertical deflections. It is important that the instrument is not affected by structure movement. Under favorable conditions, precision of $^1/_{16}$ to $^1/_{32}$ inches can be achieved.

Mechanical deflection measuring devices such as dial gages can have precision of 0.001 to 0.0001 inches and effective ranges of 0.25 to 2 inches. They are reusable, inexpensive and simple to use. However, they are not capable of being remotely monitored and are adversely affected by environmental factors such as water, sand and grit.

A commonly used electrical deflection measuring devices is the linear variable differential transducer (LVDT) which is capable of monitoring horizontal and vertical deflection, member end rotation, crack widths and joint movements. The LVDT is a very precise electro-mechanical transducer that produces an electric output proportional to the displacement of a separate movable core. Full-scale displacements of a 0.05 to 10 inches can be measured with nonlinearity of less than 0.5% over the full working range. Although expensive, LVDTs are excellent deflection measuring instruments (physically rugged with excellent linearity and sensitivity). Mounting of LVDTs involves securing the core rod on the plunger to a movable bridge component by means of a weight (5 to 50 lbs) and a spring-loaded wire.

The most common types of surface strain measuring devices are:

1) electrical resistance strain gages,

2) vibrating wire strain gages, and

3) mechanical strain indicators.

Careful selection of gage characteristics is required to optimize gage performance for the specific environmental and operating conditions of a particular test. The following factors should be considered [25]:

1) type of measurement (static or dynamic),

2) operating techniques,

3) environment,

4) ease of installation,

5) test duration,

6) required accuracy,

7) gage stability.

8) short-term or long-term use,

9) possibility of repeated use,

10) remote recording capability and acceptability of long loads, and

11) availability and cost.

Bonded strain gages consist of either electrical wire filaments or thin metal foil mounted on backing material. Hundreds of different types of wire and foil gages are available in different grid patterns with backing composed of polymides, epoxy resins, phenolic resins, and paper. The vast majority of gages in use today are the foil type. The strain gages are bonded to the structural component by means of specially formulated epoxy

adhesives and contact cements.

2.1.2 Loading and Load Placement

Test loads should be capable of producing, with good approximation, loads and deformations expected in critical elements of the bridge. Test loads should be:

1) representative of actual vehicular loads on the bridge,
2) adjustable,
3) easily maneuverable,
4) repeatable and easily stabilized with respect to weight distribution, and
5) easily transportable.

Test loads may include fully loaded vehicles with suitable weight and axle configurations, dead weight such as concrete blocks or water, and mechanically applied loads.

Static loading may be applied by the following means [25].

1) Static loading may be applied to the bridge using a specially built test vehicle with known axle weights and spacing to simulate AASHTO standard trucks or rating vehicles. For example, typical test vehicles, used by the Florida Department of Transportation and the Ontario Ministry of Transportation, consist of a tractor-trailer equipped with a crane to load itself with concrete blocks. The concrete blocks weigh approximately 2,000 pounds each.

2) For diagnostic load tests, ordinary dump trucks loaded with sand may be used as test vehicles. The weight of the sand can be easily adjusted to maximize the axle loadings. The New York Department of Transportation has used dump trucks and highway maintenance vehicles filled with sand for load tests.

3) Concrete blocks, or known weight placed on the structure from a crane may be used as static loads. The lack of maneuverability inherent in this method inhibits testing the structure for various load positions. Also, the load cannot be removed quickly should signs of distress become evident.

4) Hydraulic jacks may be used as test loads, but they are used primarily for ultimate load tests.

During static load tests, the test load must remain stationary until all deformations to be measured are stabilized.

2.2 Observed Behavior

2.2.1 Truss Bridges

In NCHRP 306, Burdette and Goodpasture have assembled, reviewed, and summarized available bridge load test data as it relates to bridge behavior and rating [7]. Trusses are generally analyzed and rated assuming simple truss theory using a pinned truss model neglecting the effect of the floor system and bracing. However, the experimental behavior often does not correlate with the simple theory. A summary of their research includes instances in which trusses could sustain high load levels in the absence of bottom chord members that had failed in tension or impact. The force normally carried by the bottom chord was sustained by the floor system composed of slab and longitudinal beams. Results from four additional load tests did not correlate well with predicted results using a simple truss model due to some restraint at the connections caused by rusted pins. Burdette and Goodpasture's report suggests that a three dimensional analysis incorporating the entire bridge structure may result in better evaluation of behavior [7].

The Ministry of Transportation of Ontario (MTO) has tested over 225 bridges in Ontario in the past several years. One of the bridges tested was a single span steel through truss with a posted vehicle weight of 2 metric tons. The test vehicle was a flatbed tractor trailer loaded with concrete blocks. During the load test, the bridge safely sustained a 70 metric ton test vehicle [5].

Load sharing between the bottom chord members has been observed in steel truss bridges. In rigid-jointed trusses, the inner component usually carries the higher share of the load. Loads to each component approach the same value at ultimate capacity of the bridge. In old pin-connected trusses, very unequal sharing of the force is observed. Bakht, et al suggest using only one of the bottom chord components for rating purposes, because brittle steel does not carry load equally at failure [5].

The observation that, in pony truss and through truss bridges, the floor system takes a large portion of the tensile force in the trusses has been made many times. If the stringers of the floor system of the bridge are connected to the truss nodes in such a way that the bottom chord between adjacent nodes cannot deform without engaging the stringers, then the floor system will sustain a portion of the axial load. Bahkt, et al found the bottom chord strains in the Finney Bridge and the Stephenson Line Bridge to be smaller, by a factor of about 15, than the strains that would have occurred if the chord sustained all of the force itself [5].

In addition to sharing the load with the bottom chord, the floor system may take some of the applied load directly by spanning between the truss supports, thus providing some relief to the trusses. In a test on a relatively short steel prototype bridge, it was found that the moments taken by the trusses constituted only about 92% of the applied load moments.

The flexural stiffness of the floor system was found to be about one-eighth of the combined stiffness of the two trusses [5].

In some cases the actual failure load of a bridge is less than the predicted load. A steel through-truss bridge, called the North West Ann Bridge, was tested to failure. Under the test load the bridge failed prematurely due to local buckling of the cover plate of the built-up section of an inclined chord. This local failure reduced the failure load of the bridge to about two-thirds of the predicted failure load. The need for inspection in addition to field testing is critical for an accurate rating evaluation of any bridge [5].

If stresses inferred from load tests are lower than predicted, slab-on-girder bridges may be exhibiting greater flexural stiffness than was considered in the analyses. Reasons for this include, but are not limited to, a very high modulus of elasticity of concrete, secondary component interaction of the barrier walls and bracing, and unintended composite action [5].

2.2.2 Unintended Continuity

Unintended continuity or restraint at the end of a longitudinal member framing into a transverse member results in reduced midspan stresses in longitudinal members. Since the longitudinal stringer to transverse floor beam connections are typically designed as simply supported in truss bridges, some degree of unintended continuity might be expected in the rating analysis. Barkton and McKeel observed this restraint and found correlation between experimental data and predicted load-deflection behavior assuming continuity [7]. However, Barkton and McKeel concluded that it is impossible to predict the amount of continuity without testing a particular bridge.

2.2.3 Transverse Load Distribution

Burdette and Goodpasture identified the distribution of wheel loads across a bridge deck as one of the most critical factors in correctly determining bridge load capacity. Errors in estimating the distribution of load can lead to incorrect assumptions regarding continuity and composite action when analyzing an experimental study or otherwise rating a structure [7]. AASHTO distribution factors are generally considered conservative for many bridge geometries. When analyzing a structure, it may be necessary to refine these distribution factors. An alternate procedure for calculating load distribution was presented in NCHRP 306, and has resulted in a modest increase in predicted load capacity [7].

Bakht, et al reported that in bridges with no mechanical shear connection between the deck slab and girders, a deterministic transverse load distribution analysis is difficult, if not impossible, because of the uncertain degree of participation of the deck slab with the various girders. This point is illustrated by an example drawn from a load test reported by Bakht. The uncertain degree of composite action results in uncertain values of the effective flexural rigidities of the girders. As a result, the actual distribution factors are not bracketed by analytical distribution factors assuming composite and noncomposite behavior. The extent of composite action can vary from one girder to another even in the same bridge [5].

2.2.4 Unintended Composite Action

Results from Bridge Test 4 in Tennessee showed composite behavior in a bridge designed to act noncompositely [7]. These results have received much publicity and have contributed to the idea that composite action will exist whether the member was designed as composite or noncomposite. Burdette and Goodpasture summarize the results of Tennessee Bridge Test 4 and many other tests regarding the validity of this kind of

assumption [7]. In this section a brief description of the bridge or test set-up is given followed by a summary of the findings regarding the presence of unintended composite behavior.

Newmark, et al [24] tested 15 simple span, I-beam bridges constructed to quarter scale. All bridges were concrete slabs on 5 stringers. The variables were span length, amount of slab reinforcement, and presence of shear connectors. In six of the bridges tested, strains were monitored at stringer top and bottom flange and at various locations across the top and bottom of the slab. Strains were monitored before and after the slab was cracked. These bridges differed only in the nature of bond between slab and beam as listed below:

Bridges W5a & W5b - Top of beam flanges waxed to destroy bond

Bridges N5a & N5b - Natural bond between slab and beams

Bridges S5a & S5b - Shear connectors provided positive mechanical bond

In tests before cracking, W5a behaved as if the bond had been entirely destroyed by waxing, while W5b displayed almost complete composite action. Similarly, bridge N5a behaved compositely, however, N5b showed little composite action even with natural bond. In the two bridges showing the least noncomposite action, top flange strains were less than bottom flange strains by about 75%. The top flange strains increased to approximately 90% of the bottom flange strains after cracking, suggesting that partial composite action decreases after the bridge has been cracked. Once all natural bond is lost, friction between the slab and stringer is the only remaining mechanism to prevent slip and provide slab-beam interaction. The authors suggest that this friction would be reduced after cracking disrupts the continuity in the slab.

Slip between slab and beam was measured for the six tested bridges. Slip was

measured only for the center beam. Once this first slip occurred in bridges W5b and N5a, partial composite action existed in all four bridges to similar degrees as was determined by comparing top and bottom flange strains.

Top flange strains measured 55% to 65% of bottom flange strains before cracking and 85% of bottom flange strains after cracking in bridge N15a which was designed to act noncompositely Slip was measured at the ends of the center beam. In bridges N15a and N15b, slip was recorded at one end after application of the first 500 pound load increment. In bridge N15a, slip at the other end was only 0.0005 inches at the maximum load of 3000 pounds. It was concluded that bond had not been broken over the whole length of the beam. Slip occurred suddenly at the other end of the beam when the load reached 3000 pounds and the destruction of bond was assumed at this point [24].

Burdette and Goodpasture tested one noncomposite steel girder on slab bridge to failure. The bridge was composed of a 7 inch slab supported by four 27 inch steel rolled beams. Load-deflection curves were developed using composite and noncomposite section properties. Composite load-deflection values matched measured data almost exactly up to a load near the capacity of the bridge. In addition, strain data indicated that a substantial amount of composite action was present up to a load approaching noncomposite yield in the stringers. Once the load exceeded yield load in the noncomposite stringers, slip occurred and composite deflections no longer matched experimental deflection [7].

Kissan performed full scale laboratory tests on a steel beam supporting a 6 inch noncomposite deck. Prior to pouring the slab, the steel beam was sanded to remove mill scale and lightly oiled to prevent chemical bond. Ratios of tension and compression flange strains were used to measure the position of the neutral axis. Some composite action was

observed, and its degree increased as the load was increased indicating that friction between slab and beam was the major contributor in developing bond stress between surfaces. A maximum 10% increase in section modulus S_b over the noncomposite modulus existed [7].

Kissan also tested a 146 foot truss using two identical load trucks. Results showed that the neutral axis shifted 0.82 inches above the noncomposite neutral axis but was considered inconsequential in light of the 300 psi experimental error [7].

Bahkt and Csagoly field tested a slab girder bridge. The slab was supported by transverse floor beams which then transferred the load to longitudinal stringers. Composite action was observed, but the amount varied from beam to beam and could not be counted upon. This geometry is different than bridge 58-14-3244 in the present study, in which the slab is supported by longitudinal stringers which then transfer the load to transverse floor beams [7].

The AASHTO Road Test incorporated 18 bridge tests of slab-on-girder bridges. The test results of the six noncomposite bridges built are relevant to this report. All beams were coated with 1:4:3 mixture of graphite and linseed oil to inhibit bond. The bridges were subjected to repeated stress cycles, and strains were measured in top and bottom flanges at the midspan of the girders. Neutral axis positions were determined assuming a linear strain distribution. The results indicated that all bridges built and designed to act noncompositely behaved with little or no composite action [7].

Thomas tested 1:3 scale bridge using 8 inch stringers spaced at 3 feet supporting a 3 inch slab. The slab was cast independently of the steel beams to minimize bond. Results showed partial composite action when the deck was still uncracked. Once the deck had cracked, slightly less composite action was present, and in both cases, the degree of

composite action increased in the proximity of the load [7].

Siess and Viest tested 1:4 scale model of a slab on 5 steel beams. The beam top flanges were coated with wax prior to the construction. Concentrated loads simulating one, two, and four trucks resulted in no composite action [30].

Tharamabala field tested the noncomposite, 70 foot pony truss Flack River Bridge. Two heavily load trucks designed to deliver the Ontario Highway Bridge Design Code ultimate limit states load were used. Experimental moments were compared to theoretical moments using composite and noncomposite section properties. Even at this high load level, test results correlated better with analytical composite predicted values [7].

Patel field tested Irvin Creek Bridge, a two lane, 104 ft span truss with 6 I-beam stringers evenly spaced at 1346 millimeters. The bridge was loaded with 175 and 200 kip load trucks. Comparisons showed that theoretical moments were between moments calculated using experimental stresses and both composite and noncomposite properties, and they correlated more closely to experimental composite moments. Floor beam composite moments correlated very well with theoretical grid analysis moments suggesting full composite action in the floor beams [7].

Unintended composite action can be a very influential factor in correctly predicting the stresses and deflection in a slab on girder bridge. Natural and chemical bond are the most significant factors in causing this composite behavior, but friction is also influential as can be seen by partial composite behavior even when bond was inhibited by oil or wax. In all cases in which these coatings were applied, the amount of composite action was small if present at all. It is more difficult to categorize results when a test was performed on slab and girders that were built using typical construction practices. In some cases the degree of

composite action was near full, in others partial, and not present at all in the case of "Kissan's truss bridge" [7].

An ultimate load test of a slab-on-girder bridge produced data suggesting that in the absence of mechanical shear connectors, the composite action between a girder and the deck slab breaks down completely as the failure limit state for the girder is approached (when stress equals yield stress of girder). At low levels of load, the neutral axis in the girders was well above the neutral axis of the steel girder alone. However, as the load approached failure, the neutral axis dropped to the neutral axis of the girder [6] .

2.3 Summary

A review of relevant bridge testing research has revealed many sources of reserve load capacities in truss bridges. Unintended composite action, continuity, and load sharing between the bottom chord and floor system are potential sources of capacity not considered in current Indiana bridge rating. Unfortunately, it may be necessary to load test a particular bridge in order to quantify the effects of these phenomena.

An overly conservative method for lateral load distribution will result in an unreasonably low bridge rating capacity. The previous AASHTO Standard Specifications for Highway Bridges [1] give criteria for lateral load distribution that are generally considered to be conservative. These criteria are intended for the design of new bridges. Therefore, some adjustment to the lateral load distribution procedure may be justified in order to achieve a rating that is not overly conservative.

CHAPTER 3 - EXPERIMENTAL PROGRAM

3.1 Bridge Structure No. 58-14-3244

3.1.1 Bridge Description

The load test of bridge structure #58-14-3244 (SR 58 Bridge) is described in the experimental phase of this study. The bridge is located in Daviess County and carries State Route 58 over the White River as shown in Figure 3.1.1.1. SR 58 Bridge is a three span simply-supported steel Pratt through truss (See Figure 3.1.1.2). Each 119 ft - 11 in. span has 10 panels at 19 ft.-9.5 in. as shown in Figure 3.1.1.3. The north and south trusses are separated by 19 ft.- 8 in. Located between the trusses is a 17 ft. roadway with 6 in. wide curbs on both sides (See Figure 3.1.1.4). As shown in Figures 3.1.1.5 and 3.1.1.6, the lower joints are pins which connect the vertical, diagonal, bottom chords, and floor beam. The top chords are connected to each other with riveted gusset plates. The truss sections are listed in Table 3.1.1.1.

The deck is a reinforced concrete slab varying in thickness from 6 in. at the edge of the curb to 7.5 in. at the center of the roadway. Longitudinal slab reinforcement consists of #4 bars spaced at 12 in. at the top of the slab and #4 bars spaced at 6 to 8 in. at the bottom of the slab. Transverse slab reinforcement consists of #5 steel reinforcing bars. Grades of concrete and reinforcing steel are not available from bridge drawings. The deck is supported in the direction of the traffic by 15 closely spaced longitudinal stringers shown in Figures

3.1.1.7 and 3.1.1.8. These steel stringers are supported at their ends by transverse floor beams every 19.8 ft. along the span. The stringer is a S10 x 25.4 and the floor beam is a built up S20 x 65.4 with a longitudinal stiffener and a bottom cover plate spanning 19 ft. 8 in. The cover plate is a 17 ft. long field welded 10 in. x $^5/_8$ in steel plate. The longitudinal stiffeners are two angles 7 in. x 4 in. x $^1/_2$ in. field welded to the web of the floor beam.

The SR 58 Bridge carries only one lane of traffic over the White River. The SR 58 Bridge experiences a very low average daily truck traffic, therefore, it was an ideal candidate for bridge closure and load testing. Span 2 of the bridge was accessible from the east side of the bridge. Span 3 and a portion of span 2 was over water, and was inaccessible. Span 1 had a damaged vertical member on the south truss, and span 2 was chosen for instrumentation.

The stringers are connected to the top flange of the floor beams at their ends with 2 bolts or 2 longitudinal welds. No shear connectors are provided on the stringers as they were designed to act noncompositely. The slab encases the top and sides of the top flange of the stringer. Transverse cracks in the slab were observed across the entire bridge deck over each floor beam.

The SR 58 Bridge was built in 1925. The reinforced concrete slab was replaced and new stringers were added in 1976. Although rust was evident on most truss members, no significant reduction in area was noted. The overall structure appeared to be in good condition.

3.1.2 Instrumentation

Strains were measured in the truss and floor system members with electrical resistance strain gages provided by Micro-Measurement of Raleigh, NC. Type CEA-06-250UN-350

foil gages were attached to critical areas. Strain gages were concentrated in panel 2 and panel 3 of the south span of span 2. Figure 3.1.2.1 shows the location of the strain gages on the truss. Figures 3.1.2.2 and 3.1.2.3 show the instrumented truss member sections and location of individual strain gages.

Several stringers and a floor beam were instrumented in panel 3 of span 2. Figure 3.1.2.4 shows instrumentation locations along the length of the members the stringers and floor beam. Figure 3.1.2.5 shows the locations of individual strain gages on the stringer and floor beam cross-sections. Gages at the midspan of stringers were placed on the bottom flange and on the web. One strain gage was placed on the bottom flange of the stringer 1 ft. from the end. Figure 3.1.2.6 shows locations and identification labels for the floor system gages. Figure 3.1.2.7 shows a photo of a typical installed gage.

Selected deflection measurements were made of the overall truss using a laser level. Small metal rulers were attached to the vertical truss members, and were used to measure deflections. The laser level was located on the west end of span 1. Span 1 is separated from span 2 by an expansion joint across the width of the deck.

3.1.3 Instrumentation Procedure

Strain gages were attached directly to the bare metal. Paint and rust were removed with a hand-held grinder. Further removal of surface defects and cleaning of bare metal were accomplished with fine sand paper and cleaning agents provided by Micro-Measurements. Sanding and grinding of the surface were performed in the direction parallel to the assumed stress field. Type CEA-06-250UN-350 strain gages were attached to the surface with Micro-Measurements M Bond adhesive.

AWG 22 twisted, shielded cable was connected to each strain gage. After the gages were attached to the surface and connected electrically to the cable, they were coated with polyurethane, wax, and a rubber sealant to prevent moisture and dirt from damaging the gages.

The stringers and floor beam were accessed from below using temporary scaffolding. A portable generator was used as a field power supply for the grinder, soldering irons, lamps, and a hot plate. The bottom chords, diagonals, and vertical were instrumented from the bridge deck without the use of additional equipment. The top chords were accessed by a bucket truck provided by the local INDOT district. The bridge was completely closed for approximately 10 hours while the top chord members were being instrumented.

Small metal rulers were attached vertically to selected vertical members of the truss.

3.1.4 Recording Station

The recording station comprised a data acquisition system (DA) capable of reading 200 channels and a portable laptop computer. Cables 30 ft. in length were connected from the DA to the ends of the gage wire. The recording station was placed off the roadway on top of member L2L3 on the north truss as shown in Figure 3.1.4.1. This enabled the person conducting the movement of test vehicles to be in constant contact with the person monitoring the strains in the instrumented members.

3.1.5 Load Test

Load testing was performed with one and two tandem axle highway trucks furnished by INDOT. The truck identification numbers and axle weights are given in Table 3.1.5.1. The axle weights and spacing of each test vehicle is shown in Figure 3.1.5.1. Descriptions of the loading conditions are given in the following sections and in Table 3.1.5.2.

3.1.5.1 Loading Condition #1

Figures 3.1.5.1.1 and 3.1.5.1.2 show the transverse and longitudinal positions of the test vehicle during LC #1. Figure 3.1.5.1.3 shows a photo of LC #1 during the actual load test. The objectives of LC #1 were:

1. to maximize strains in stringers,
2. to study transverse load distribution across the deck,
3. to investigate possible continuity over floor beams, and
4. to determine the degree of composite action between slab and stringers.

3.1.5.2 Loading Condition #2

Figures 3.1.5.2.1 and 3.1.5.2.2 show the transverse and longitudinal positions of the test vehicles during LC #2. A photo of LC #2 is shown in Figure 3.1.5.2.3. The objectives of LC #2 were:

1. to maximize strains in floor beams,
2. to study load distribution to trusses, and
3. to simulate influence line loading.

3.1.5.3 Loading Condition #3

Figures 3.1.5.3.1 and 3.1.5.3.2 show the transverse and longitudinal positions of LC #3. A photo of the LC #3 during the load test is shown in Figure 3.1.5.3.3. The objectives of LC #3 were:

1. to maximize strains in stringers,
2. to maximize strains in floor beams, and
3. to evaluate deck deflections at truss midspan.

3.2 Bridge Structure No. 46-11-1316

3.2.1 Bridge Description

Bridge structure 46-11-1316 was used as the test structure. Structure # 46-11-1316 is located on State Road 46 over the Eel River in Clay County, Indiana and will be referred to throughout this report as SR 46 bridge. SR 46 bridge was chosen because Average Daily Traffic was low and members could be conveniently accessed. The first three panels of the west span are over land, eliminating the need for a barge or costly hanging scaffolding for deck instrumentation. Turn offs on both sides of this bridge allowed placement of the generator and recording station. A lift vehicle was used to access truss members from the north lane while traffic proceeded in the south lane. Therefore, this bridge could be instrumented and tested with minimal down time to traffic.

The SR 46 bridge is a steel Pratt through-truss consisting of two 198 foot spans and is shown in Figure 3.2.1.1. A 25 foot wide concrete deck, $7^{7}/_{16}$ to $10^{11}/_{16}$ inches thick, is supported on a steel grid of longitudinal stringers and transverse floor beams. Longitudinal, number 4 bars at 12 inch spacing and transverse number 4 bars at 6 inch spacing were provided as top reinforcement. Number 4 bars at 6 inches were used in both directions as the bottom reinforcement. Top and bottom cover is $2^{1}/_{2}$ inches and 1 inch, respectively. Class C concrete was used in the roadway slab but reinforcing steel yield strength was not listed in drawings. Figure 3.2.1.2 shows a typical deck cross section. Figures 3.2.1.3 through 3.2.1.5 show the truss and floor system in detail. Truss member sections and areas are listed in Table 3.2.1.1. Figures 3.2.1.6 and 3.2.1.7 show truss gusset plate connections. Figure 3.2.1.8 shows a typical connection between floor beam and truss members. Stringers are transversely spaced at approximately 2 feet 4 inches and span 18 feet between floor

beams. Stringers frame into floor beams with a simple web to web bolted or riveted connection as shown in Figure 3.2.1.8.

3.2.2 Description of Instrumentation

Strains were measured in the truss and floor system members by using electrical resistance strain gages. Load test results obtained from the SR 58 bridge showed that measured strains in truss members in two panels correlated well with strains predicted by an idealized truss model. Therefore, only one truss panel was instrumented in this bridge. In all following figures, the symbol "o" refers to the placement of each strain gage or LVDT on the member. Figure 3.2.2.1 shows a schematic of the placement of the strain gages throughout the north truss. Strain gage placement along the cross section of each member is shown in Figures 3.2.2.2a and 3.2.2.2b. Gages were placed at the midspan of truss members to limit any bending effect near connections.

Figure 3.2.2.3 shows placement of strain gages on stringers and the floor beam in the third deck panel from the west abutment. Stringers were gaged at three vertical locations along the depth of the member both at midspan and 17 inches from the connection to the floor beam as shown in Figure 3.2.2.4. This placement was used to investigate strain distribution through the steel section and possible continuity at the floor beam. Figures 3.2.2.5 and 3.2.2.6 show the longitudinal and vertical placement of gages used to investigate the strain distribution and amount of possible composite action between the slab and floor beam three (FB3).

Deflection transducers were used to measure relative deflections in the floor system and overall deflections in the north truss. Deflection measurements were taken at the

midspan of stringers S1 through S5 and the midspan of bottom chord L2L3 as shown in Figure 3.2.2.7. Linear Variable Differential Transducers (LVDT) were mounted on stands underneath the bridge and a 5 pound weight was hung underneath each LVDT to induce tension in 11 millimeter diameter, 7 strand abraded aircraft cable, suspended from floor members.

Overall deflection measurements were recorded using a transit and leveling rod at the north truss midspan.

3.2.3 Instrumentation Procedure

Instrumented members were first ground at the intended gage site using a 4 inch disc grinder and then "wet sanded" using 400 grit sand paper and applications of conditioner and neutralizer solutions. In all cases, grinding was performed parallel to the assumed direction of stress. Electrical resistance CEA-06-250UN-350 Micromeasurements strain gages were bonded to all floor system and truss members using Mbond 200 adhesive. Gage 22 twisted, shielded cable was soldered to strain gages directly without the use of separate solder terminals. Once bonded and wired, gages were covered with Mcoat A, microsilicon wax, and Mcoat J rubber sealant for protection against moisture and mechanical damage.

Floor system members were accessed with scaffolding that extended to a height of approximately seven feet. A 5000 Watt portable generator and four foot grounding rod assembly was used as the power supply for soldering, grinding, lighting, and wax melting operations. INDOT lift trucks were used to access north truss members from the north lane requiring closure of one lane of traffic for one and a half business days.

Abraded aircraft cable was attached to the deck members using a 3 inch long

aluminum angle mounted to the stringer bottom flanges using epoxy and C-clamps. Number 4-40 threaded rod was then mechanically connected to the aircraft cable just above the LVDT and a similar mechanical connector was used to suspend the 5 pound weight to the threaded rod bellow the LVDT. Figures 3.2.3.1 and 3.2.3.2 show the LVDT set up from underside of deck to ground level.

Strains and deflections were recorded and stored using a multichannel Data Acquisition System (DA) and portable personal computer.

3.2.4 Load Test Procedure

Load testing was performed using combinations of one, two, and three tandem axle dump trucks with the vehicle axle weights listed in Table 3.2.4.1. Figure 3.2.4.1 shows the axle and tire spacings of a typical test vehicle. Four different loading conditions were prescribed to maximize stresses and investigate critical behavior. Table 3.2.4.2 summarizes the transverse and longitudinal vehicle placements for these four loading conditions.

3.2.4.1 Loading Condition One (LC #1)

Vehicles #5460 and, #5329 were positioned back to back starting with the outside tires approximately 12 inches from the north curb. This two vehicle configuration was centered over floor beam three (FB3). Strain measurements were recorded, and the vehicle configuration was then centered over the midspan of the stringers in bridge panel three (P3). The vehicle configuration was then positioned over floor beam two (FB2) and then over the stringer midspans in panel two (P2). The Vehicle configuration was positioned transversely such that the outside wheels of the back axles were 12 inches from the north curb. Once

strain readings were taken at these four locations, the trucks were driven off the span and the DA was rebalanced.

These four longitudinal loading positions and DA rebalancing were repeated for two more transverse locations across the deck of the bridge: trucks centered over bridge centerline, and south outside wheels 12 inches from south curb. Figure 3.2.4.1.1 shows these longitudinal and transverse positions. It is important to emphasize that gage rebalancing was performed after every four longitudinal test locations were monitored. A maximum drift of 20 microstrains was observed over a 30 minute period. Frequent rebalancing resulted in a difference in no-load strain readings before and after testing of 6 microstrains. This is only a possible error of 5% for the maximum strain measurement of 120 microstrains.

LC #1 truck positions were prescribed to maximize stresses in longitudinal stringers. Transverse load distribution from the concrete deck to the five instrumented stringers was investigated by analyzing the change in measured strains as the trucks were moved across the deck.

A vehicle configuration centered directly over the midspan of floor beam three (LC #1-FB3-Center) maximized strains at midspan. Load trucks were moved off the instrumented panel to determine the amount of continuity over the floor beam. This was done by examining strains near the end and at midspan of the off- panel stringers.

3.2.4.2 Loading Condition Two (LC #2)

Vehicles #5460 and, #5329 were positioned back to back and strain measurements were taken at every panel point (centerline of truck configuration centered over every floor

beam). These longitudinal truck positions were prescribed for north outside wheels 12 inches from the north curb and vehicle centerline over bridge centerline. LC #2 - FB8-North is the abbreviation for data acquired when the test vehicles were positioned next to the north curb over floor beam eight. The truck placements for loading condition two are shown in Figures 3.2.4.2.1. Again, gages were balanced after every set of longitudinal positions resulting in a maximum drift of 24 microstrain between NL readings, 18% of the maximum measured strain.

Experimental truss member forces were calculated for each truck position in LC #2. Experimental forces are compared to calculated forces to evaluate the assumptions of simple truss theory commonly used in analysis. Load distribution to each truss is evaluated from forces measured in each of the two transverse load positions.

Deflection measurements were also taken at bottom chord member L2L3 midspan with the load centered over every floor beam, enabling the comparison of analytical and experimental deflections.

3.2.4.3 Loading Condition Three (LC #3)

Due to the low measured strains recorded in loading conditions one and two, a third vehicle was incorporated into the load test. Three different sets of truck placements were used in loading condition three.

LC #3-1 places vehicles #5460 and #5329 back to back, outside wheel 12 inches from the north curb. Truck #5019 was south of the first two trucks with the north outside wheel 11 feet from the north curb. This three-truck configuration was longitudinally centered over midspan panel three (P3), floor beam three (FB3), and midspan panel four (P4). Figure 3.2.4.3.1 shows the longitudinal and transverse vehicle positions.

LC #3-2 positioned trucks #5460 and #5019 side by side with the first tandem axle located directly over the midspan of panel three. The center of the tandem axles of Truck #5329 is placed over the midspan of panel four. Figure 3.2.4.3.2 shows the transverse and longitudinal truck placements for LC#3-2.

LC #3-3 used trucks #5460 and #5329 side by side, positioned over the deck centerline, back to back with truck #5019 also placed over the roadway centerline. Truck #5019 faced west and #5460 and #5329 faced east. The three vehicle configuration is centered over midspan of panel three (P3), over floor beam three (FB3), and over truss midspan (P5). Figure 3.2.4.3.3 shows longitudinal and transverse vehicle positions for LC #3-3.

LC #3-1 was one of several attempts to use the three load vehicles present to achieve maximum strains in floor beams and exterior stringers. LC #3-2 was used to investigate the presence of continuity over the floor beam by maximizing strains in gages at stringer ends. LC #3-3 was designed to induce the maximum moment to floor beams. This loading position was also used to induce the maximum truss deflection measured at truss centerline.

3.2.4.4 Loading Condition Four (LC #4)

Truck #5460's tandem axles were positioned over the midspan of panel three in the North, Center, and South transverse locations shown in Figure 3.2.4.4.1. During testing it was noticed that placing a double truck configuration over a panel midspan such in LC #1 did not result in tire loads over the panel midspan. Therefore, LC #4 attempted to increase midspan stringer moments by centering the tandem axle of a single truck over the midspan of panel three.

CHAPTER 4: BRIDGE ANALYSIS AND RATING SYSTEM

ANALYSIS ASSUMPTIONS

4.1 Introduction

The Indiana Department of Transportation (INDOT) periodically rates its state bridges. Often, bridge rating is required prior to granting a permit to a vehicle which exceeds the legal load for a particular structure. INDOT uses the BARS software to perform these ratings [3].

The term "rating" is defined as the load-carrying capacity of a bridge in accordance with an AASHTO H and HS truck configuration. The rating of a bridge is a number that expresses the percentage of the maximum gross load of an AASHTO H or HS axle configuration vehicle that can be supported by the structure. For example, a rating of HS19.8 indicates a capacity of 99% of the standard HS20-44 vehicle.

BARS can be used to rate a bridge by analyzing each element of the structure that has been selected by the analyst. A structural element may be a flexural member (stringer or floor beam) or a truss member. In BARS, each selected element is analyzed individually until all elements which are considered critical by the analyst have been processed. The method of structural analysis used is based upon the type of member and its boundary conditions.

The primary analysis tasks are:

1. establish allowable stresses,
2. establish section properties,
3. generate influence lines,
4. calculate dead load effects,
5. determine live load distribution,
6. calculate maximum live load effect,
7. calculate impact effect, and
8. rate structural element.

The scope of this study involves evaluating the BARS ratings for steel through truss bridges. The methods used by BARS to generate influence lines, live load distribution factors, dead load effects, and impact effects will be discussed in this chapter. Allowable stress for inventory rating is 55% of the yield stress of the steel. Dead load and impact effects were not investigated in this study.

4.2 Truss Member Rating Assumptions

Because structural response to live loads was the principal topic of investigation during the field test, the method used by BARS for calculating dead loads is discussed only briefly.

Live load effects are calculated by placing the load configuration of a rating vehicle on a truss influence line. These influence lines are generated using simple truss theory. Members are assumed to be prismatic, axially loaded, and connected with simple pin connections at all joints. Truss member forces calculated using BARS are found by placing

the load configuration of the vehicle to be rated on these influence lines. As the truck is moved along the influence line the maximum force calculated is saved and compared to the load capacity. The percentage of the maximum calculated force to the force capacity is then multiplied by the rating vehicle weight to determine the member rating.

4.3 Floor Member Rating Assumptions

In a similar manner to the truss, BARS is used to create flexural influence lines for each member that is rated. In through truss bridges, stringers and floor beams are typically designed simply supported and noncomposite unless otherwise noted. Member supports are standard rating positions for shear. The standard rating position for flexure is member midspan.

Dead load effects are calculated by multiplying default specific weights by tributary areas determined by member dimensions and spacings. Live load effects are calculated by applying a live load distribution factor to the load that is in a parallel plane to the plane of the member being rated. Live load distributions are different for longitudinal stringers and transverse floor beams. For longitudinal flexural members, the load associated with one line of wheels is multiplied by a live load distribution factor and then placed directly over the member being rated in a position to achieve maximum shear or moment. Live load distribution factors used in BARS are found in the previous version of the AASHTO [1].

Floor beam moments are calculated by first determining the maximum stringer reaction to the rated floor beam. One span of stringer reactions is applied in the case of an end floor beam, and two spans for and intermediate floor beam. Once the maximum live load reaction is determined, it is placed on the floor beam to maximize stresses. The entered

roadway width allows BARS to determine how many lanes can be loaded. For instance, when a simple beam is subjected to a group of nonsymmetric concentrated loads, the maximum bending moment generally does not occur at midspan. To achieve the maximum moment in a floor beam, the live load is placed such that the centerline of the floor beam is halfway between one wheel load and the resultant of all loads on the span. In the case of a single truck, this would result in the centerline of the truck being placed over the centerline of the floor beam in a longitudinal position that produced maximum reactions from the stringers.

4.4 Impact Factor

An impact factor is calculated for each flexural and truss member being analyzed. The impact factor is calculated using the equation: $I = 50/(L + 125)$, where L is the length of the member (in feet) that can be loaded [1]. The impact effect is calculated as the impact factor multiplied by the live load effect.

4.5 Element Rating

The final step in the BARS analysis is the assignment of a rating number to a structure. This number indicates whether or not the structure can safely sustain a designated live load without overstressing any of its members. The rating number depends on the rating factor. The rating factor is the ratio of the capacity of the bridge member available to support live load plus impact (LL + I) to the actual maximum (LL + I) effect produced by the vehicle. A factor of less than one indicates the member is overstressed at the level of allowable stress specified by rating analysis.

The truss member capacity can be expressed as the allowable stress multiplied by the available area. The available capacity for (LL + I) equals the member capacity minus dead load forces. The moment capacity of structural steel flexural members is the allowable stress multiplied by the section modulus. The available capacity for rating is equal to the dead load moment minus the moment capacity.

The member in the structure with the lowest rating factor limits the bridge rating. The rating number is given in two possible forms. In the case of a standard AASHTO H or HS truck, the rating factor is multiplied by the designated vehicle number (20 for and HS20-44). For a non-AASHTO vehicle, the rating number is the product of the rating factor and the gross weight of the vehicle being rated. This rating is only valid for the particular wheel configuration of the truck used in the calculations. Although the BARS software can be used to calculate shear effects at supports, rating of floor members is based solely on flexural moment capacity.

CHAPTER 5 - EXPERIMENTAL RESULTS AND ANALYSIS

5.1 Bridge Structure No. 58-14-3244

5.1.1 Analysis Assumptions

Measured strain data and experimental stress data for each gage are found in Tables A.1 and A.2, respectively [22]. Experimental stresses are calculated by multiplying the corresponding measured strain by an assumed modulus of elasticity of steel (E_s = 29,000 ksi).

The maximum experimental stresses for the individual truss member components were calculated by multiplying the appropriate maximum strain by 29,000 ksi. The maximum stresses are shown in Table 5.1.1.1. Theoretical forces in the truss members and theoretical deflections of truss panel points were determined using a simple truss model in which all joints were assumed pinned. Strain distributions were assumed linear in the analysis of the experimental results. The experimental stresses in all truss members were calculated by multiplying the average strain across the member by an assumed modulus of elasticity of the steel (E_s = 29,000 ksi). The experimental forces were determined by multiplying the above mentioned experimental stress by the gross area of each member. The gross area of each section was taken from original bridge drawings provided by INDOT. The use of gross area from the original drawings was justified based on visual inspection.

The following assumptions were made in the analysis of the stringers and floor beams:

$f'_c = 4{,}000$ psi

$E_s = 29{,}000$ ksi

$E_c = 3{,}600$ ksi.

Strain distributions at the midspan of the stringers were determined by straight line interpolation between the flange gage (MF) values and the web gage (MW) values. A modular ratio of 8 was used in calculations involving composite section properties.

5.1.2 Truss Analysis and Behavior

5.1.2.1 Maximum Stresses

Table 5.1.2.1.1 shows the maximum experimental stress in each instrumented truss member. Also included in the table are the loading condition and the longitudinal and transverse positions of the test vehicle(s).

5.1.2.2 Individual Component Behavior

Influence line loading was performed in LC #2 to determine the force in each instrumented truss member as the test vehicles moved along the bridge span. The experimental forces determined from LC #2 were compared to theoretical forces. The theoretical forces were calculated by placing the appropriate load configuration on influence lines generated for the truss.

Strain measurements from the five member U1U2 strain gages are plotted against load position in Figure 5.1.2.2.1. When the test vehicles are placed on FB1 and FB2, a small

amount of bending strain is evident. This bending is not noticeable as the test vehicles move away from the member U1U2. This suggests that a small degree of frame action is present in the top chord, but only when the test vehicle is placed near the member producing the largest stresses. A comparison of the experimental and theoretical forces is shown in Figure 5.1.2.2.2. The maximum force in member U1U2 can be calculated within +/- 1% using simple truss theory. A similar behavioral trend is observed in member U3U4. Strain load position from the four member U3U4 strain gages are plotted against load position in Figure 5.1.2.2.3. Again, a small amount of bending strain is apparent at the heavily loaded floor beams (FB3 - FB4). The top chord acts like a pinned-pinned truss instead of a frame. A comparison of the experimental and theoretical forces is shown in Figure 5.1.2.2.4. The maximum force in member U3U4 can be calculated within +/- 3% using simple truss theory.

Strain measurements from the interior and exterior strain gages on member L1L2 are plotted against load position in Figure 5.1.2.2.5. The interior component of the bottom chord carries more share of the load than the exterior component. The exterior component carries an average of 75% of the load on the interior member. The experimental forces are compared with the theoretical forces in Figure 5.1.2.2.6. The experimental forces range in value from 20% - 60% of the theoretical forces depending on the position of the load vehicles.

Similar behavior is observed in the bottom chord member L3L4. Strain measurements from the four bottom chord components are plotted against load position in Figure 5.1.2.2.7. Strain gage L3L4-1 is the outer gage, and strain gage L3L4-4 is the inner gage. As with member L1L2, the inner gage (L3L4-4) experiences a higher share of the strain than the other three components. The experimental forces are compared with the

theoretical forces in Figure 5.1.2.2.8. The experimental forces range in value from 50% - 65% of the theoretical forces.

Strain measurements from the interior and exterior gages of vertical member U1L1 are plotted against load position in Figure 5.1.2.2.9. The strain measured in the inner component of the vertical member is always substantially higher than that measured in the outer component. The exterior component carries only half as much strain as the inner component. Figure 5.1.2.2.10 shows a comparison between the experimental forces and theoretical forces calculated for member U1L1. The maximum force in member U1L1 can be calculated within +/- 14% using simple truss theory.

Strain measurements for the interior and exterior gages of the diagonal member U1L2 are plotted versus load position in Figure 5.1.2.2.11. The interior component carries a higher share of the load than the exterior component. Experimental forces are compared with theoretical forces in Figure 5.1.2.2.12. Experimental forces correlate well with theoretical forces. Experimental forces reach a maximum of 110% of the theoretical forces in the heavily loaded panels.

Strain measurements for the interior and exterior gages on member U3L4 are plotted in Figure 5.1.2.2.13. Once again, the inner component carries a higher share of the load than does the exterior component. Figure 5.1.2.2.14 shows a comparison between the experimental forces and theoretical forces for member U3L4. The force in member U3L4 can be calculated within +/- 1% using simple truss theory.

Figure 5.1.2.2.15 shows a comparison of experimental and theoretical forces. The experimental forces follow the same trend as do the theoretical forces, but the value of the experimental forces are always much higher than the theoretical values. The critical

buckling load of the member is only 75 lbs. This evidence suggests that the member buckled. Nevertheless, member U4L3 is a counter, and is only expected to resist tension.

From the preceding results, the following conclusions can be made concerning truss behavior of this type of bridge.

1) Bending or frame action in the top chord is negligible.

2) The actual force in the bottom chord can be as low as 20-60% of the theoretical force. This fact indicates that the floor system, especially the exterior stringers, share the load in the bottom chord. As the load vehicle moves away from the bottom chord in question, more of the floor system is developed, which results in a higher share of the force being carried by the floor system. This will be discussed in more detail in Section 5.3.

3) The inner component of the bottom chord and diagonals carry more load than the outer components. As the floor system shares some of the bottom chord force, the load on the exterior component of the bottom chord decreases more than the load on the interior component. This is specific to pin connected trusses where the effective bottom chord consists of multiple individual components as well as part of the floor system. As the floor system draws a share of the load away from the actual bottom chord of the truss, the centroid of the effective bottom chord shifts toward the center of the bridge. This shift causes the load in the exterior component to be less than load in the interior component.

4) Significant bending occurs in vertical member U1L1 due to the detail of the floor beam to vertical connection shown in Figures 3.1.1.5 and 3.1.1.6. Assuming a simply supported beam, the inner component (U1L1-I) will share more of the load than the outer component (U1L1-E).

5.1.2.3 Load Distribution to Truss

In Section 5.1.2.2, the theoretical forces in the truss were calculated using half of the truck loads (one line of wheels) and placing them on one truss. The experimental forces were taken from LC #2 - CENTER so that the two comparisons would be compatible. In this section, the load distribution to the trusses is investigated when the truck is placed off of the center of the bridge (eccentric loading).

Comparisons of experimental force and theoretical force in each member are made in this section for LC #2 - SOUTH. The experimental forces are calculated using the following steps: 1) assume floor beam to be simply supported, 2) place appropriate load configuration (LC #2 - SOUTH) on floor beam and calculated percentage of applied load to south support, and 3) place calculated percentage of applied load on influence lines for each member.

Figures 5.1.2.3.1 through 5.1.2.3.8 show the comparisons described above. The experimental and theoretical forces in the truss members correlate well. The only exceptions are the bottom chord members (L1L2 and L3L4) and the counter (U4L3). The explanations for these exceptions were covered in the preceding section (5.1.2.2).

5.1.2.4 Truss Deflections

Deflection measurements were taken at a few selected points during LC #2 and LC #3. The actual deflection measurements are compared with the theoretical truss deflections in Table 5.1.2.4.1. The ratio of measured to theoretical deflections ranges from 73% - 80%. The actual structure is stiffer than the theoretical structure. Participation of the floor system with the bottom chord helps to enhance the flexural stiffness of the structure, and thereby the measured deflections are reduced with respect to the expected values. It should be noted that in all cases the bridge experienced full recovery of deflection upon unloading.

5.1.3 Stringer Analysis and Behavior

5.1.3.1 Maximum Stresses

The maximum stresses produced in the stringers during the load test are shown in Table 5.1.3.1.1. The maximum tensile stresses in the bottom flanges at midspan were produced by LC #3, when the test vehicles were centered over the midspan of panel 3 (MS-P3). The maximum tensile stress in the bottom flange at the stringer end was produced by LC #2, when the test vehicles were centered over floor beam 2 (FB2). A maximum compressive stress of 2.4 ksi was experienced by S1-EF in LC #1 when the test vehicle was centered over the midspan of panel 2.

Figure 5.1.3.1.1 shows the distribution of bottom flange stresses across one-half of the bridge for six transverse test vehicle positions. The instrumented stringers are S1, S2, S3, S6, and S8. Stress values for S4, S5, and S7 are calculated assuming linear stress distribution between adjacent instrumented stringers. This is only done for the purpose of making the graphs easier to read, not to represent the actual stresses in stringers S4, S5, and

S7. Stringer S1 had a live load stress of 4.6 ksi during LC #1 - SCET. The stress in S1 decreased from 4.6 ksi to 3.9 ksi and 1.6 ksi when the test vehicle was moved to transverse positions SWLET and CLET, respectively. The stresses produced in S1, S2, and S3 (south side of bridge) were very low (0.7 ksi to 0.9 ksi) when the load truck was positioned against the north curb. Stringer S1 has a maximum live load stress of 5.6 ksi during LC #3.

5.1.3.2 Live Load Distribution

Figure 5.1.3.2.1 shows the experimental distribution of moment across the entire bridge deck. The experimental moment was calculated using the following steps: 1) assume a linear strain distribution in the steel stringer, 2) calculate tension force and compression force in steel (if any), 3) determine compression force in concrete to balance forces such that T = C (neglecting tension in concrete), 4) assume concrete compressive force acts at the centroid of the slab and calculate moment arm, and 5) multiply the compression or tension force by the moment arm. Moment values were determined for S4, S5, and S6 assuming a linear moment distribution between adjacent instrumented stringers. Symmetry was used to model the north half of the bridge deck. Experimental moment values are used as qualitative estimates of moment, not as accurate calculations of the actual moments.

The experimental moments for LC #1 when trucks are facing east are shown in Figure 5.1.3.2.1. The total moment across the entire bridge deck for each of the three transverse test vehicle positions are equal. The experimental moments for LC #1 when test vehicles were facing west are shown in Figure 5.1.3.2.2. The experimental moments for LC #1 are shown in Figure 5.1.3.2.3 and Figure 5.1.3.2.4.

The total experimental moment across the entire bridge deck for each loading

condition was determined and is compared with the theoretical total moment in Table 5.1.3.2.1. The theoretical total moment was calculated using the following steps: 1) assume simply supported stringer, 2) apply appropriate axle loads and spacing to the stringer corresponding to the particular load position, and 3) calculate midspan moment. Note that the sum of the experimental moments for each position in LC #1 are equal. The same is true of LC #2. It follows that LC #3 should produce a total experimental moment twice as large as that which LC #1 produces. This correlation is shown in Table 5.1.3.2.1.

The discrepancy between the experimental and the theoretical total moment may be explained by the interaction of three behavioral aspects. The three behavioral aspects are: a) A small amount of bending exists in the top chords due to the semi-rigid gusset plate connections at the upper truss joints. This frame-action of the top chords, however small, does attract moment away from the floor system; b)The assumed location of the concrete compressive force may not be valid. The actual distribution of stress in the slab is in all likelihood different than that which was assumed. If the concrete displayed a triangular distribution of stress and if the neutral axis of the section were into the slab, the moment arm and resulting experimental moment would be greater; and c) when calculating the theoretical moment, the stringer was assumed simply-supported. If, however, there was some continuity or restraint at the end of the model stringer, the theoretical moment would be smaller because of offspan placement of the front axle of the truck to counter the effect of the two back axles. Restraint stresses are present at the end of the stringers, but not to a significant degree. Although individually the effect of these behaviors may be small, together they may contribute to a noticeable difference between theoretical and experimental values.

A comparison of maximum experimental and theoretical moments is shown in Figure 5.1.3.2.5. The maximum experimental moments (MEM) are determined from the MEMs in LC #1. For example, LC #1 SCWT produces the MEM in stringers S1, S2 and S3, whereas LC #1 SWLET and LC #1 CLET produce the MEM in stringers S6 and S8, respectively. The experimental moments are compared with the theoretical moments assuming live load distribution factors from the current AASHTO and a proposed revision [2]. The theoretical moments are calculated using the following steps: 1) using one line of test vehicle wheels, calculate the moment on a simply supported beam, and 2) multiply the moment in Step 1 by the appropriate transverse live load distribution factors for stringers.

The values of the distribution factors are shown in Table 5.1.3.2.2. The current AASHTO method produces a moment 75% greater than the experimental method. The revised AASHTO method, however, produces a moment only 15% greater than the experimental method. The revised AASHTO method produces a distribution of moments similar to that of the experimental method.

5.1.3.3 Composite Action

The position of the experimental neutral axis of each stringer under LC #1 SCET MS-P3 is shown in Figure 5.1.3.3.1. This neutral axis position was determined by assuming a linear strain distribution throughout the steel stringer and concrete slab and locating the point of zero strain according to the flange and web gages. The positions of the experimental neutral axes closely match those of full composite behavior. The full composite moment of inertia (I_{comp}) was calculated with an effective width (b_{eff}) equal to one-half of the stringer spacing to each side and a modular ratio of 8. The neutral axis (NA) positions of S1 and S2

are above the theoretical composite NA positions. The experimental NA positions of S6 and S8 are below those corresponding to full composite behavior. This trend of varying degrees of composite action repeats itself for LC #1 SWLET, LC #1 CLET and LC #3 shown in Figure 5.1.3.3.2, Figure 5.1.3.3.3 and Figure 5.1.3.3.4, respectively.

A plot of maximum experimental stresses is shown in Figure 5.1.3.3.5. The solid boxes represent the maximum stresses in the bottom flange of the each stringer for LC #1. Note that these values are below all theoretical stresses. The experimental stresses are compared with the theoretical stresses obtained using the previos AASHTO (Method 1) and present AASHTO (Method 2) in conjunction with noncomposite and composite section properties. The composite and noncomposite section properties of the stringers are shown in Table 5.1.3.3.1.

The use of Method 1 (noncomposite) results in theoretical stresses of 16 ksi for the exterior and 6.5 ksi for the interior stringers. The use of Method 2 (noncomposite) results in a much lower value of 10.5 ksi for the exterior stringer and a slightly higher value of 7.2 ksi for the interior stringers. The shape of the stress distribution given by Method 2 (noncomposite) better represents qualitatively the actual distribution of stresses across the bridge deck. However, a gap of at least 3 ksi still exists between experimental stresses and those calculated by Method 2 (noncomposite). Figures 5.1.3.3.1 through 5.1.3.3.4 indicate that there is at least partial composite action in each stringer. Comparisons of Method 1 (composite) and Method 2 (composite) are made with the experimental stresses and plotted in Figure 5.1.3.3.5. Again, Method 2 results fit the behavior of the actual bridge more closely than Method 1 results. In addition to matching the shape of the graph, the use of Method 2 seems to result in values close to actual bottom flange stresses.

The location of the neutral axis for the same stringer varies only slightly for different load cases. Table 5.1.3.3.2 shows the location of the NA of each stringer for several loading conditions. Stringers S6 and S8 consistently have experimental neutral axis positions below full composite neutral axis positions by $^1/_2$ to 1 $^1/_2$ inches. The amount of composite action varies from LC #1 to LC #3 and from S1 to S8. The locations of the load influences the amount of composite action in each stringer.

Although Method 2 (composite) reflects the maximum bottom flange stress fairly well, it does not describe behavior of the section. Referring back to Figures 5.1.3.3.1 through 5.1.3.3.4, the NA positions for S1 and S2 are consistently above the full composite action neutral axis position. This does not seem to be possible, however, the proposed reason for this shift of the $NA_{experimental}$ above the $NA_{composite}$ is the addition of an axial tension throughout the section.

5.1.3.4 Interaction of Floor System with Bottom Chord

The experimental strain distributions in S6 and S8 indicate that there in partial composite action. The experimental strain distributions in S1 and S2 indicate that there is more than full composite action. This, however, is an incorrect conclusion. The addition of axial tensile stress distributions to the already present bending stress distributions in the exterior stringers raises the experimental neutral axes. This appears to be the case since the bottom chord of the truss is "missing" approximately 50% of its theoretical force. Also, the stringers are detailed such that when the bottom chord elongates, the stringers will be engaged and will carry some of the load.

5.1.4 Floor Beam Analysis and Behavior

5.1.4.1 Maximum Stresses

The maximum stresses in the floor beam are shown in Table 5.1.4.1.1. LC #2 resulted in the maximum floor beam stresses when the test vehicles were placed over floor beam 2 (FB2) at the SOUTH and CENTER transverse positions.

5.1.4.2 Composite Action

The load path existing between the test vehicle and the floor beams consists of a 6 to 7 $^{1}/_{2}$ inch reinforced concrete slab on top of fifteen stringers that are bolted or welded to the top flange of the floor beam. Comparisons of experimental stresses with theoretical composite and noncomposite stresses are shown in Figures 5.1.4.2.1 through 5.1.4.2.5. The theoretical composite moment of inertia (I_{comp}) was determined by assuming a 7 inch slab acting compositely with the floor beam. It is evident that full composite action of the floor beam and slab does not exist. Experimental values lie within the theoretical composite and noncomposite values.

A refined approximation of the actual bottom flange stress is computed when the floor beam, stringers and slab are modeled as a Vierendeel truss as shown in Figure 5.1.4.2.6. A tributary width of slab and stringer is assumed as the floor beam span divided by four. Table 5.1.4.2.1 shows a comparison of stresses for two load positions using different calculation methods.

5.1.4.3 Restraint

Restraint stresses calculated at one foot from the end of the floor beam are very small as shown in Figures 5.1.4.2.1 through 5.1.4.2.5. Some restraint does exist at the end of the

floor beam. This is evident in the bending of member U1L1. The restraint, however, does not affect the floor beam, because the stiffness of the floor beam is large compared to the stiffness of U1L1.

5.2 Bridge Structure No. 46-11-1316

5.2.1 Data Analysis Assumptions

Measured deflections and strain values, and experimental stresses are found in Tables A.3, A.4, and A.5 respcetively of reference[12].

The truss model used to calculate analytical forces and deflections is assumed to have pinned connections such that the truss members are subjected only to axial forces. The total strain in each gage was calculated by averaging the no load (NL) strain measurements before and after loading and subtracting this average NL from all strain measurements. The following procedure was used when calculating "measured forces" in the truss top chord.

1) Average strain from gages 1 and 3 (see figure 3.2.2.2a).
2) Assume linear strain distribution across member.
3) Calculate average strain in both channels and top plate.
4) Convert average strain in each section to average stress (E_s=29,000 ksi).
5) Calculate force in each section (see Table 3.2.1.1 for member areas).
6) Calculate total member force as the sum of the forces in each section.

In members U2L2, L2L3, and L2U3 (Figures 3.2.2.2a and 3.2.2.2b), where gage placement was symmetric, the average stress in the member was calculated by multiplying the average of the strain measured in each gage by the elastic modulus of steel (E_s). Total force was then calculated as described above.

The following assumptions were made for flexural analysis: f'_c = 4,000 psi, E_s= 29,000 ksi, and E_c=3,600 ksi. In all loading conditions where instrumented members were highly stressed, a near linear strain distribution was observed. Figures 5.2.1.1 and 5.2.1.2 show

typical strain distributions that were assumed based on the actual strain measurements in the floor beam and stringers respectively. In the following figures, "measured stresses" were calculated by multiblying the recorded strain by E_s.

As shown in Figures 3.2.2.3 and 3.2.2.7, only half of the bridge deck was instrumented. Deflection and strain measurements recorded during LC #1-North in stringer S5 are practically equal to measurements recorded in stringer S4 during LC #1-South. Using this observed symmetry, experimental deflections, moments, and stresses will be estimated for stringers S6 through S8.

5.2.2 Truss Analysis and Behavior

5.2.2.1 Maximum Stresses

The maximum stress in each strain gage of each member is listed in Table 5.2.2.1.1 with its corresponding loading condition and longitudinal and transverse vehicle placement.

5.2.2.2 Individual Component Behavior

Measured member forces were developed by calculating the force in a given member for each truck position in loading condition two. The center of the vehicle configuration was positioned over every floor beam resulting in eleven forces for each truss member. Analytical forces were developed by loading a member influence line with the test load configuration at each panel point. Overall truss behavior can be inferred from the comparison of measured to predicted member forces as a load truck moves across the bridge.

In an ideal truss, deformations in each member would be uniform across the entire cross section. Strain measurements from the three strain gages located on top chord U2U3 are plotted in Figure 5.2.2.2.1. When the load configuration was positioned over FB2, FB3, and FB4 more compression was present in the top plate gage than in the gages located on channel bottom flanges. This behavior reversed when the load was placed over FB5 and FB6, and there was more compression in the bottom flanges of the top chord. Axial force and bending would be present if end moments were developed between the top chord and vertical. This partial frame action was localized to the truss panels near top chord U2U3. Measured versus predicted forces for top chord U2U3 are plotted in Figure 5.2.2.2.2. Because bending was minor, the observed average member force was within 10% of that predicted by the simple truss model.

Figure 5.2.2.2.3 plots strain measurements within the cross section of the vertical L2U2. Bending about the north-south axis was observed when the vertical member was loaded in compression. Again, bending was small and axial force was the predominate load carrying mechanism. Although measured and predicted forces do not coincide exactly, Figure 5.2.2.2.4 shows that the analytical truss model can be used to reasonably predict truss member forces within 35% of the actual forces.

The strain distribution in diagonal L2U3 shows predominately axial force as seen in Figure 5.2.2.2.5. Actual measured forces in the diagonal are within 25% of predicted values, as shown in Figure 5.2.2.2.6, suggesting simple truss behavior with some small localized bending.

It is clear from Figure 5.2.2.2.7 that strains were virtually equal on each plate in bottom chord L2L3, and it can be concluded that each section in the bottom chord L2L3 shared the load equally. Unlike the top chord, vertical, and diagonal members in the instrumented panel, measured forces in the bottom chord L2L3 are only 50% of the predicted values as shown in Figure 5.2.2.2.8. Therefore, by cutting a section through members U2U3, U2L3, and L2L3 and summing forces, it is clear that the section is not in equilibrium and an additional horizontal force must be present in the actual structure to maintain equilibrium. The absence of 50% of the tensile force suggests that member L2L3 and some additional mechanism are acting together to sustain the expected force in the bottom chord. As mentioned in section 2.3.1, previous load tests have found that the intended bottom chord and longitudinal deck components often act together in sustaining axial tension forces.

If load sharing between the bottom chord and the bridge deck exists, there must be a load path to transfer axial force from the slab and stringer(s) through the "pin" to truss diagonals. The connection between the floor beam and truss is shown in Figure 3.1.8. Because the web and bottom flange of the floor beam are connected to the truss joint, the bottom chord in unable to deform independently of the deck diagonals and at least one outside stringer. The exact load path cannot be derived from the experimental data obtained from this study, however, the magnitude of the missing force in the bottom chord and the existence of a possible load path suggests that at least a portion of the slab and the exterior stringer carry an axial tension force.

5.2.2.3 Live Load Distribution to Each Truss

Truck axle loads were placed on a simple beam spanning the center to center distance between trusses. The beam reaction was then placed longitudinally on the truss member influence line corresponding to the longitudinal truck location. These predicted forces correlate well with forces measured during LC #2-North (Figures 5.2.2.3.1 through 5.2.2.3.4), indicating that the truss distribution can be easily determined assuming the bridge deck as a simple beam spanning the center to center distance between trusses.

5.2.2.4 Deflections

Deflection measurements were recorded on the north truss at the midspan of L2L3 using an LVDT. Overall deflection at truss midspan was measured during LC# 3-3 using a surveying level. An overall truss deflection of .313 inches was recorded, which rebounded completely after unloading. The analytical truss model was "loaded" with the test vehicle configuration in LC# 2-Center. Midpoint deflections in bottom chord L2L3 are plotted versus the average analytical deflections for truss points L2 and L3 in Figure 5.2.2.4.1. The actual stiffness of the truss is substantially greater than the theoretical stiffness due to the interaction between the bottom chord and the bridge deck. Therefore, it is not surprising that measured deflections were substantially less than those predicted by the analytical model.

5.2.3 Stringer Analysis and Behavior

5.2.3.1 Maximum Stresses

The maximum stress in each strain gage of each member is listed in Table 5.2.2.1.1 with its corresponding loading condition and longitudinal and transverse vehicle placement.

5.2.3.2 Live Load Distribution

As was mentioned in Section 2.3.4 of the literature review, the distribution of live load to each stringer in bridges with decks supported by a grid of steel members is often overestimated by current AASHTO guidelines. It is also known that mistakes in estimating live load distribution and hence load sharing between deck members can lead to an inaccurate evaluation of test measurements. This section identifies the actual live load distribution between deck members for different loading conditions. Once the actual amount of load sharing between adjacent stringers is determined, the relative importance of other factors such as unintended composite action can be evaluated.

It was assumed that the strain distribution measured at stringer midspan accurately represents strong axis bending in the steel stringers. Section 5.2.3.3 will show that although a considerable degree of interaction was present between stringers and the concrete slab, full composite action was not present. Because the strain distribution in the concrete slab was not measured, and full composite action cannot be assumed, the following procedure was used when calculating midspan stringer moments:

1) Assume a linear strain distribution in steel stringer.

2) Calculate tension (T_s) and compression (C_s) force in steel section.

3) Neglecting tension in concrete, calculate concrete compression force (C_{conc}) assuming $C_{conc}=T_s-C_s$.

4) Assuming C_{conc} is resolved at h/2 of slab, calculate moment arm (d') and moment (M=Td').

This method will most likely underestimate the actual distance from the bottom of the slab to C_{conc}. However, because tension in the concrete and the bottom mat of slab reinforcement is neglected, and C_{conc} is small compared to C_s and C_c, a small error in its location will not significantly effect the calculated moment. In the case of the exterior stringer S1, the position of the measured neutral axis is believed to be artificially high due to the presence of axial tension. Therefore, the moment calculated using the measured strain distribution in S1 is not valid and is not plotted in the following pages. Predicted moments were calculated assuming AASHTO distribution factors and a simply supported stringer. Distribution factors from AASHTO 1992 [1] and Revised AASHTO 1992 [2] are listed in Table 5.2.3.2.1. Although only three transverse truck positions were prescribed for this test, the strains measured during the North and Center transverse truck positions are believed to represent the range of maximum strains any stringer would experience for random transverse truck placements. Figure 5.2.3.2.1 plots moments for the North and Center transverse positions of LC #1. In both load positions, moments are maximized in the stringers nearest to the load, as expected. The maximum stringer moment was observed in stringer S2. The overall deflection of the midspan of the stringers is shown in Figure 5.2.3.2.2. Deflections are nearly equal in S1 and S2 and they steadily decrease in stringers away from the load. Although the moment in the exterior stringer cannot be accurately calculated, comparing deflections suggests that if axial

tension were not present in S1, the moments in S1 and S2 would be nearly equal. Predicted moments calculated from current distribution factors are 30% to 50% higher than moments calculated from measured strains. Revised distribution factors predict moments within plus or minus 10% of experimental moments with the exception of S1, where a comparison cannot be made. It is clear that the revised distribution factors better represent the experimental moment distribution for LC #1.

Figures 5.2.3.2.3 and 5.2.3.2.4 plot LC #3 experimental moments versus moments developed using AASHTO distribution factors for two loaded lanes. Moments currently predicted by AASHTO are 27% to 30% higher than experimental moments but those predicted using revised AASHTO are again within plus or minus 10% of experimental moments.

If the instrumented span were truly simply supported the total theoretical moment for the known vehicle load should correspond exactly with the sum of the experimental moments in each stringer. Theoretical and experimental total moments compare very closely as shown in Table 5.2.3.2.2.

5.2.3.3 Composite Action

Most truss bridges were built using noncomposite construction. Considerable laboratory and field research has found that composite behavior can exist in varying degrees up to full composite action, even though no mechanism for shear transfer has been provided. The amount of interaction between steel stringers and the concrete slab can be inferred by analyzing the strain distribution in the steel stringers.

The strain distribution measured in each of the stringers S1 through S5 are plotted in Figure 5.2.3.3.1. If no interaction were present between the steel beam and slab, the measured neutral axis would coincide with the stringer midepth of 8 inches, while for complete composite action, the neutral axis would lie in the concrete slab. Therefore, the neutral axis position in all instrumented interior stringers shows the existence of partial composite action. The measured neutral axis position of stringer S1 is higher than 16.5 inches, the neutral axis position expected for complete interaction between stringer and slab. It should be noted that if the measured strain distribution were assumed to extend linearly into the slab, the neutral axis position would fall into the 6 inch curb for some loading conditions. As previously mentioned, the measured strain distribution in S1 is not the result of simple bending alone, and will not be used to investigate composite behavior.

Neutral axis positions are plotted for one truck positioned over the midspan of panel three in Figure 5.2.3.3.2, two trucks back to back in Figure 5.2.3.3.3, and three trucks in Figure 5.2.3.3.4. In all cases partial composite action is present. The neutral axis position when one truck was used in LC #4 was generally lower than for two and three truck loadings.

However, the neutral axis position in stringer S4 changed independently of load and load placement. Secondly, it was not possible to load the exact same area of the bridge with an increased load increment, as has been done in hydraulic load tests. Therefore, it is not possible to conclude whether the degree of interaction between deck components increases as the load increases in this test.

It is clear that partial composite action is present in all of the instrumented stringers, and the degree of composite action will substantially reduce stresses over those expected for

a noncomposite section. However, the amount of composite action varies by stringer and loading condition and could not be confidently predicted for another bridge of similar geometry.

5.2.3.4 Interaction Between Floor System and Bottom Chord

Previous references to the interaction between the bottom chord and exterior stringer have been made throughout this chapter. This section will summarize the findings of this study and those in other sources supporting this conclusion. Bakt and Jeager [5] and Elleby et al. [7] found that truss bridges were capable of sustaining considerable loads even when the bottom chord was missing. Bakt and Jeager also found that the connection between the bottom chord and the bridge deck dictated the ability of the floor system to share load with the deck.

As shown in Figure 3.2.1.8, the bottom chord is attached to the floor system by bolting the web of the floor beam to a gusset plate, framing the bottom chord to the vertical. The bottom chord is also connected to the bottom flange of the floor beam and deck cross bracing. Theoretically, the reaction from the floor beam would load the truss "pin", initiating deformations in the truss members. However, if the truss and floor system are connected such as with the bottom chord, exterior stringer, slab, and deck cross bracing, these components will resist deformation as one, multiple-section member. Load would be distributed proportional to the relative axial stiffness and distance between each component. It is reasonable that the exterior stringer behaving partially composite with the slab would be

sufficiently stiff and close enough to the the floor beam/truss joint to attract some of this axial load.

The predicted force in bottom chord L2L3 was twice that calculated from measured strain values, while all other instrumented truss members framing into joint L2 carried near the expected axial force. A large change in the measured strain distribution in exterior stringer S1, as compared to stringers S2 through S5 was a further indication that S1 interacts with L2L3 in carrying axial tension. Figures 5.2.3.4.1 and 5.2.3.4.2 show the strain distribution at stringer midspan for LC #1-P3-North and LC #4-Center, respectively. If the measured strain distribution were the result of pure bending, the degree of interaction between stringer and slab would exceed full composite interaction. Measured deflections and bottom flange strains for LC #3-3 are plotted in Figures 5.2.3.4.3 and 5.2.3.4.4, respectively. The measured strain in the bottom flange of stringer S1 increased slightly relative to that in S2, where as deflections consistently decrease away from the load, further suggesting that axial tension effects the exterior stringer S1. Although it is possible that some force is carried in the interior stringers S2-S5, there is no indication that axial tension existed in these interior stringers.

5.2.4 Floor Beam Analysis and Behavior

5.2.4.1 Maximum Stress

The maximum stresses observed in each strain gage of each member are listed in Table 5.2.4.1.1 corresponding to the loading condition and longitudinal load placement.

5.2.4.2 Floor Beam Behavior

Typical strain distributions for the three longitudinal gage locations are shown in Figure 5.2.4.2.1. A change in the neutral axis position from 16.7 inches in the case of no composite action to the measured range of 18.1 in. to 19.4 in. is small relative to the 33 in. member depth. It can be concluded that partial composite action is present in floor beams but will not significantly reduce the stresses over those predicted for a noncomposite section.

Figure 5.2.4.2.2 shows the measured stresses versus predicted stresses for LC #1-FB3-Center. Predicted stresses are calculated using the BARS load distribution to transverse members, as described in Section 4.3. It is not surprising that measured stresses were considerably lower than those predicted by this simple analysis. Figures 5.2.4.2.3 and 5.2.4.2.4 compare predicted versus measured stresses for eccentric and symmetric three vehicle loading conditions.

The low stresses measured in the transverse floor beam are most likely the result of the following. The simple model used for analysis assumes that the total reaction from each line of wheels is concentrated at one of the two transverse wheel locations along the floor beam. Because there is considerable load sharing between longitudinal members away from the floor beams, the wheel loads will actually be delivered to the floor beams as a distributed

load from the slab and a series of stringer reactions, decreasing in magnitude away from the load. In the case of a tandem axle vehicle, only one rear axle delivers its full load as a point load and load from the remaining axle is spread out before it reaches the floor beam.

Secondly, stresses are calculated assuming the floor beam acts alone in resisting the applied moment. It has been shown that little interaction is present between the floor beam and the slab. However, a concrete slab 8 to 10 inches thick, spanning 25 $^1/_2$ feet, would attract applied moment relative to its flexural stiffness.

Low bottom flange strains were measured near the support and closely coincide with theoretical strains for a simply supported span, suggesting that moment restraint at the floor beam truss joint is negligible. Only a small amount of bending was observed in vertical member L2U2 due to the floor beam, also supporting this conclusion.

CHAPTER 6 - EVALUATION OF BARS ASSUMPTIONS FOR TRUSS BRIDGE RATING

6.1 Bridge Structure No 58-14-3244

6.1.1 Truss

During the experimental phase of this study, influence line loading and load distribution to the trusses were investigated in Loading Condition #2. The trucks were placed at 9 longitudinal positions along span 2 corresponding to FB1 through FB9. Table 6.1.1.1 shows a comparison of the maximum live load stress in each instrumented truss member. It can be concluded that the current BARS rating procedure for truss members is sufficient and no change to the rating procedure is needed.

6.1.2 Stringers

In Chapter 5, only live load stresses in the stringers were discussed. This section discusses dead load stress, live load plus impact stress, and total stress in the stringers. Dead load was calculated as follows: 1) Assume a tributary width of slab for each stringer; 2) Determine the average slab thickness and calculate weight of slab per foot, 3) Add the weight per foot of the stringer to the weight per foot of the slab to determine total wight per linear foot supported by the stringer. Assuming a simply-supported beam with noncomposite properties, the dead load moment and corresponding dead load stress were calculated.

Impact was included by multiplying the live load stress by the impact factor defined in AASHTO [1]. The impact factor for the stringers was 0.3. Comparisons of stresses are shown in Table 6.1.2.1. The total stress calculated for the exterior stringer by the BARS I method is 130% higher than the experimental stress. The total stress calculated for the exterior stringer by the BARS II method is 65% higher than the experimental stress.

6.1.3 Floor Beam

It was seen in Section 5.1.4.2 that the live load stresses calculated using the BARS assumptions were, for all loading conditions, higher than the experimental stresses. The effect of impact and dead load have been added to the live load stresses in the same manner as for the stringers described in Section 6.1.2. A comparison of stresses is shown in Table 6.1.3.1.

The total stresses calculated for the floor beam by BARS I are 27% higher than the experimental stresses. The assumption that all wheel loads are delivered to the floor beam as point loads is an oversimplification of the actual behavior. If the floor beam is found to be the critical member limiting bridge rating, further refinement of the load distribution assumptions is justified. Such a refinement could result in a significant increase in member capacity.

6.2 Bridge Structure No. 46-11-1316

6.2.1 Truss Evaluation

Section 5.2.2.1 identified that an idealized pinned truss model was sufficient to accurately predict member forces with the exception of the bottom chord. Considerable load sharing between the bottom chord and the bridge deck resulted in experimental forces in the bottom chord that were only 50% of those predicted. The average total stresses calculated for each member are shown in Table 6.2.1.1. Total stresses are calculated by adding the effect of dead load and impact to the maximum experimental and predicted live load forces shown in Figures 5.2.2.2.1 to 5.2.2.3.4. Stresses due to live load plus impact and dead load are listed in Table 6.2.1.2. Dead load stresses and the impact factors used for the calculation of live load plus impact were taken from BARS output for the SR 46 bridge. BARS identified the critical member in the SR 46 bridge to be the diagonal member L5U6. This member was not instrumented.

Predicted live load forces do not coincide exactly with those calculated in the SR 46 BARS output. This is because predicted forces shown in Figures 5.2.2.2.1 to 5.2.2.3.4 were calculated based on the actual truck placements used in the load test. These truck locations are not exactly the same as those used by BARS to calculate maximum member forces. The analytical forces shown in this report were calculated based upon BARS assumptions, and would match BARS output exactly if the truck placements were identical. By comparing the total stresses, it can be concluded that the current BARS rating analysis for truss members is sufficient.

6.2.2 Stringer Evaluation

In Chapter 5, the moments in each stringer were estimated such that the live load distribution between longitudinal stringers could be evaluated. However, BARS rates bridge members by limiting individual member stresses to a prescribed value (55% of yield for steel). Therefore, the stresses calculated from measured strains have been compared to those predicted by BARS to evaluate the accuracy of the stringer rating.

The maximum stresses measured in each stringer for the three transverse truck positions in LC #1 are plotted in Figure 6.2.2.1. It was shown in Chapter 5, that experimental moments may be closely predicted using the present AASHTO [2] distribution factors. Even though experimental moments in stringers S1 and S2 exceeded predicted moments, experimental stresses are equal to or less than predicated stresses, calculated assuming noncomposite section properties. The existence of partial composite action results in a lower experimental than predicted stresses in stringers S3 through S6 where predicted and experimental moments were nearly equal. Although partial composite action exists, it is clear that the predicted stresses calculated assuming full composite action would significantly underestimate measured stresses.

Experimental versus predicted stresses for LC #3-1 and LC #3-3 are plotted in Figures 6.2.2.2 and 6.2.2.3. Stresses calculated assuming previous AASHTO [1] distribution factors exceed experimental stresses by 35% to 80%, whereas predicted stresses are higher than experimental stresses by up to only 35% when revised distribution factors are assumed.

Previously, only live load stresses and moments have been presented. However, estimation of the total stress in a member is necessary to evaluate its BARS rating. Total

experimental stresses were calculated by the following procedure. 1) Assume stringers are simply supported and noncomposite. 2) Calculate the dead load stress induced by the beam and slab self-wight (values taken from BARS output). 3) Increase the experimental stress by the calculated impact effect of 30%[1]. 4) Sum the experimental live load plus impact and dead load stresses. Figure 6.2.2.4 shows the effect of the total load applied to the stringers for LC #1-P3. The comparison between total experimental and predicted stresses can be seen in Table 6.2.2.1. It was shown in Section 2.2.4 that considerable interaction between slab and beam often exists unless special care is taken during construction to eliminate bond between the two surfaces. Therefore, even if the moment in a member is predicted exactly during rating, experimental stress will be overestimated by stresses calculated assuming a noncomposite section, which explains the difference between experimental and predicted BARS-2 values (BARS-2 notation described in table).

As in the previous section, predicted values shown in Table 6.2.2.1 were calculated based on BARS assumptions for the exact test vehicle locations prescribed in the load test. Table 6.2.2.2 shows the maximum stringer stress as calculated from BARS output. It is not reasonable to compare the BARS output directly with the experimental stresses from the load test due to the differing load placements. It can be seen that the maximum stress in an interior stringer, as computed by BARS, is 11.2 ksi. In the next section the maximum floor beam stress calculated by BARS for the same loading condition (LC#1) is shown to be 14.7 ksi. Therefore, in this bridge the floor beam and not the stringer is the floor member rated as critical.

6.2.3 Floor Beam Rating Evaluation

It was seen in Section 5.2.4.2, that the live load stresses calculated using BARS assumptions were, for all loading conditions, higher than experimental stresses. The effect of impact and dead load have been added to the experimental and predicted stresses using the procedure described in the previous section. The total stresses in the instrumented floor beam for LC #3-3 are shown in Figure 6.2.3.1. The maximum predicted stress was only 22% higher than the total estimated stress in the bottom flange of the floor beam. Table 6.2.3.1 lists the maximum total stresses for the three loading conditions designed to maximize moments in the floor beam. "Predicted (BARS)" values shown in Table 6.2.3.1 were calculated based upon BARS assumptions using the exact truck placement in the load test. It should be noted that the actual truck placement and the load placement used by BARS are nearly equal, resulting in the same total stress after round off.

Although it would be ideal to rate every bridge structure understanding and accounting for all of its capacity, this is not realistic. However, despite simplistic assumptions, the error observed in the floor beam rating is small. BARS rates floor beams assuming the following. 1) Members are simply supported, and resist the entire applied moment with a noncomposite section. 2) All wheel loads, regardless of longitudinal placement, are assumed as point loads over the floor beam. It has been shown that, in the SR 46 bridge, little composite action exists, and the floor beam ends are simply supported. However, the slab does resist applied moment relative to its flexural stiffness, reducing the moment applied to the beam. Also, the assumption that all wheel loads are delivered to the floor beam as point loads is known to be an oversimplification of actual behavior. Due to these conservative assumptions, predicted live load stresses are 35% to 75% higher than

experimental stresses. If the floor beam is found to be the critical member limiting bridge rating, further refinement of the load distribution assumptions is justified. Such refinement could result in a significant increase in member capacity. However, under the current BARS procedures, such refinement is not feasible within the constraints of load distribution.

CHAPTER 7 - CONCLUSIONS AND IMPLEMENTATION

7.1 Summary of Findings

This section summarizes the results described in Chapter 5.

7.1.1 Bridge Structure No. 58-14-3244

Based on the results discussed in Section 5.1.2, the following conclusions can be made concerning the truss.

1. Truss theory can be used to calculate truss forces within 15%.
2. The experimental force in the bottom chord ranged from 20% to 60% of the theoretical bottom chord force.
3. Interior truss member components carry more load than exterior truss member components. No estimate of the amount of axial force in the floor system was made because instrumentation was not installed on member L2L3. Member L2L3 is adjacent to the instrumented deck panel (Panel 3).
4. Bending occurred in the vertical member U1L1.
5. Load distribution to the trusses may be determined by assuming that the floor system spans between the trusses as a simply supported element.

The following conclusions about stringer behavior may be made based on the results discussed in Section 5.1.3.

1. Partial composite action was observed in the stringers, causing the neutral axes of the stringers to be higher than the neutral axes of bare beams.
2. Axial tension force exists in the exterior stringers, causing the experimental neutral axes to be higher than the neutral axes of fully composite members.
3. Experimentally determined bottom flange stresses were less than those calculated using current and revised live load distribution factors considering both composite and noncomposite section properties. For the case of the AASHTO live load distribution factors [2], the degree of conservatism, in terms of live load stress only, was at least 230% with noncomposite section properties. In this bridge, the rating is controlled by the exterior stringer and the degree of conservatism is 130% in terms of total stress. The degree of conservatism was computed by dividing the calculated stress by the experimental stress and subtracting one from this result. Refer to Table 6.1.2.1 for stress values.

The following conclusions concerning the floor beams may be made based on results discussed in Section 5.1.4.

1. Experimentally determined stresses were greater than theoretical composite stresses and less than theoretical noncomposite stresses.
2. No restraint was present at the ends of the floor beams.

7.1.2 Bridge Structure No. 46-11-1316

Based on the results developed in Section 5.2.2, the following conclusions can be made regarding the behavior of the trusses in the SR 46 bridge.

1) An idealized truss model can be used to predict truss member forces within plus or minus 35% of experimental forces, with the exception of the bottom chord.

2) The maximum predicted force in the instrumented bottom chord was twice the experimental force.

3) Although truss joints have some bending rigidity, little bending was observed in the instrumented top chord, diagonal, and vertical members. Therefore, for the purpose of rating, all truss members can be assumed to carry axial force exclusively.

4) Load distribution to each truss can be determined assuming that the bridge deck is a simple beam spanning the center to center distance between trusses.

The results from Section 5.2.3 support the following conclusions concerning behavior of the longitudinal stringers.

1) Moments calculated using AASHTO [1] live load distribution factors were 30% to 50% higher than experimental moments.

2) Moments calculated using AASHTO [2] live load distribution factors may be used to predict the maximum experimental moment within plus or minus 10%.

3) Experimental bottom flange stresses never exceeded stresses calculated using revised AASHTO live load distribution factors, regardless of truck placement.

4) Partial composite action exists in all instrumented stringers, but in no instance was full interaction between beam and slab observed.

5) Axial tension in the deck is believed to result in higher than calculated bottom flange stresses in exterior stringers.

The results from Section 5.2.4 support the following conclusions concerning floor beam behavior.

1) No restraint was observed at the ends of floor beams.

2) Partial composite action was observed between beam and slab, but the amount of interaction does not result in a significant reduction in the stresses predicted assuming noncomposite behavior.

3) Maximum experimentally determined stresses ranged from 35% to 75% of the maximum theoretical bottom flange stresses.

7.2 Extrapolation of Findings to Other Truss Bridges

In Chapter 2, several instances were discussed where truss bridges sustained loads well in excess of those predicted by simple truss theory. The existence of rusted pins and damaged members often requires the entire bridge structure to behave more like an arch or frame than an ideal truss. However, the behavior observed in these two truss bridges suggests that rating a truss bridge using an idealized truss model is not overly conservative. This study and many previous studies have found that the actual stresses in the bottom

chords of trusses are much less than the theoretical stresses. However, this behavior is specific to the details that will transfer force between the truss joint and floor system. Truss bridges in the state of Indiana vary in geometry, and it is unrealistic to suggest that the rating capacity of the bottom chord should somehow be increased for all bridges.

Composite action was also observed in varying degrees and locations throughout the bridge decks of both bridges even though no shear connectors were used in construction. This phenomenon is discussed in Chapter 2 and the following conclusions can be made. Unless bond between the concrete slab and steel beams is intentionally eliminated during construction, significant interaction between the two components will often exist. Even if this bond is eliminated during construction or subsequently broken during the service life of a bridge, partial composite action will exist to some degree due to the friction between the beam and slab.

Because bridge rating is designed to limit stresses well below yield, it would be reasonable to incorporate this unintended composite action in bridge rating if it could be proven to consistently exist. The behavior observed in the SR 46 bridge is a textbook example of the overall behavior on the subject of unintended composite action. In all stringers, partial composite action was observed to some degree and resulted in experimental stresses which are lower than those calculated in a noncomposite rating. However, full composite action was not observed, and it would be unconservative to rate this bridge using full composite section properties. Secondly, the detail between the floor beam and slab was identical to that between the slab and stringers (beam top flange partially incased in concrete) but little composite action was observed. Also, in the SR 58 bridge, composite action was observed to varying degrees, but full interaction was not observed in all stringers

under all loading conditions. Therefore, it is recommended that unless shear connectors are used in design, noncomposite section properties should be used for the rating of bridges with slab on girder decks.

It is recognized by the authors that experimental moments cannot be accepted with the same degree of confidence as experimental stresses calculated from measured strains. Therefore, the actual distribution of load throughout the bridge deck can only be evaluated to the degree that the reader accepts these experimental moments. However, by examining the experimental stresses, it is clear that new AASHTO [2] distribution factors better represent the actual magnitude of stresses in both bridges than stresses calculated using past AASHTO [1] factors. It is also clear that, although full composite action cannot be depended upon when rating a structure, partial interaction will most likely introduce an additional factor of safety into the rating of a noncomposite stringer. Results from these two bridge tests indicate that the use of new AASHTO [2] distribution factors would result in a better estimate of the stringer load capacity for these two bridges than those currently used by BARS. Secondly, the revised distribution factors are being proposed for the design and not analysis of new bridges, suggesting that a certain degree of conservatism in the lateral load distribution will remain. Therefore, it is believed that the new AASHTO distribution factors proposed for the design of new bridges can safely be extrapolated to other slab on steel girder bridges when performing a rating analysis.

7.3 Implementation

It is widely known that previous AASHTO [1] live load distribution factors are conservative. These distribution factors have previously been accepted because they were developed for design and not analysis of bridges. Many designers and analysts concerned with the long term life of bridge structures see this conservatism as a safeguard against increasing gross vehicle weights. However, for the purpose of rating for a known overload vehicle, a more realistic assessment of the actual load distribution in a bridge is justified. Therefore, it is recommended that the Indiana Department of Transportation incorporate the new AASHTO [2] live load distribution factors when rating truss bridges.

For the SR 58 bridge, the adoption of the new LRFD AASHTO distribution factors would change the member controlling the rating from the stringer to the floor beam. The rating of the floor beam would not be affected by the new distribution factors. The critical floor member in SR 46 bridge was determined to be the floor beam. The diagonal member L5U6 controlled the BARS rating for the entire bridge. Therefore, a change in the live load distribution factors would not result in an increase in rating capacity for the SR 46 bridge.

Table 3.1.1.1 SR 58 Bridge Truss Sections

Truss Member	Section	Gross Area (in^2)
L0L1	(2) Bars 4" x $1^1/_4$"	10.00
L1L2	(2) Bars 4" x $1^1/_4$"	10.00
L2L3	(4) Bars 4" x $^{15}/_{16}$"	15.00
L3L4	(4) Bars 4" x $1^1/_8$"	18.00
L4L5	(4) Bars 4" x $1^3/_{16}$"	19.00
L0U1	(2) C12x20.7 (1) Plate 20" x $^1/_2$"	22.06
U1U2	(2) C12x20.7 (1) Plate 20" x $^1/_2$"	22.06
U2U3	(2) C12x20.7 (1) Plate 20" x $^1/_2$"	22.06
U3U4	(2) C12x25 (1) Plate 20" x $^1/_2$"	26.64
U4U5	(2) C12x25 (1) Plate 20" x $^1/_2$"	26.64
U1L1	(2) Angles $3^1/_2$" x $2^1/_2$" x $^5/_{16}$"	3.56
U2L2	(2) C8x11.5	6.76
U3L3	(2) C8x11.5	6.76
U4L4	(2) C8x11.5	6.76
U5L5	(2) C8x11.5	6.76
U1L2	(2) Bars 4" x $^7/_8$"	7.00
U2L3	(2) Bars 3" x $^7/_8$"	5.25
U3L4	(2) Bars $2^1/_2$" x $^3/_4$"	3.75
U4L5	(2) Bars $2^1/_2$" x $^3/_4$"	3.75
U4L3	(1) Rod 1" diam.	0.875
U5L4	(1) Rod 1" diam.	0.875

Table 3.1.5.1 Test Vehicle Identification and Weights

	Weight (lbs)			
Truck Identification	Front Axle	Front Tandem Axle	Back Tandem Axle	Gross Vehicle Weight
# 66184	14,200	22,000	22,000	58,000
# 10326	13,700	22,000	22,000	57,000

Table 3.1.5.2 Loading Condition Descriptions

Loading Condition	Abbreviation	Description
#1	LC #1	Single tandem axle truck. Center of load was assumed at center of back axles.
#2	LC #2	Two tandem axle trucks aligned back to back longitudinally. Center of load was assumed at back edge of trucks.
#3	LC #3	Two tandem axle trucks aligned side by side transversely facing in opposite directions. Center of back axles of both trucks was aligned and assumed to be the center of load.

Transverse Position	Description
SCET	South curb, truck facing East
SWLET	1 $^1/_2$ ft from south curb, truck facing East
CLET	Center of bridge, truck facing East
NWLET	1 $^1/_2$ ft from north curb, truck facing East
NCET	North curb, truck facing East
SCWT	South curb, truck facing West
CLWT	Center of bridge, truck facing West
NCWT	North curb, truck facing West
SOUTH	1 $^1/_2$ ft from south curb
CENTER	Center of bridge
NORTH	1 $^1/_2$ ft from north curb

Longitudinal Position	Description
MS-P3	Midspan of panel 3
FB2	Floor beam 2
MS-P2	Midspan of panel 2
FB1	Floor beam 1

Table 3.2.1.1 SR46 Truss Sections

Truss Member	Section	Gross Area (in^2)
L0L1	(4) Angles 6" x 4" x $^3/_{16}$"	16.76
L1L2	(4) Angles 6" x 4" x $^3/_{16}$"	16.76
L2L3	(4) Angles 6" x 4" x $^1/_8$" (2) Plates 13" x $^3/_8$"	22.93
L3L4	(4) Angles 6" x 4" x $^1/_2$" (2) Plates 15" x $^7/_{16}$"	29.38
L4L5	(4) Angles 6" x 4" x $^1/_2$" (2) Plates 15" x $^7/_{16}$"	29.38
L5L5'	(4) Angles 6" x 4" x $^3/_4$" (2) Plates 13" x $^3/_{16}$"	31.04
L0U1	(2) C15x45 (1) Plate 18$^1/_2$" x $^1/_2$"	35.58
U1U2	(2) C15x35 (1) Plate 18$^1/_2$" x $^1/_2$"	29.71
U2U3	(2) C15x45 (1) Plate 18$^1/_2$" x $^7/_{16}$"	34.43
U3U4	(2) C15x50 (1) Plate 18$^1/_2$" x $^7/_{16}$"	37.37
U4U5	(2) C15x50 (1) Plate 18$^1/_2$" x $^1/_2$"	38.53
U5U5'	(2) C15x50 (1) Plate 18$^1/_2$" x $^1/_2$"	38.53
U1L1	(2) C10x15.3	8.94
U2L2	(2) C10x20	11.72
U3L3	(2) C10x15.3	8.94
U4L4	(2) C10x15.3	8.94
U5L5	(2) C10x15.3	8.94

Table 3.2.1.1 SR46 Truss Sections (continued)

Truss Member	Section	Gross Area (in^2)
U1L2	(2) Angles 4" x $3^1/_2$" x $^1/_2$"	12.00
U2L3	(2) Angles 7" x 4" x $^1/_2$"	8.71
U3L4	(2) Angles 7" x 4" x $^3/_8$"	6.76
U4L5	(2) Angles 4" x $3^1/_2$" x $^7/_{16}$"	5.30
U5L5'	(2) Angles $3^1/_2$" x 3" x $^3/_8$"	3.20
U5L4	(2) Angles $3^1/_2$" x 3" x $^3/_8$"	3.20
U5'L5	(2) Angles $3^1/_2$" x 3" x $^3/_8$"	3.20

Table 3.2.4.1 Test Vehicle Weights

Truck Identification	Weight in Pounds		
	Front Axle	First Tandem Axle	Second Tandem Axle
# 5460	13,000	20,000	20,000
# 5329	13,000	20,000	20,000
# 5019	13,000	16,000	16,000

Table 3.2.4.2 Summary of Truck Placement by Loading Condition

Loading Condition	Abbreviation	Description
#1	LC #1	Two tandem axle trucks aligned back to back longitudinally. Center of load was assumed at back edge of trucks (4'-2" from the second tandem axle of each truck)
#2	LC #2	Two tandem axle trucks aligned back to back longitudinally. Center of load was assumed at back edge of trucks (4'-2" from the second tandem axle of each truck)
#3	LC #3-1	Two tandem axle trucks aligned back to back longitudinally, identical to LC #1 & #2. A third tandem axle truck with the center of the tandem axles lined up with center of the two truck configuration.
	LC #3-2	Two tandem axle trucks side by side transversely. Center of load assumed at first tandem axle. A third tandem truck one panel East. Center of load assumed at first tandem axle.
	LC #3-3	Two tandem axle trucks side by side. Third tandem axle truck back to back of first two. Center of load was assumed at back edge of trucks (4'-2" from the second tandem axle of each truck)
#4	LC #4	Single tandem axle truck. Center of load assumed at center of back axles.

Transverse Position	Description
SOUTH	Outside edge of back tires placed 1' from south curb.
CENTER	Center of bridge
NORTH	Outside edge of back tires placed 1' from north curb.

Table 3.2.4.2 Summary of Truck Placement by Loading Condition (continued)

Longitudinal Position	Description
P2	Assumed center of load placed at midspan of panel 2
FB2	Assumed center of load placed over Floor beam 2
P3	Assumed center of load placed at midspan of panel 3
FB3	Assumed center of load placed over Floor beam 3
P4	Assumed center of load placed at midspan of panel 4
P5	Assumed center of load placed at midspan of panel 5

Table 5.1.2.1.1 Maximum Experimental Stresses in Truss Members

Member	Gage	σ_{max}, ksi*	LC #	Longitudinal Position	Transverse Position
U1U2	U1U2-1	-3.9	2	FB3	SOUTH
	U1U2-2	-3.9	2	FB3	SOUTH
	U1U2-3	-3.9	2	FB3	SOUTH
	U1U2-4	-4.2	2	FB2	SOUTH
	U1U2-5	-4.0	2	FB2	SOUTH
U3U4	U3U4-2	-3.8	2	FB5	SOUTH
	U3U4-3	-4.1	2	FB4	SOUTH
	U3U4-4	-4.1	2	FB4	SOUTH
	U3U4-5	-4.0	2	FB4	SOUTH
L1L2	L1L2-I	2.7	2	FB1	SOUTH
	L1L2-E	2.1	2	FB1	SOUTH
L3L4	L3L4-1	2.4	2	FB3	SOUTH
	L3L4-2	3.0	2	FB3	SOUTH
	L3L4-3	3.4	2	FB3	SOUTH
	L3L4-4	3.3	2	FB3	SOUTH
U1L1	U1L1-I	12.4	2	FB1	SOUTH
	U1L2-E	8.1	2	FB1	SOUTH
U1L2	U1L2-I	7.2	2	FB3	SOUTH
	U1L2-E	6.9	2	FB3	SOUTH
U3L4	U3L4-I	7.2 (-5.4)**	2 (2)	FB5 (FB2)	SOUTH (SOUTH)
	U3L4-E	6.8 (-2.3)	2 (1)	FB5 (MS-P3)	SOUTH (SCET)
U4L3	U4L3	11.1 (-10.7)	2 (2)	FB2 (FB5)	SOUTH (SOUTH)

* (-) indicates compression

** load reversal for diagonals

Table 5.1.2.4.1 Truss Deflections

LC #	Longitudinal Position	Deflection at L5 (in.)		Ratio of Measured to Theoretical Deflection
		Theoretical	Measured	
2	FB5	0.70	0.56	80%
	FB6	0.68	0.50	73%
	FB7	0.50	0.38*	75%
3	FB5	0.83	0.63	75%

Note: All loads are centered on the roadway.

* Measurement taken at center of roadway.

Table 5.1.3.1.1 Maximum Experimental Stress in Stringers

Member	Gage	σ_{max}, ksi	LC #	Longitudinal Position	Transverse Position
S1	S1-MF	5.6	3	MS-P3	-
	S1-MW	2.2	3	MS-P3	-
	S1-EF	-2.4	1	MS-P2	SCWT
S2	S2-MF	4.9	3	MS-P3	-
	S2-MW	1.8	3	MS-P3	-
	S2-EF	1.6 (-1.2)	3 (1)	FB2 (MS-P2)	- (SCET)
S3	S3-MF	4.2	3	MS-P3	-
	S3-MW	1.0	3	MS-P3	-
	S3-EF	2.1 (-0.6)	3 (1)	FB2 (MS-P2)	- (SCET)
S6	S6-MF	3.7	3	MS-P3	-
	S6-MW	0.6	2	FB3	CENTER
	S6-EF	1.8 (-0.5)	3	FB2 (MS-P2)	- (SWLET)
S8	S8-MF	4.0	3	MS-P3	-
	S8-MW	0.8	3	MS-P3	-
	S8-EF	2.5 (-0.6)	3 (1)	FB2 (MS-P2)	- (CLET)

Note: (-) indicates compression

Table 5.2.3.2.2 Experimental Total Moments and Theoretical Total Moments

LC #	Transverse Position	Longitudinal Position	Total Moment (ft - kips)	
			Experimental	Theoretical
LC #1	SCET	MS-P3	120	170
	SWLET	MS-P3	120	170
	CLET	MS-P3	120	170
	SCWT	MS-P3	120	170
	CLWT	MS-P3	120	170
LC #2	SOUTH	FB3	110	125
	CENTER	FB3	110	125
LC #3	-	MS-P3	240	340

Note: Experimental moments rounded to nearest 10 ft-kips

Table 5.1.3.2.2 Transverse Live Load Distribution Factors for Stringers

Stringer	1992 AASHTO		Revised AASHTO	
	One Lane	Two Lanes	One Lane	Two Lanes
S1 (exterior)	0.386	0.386	0.249	0.335
S2 (1st interior)	0.228	0.290	0.212	0.282
S3 (2nd interior)	0.152	0.193	0.172	0.224

Table 5.1.3.3.1 Stringer Section Properties

	Noncomposite		Composite	
Stringer	I_{nc} (in^4)	NA* (in)	I_{comp} (in^4)	NA* (in)
S1	122	5	460	10.2
S2	122	5	520	10.5
S3	122	5	410	9.8
S4	122	5	440	9.9
S5	122	5	470	10.1
S6	122	5	500	10.2
S7	122	5	540	10.3
S8	122	5	570	10.4

* Neutral axis position is measured from bottom flange.

Table 5.1.3.3.2 Experimental Neutral Axis Positions

LC#	Transverse Position	Neutral Axis Position from Bottom Flange (in)							
		S1*	S2*	S3*	S4	S5	S6*	S7	S8*
LC #1	SCET	11.3	11.2	9.5	9.1	8.6	8.1	9.1	10.0
	SWLET	11.4	11.3	9.3	8.9	8.5	8.1	8.5	8.9
	CLET	11.7	11.6	10.1	9.3	8.6	7.9	8.8	9.7
	SCWT	11.2	11.1	9.7	9.2	8.7	8.1	9.1	10.1
	CLWT	11.3	11.2	9.9	9.2	8.6	8.0	8.7	9.5
LC #3	-	11.6	11.2	9.7	9.3	8.8	8.4	8.8	9.3

Note: Longitudinal position is MS-P3 for all cases.
* Instrumented stringers.

Table 5.1.4.1.1 Maximum Experimental Stress in Floor Beam

Member	Gage	σ_{max}, ksi	LC #	Longitudinal Position	Transverse Position
FB2	FLBM-M	7.3	2	FB2	CENTER
	FLBM-Q	5.5	2	FB2	SOUTH
	FLBM-E	2.8	2	FB2	SOUTH

Table 5.1.4.2.1 Floor Beam Midspan Stresses

LC #	Transverse Position	Midspan Stress (ksi)			
		Theoretical Noncomposite	Theoretical Composite	Experimental	Vierendeel Truss Model
LC #1	CLET	7.8	2.8	4.4	6.0
LC #2	CENTER	11.5	4.1	7.3	8.5

Note: Longitudinal position is FB2 for both loading conditions.

Table 5.2.2.1.1 Maximum Truss Member Stresses

Member	Gage	Stress, ksi	LC#	Longitudinal Position	Transverse Position
U2U3	U2U3-1	-2.9	3-1	P4	①
	U2U3-2	-3.9	3-1	FB3	①
	U2U3-3	-3.0	3-1	P4	①
U2L2	U2L2-4	-2.2 (2.0)	2 (1)	FB4 (P2)	N (N)
	U2L2-5	-2.9 (2.3)	2 (1)	FB4 (P2)	N (N)
	U2L2-6	-2.9 (1.8)	2 (1)	FB4 (P2)	N (N)
	U2L2-7	-2.3 (1.7)	2 (1)	FB4 (P2)	N (N)
U2L3	U2L3-8	3.7 (-1.7)	3-1 (1)	P4 (P2)	① (N)
	U2L3-9	3.6 (-1.5)	3-1 (1)	P4 (P2)	① (N)
	U2L3-10	3.3 (-1.6)	3-1 (1)	P4 (P2)	① (N)
	U2L3-11	3.7 (-1.4)	3-1 (1)	P4 (P2)	① (N)
L2L3	L2L3-12	2.0	3-1	P3	①
	L2L3-13	2.0	3-1	P3	①

① - See Figure 3.2.4.3.1 for transverse position
N - NORTH

Table 5.2.3.1.1 Maximum Stringer Stresses

Member	Gage	Stress, ksi	LC #	Longitudinal Position	Transverse Position
S1	S1-A	-1	3-2	②	②
	S1-B	-0.9	3-3	FB3	③
	S1-C	1.3	3-3	FB3	③
	S1-D	1.5	3-2	②	②
	S1-E	2.3	3-2	②	②
	S1-F	3.7	3-2	②	②
	S1-G	3.8	3-2	②	②
S2	S2-A	1.6	3-3	P3	③
	S2-B	2	3-3	P3	③
	S2-C	1.1	3-3	P3	③
	S2-D	-0.7	4	P3	NORTH
	S2-E	0.9	3-2	②	②
	S2-F	3.2	3-2	②	②
	S2-G	3.4	3-2	②	②
S3	S3-A	1.3	3-3	FB3	③
	S3-B	2.1	3-1	FB3	①
	S3-C	1.5	3-3	P3	③
	S3-D	-0.7	4	P3	NORTH
	S3-E	1.5	3-2	②	②
	S3-F	3.8	3-2	②	②

Table 5.2.3.1.1 Maximum Stringer Stresses (continued)

Member	Gage	Stress, ksi	LC #	Longitudinal Position	Transverse Position
S4	S4-A	0.9	3-3	P3	③
	S4-B	2.1	3-3	P3	③
	S4-C	1.6	3-3	P3	③
	S4-D	-0.6	3-1	P3	①
	S4-E	1.6	3-2	②	②
	S4-F	3.8	3-2	②	②
S5	S5-A	0.4	3-3	P3	③
	S5-B	1.1	3-3	P3	③
	S5-C	1.3	3-3	P3	③
	S5-D	-0.9	3-1	P3	①
	S5-E	1.3	3-2	②	②
	S5-F	3.8	3-2	②	②

① - See Figure 3.2.4.3.1 for transverse position
② - See Figure 3.2.4.3.2 for longitudinal and transverse position
③ - See Figure 3.2.4.3.3 for transverse position

Table 5.2.3.2.1 AASHTO Distribution Factors

	1992 AASHTO		Revised AASHTO	
Stringer	One Lane	Two Lanes	One Lane	Two Lanes
S1 (exterior)	0.58	0.58	0.33	0.45
S2-S7 (interior)	0.48	0.61	0.33	0.45

Table 5.2.3.2.2 Experimental Total Moments and Theoretical Total Moments

Load Condition	Experimental Total Moment (k-ft)	Theoretical Total Moment (k-ft)	Percent Difference
LC #1-P3-North	100	105	4%
LC #1-P3-Center	115	105	10%
LC #3-1-P3	205	217	5%
LC #3-3-P3	170	153	10%

Table 5.2.4.1.1 Maximum Floor Beam Stresses

Member	Gage	Stress, ksi	LC #	Longitudinal Position	Transverse Position
FB3	FB1-A	-1.1	3-1	FB3	①
	FB1-B	-0.2	3-2	②	②
	FB1-C	2.3	3-2	②	②
	FB2-A	-2.7	3-1	FB3	①
	FB2-B	0.8	3-1	FB3	①
	FB2-C	4.9	3-1	FB3	①
	FB3-A	-3.9	3-3	FB3	③
	FB3-B	0.5	3-3	FB3	③
	FB3-C	5.5	3-3	FB3	③

① - See Figure 3.2.4.3.1 for transverse position
② - See Figure 3.2.4.3.2 for longitudinal and transverse position
③ - See Figure 3.2.4.3.3 for transverse position

Table 6.1.1.1 Maximum Live Load Stresses in the Instrumented Truss Members

Loading Position	Member	Maximum Live Load Stress (ksi)	
		Experimental	Theoretical
LC #2 - CENTER	L1L2	2.2	4.3
	L3L4	2.6	4.2
	U1U2	-2.9	-2.9
	U3U4	-3.3	-3.3
	U1L1	7.8	8.9
	U1L2	5.5	5.1
	U3L4	5.3	5.3
LC #2 - SOUTH	L1L2	2.4	5.6
	L3L4	3.0	5.4
	U1U2	-3.9	-3.8
	U3U4	-4.0	-4.3
	U1L1	10.2	11.5
	U1L2	7.1	6.6
	U3L4	7.0	6.9

Table 6.1.2.1 Total Stresses in Stringers

Stringer	BARS I[1]	BARS II[2]	Experimental
	Live Load Stress (ksi)		
S1	16.1	10.4	4.9
S2	9.5	8.9	3.8
S3	6.4	7.2	3.2
S6	6.4	7.2	2.3
S8	6.4	7.2	2.7
	Live Load + Impact Stress (ksi)		
S1	21.0	13.5	6.4
S2	12.4	11.5	4.9
S3	8.3	9.3	4.2
S6	8.3	9.3	3.0
S8	8.3	9.3	3.5
	Dead Load Stress (ksi)		
S1	5.0	5.0	5.0
S2	4.2	4.2	4.2
S3	3.0	3.0	3.0
S6	3.0	3.0	3.0
S8	3.0	3.0	3.0
	Total Stress (ksi)		
S1	26.0	18.6	11.4
S2	16.6	15.7	9.2
S3	11.3	12.4	7.2
S6	11.3	12.4	6.0
S8	11.3	12.4	6.5

1) BARS I: Stresses calculated using BARS assumptions with previous AASHTO [1] live load distribution factors.

2) BARS II: Stresses calculated using BARS assumptions with current LRFD AASHTO [2] live distribution factors.

Table 6.1.3.1 Maximum Midspan Stress in Floor Beam

LC #	Stress (ksi)						
	Live Load		Live Load plus Impact		Dead Load	Total Load	
	BARS I	Exp.	BARS I	Exp.		BARS I	Exp.
1	7.8	4.4	10.2	5.7	6.2	16.8	11.9
2	11.5	7.3	14.9	9.5	6.2	21.1	15.7

Table 6.2.1.1 Maximum Total Stresses in Instrumented Truss Members

Loading Condition	Member	Maximum Total Stress (ksi)		Percent Difference
		Predicted (BARS)	Experimental	
LC #2 Center	U2U3	-10.3	-10.3	0%
	L2U2	-8.2	-7.5	9%
	U2L3	11.9	11.2	6%
	L2L3	13.0	11.6	12%
LC #2 North	U2U3	11.5	11.4	1%
	L2U2	9.6	8.5	13%
	U2L3	13.7	12.4	11%
	L2L3	14.3	12.4	16%

Table 6.2.1.2 Live Load Plus Impact and Dead Load Stresses in Instrumented Members

Loading Condition	Member	Predicted (BARS) Stress		Experimental Stress	
		LL + I (ksi)	DL (ksi)	LL + I (ksi)	DL (ksi)
LC #2 Center	U2U3	-2.0	-8.3	-2.0	-8.3
	L2U2	-2.5	-5.7	-1.8	-5.7
	U2L3	3.3	8.6	2.6	8.6
	L2L3	2.6	10.4	1.2	10.4
LC #2 North	U2U3	-3.2	-8.3	-3.11	-8.3
	L2U2	-3.9	-5.7	-2.8	-5.7
	U2L3	5.1	8.6	3.8	8.6
	L2L3	3.9	10.4	2.0	10.4

Table 6.2.2.1 Total Stress in Bottom Flange of Instrumented Stringers

Loading Condition	Total Stress (ksi)		
	Predicted (BARS-1)[1]	Predicted (BARS-2)[2]	Experimental
Exterior Stringer			
LC #1	8.0	6.5	6.6
LC #3-1	9.7	8.0	6.9
LC #3-2	11.8	9.6	7.2
LC #3-3	8.9	7.4	5.5
LC #4	9.6	7.6	6.7
Interior Stringers [3]			
LC #1	9.4	7.1	6.4
LC #3-1	11.1	9.0	7.9
LC #3-2	13.3	10.6	8.3
LC #3-3	10.3	8.4	7.1
LC #4	11.1	8.7	7.1

1) BARS-1: Stresses are calculated using BARS assumptions based on previous AASHTO distribution factors.
2) BARS-2: Stresses are calculated using BARS assumptions based on current AASHTO distribution factors.
3) Only values for that interior stringer with the highest measured stress are shown.

Table 6.2.2.2 Maximum Stress in an Interior Stringer from BARS Output for LC #1

Loading Condition	Maximum Total Stress in an Interior Stringer (ksi)	
LC #1	BARS Output	Experimental
	11.2	NA

Table 6.2.3.1 Total Stresses in Bottom Flange of Instrumented Floor Beam

Loading Condition	Total Stress (ksi)	
	Predicted (BARS)	Experimental
LC #1-Center	14.7	11.4
LC #1- North	10.3	8.1
LC #3-3	15.1	12.4

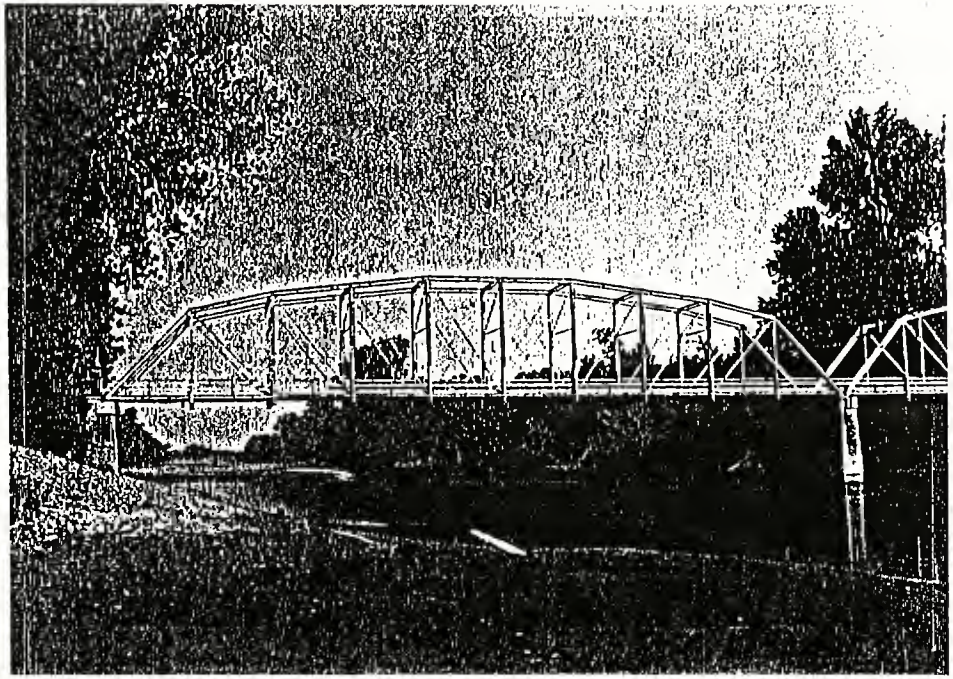

Figure 3.1.1.1 Span 3 of Bridge Structure No. 58-14-3244 facing North

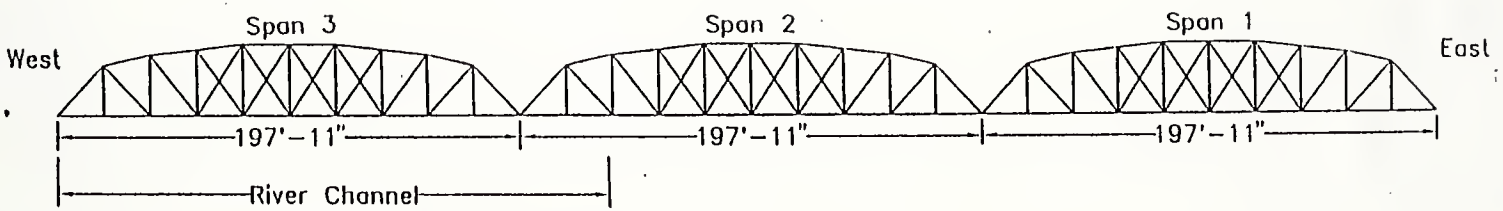

Figure 3.1.1.2 Bridge Structure No. 58-14-3244

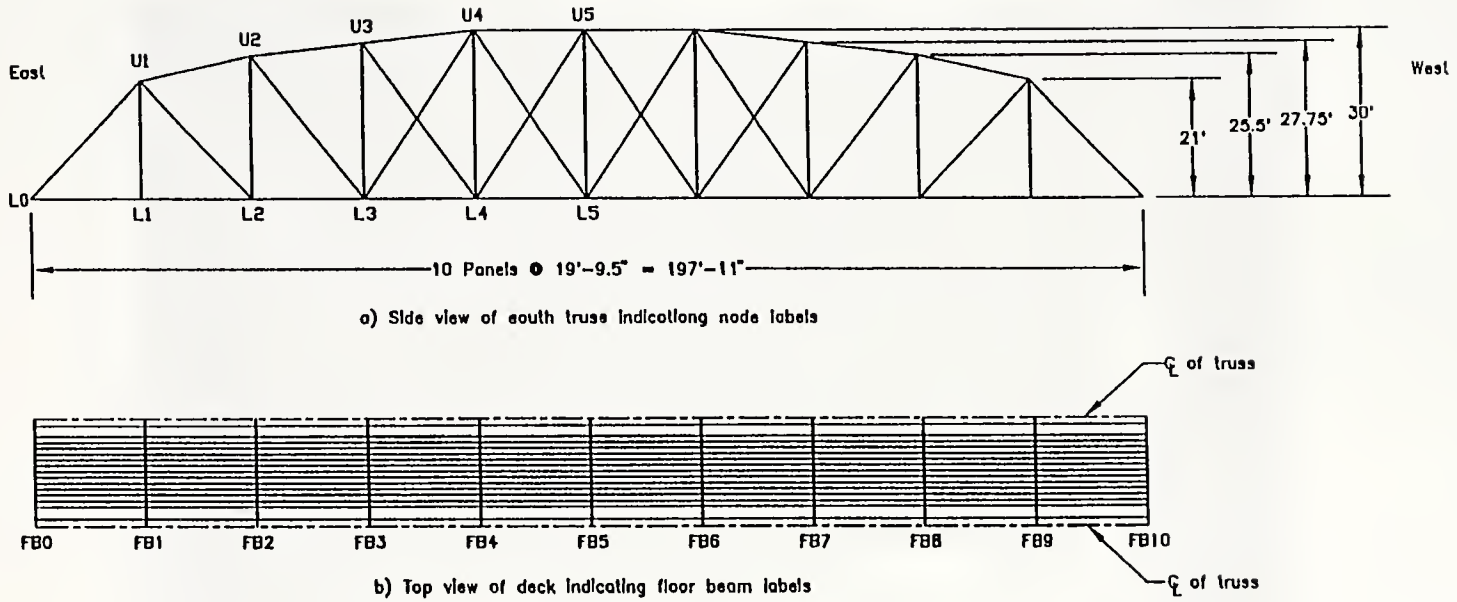

Figure 3.1.1.3 Span 2 of south truss

Figure 3.1.1.4 Roadway of Span 2 facing West

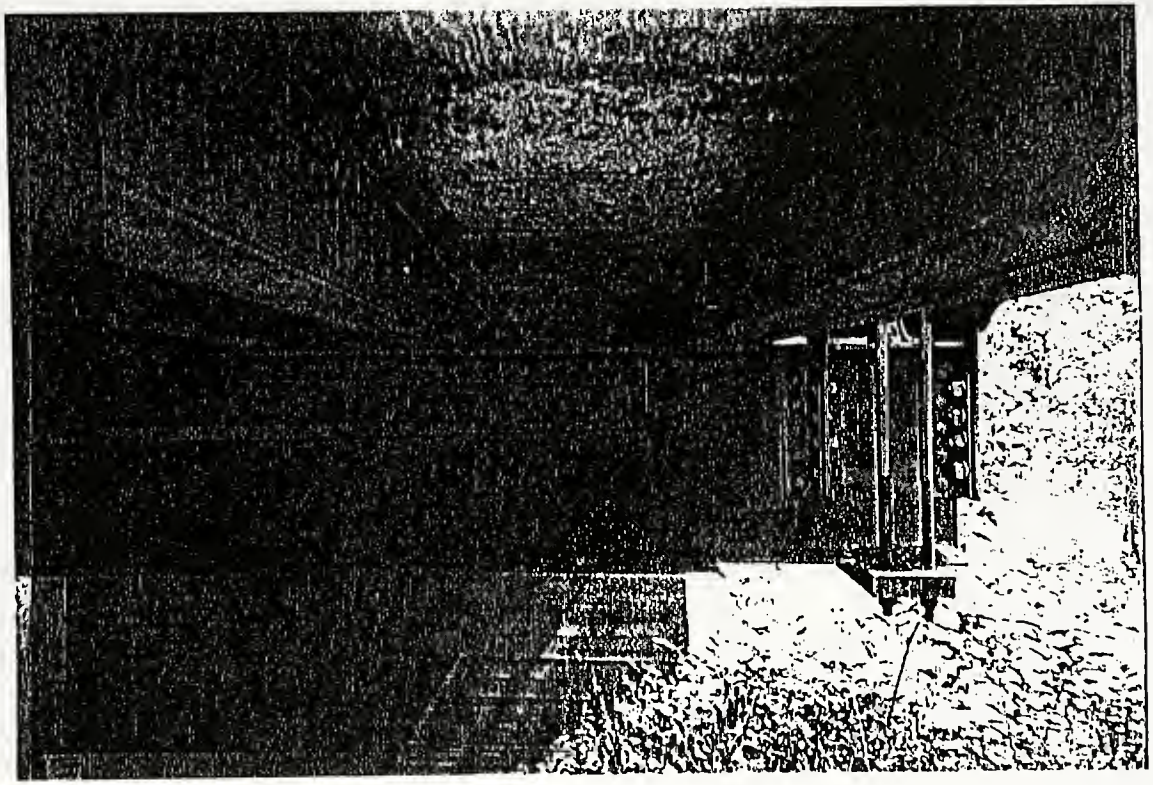

Figure 3.1.1.5 Connection of stringers, floor beam, and truss vertical

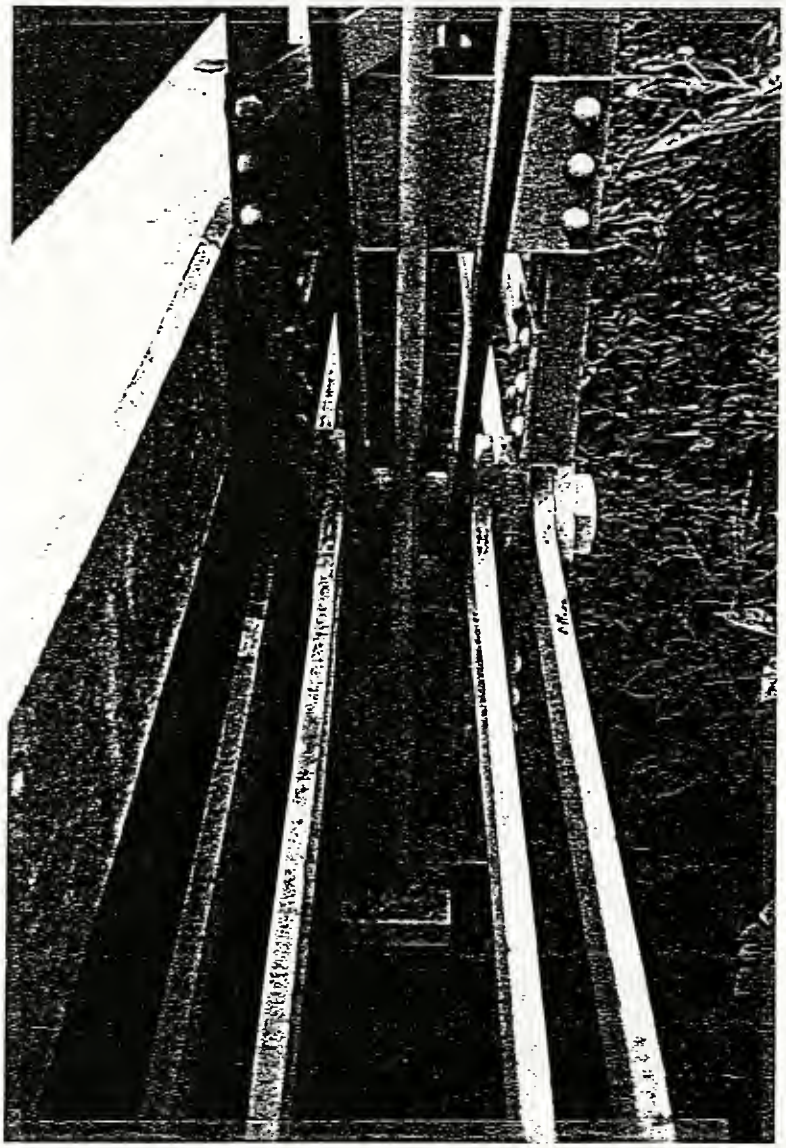

Figure 3.1.1.6 Lower truss joint (L1)

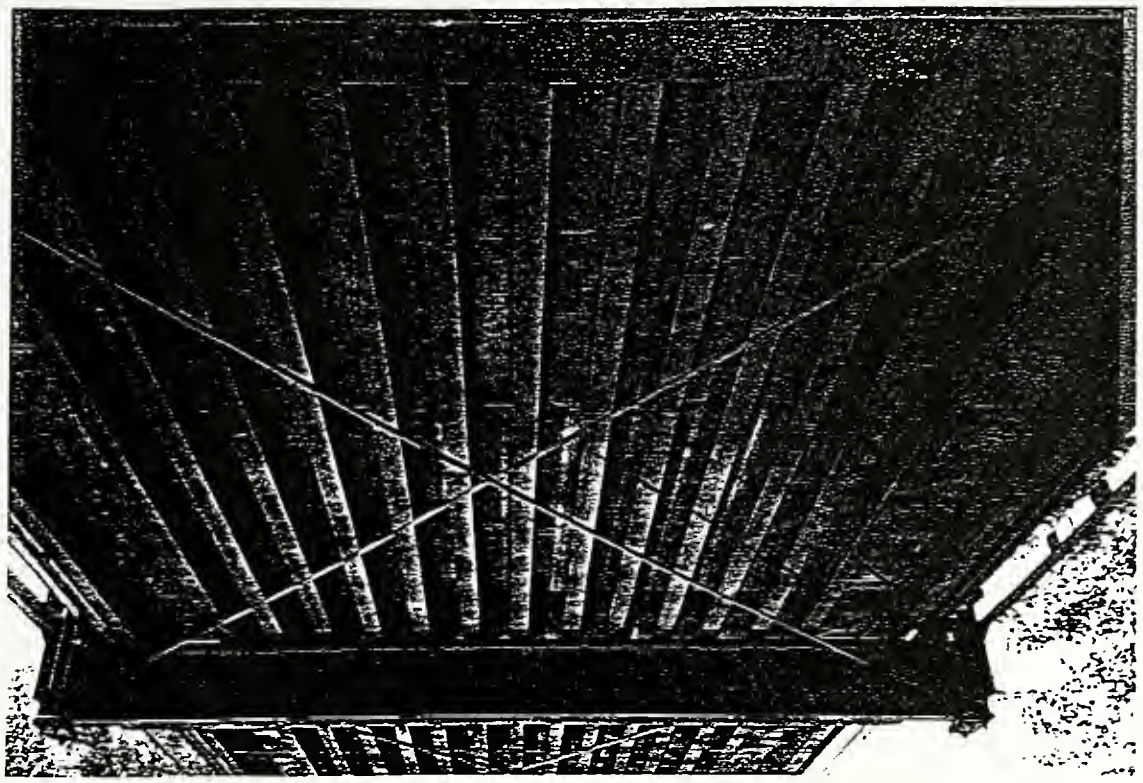

Figure 3.1.1.7 Underside of deck showing stringer and floor beam layout

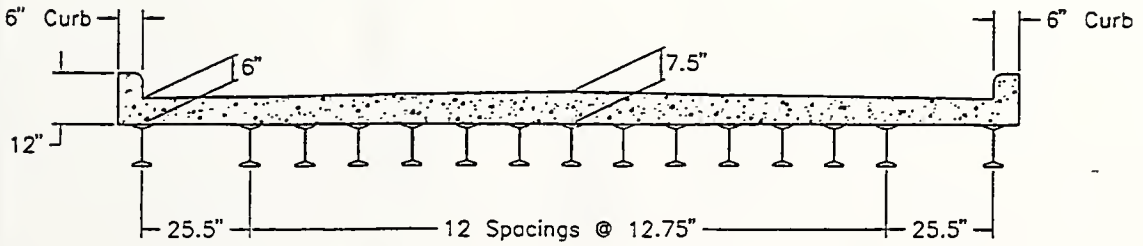

Figure 3.1.1.8 Deck cross-section

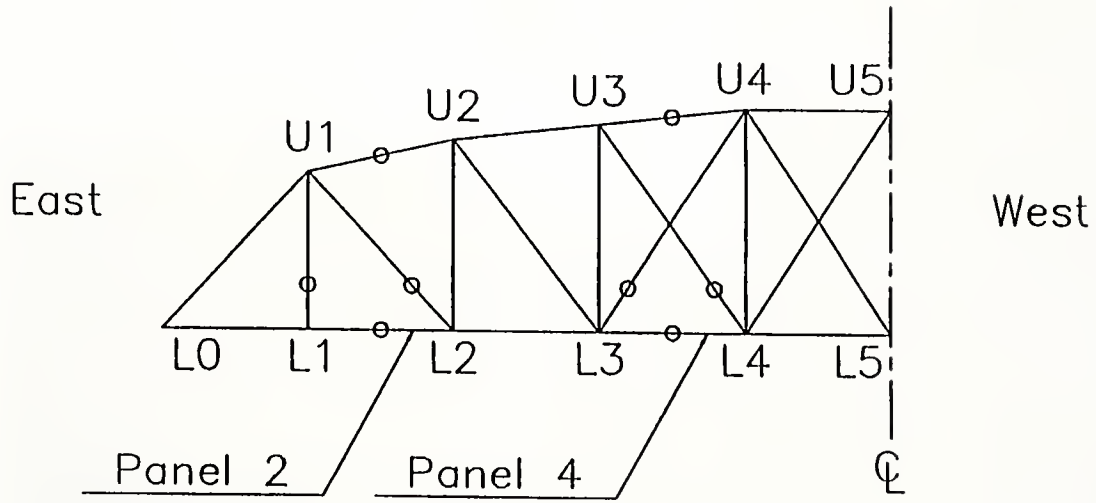

Note: The symbol ∘ denotes locations of strain gages.

Figure 3.1.2.1 Truss strain gage locations

2 bars @ 4" x 1 1/4"

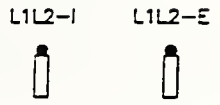

a) L1L2

2 angles @ 3 1/2" x 2 1/2" x 5/16"

b) U1L1

2 bars @ 4" x 7/8"

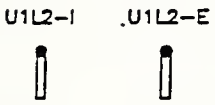

c) U1L2

2 channels @ 12" x 20.7" #/ft
1 plate @ 20" x 1/2"

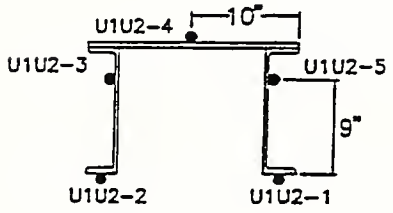

d) U1U2

Note: The symbol • denotes location of a single strain gage.

Figure 3.1.2.2 Panel 2 truss strain gage locations

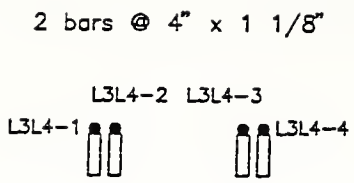

a) L3L4

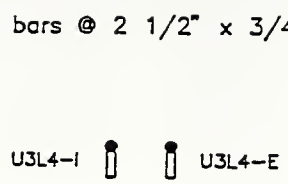

b) U3L4

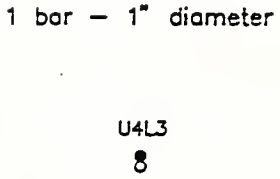

c) U4L3

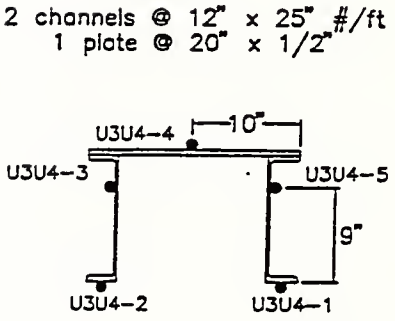

d) U3U3

Note: The symbol • denotes location of a single strain gage.

Figure 3.1.2.3 Panel 4 truss strain gage locations

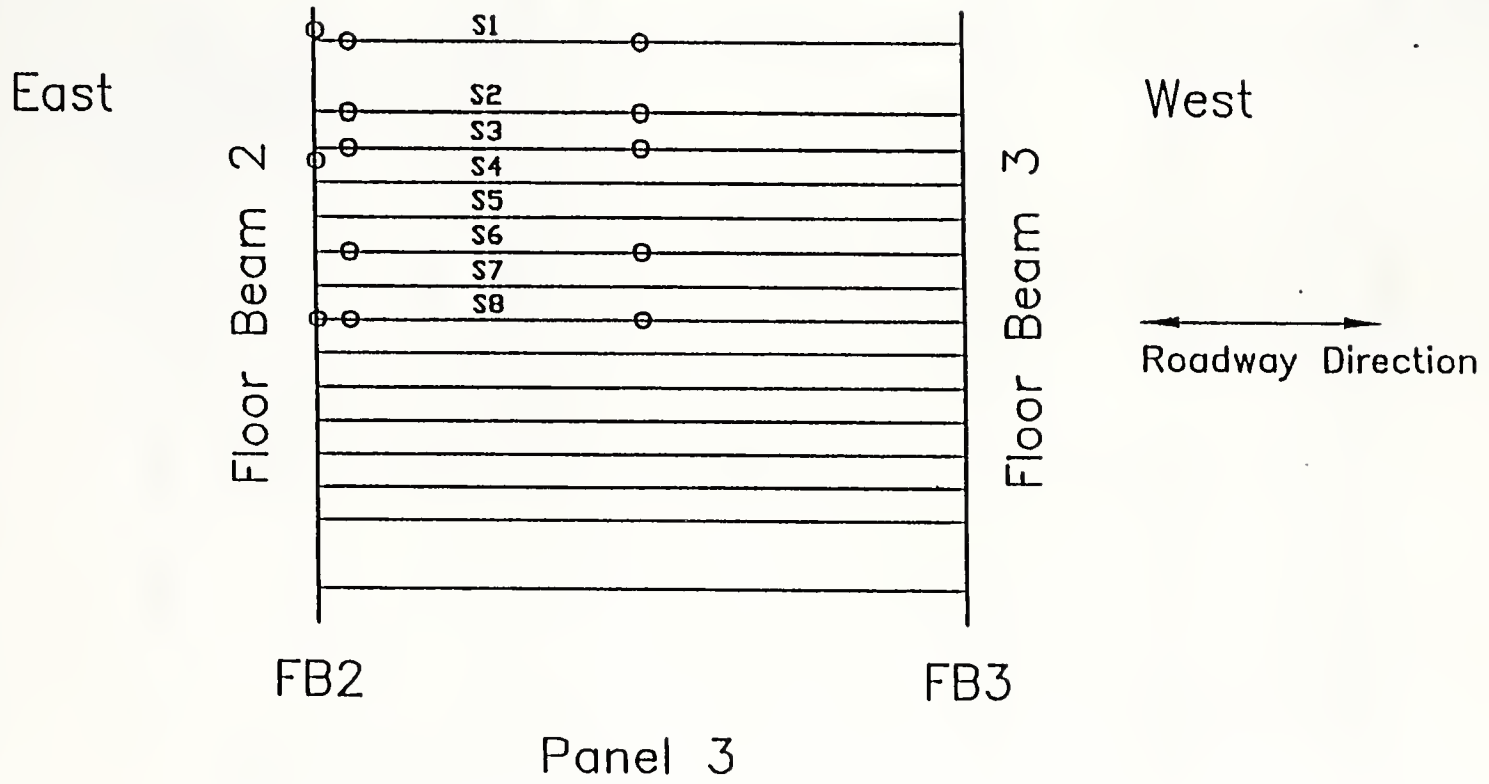

Figure 3.1.2.4 Deck strain gage locations (Plan view)

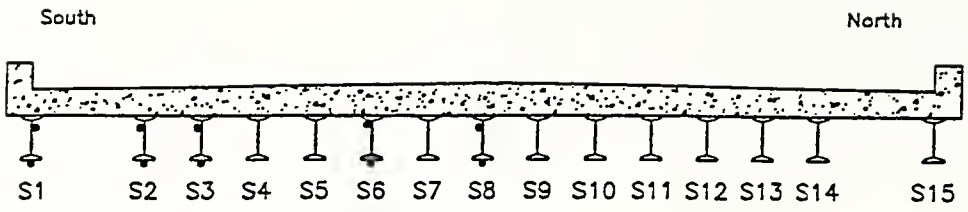

a) Deck Cross–Section at Stringer Midspan – Panel 3

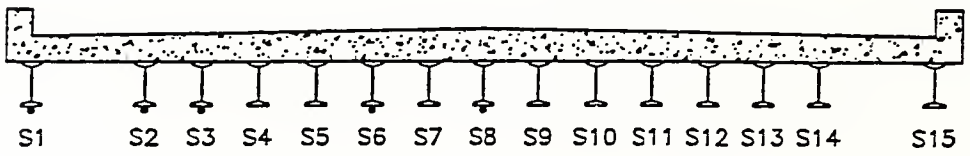

b) Deck Cross–Section at 1 ft. West of Floor Beam 2

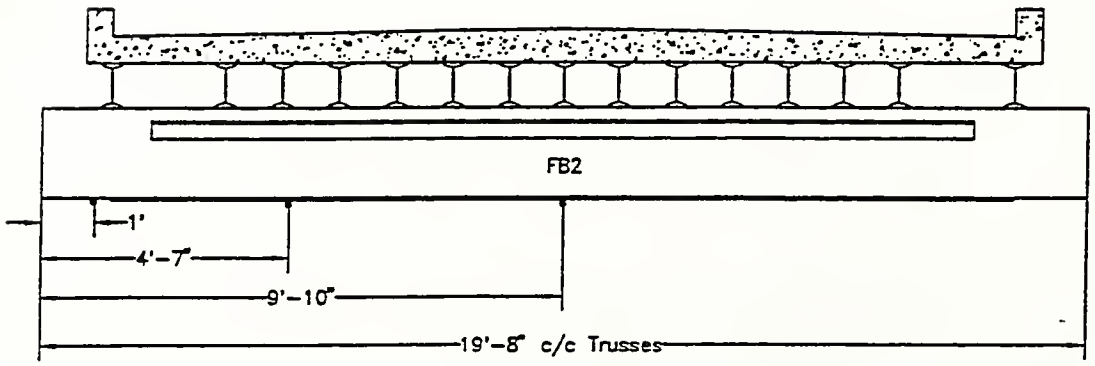

c) Deck Cross–Section at Panel Point

Figure 3.1.2.5 Deck strain gage locations (Sections)

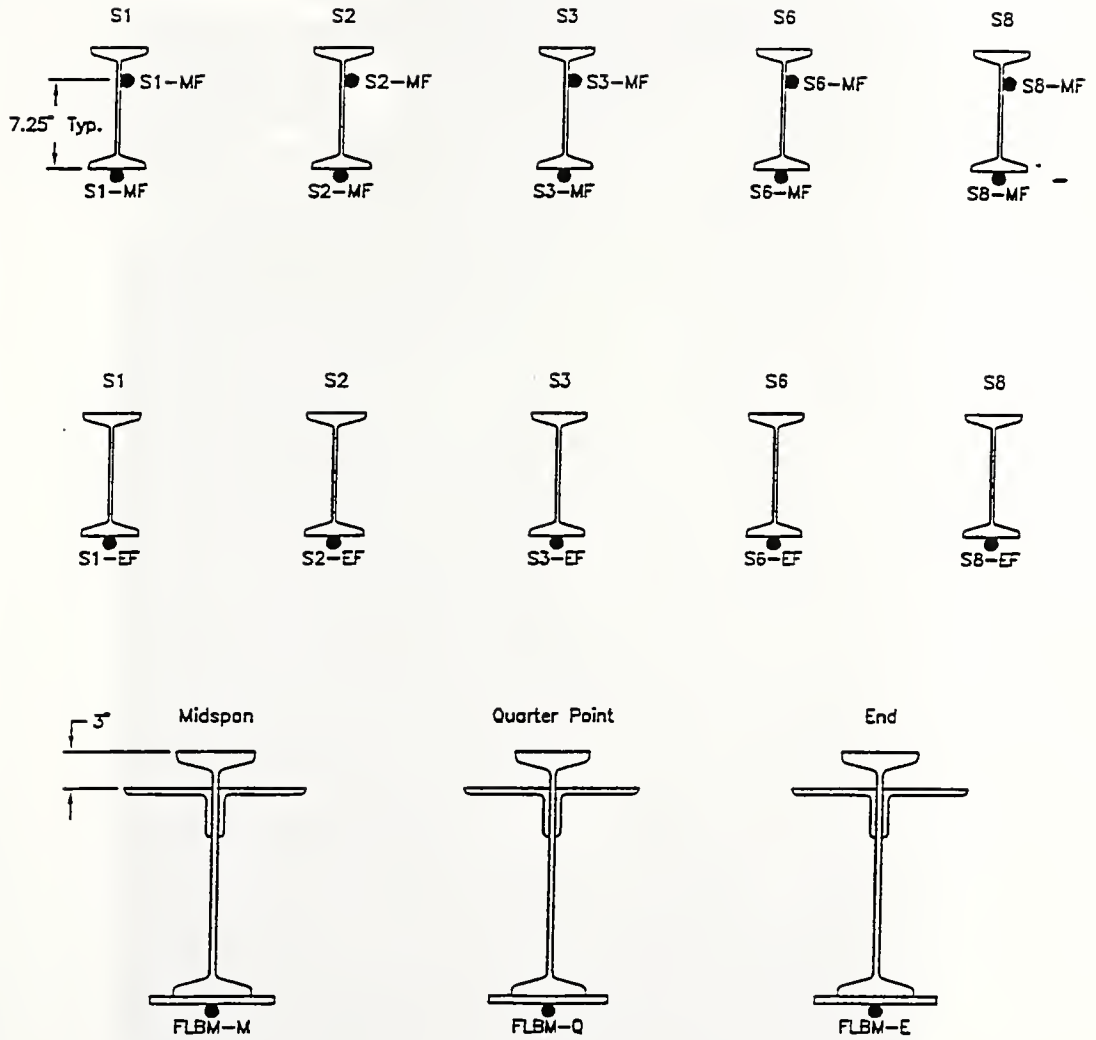

Figure 3.1.2.6 Panel 3 deck strain gage locations and identification
(S = stringer, FLBM = floor beam)

Figure 3.1.2.7 Typical strain gage installation on stringers and flqor beam

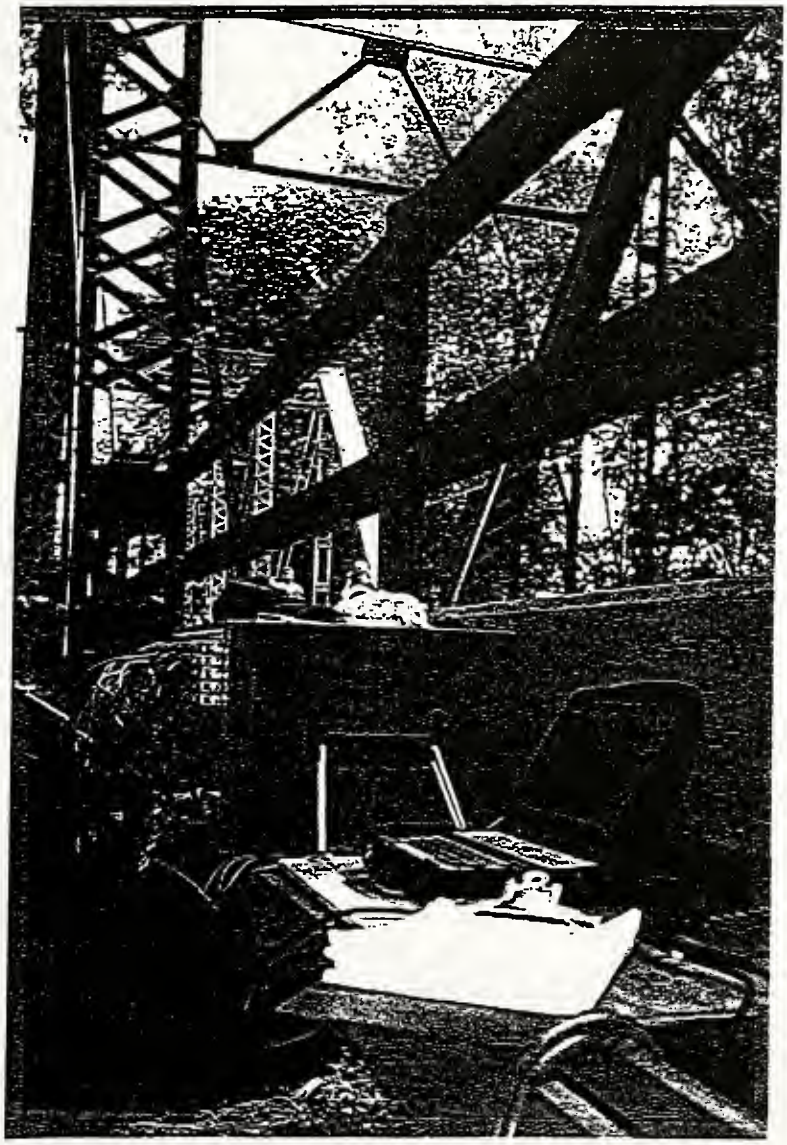

Figure 3.1.4.1 Recording station location

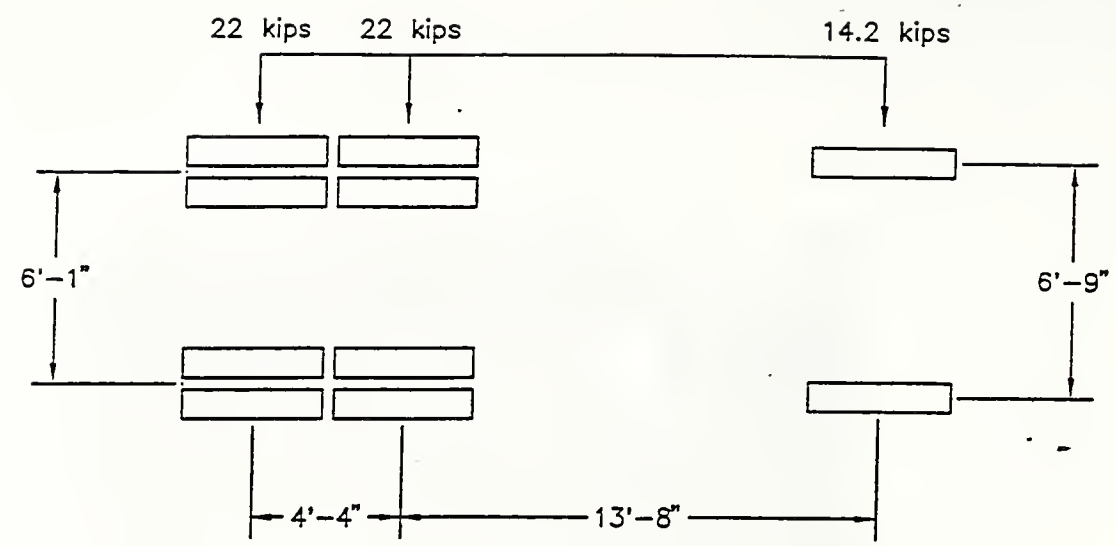

Test Vehicle #66184

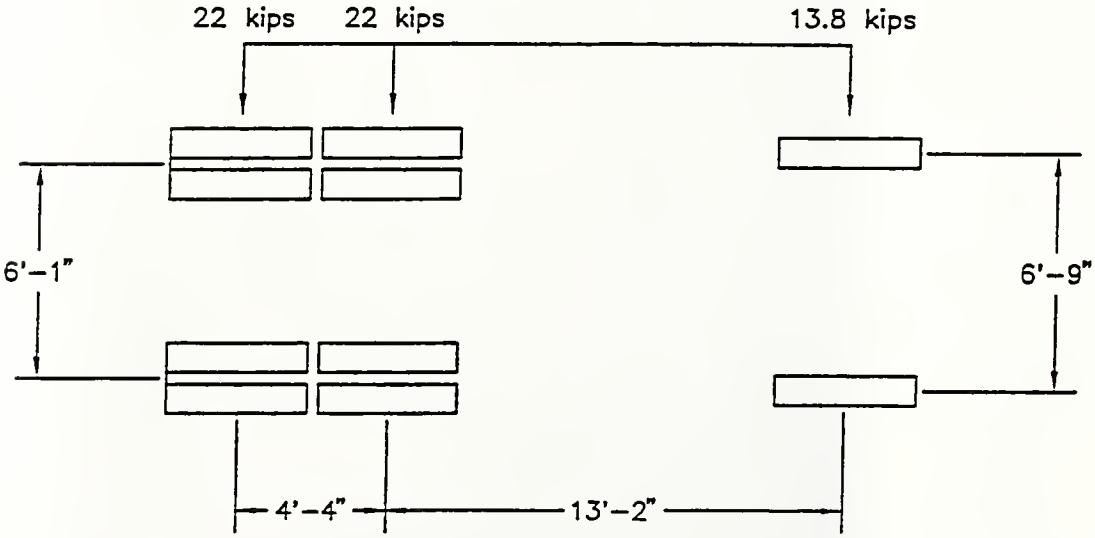

Test Vehicle #10326

Figure 3.1.5.1 Axle weights and spacing of test vehicles

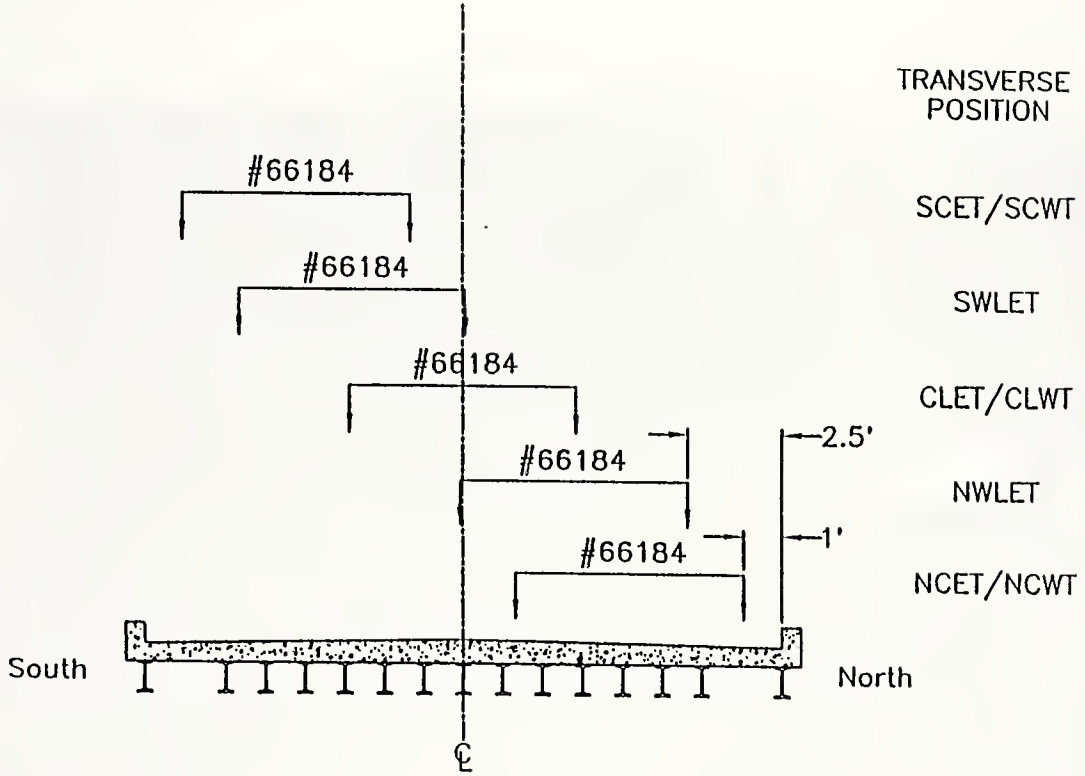

Figure 3.1.5.1.1 Loading Condition #1 - Transverse vehicle positions

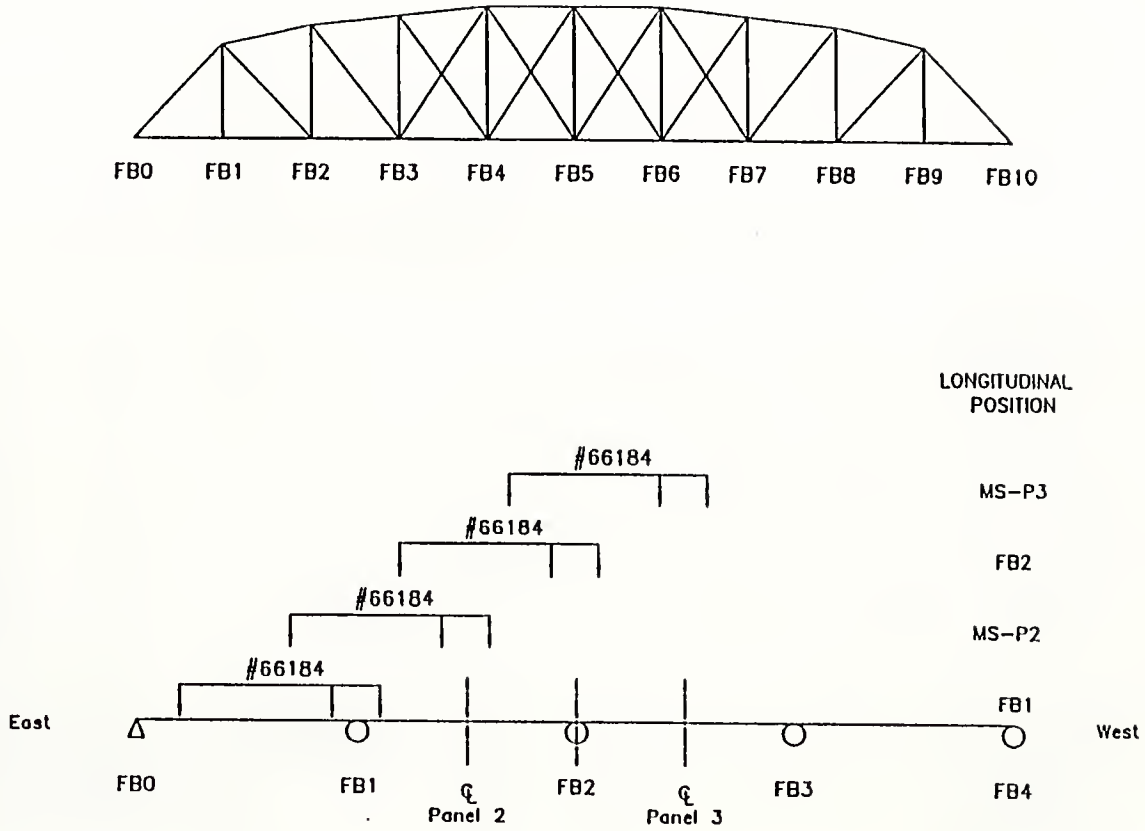

Figure 3.1.5.1.2 Loading Condition #1 - Longitudinal vehicle positions

Figure 3.1.5.1.3 Loading Condition #1 - Position of test vehicle: SCET MS-P3

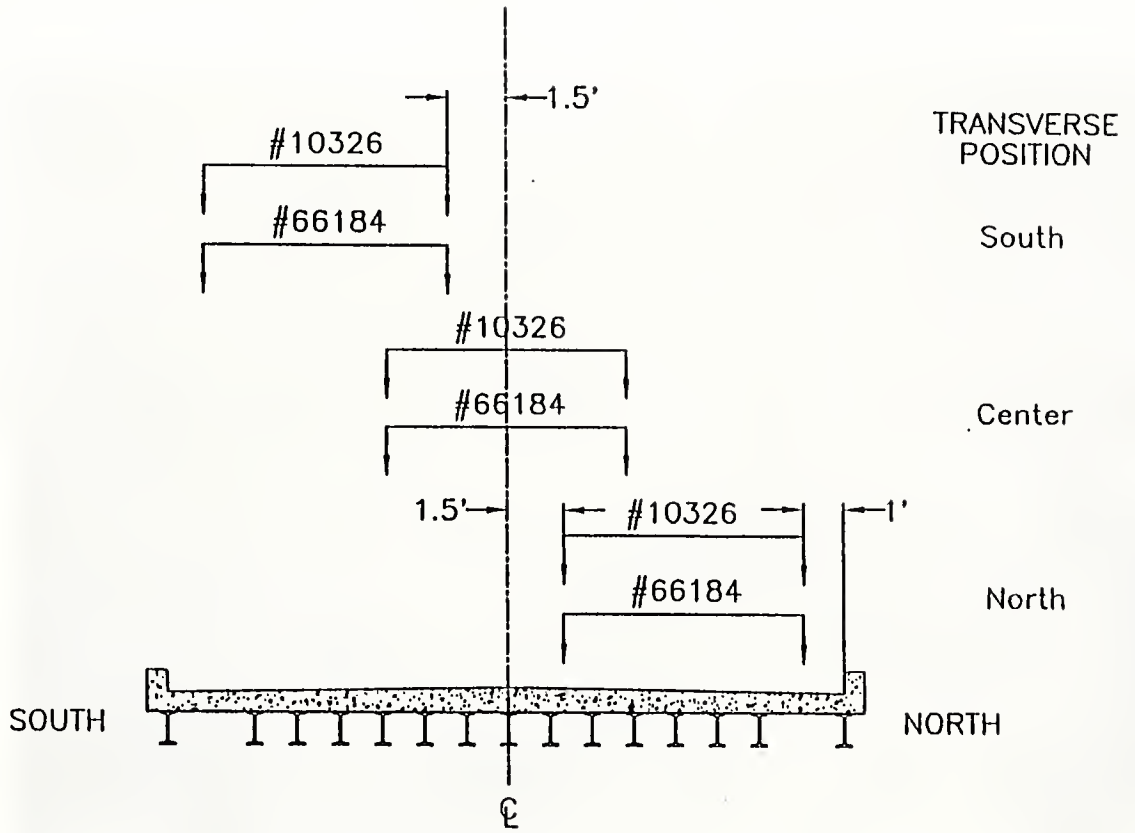

Figure 3.1.5.2.1 Loading Condition #2 - Transverse vehicle positions

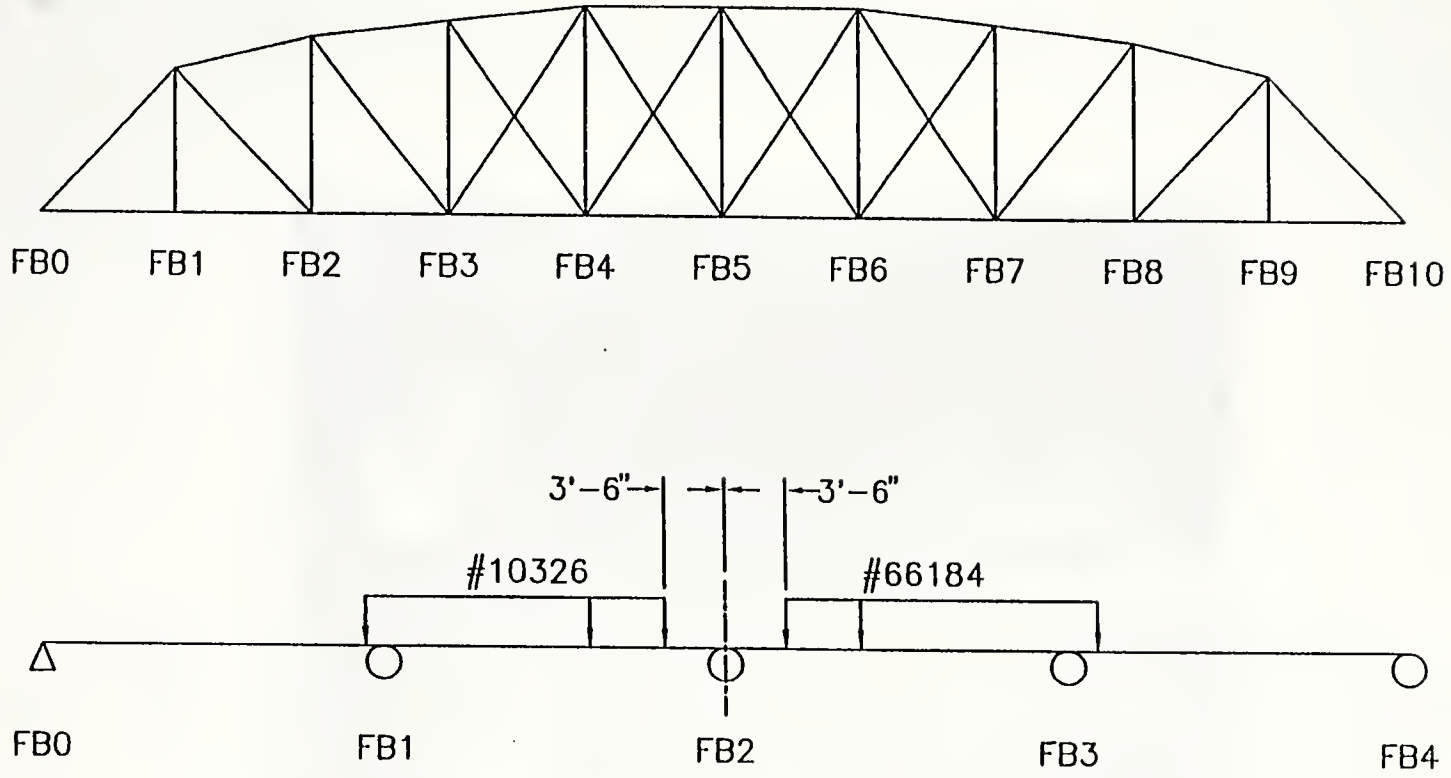

Typical vehicle loading. Similar loading at each floor beam (FB1 – FB9).

Figure 3.1.5.2.2 Loading Condition #2 - Longitudinal vehicle positions

Figure 3.1.5.2.3 Loading Condition #2 - Position of test vehicles: SOUTH FB2

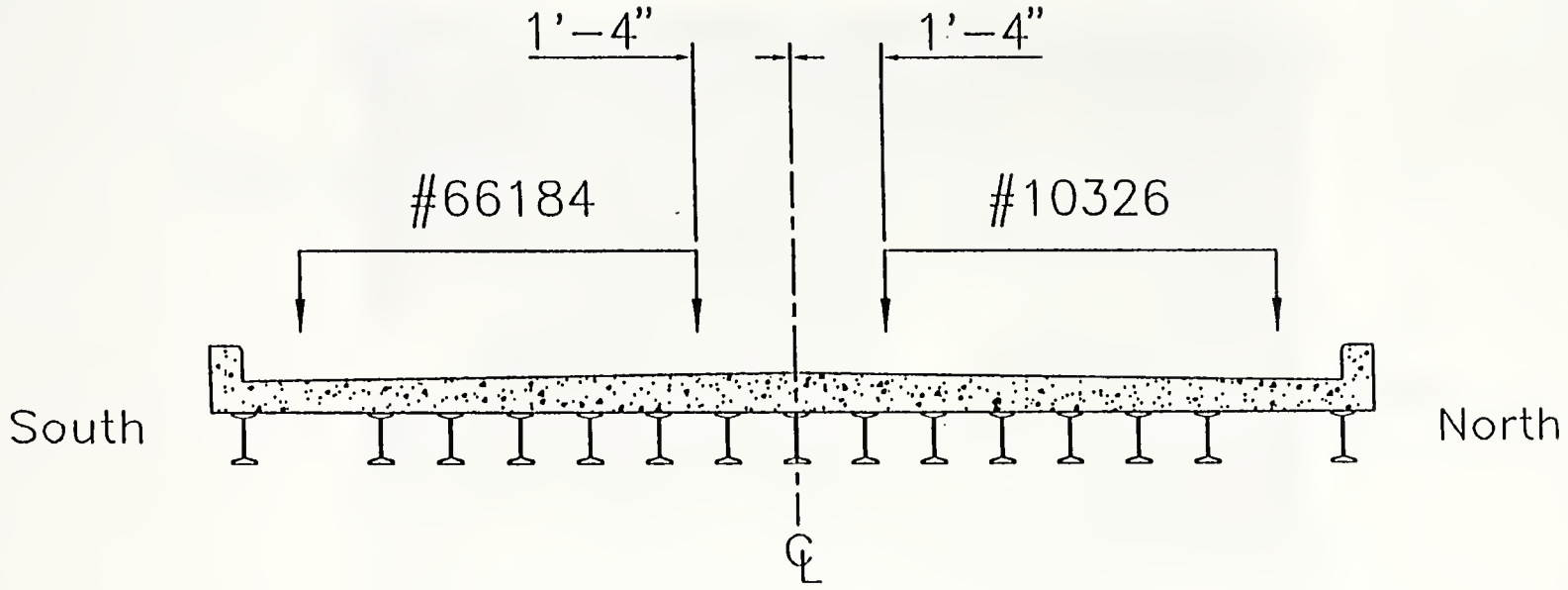

Figure 3.1.5.3.1 Loading Condition #3 - Transverse vehicle positions

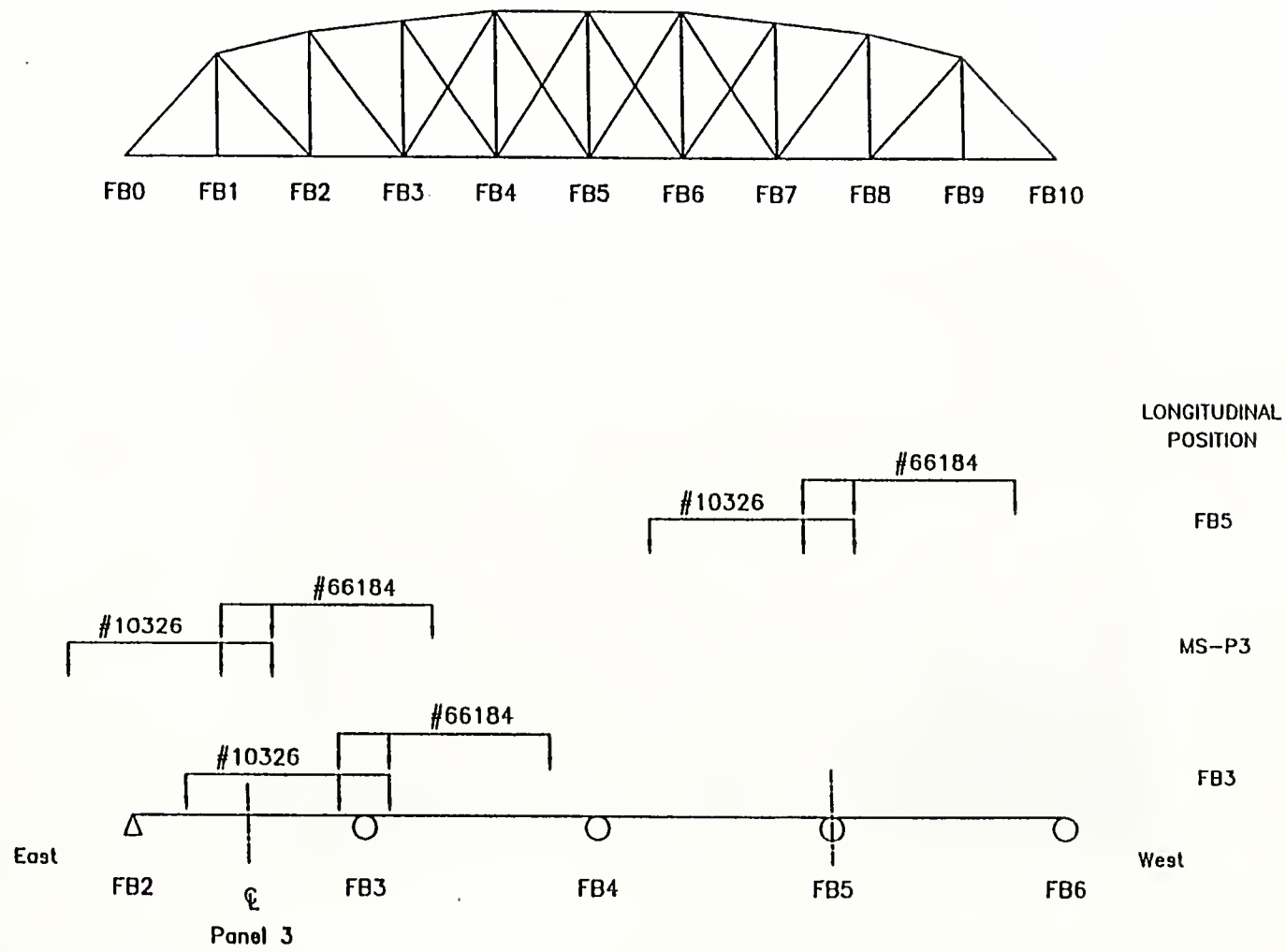

Figure 3.1.5.3.2 Loading Condition #3 - Longitudinal vehicle positions

Figure 3.1.5.3.3 Loading Condition #3 - Position of text vehicles: MS-P3

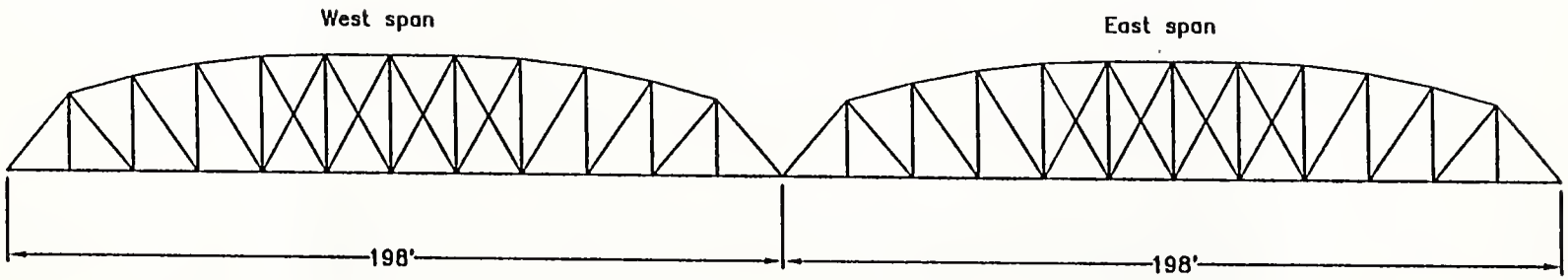

Figure 3.2.1.1 SR 45 Truss bridge

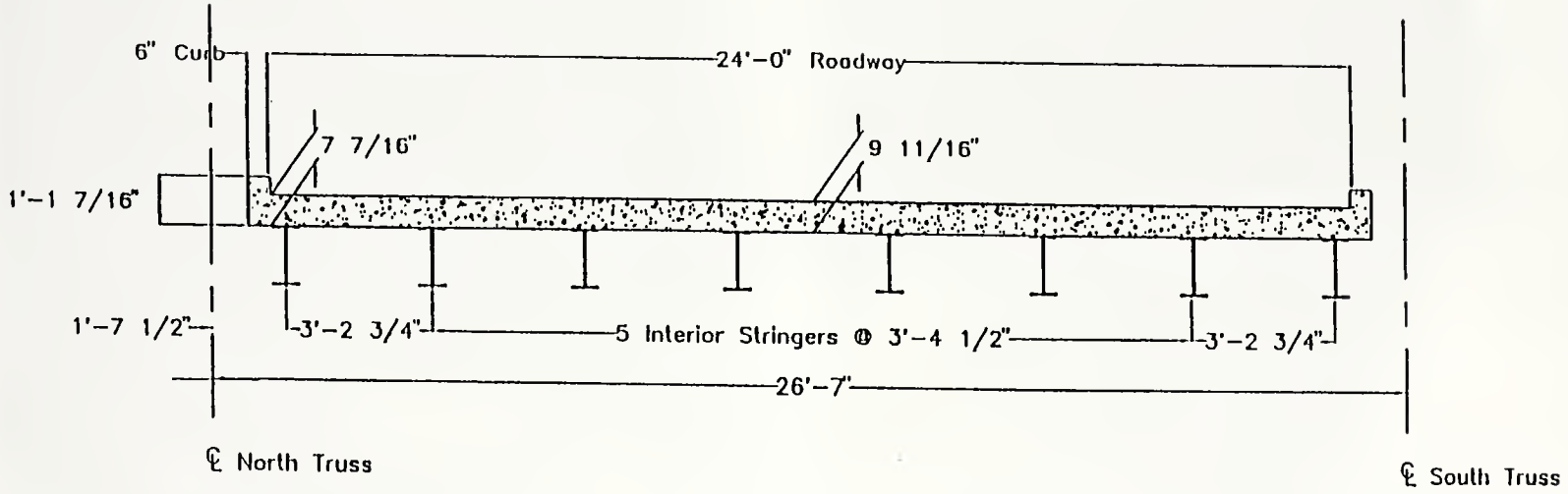

Figure 3.2.1.2 Deck cross section

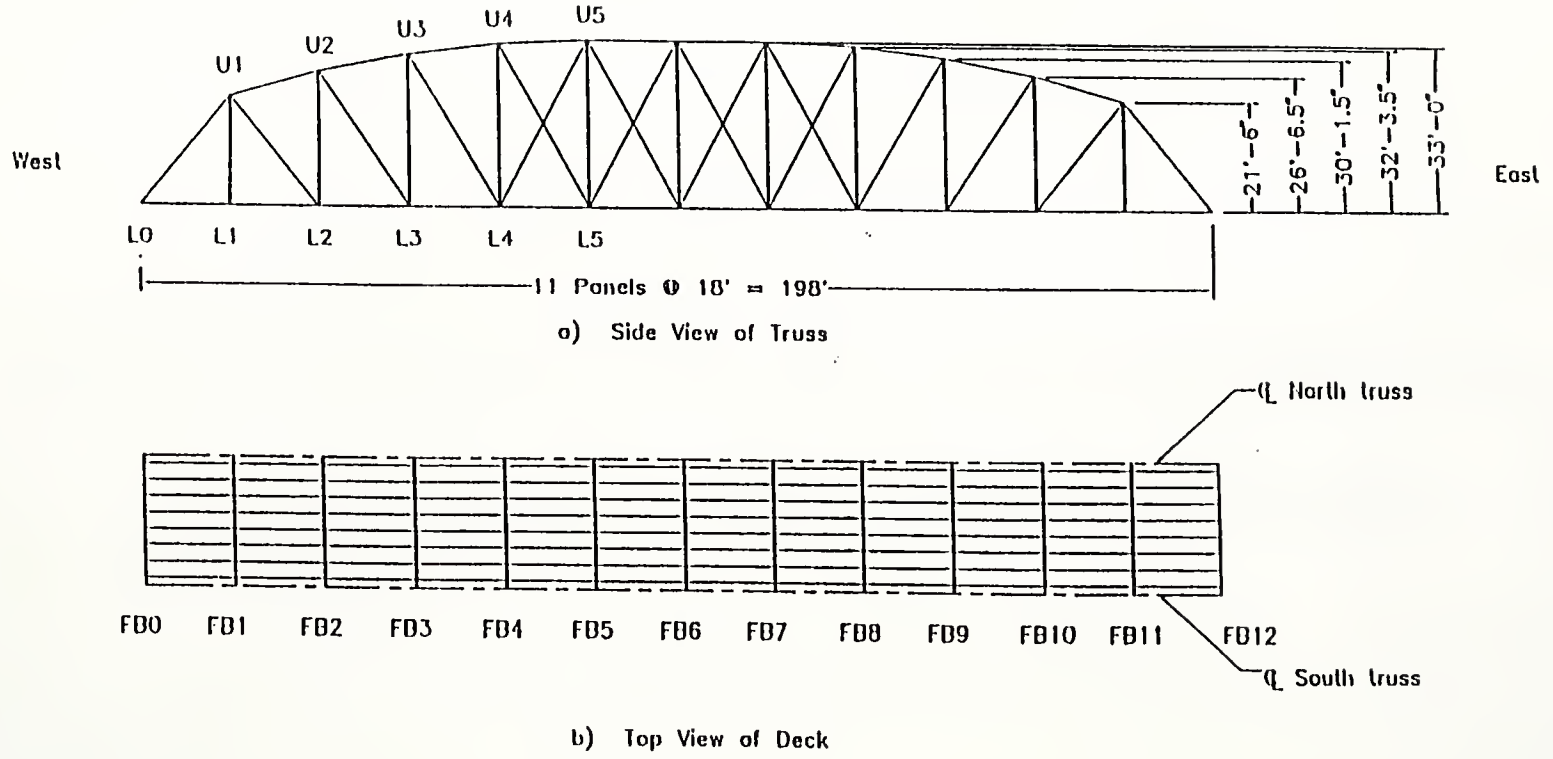

Figure 3.2.1.3 Schematic of west truss

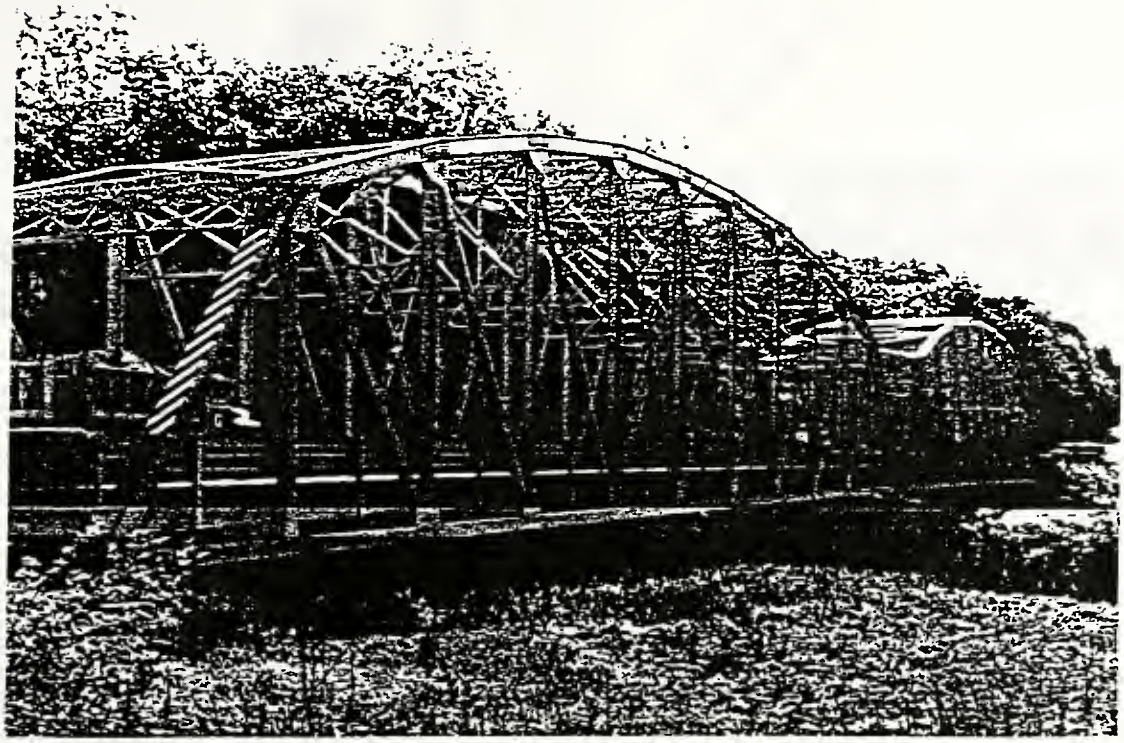

Figure 3.2.1.4 Side view of truss

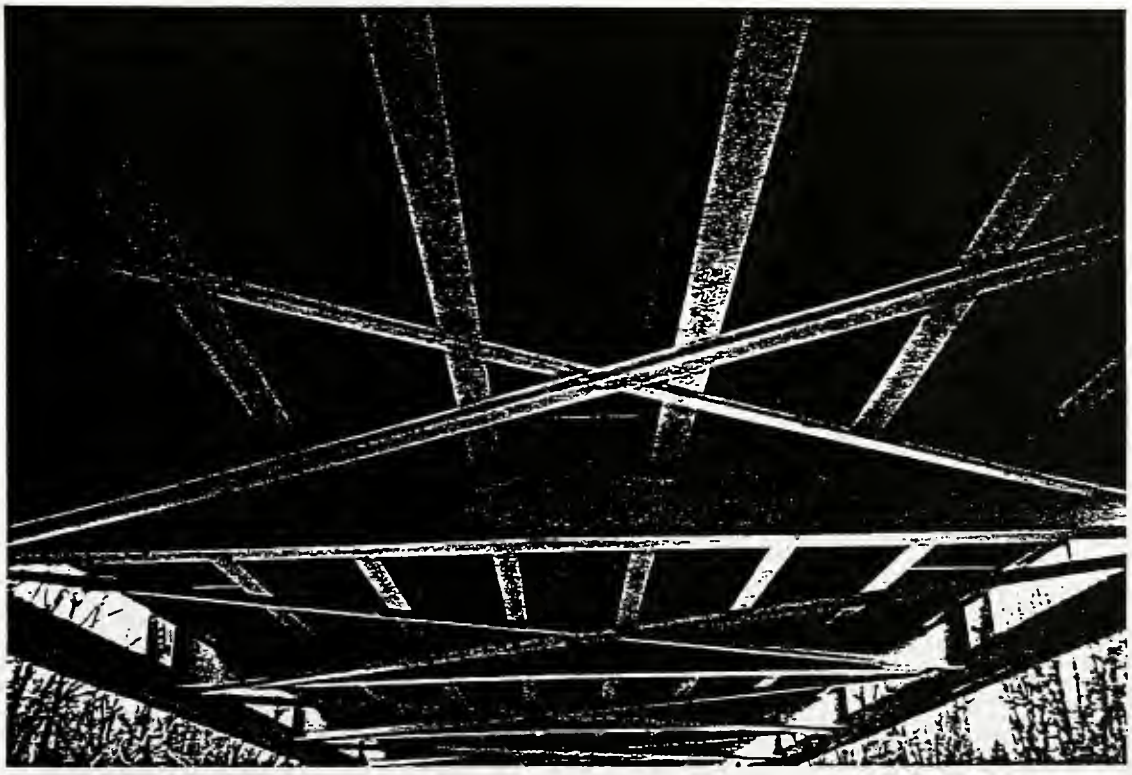

Figure 3.2.1.5 Typical floor panel

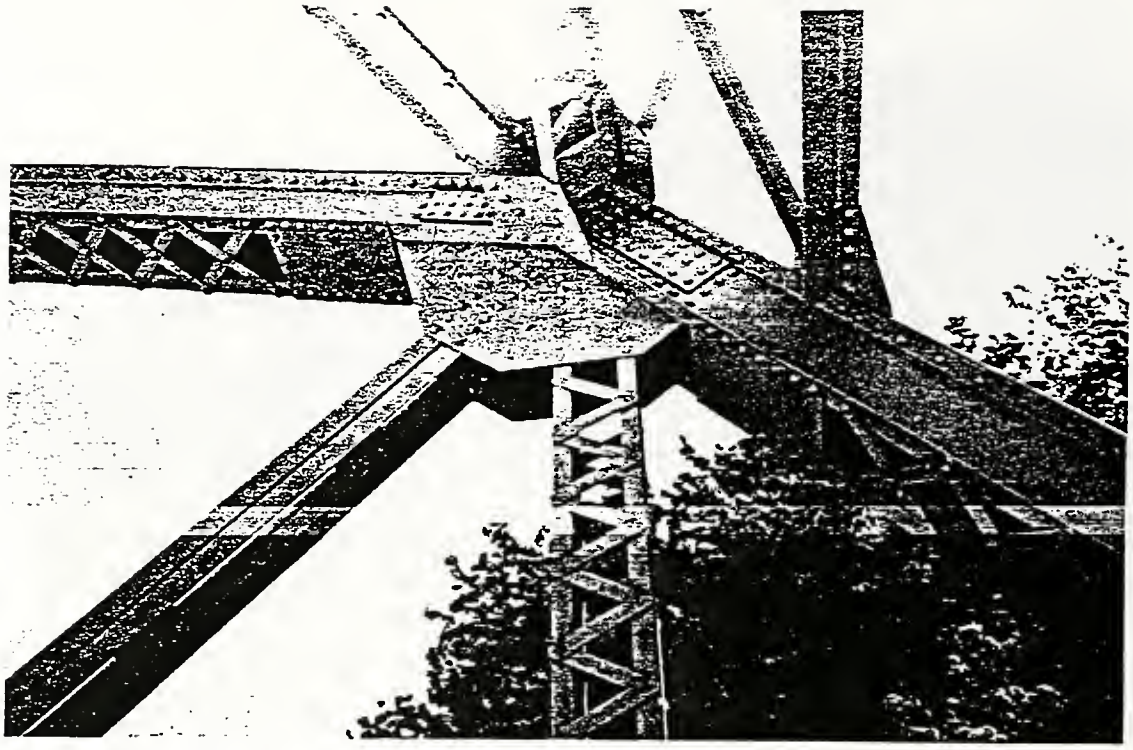

Figure 3.2.1.6 Top chord, vertical, diagonal joint detail

Figure 3.2.1.7 Bottom chord, vertical, diagonal joint detail

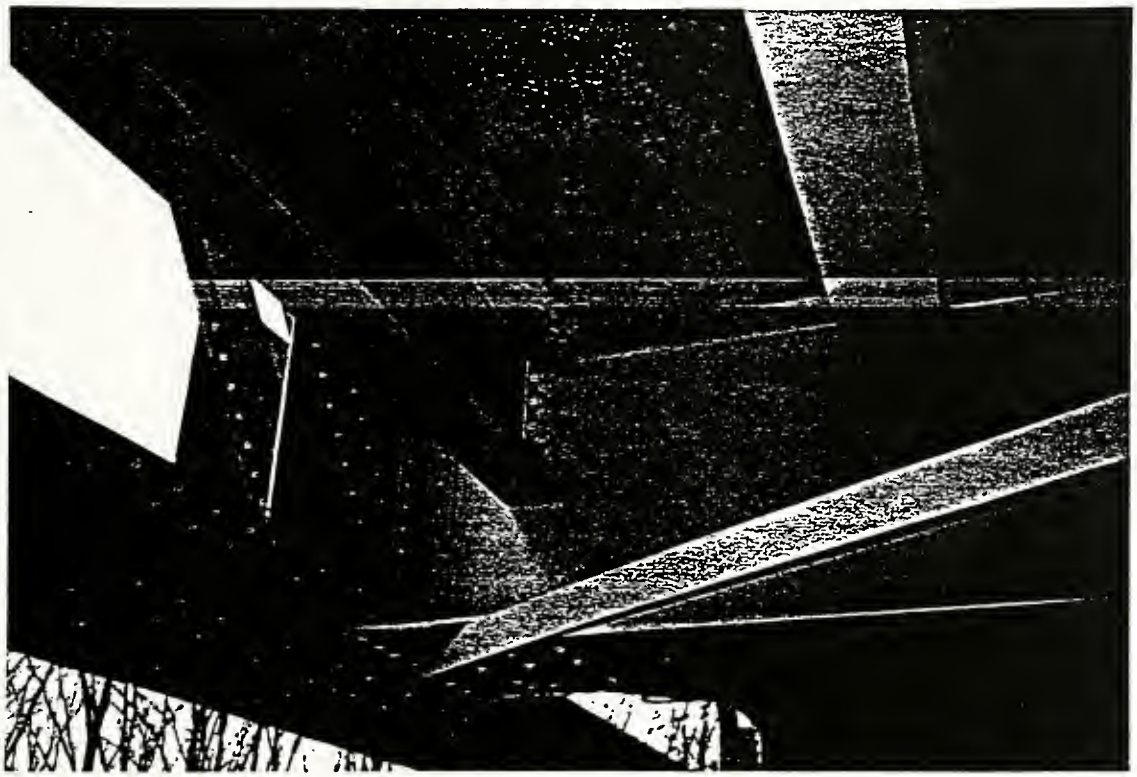

Figure 3.2.1.8 Typical floor beam to truss and floor beam to stringer connections

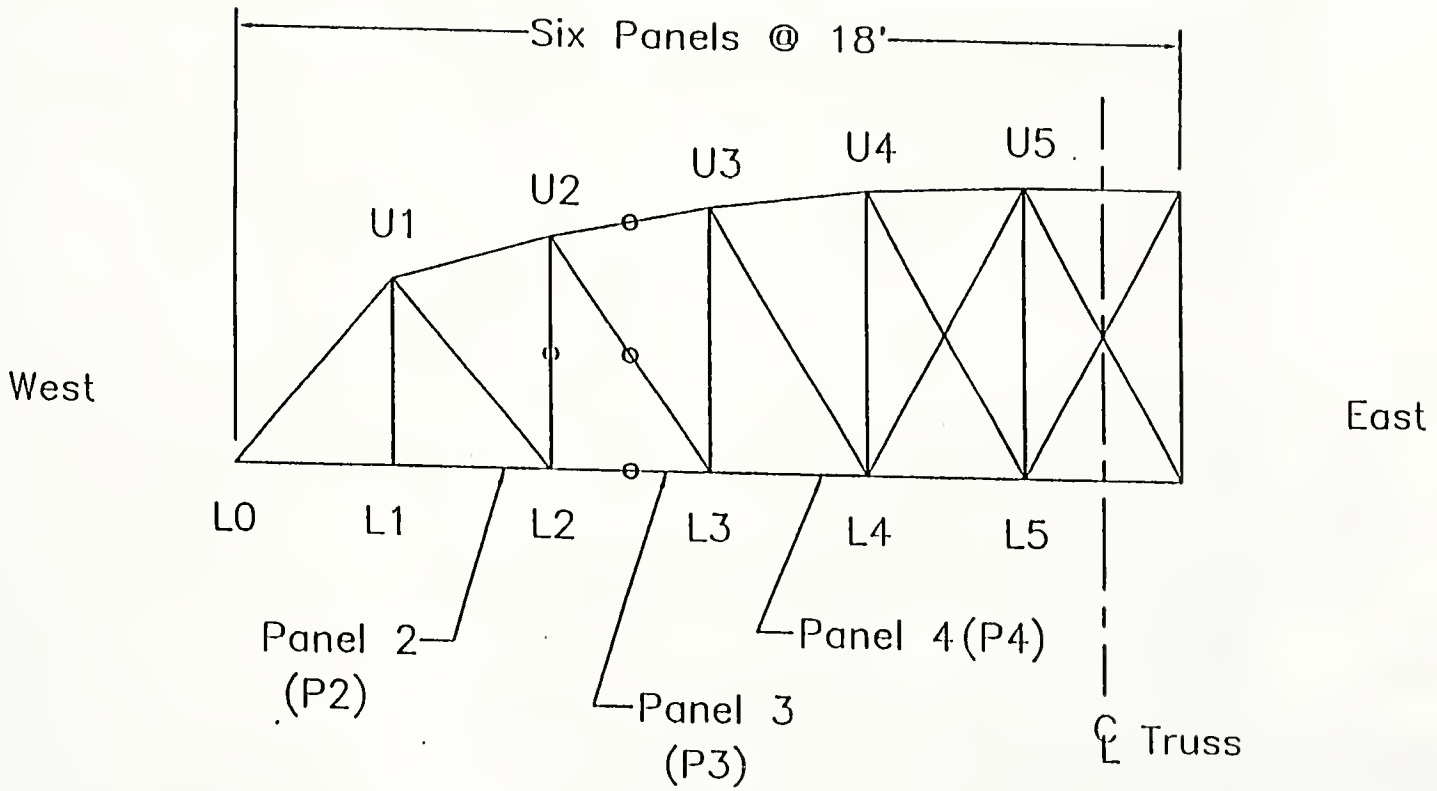

Figure 3.2.2.1 Truss strain gage locations

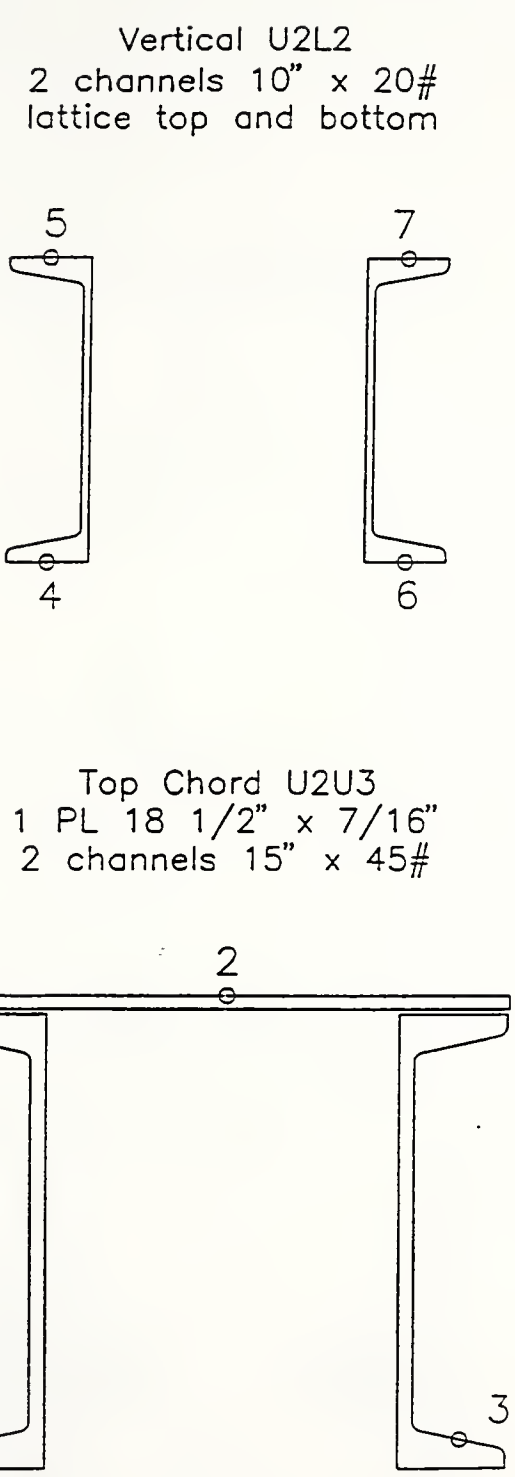

Figure 3.2.2.2a Truss member strain gage placements for U2L2 and U2U3

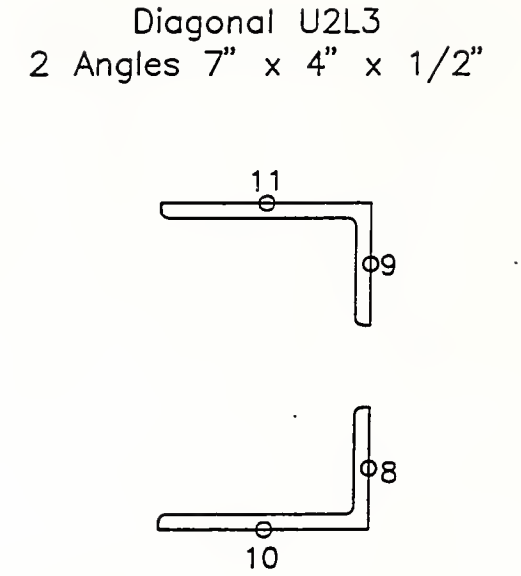

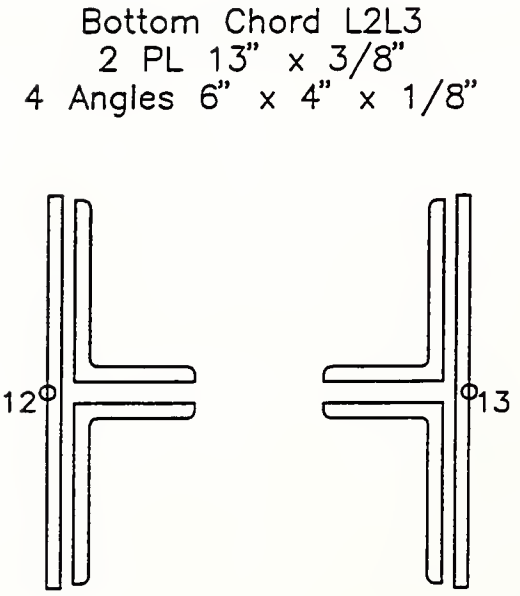

Figure 3.2.2.2b Truss member strain gage placements for U2L3 and L2L3

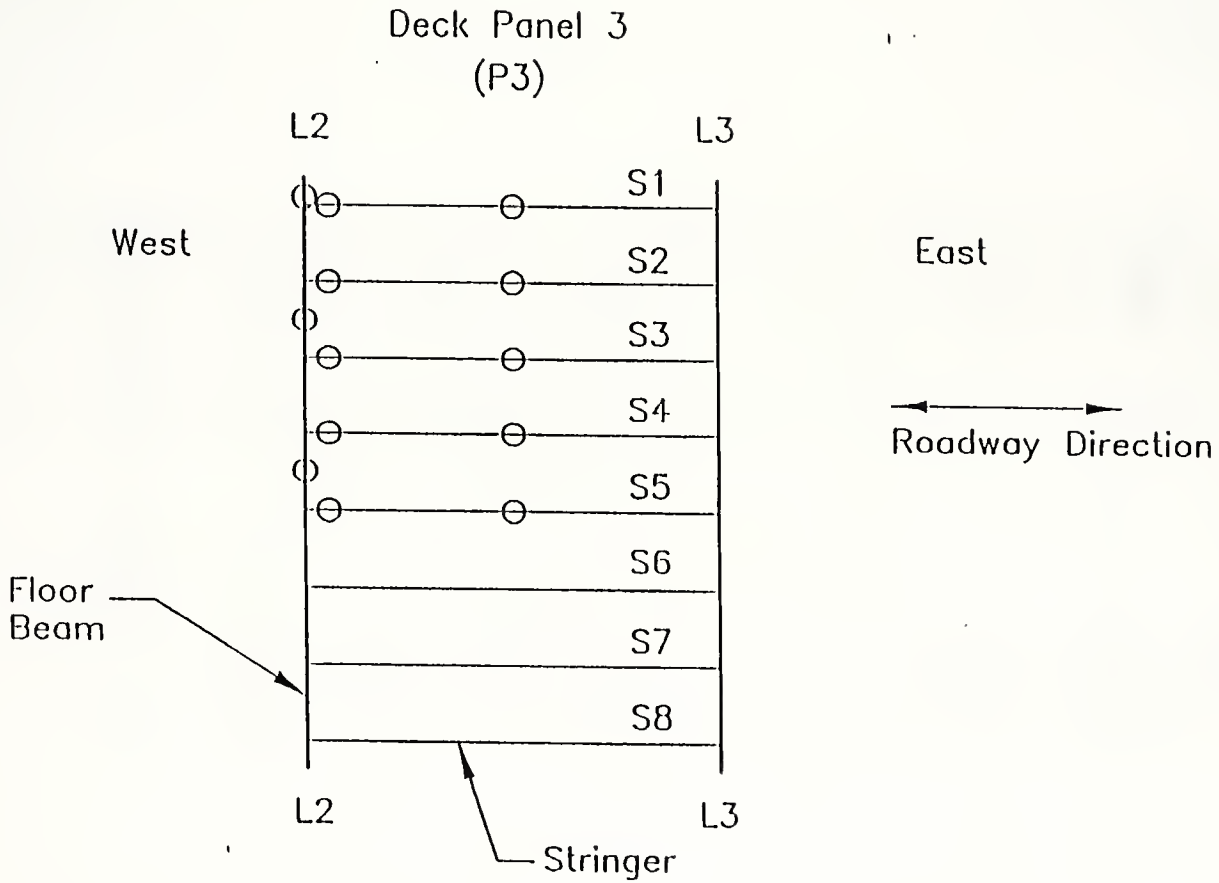

Figure 3.2.2.3 Deck strain gage locations

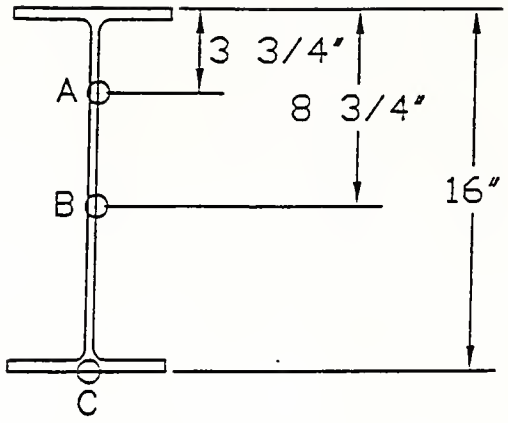

a) End of Stringer

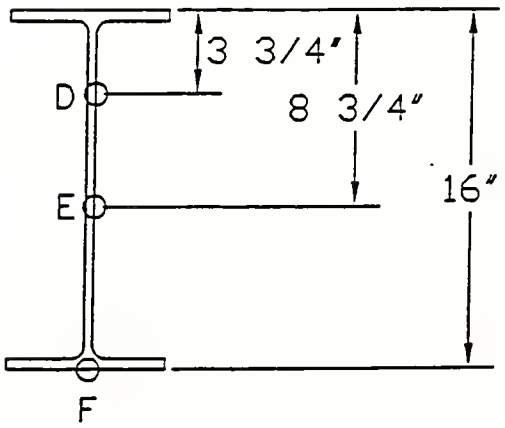

b) Midspan of Stringer

Figure 3.2.2.4 Stringer strain gage locations

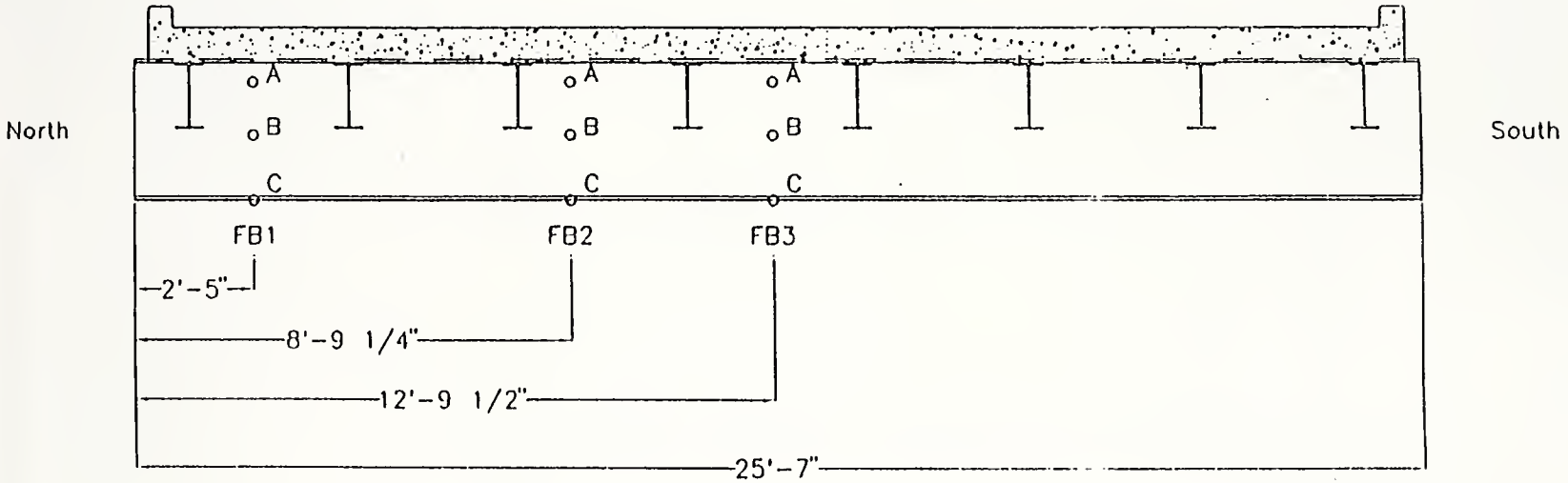

Figure 3.2.2.5 Floor beam longitudinal strain gage locations

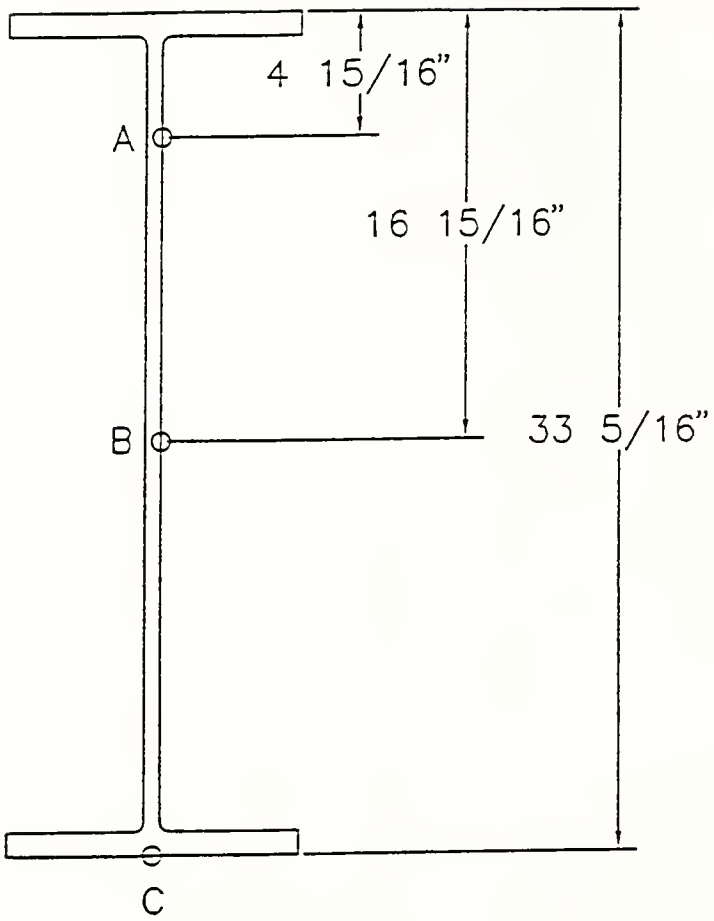

Figure 3.2.2.6 Floor beam vertical strain gage locations

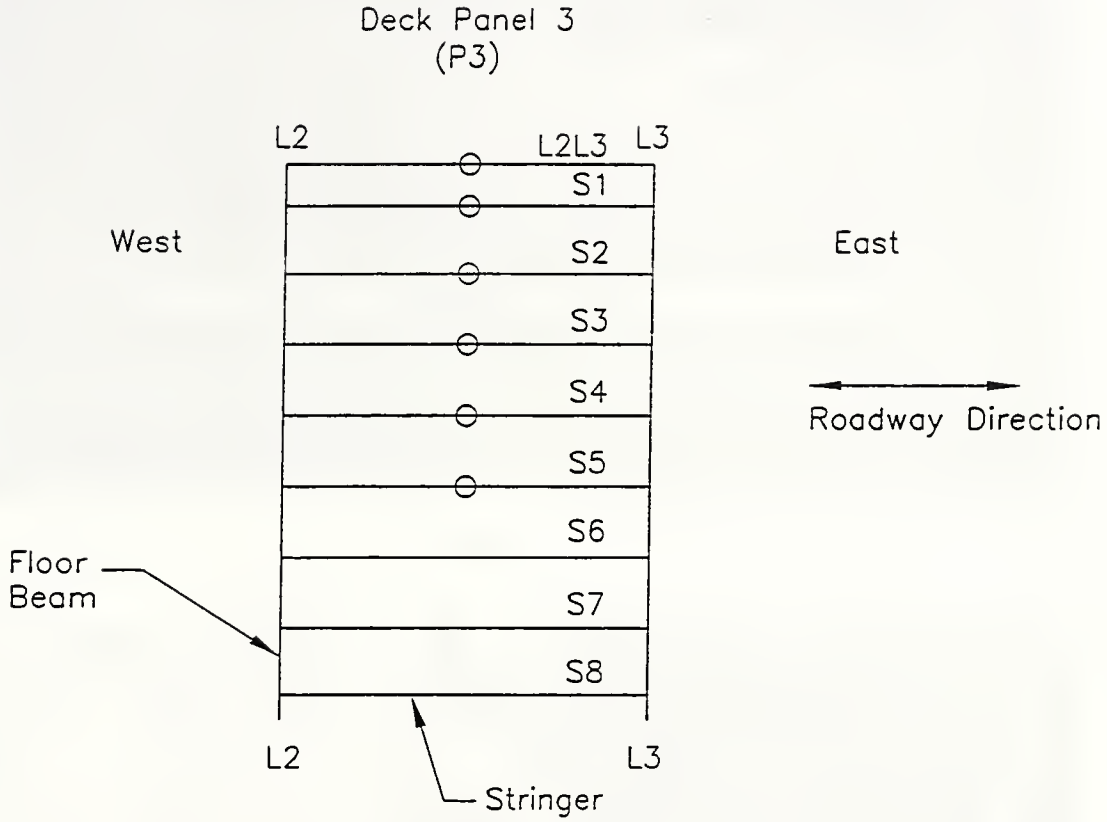

Figure 3.2.2.7 Deck LVDT locations

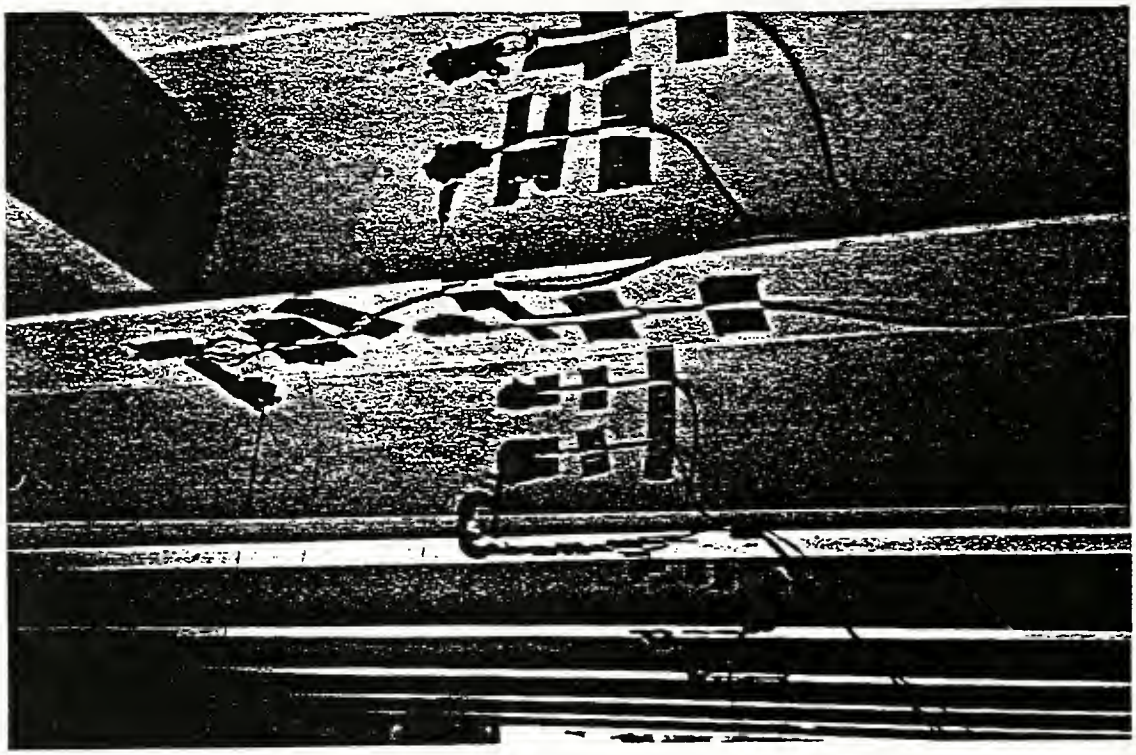

Figure 3.2.3.1 Hanger connection for LVDT cable

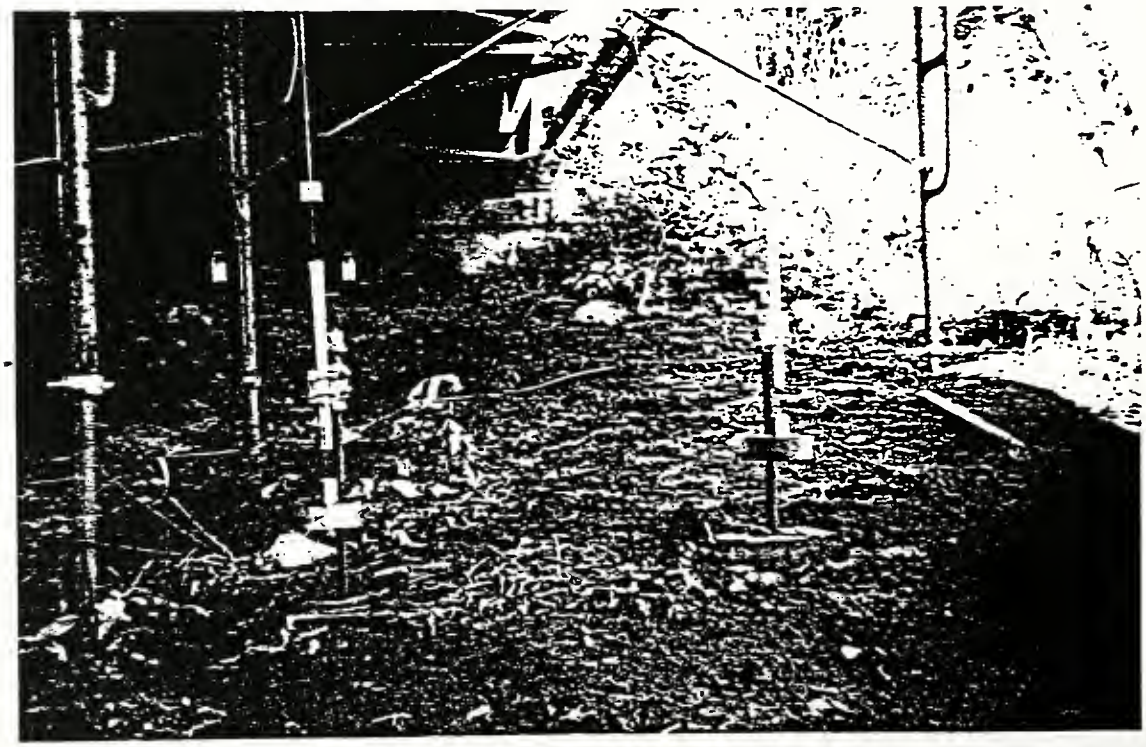

Figure 3.2.3.2 LVDT stand and weight assembly

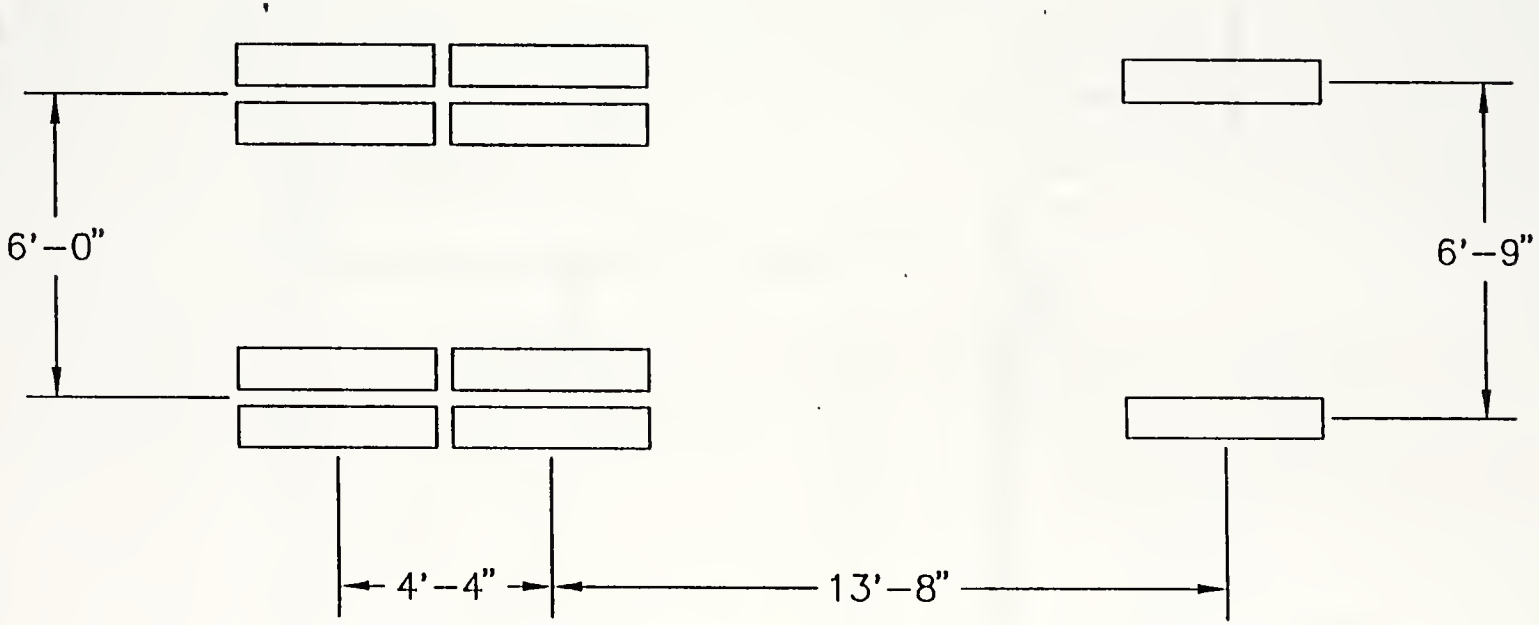

3.2.4.1 Tire and axle spacings for a typical test vehicle

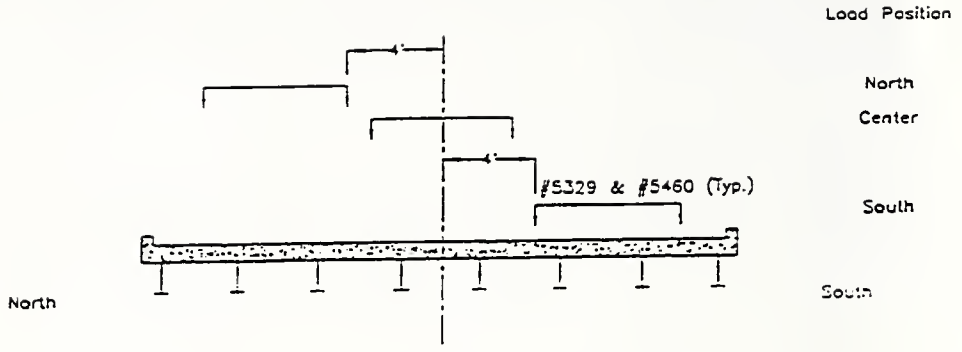

a) Transverse Vehicle Positions

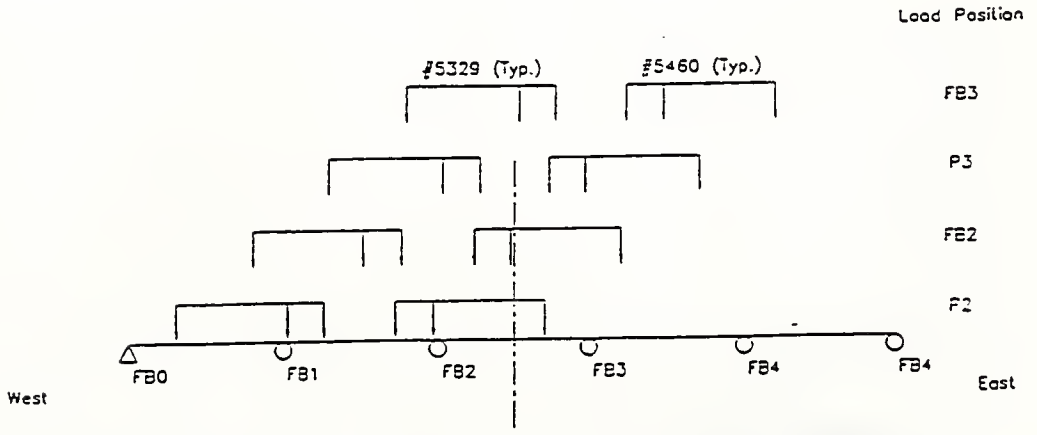

b) Longitudinal Vehicle Positions

Figure 3.2.4.1.1 Loading condition #1

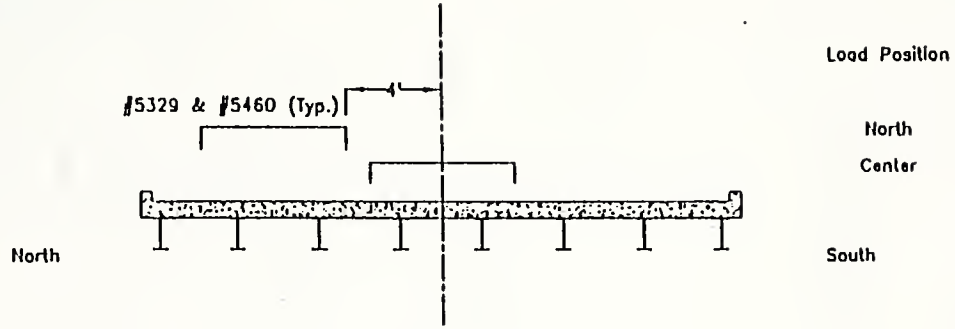

a) Transverse Vehicle Positions

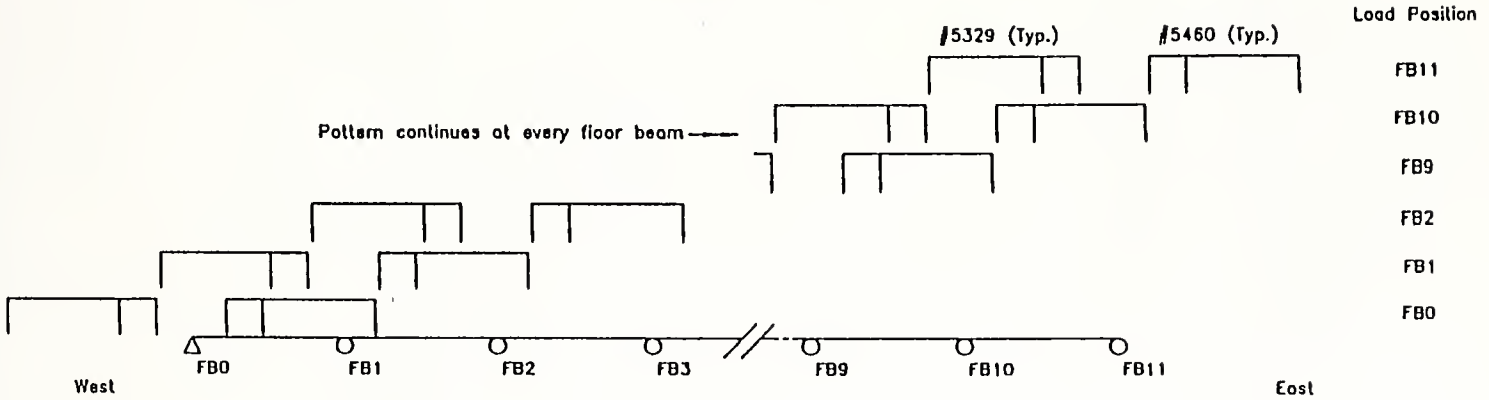

b) Longitudinal Vehicle Positions

Figure 3.2.4.2.1 Loading condition #2

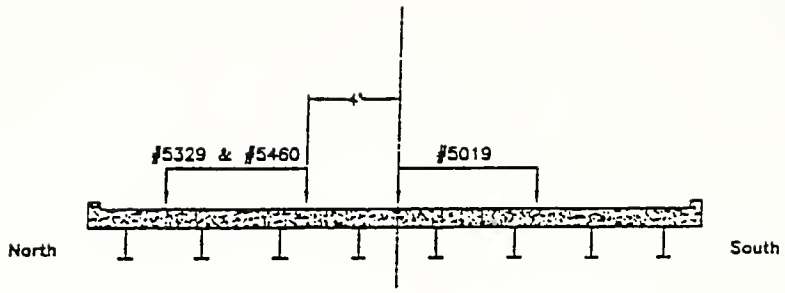

a) Transverse Vehicle Positions

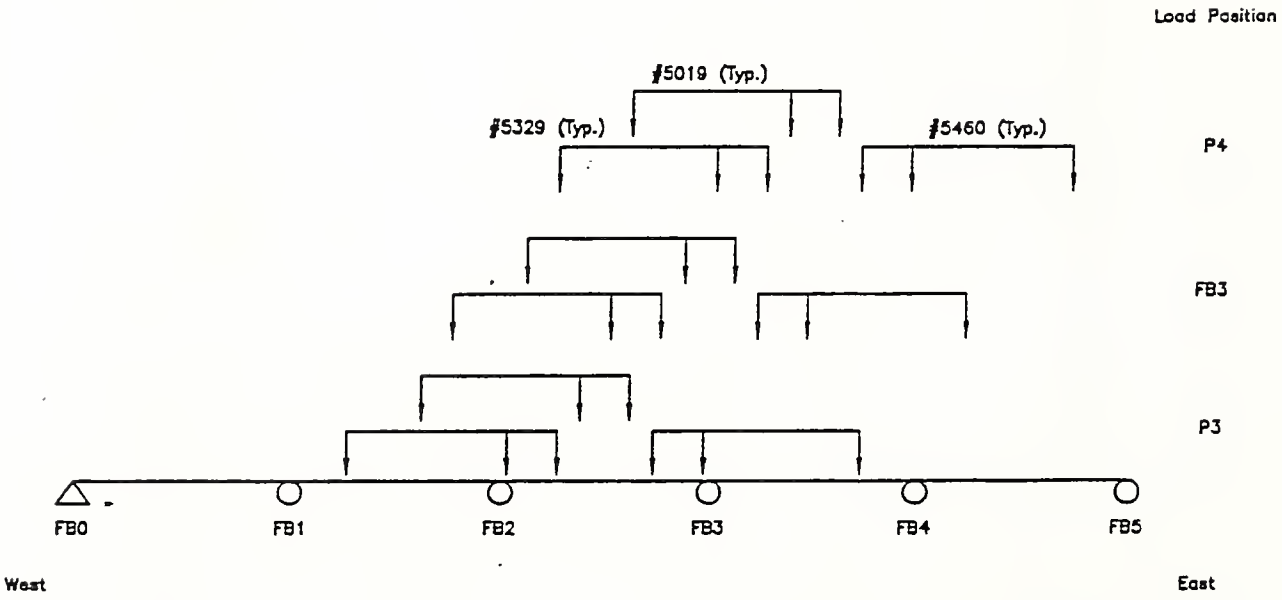

a) Longitudinal Vehicle Positions

Figure 3.2.4.3.1 Loading condition #3-1

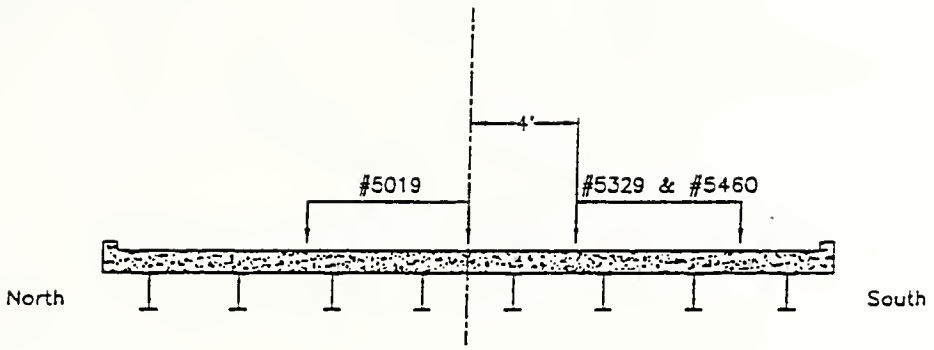

a) Transverse Vehicle Positions

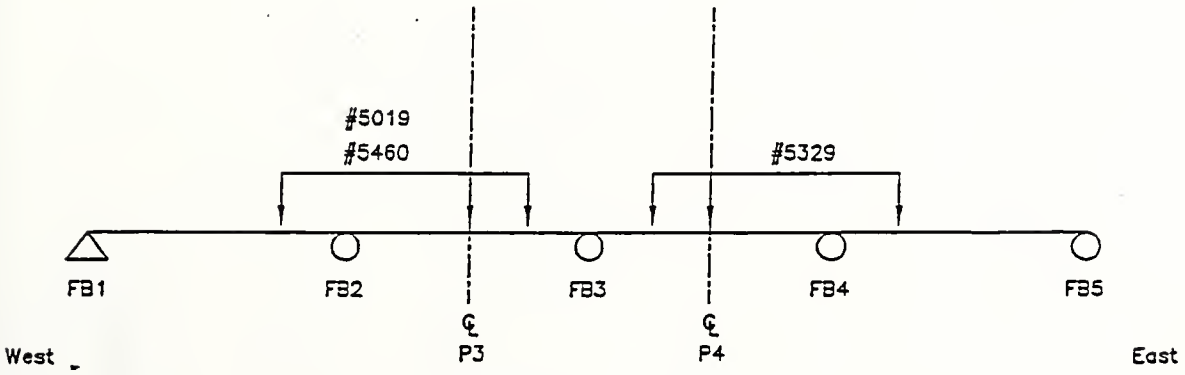

a) Longitudinal Vehicle Positions

Figure 3.2.4.3.2 Loading condition #3-2

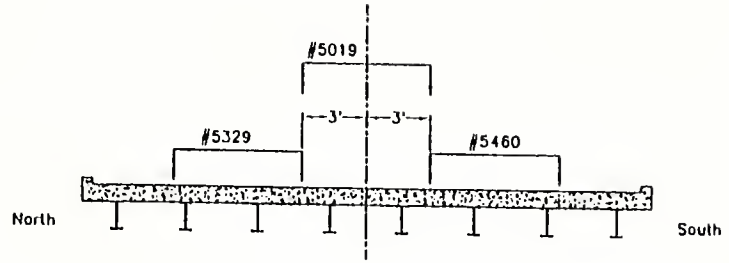

a) Transverse Vehicle Positions

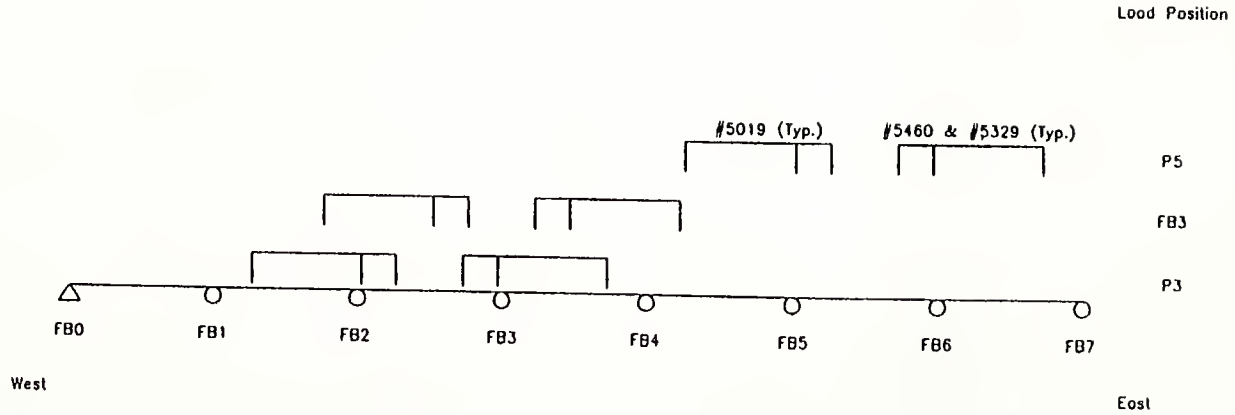

a) Longitudinal Vehicle Positions

Figure 3.2.4.3.3 Loading condition #3-3

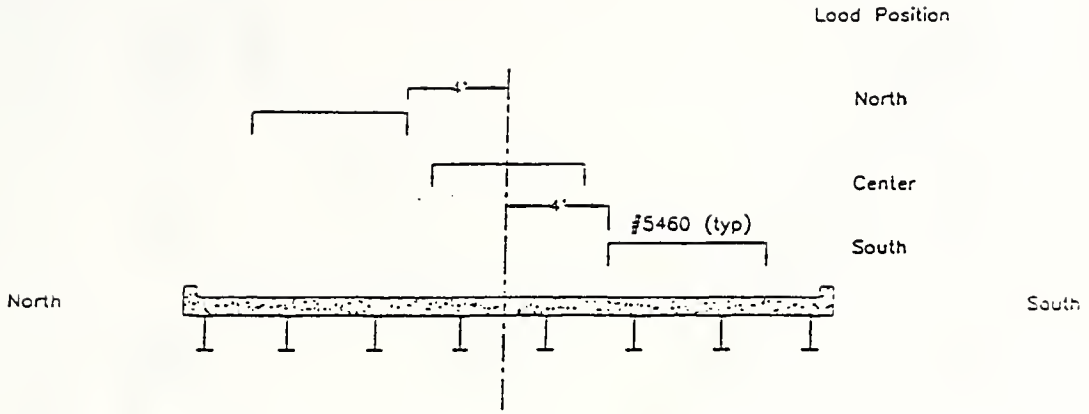

a) Transverse Vehicle Positions

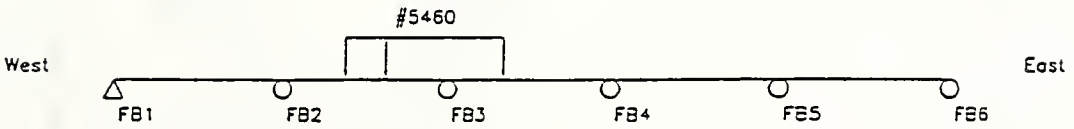

b) Longitudinal Vehicle Positions

Figure 3.2.4.4.1 Loading condition #4

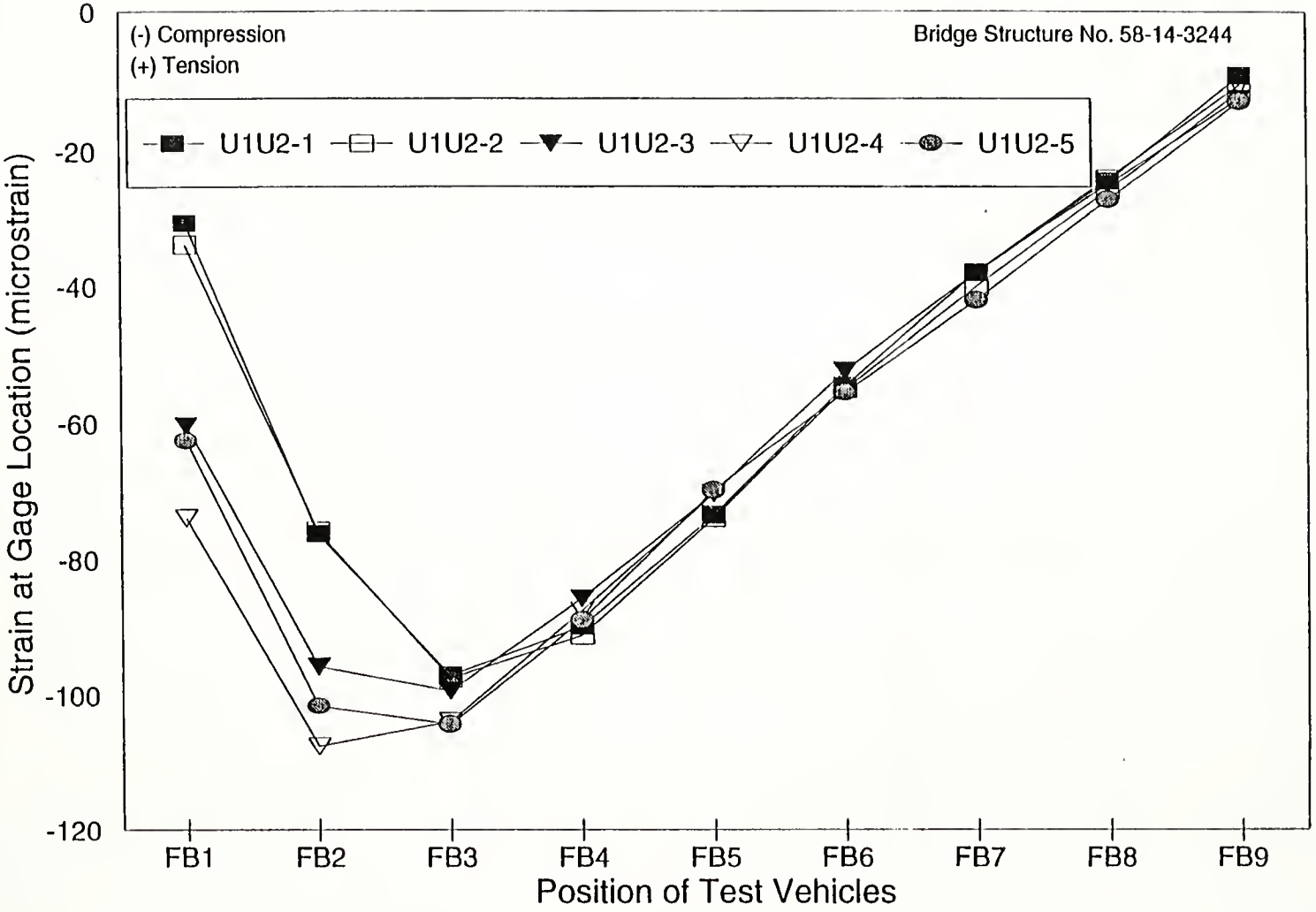

Figure 5.1.2.2.1 Strain measurements in member U1U2 for LC #2 - CENTER

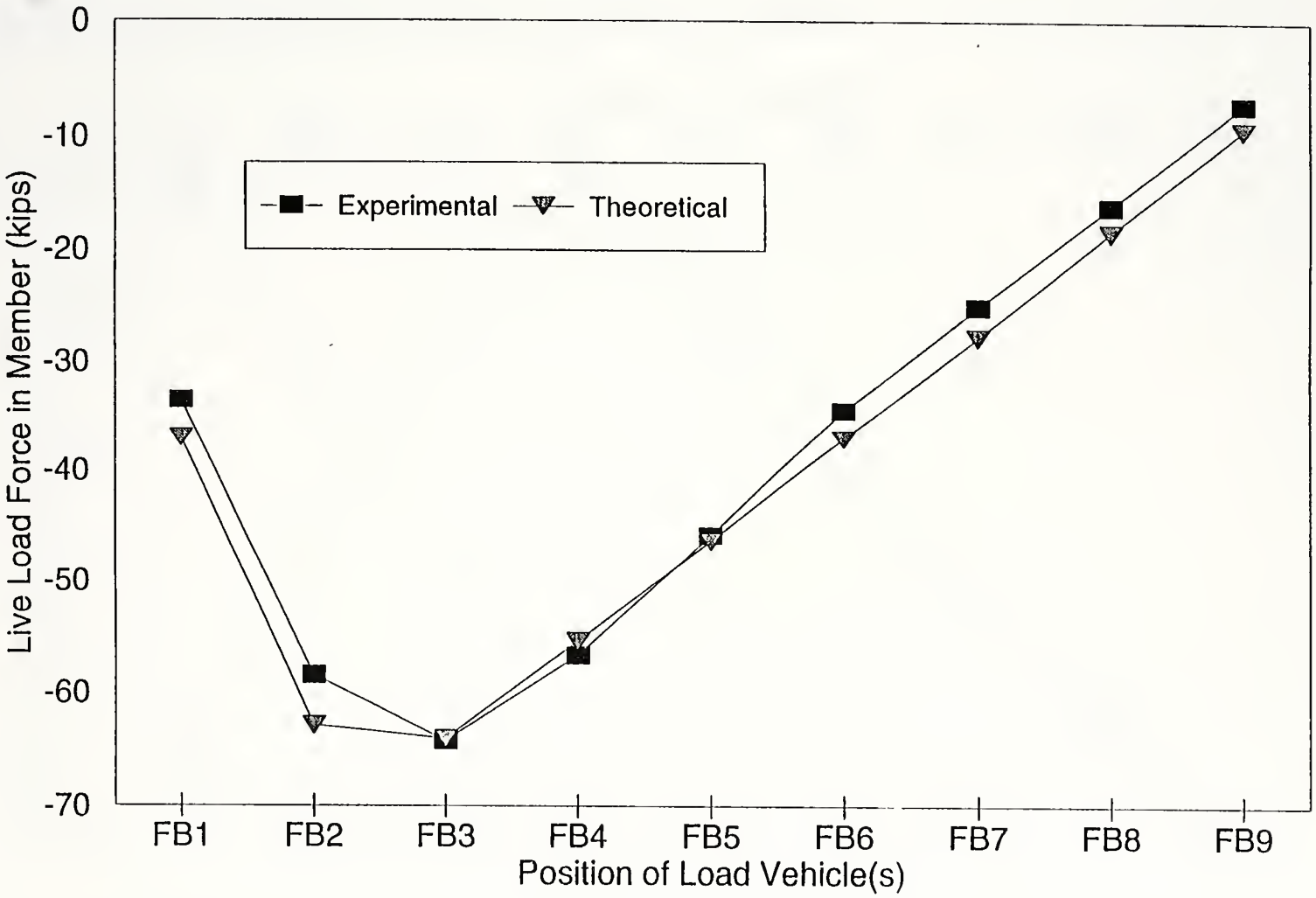

Figure 5.1.2.2.2 Force in member U1U2 for LC #2 - CENTER

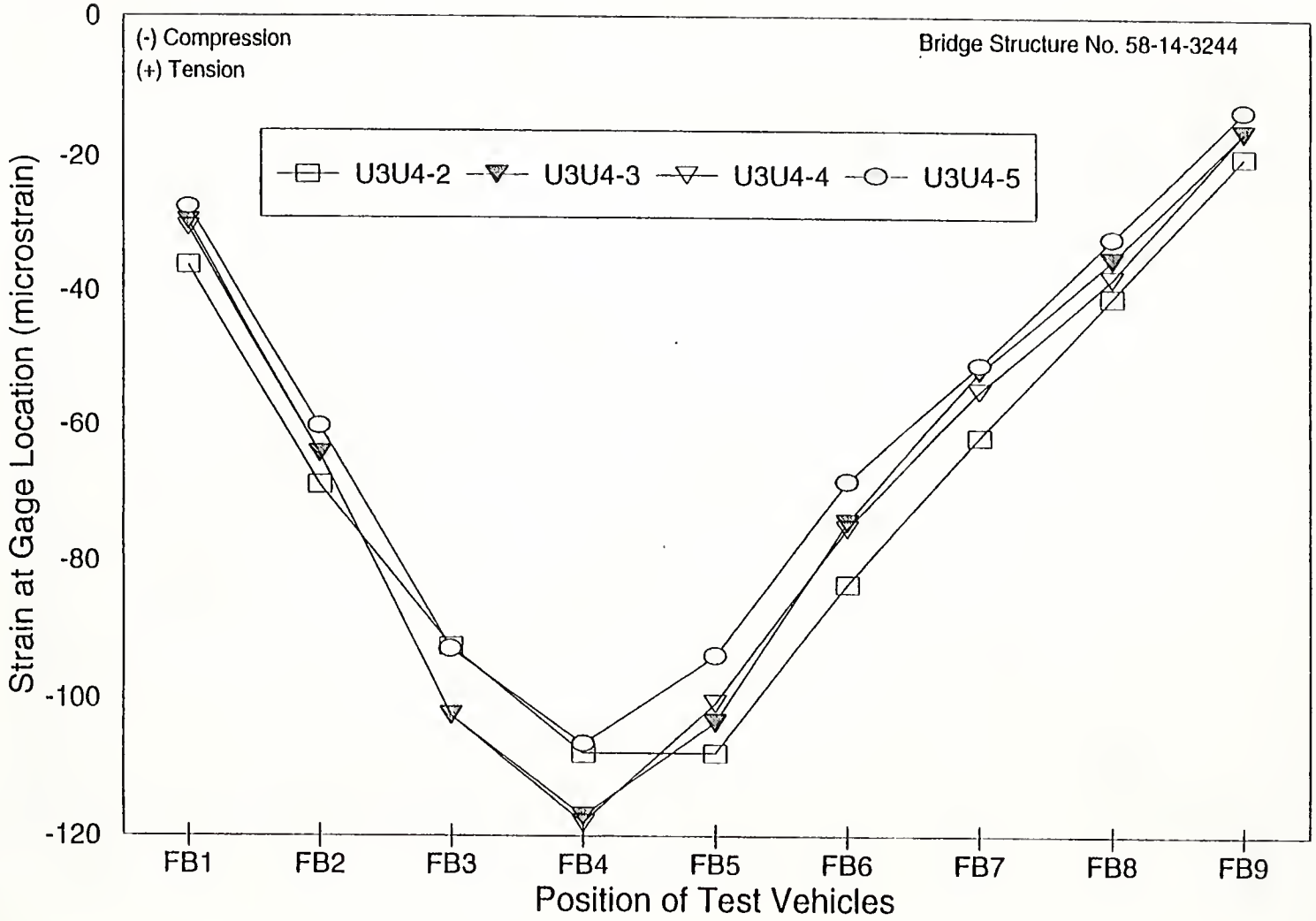

Figure 5.1.2.2.3 Strain measurements in member U3U4 for LC #2 - CENTER

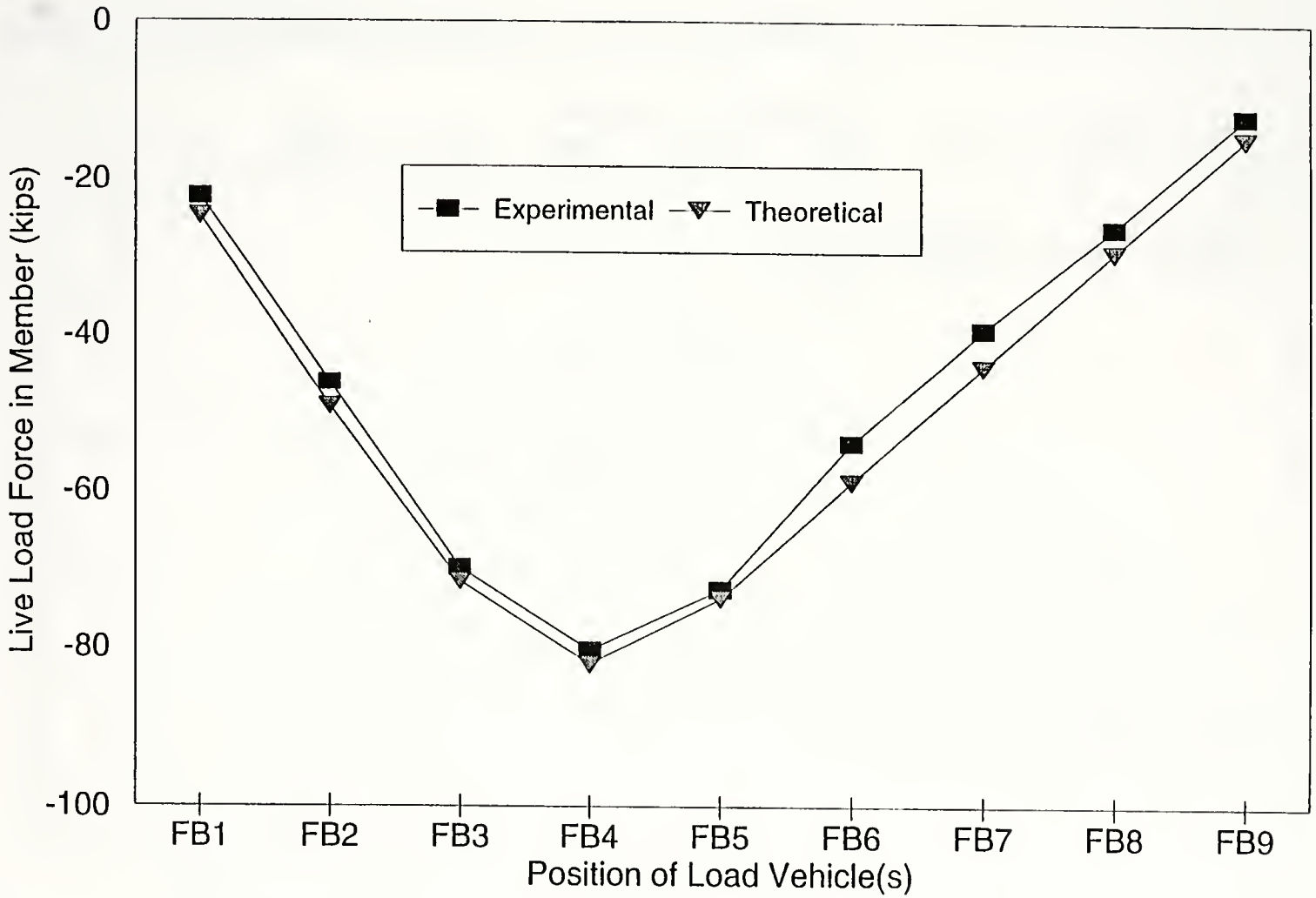

Figure 5.1.2.2.4 Force in member U3U4 for LC #2 - CENTER

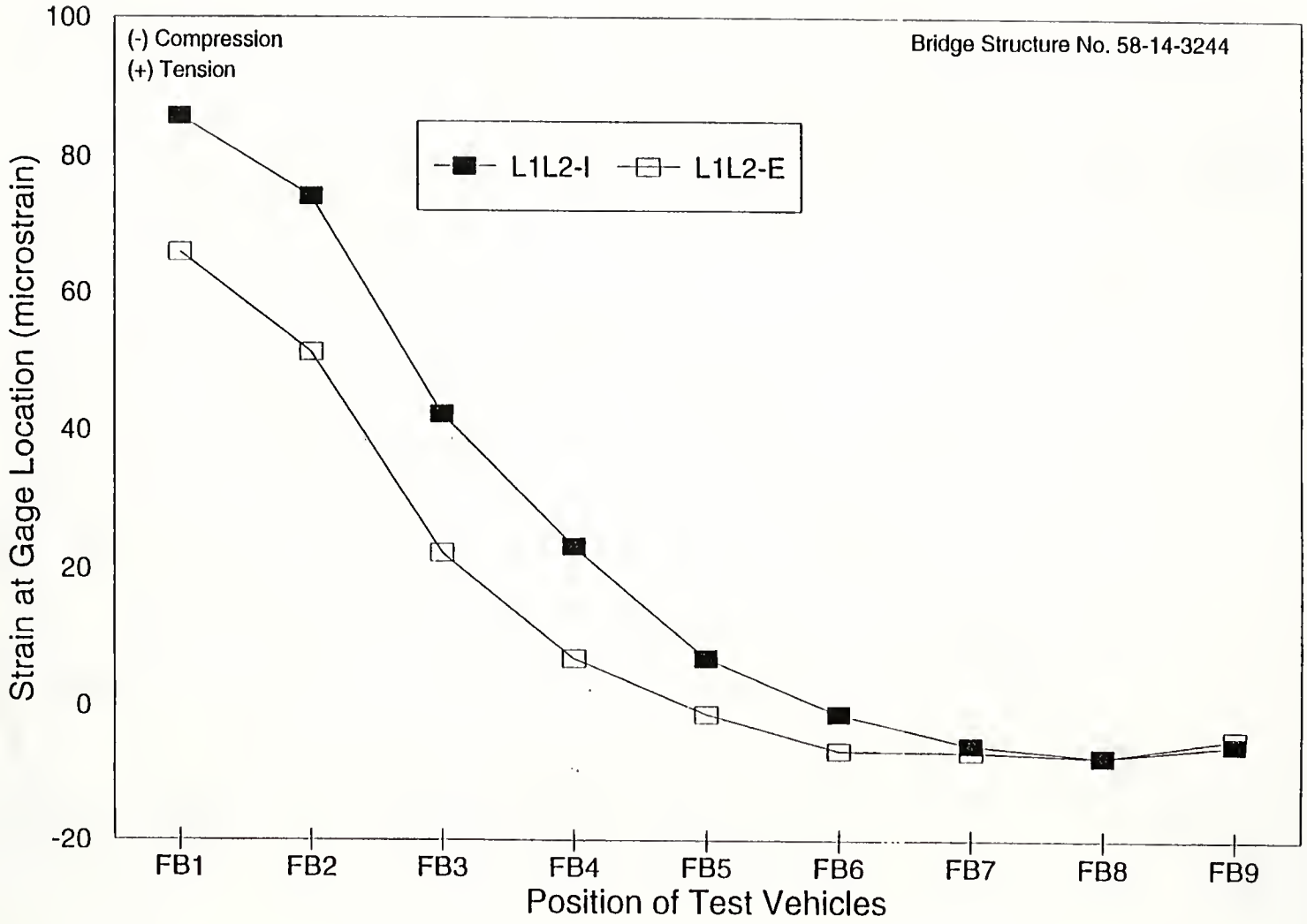

Figure 5.1.2.2.5 Strain measurements in member L1L2 for LC #2 - CENTER

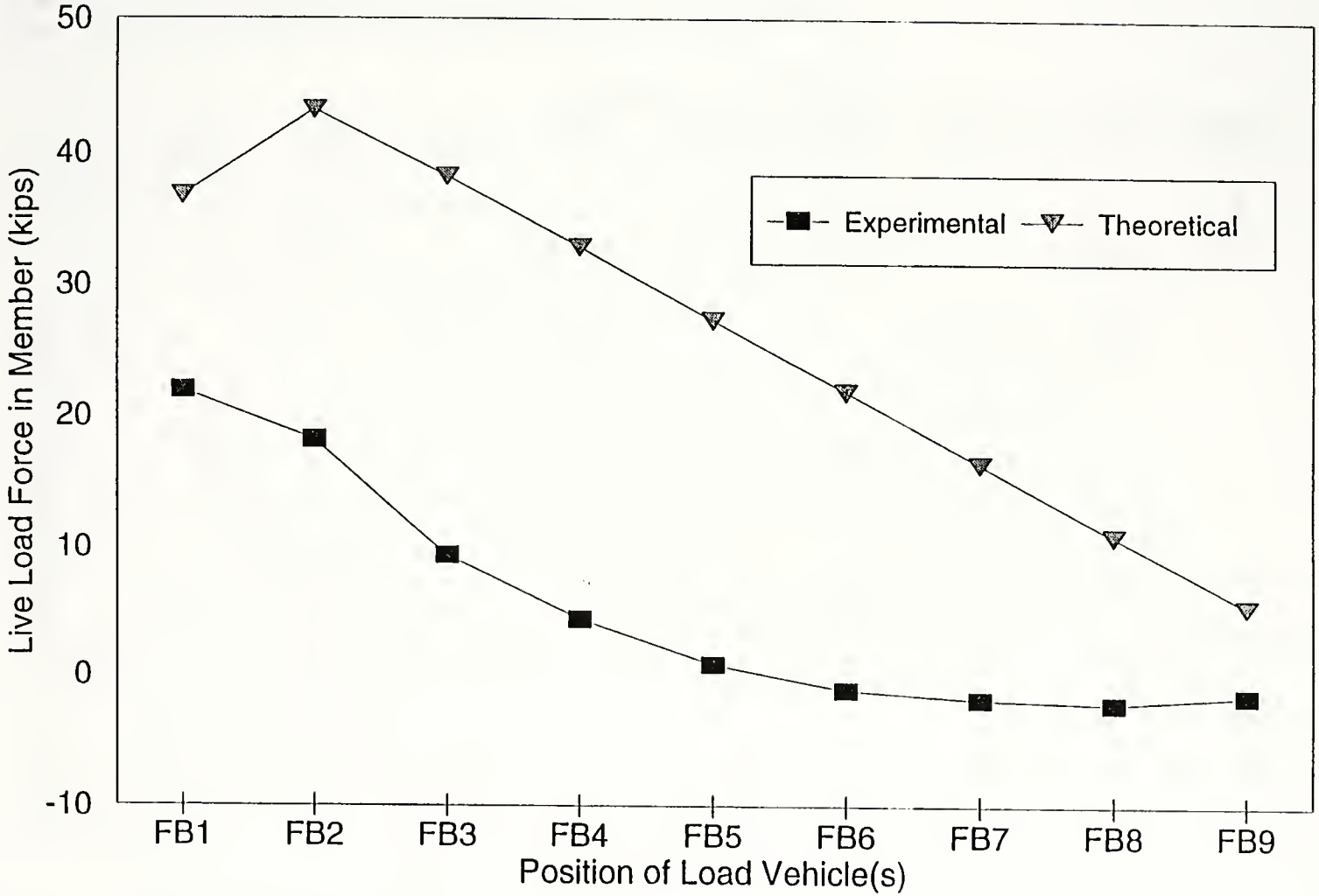

Figure 5.1.2.2.6 Force in member L1L2 for LC #2 - CENTER

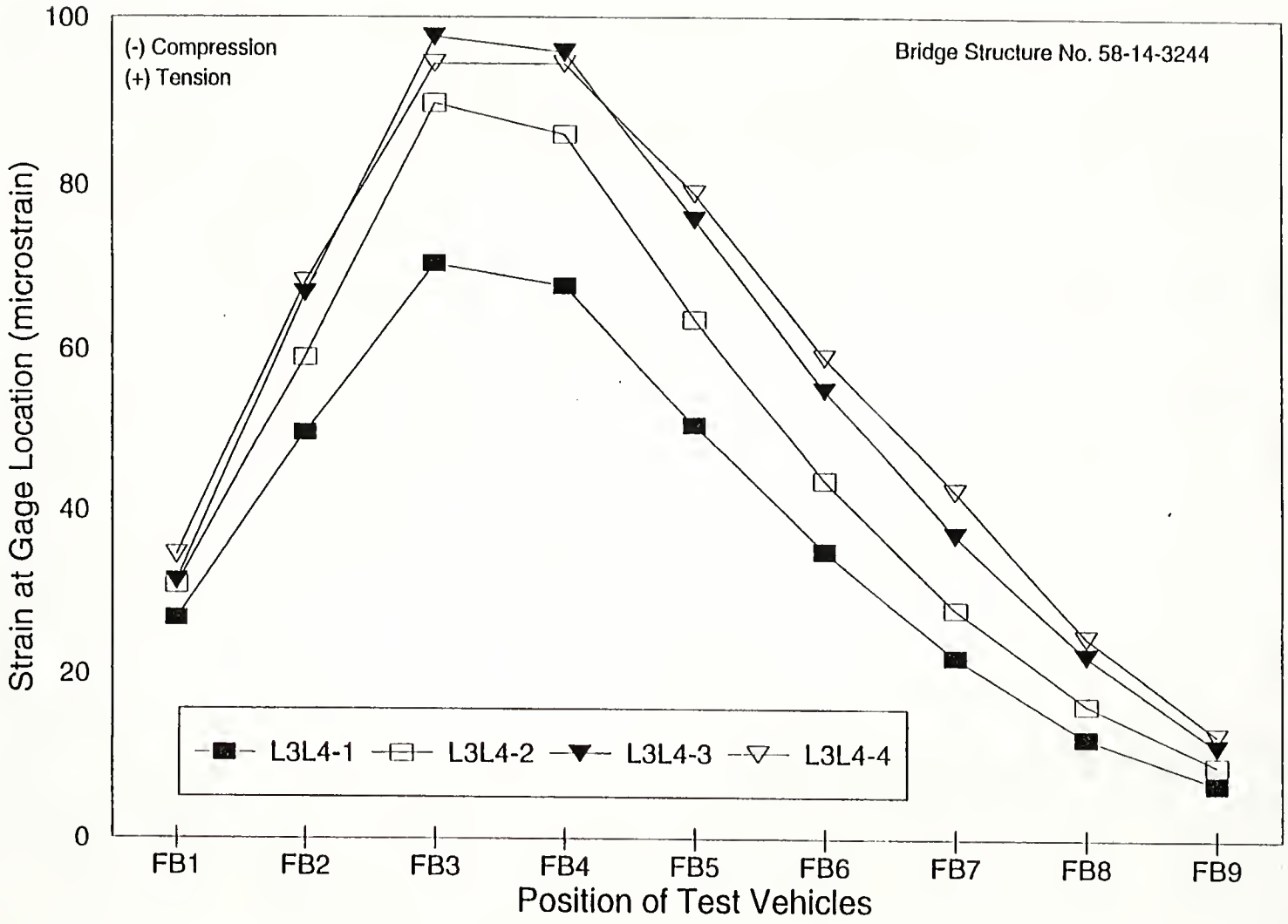

Figure 5.1.2.2.7 Strain measurements in member L3L4 for LC #2 - CENTER

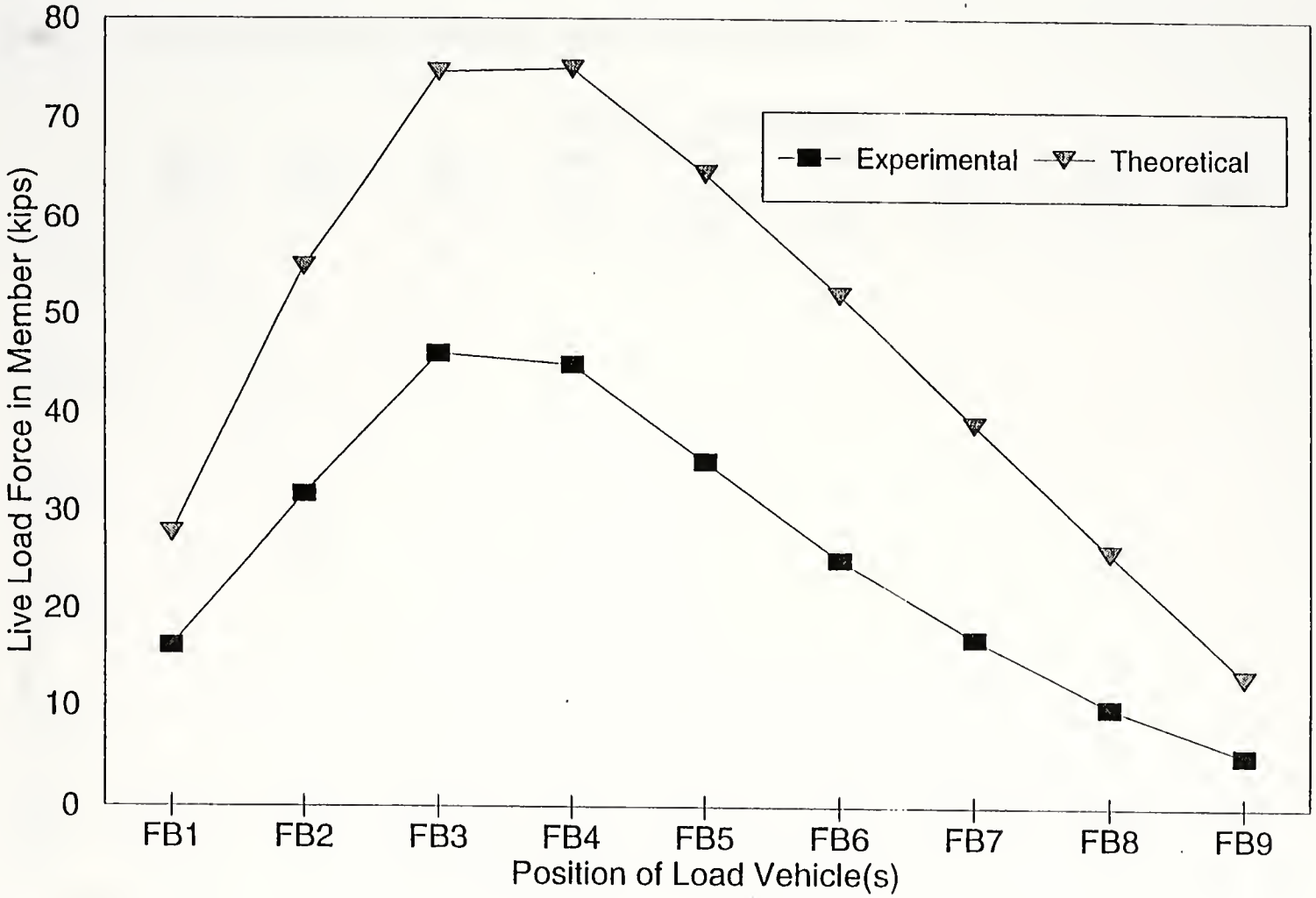

Figure 5.1.2.2.8 Force in member L3L4 for LC #2 - CENTER

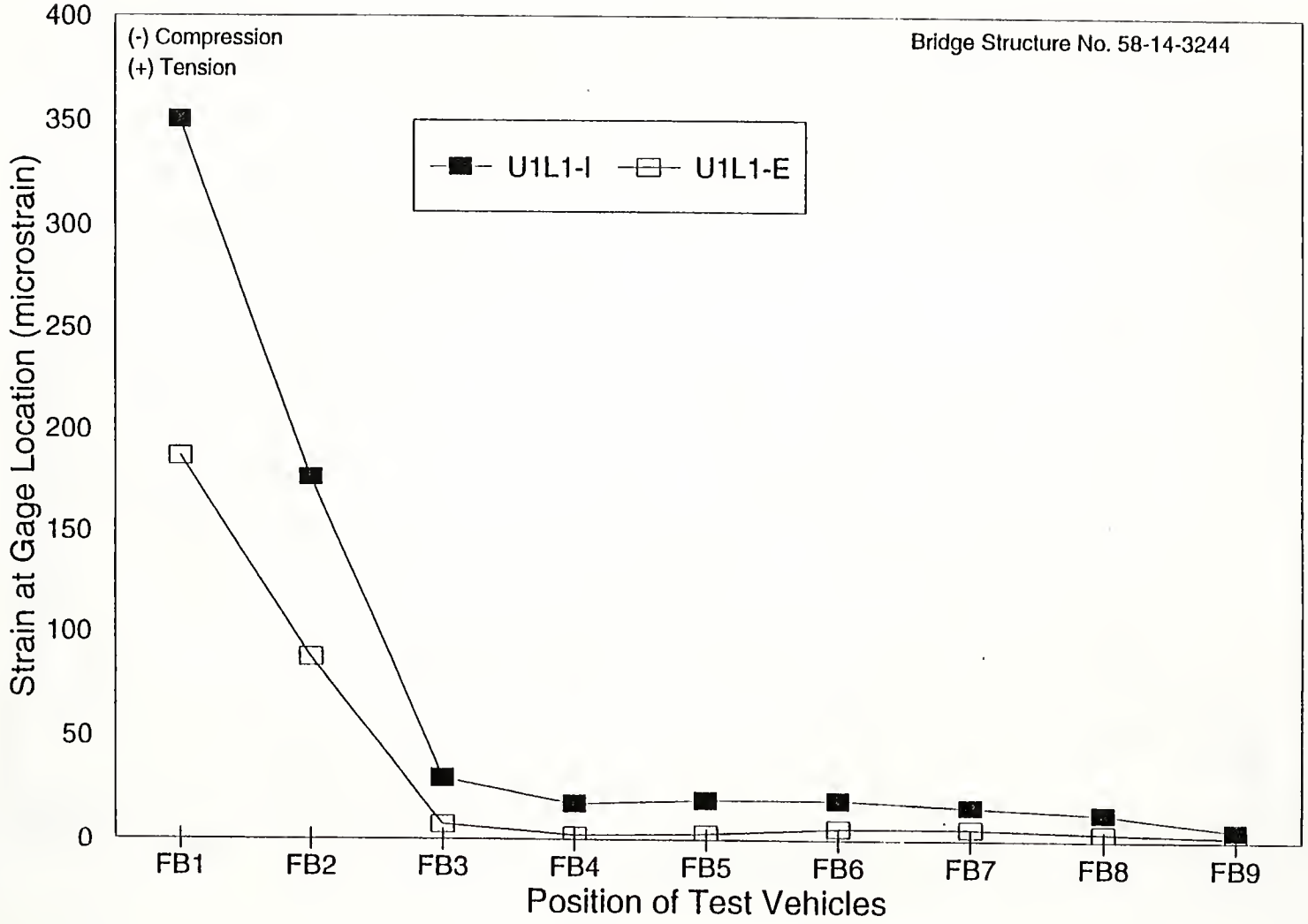

Figure 5.1.2.2.9 Strain measurements in member U1L1 for LC #2 - CENTER

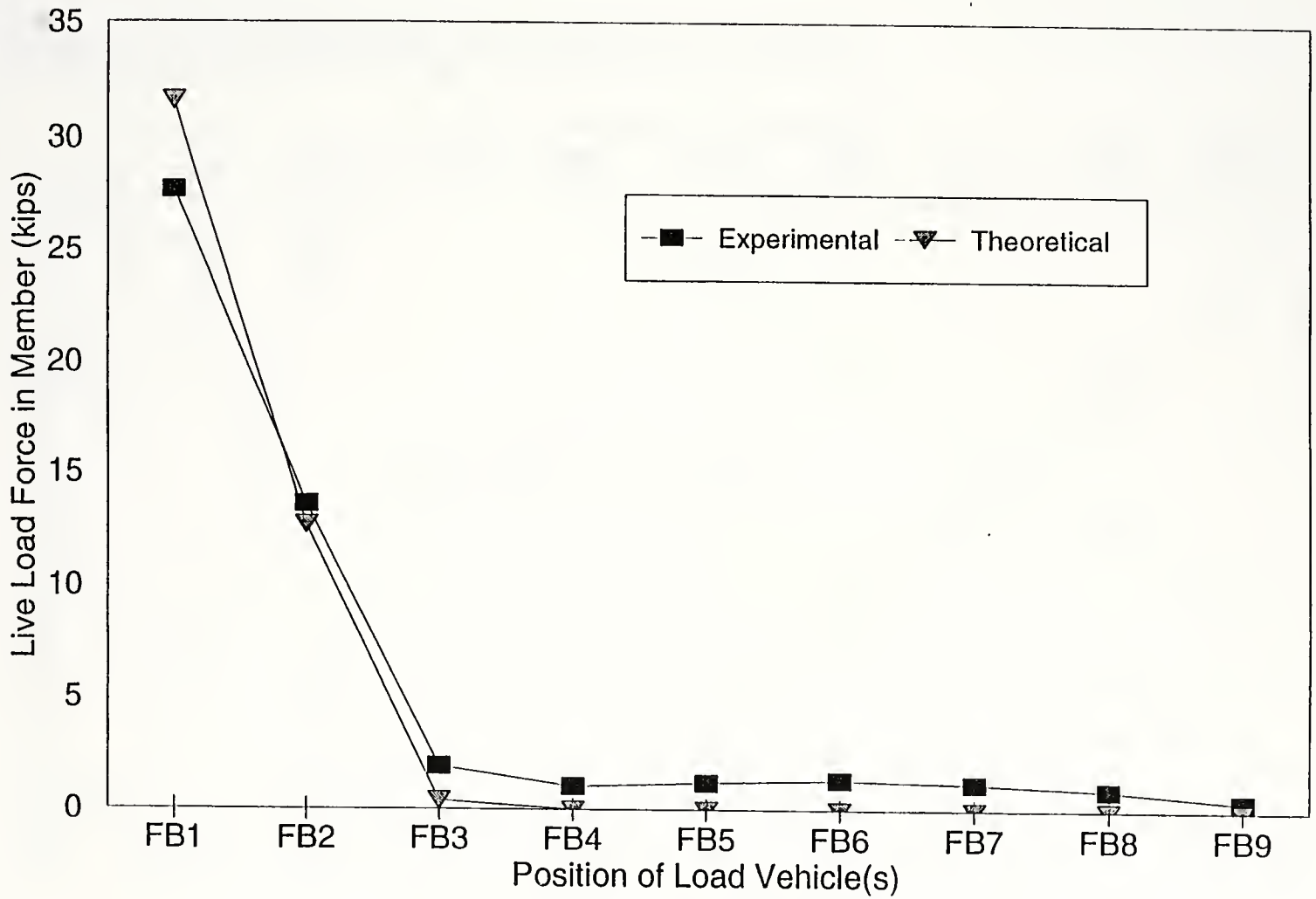

Figure 5.1.2.2.10 Force in member U1L1 for LC #2 - CENTER

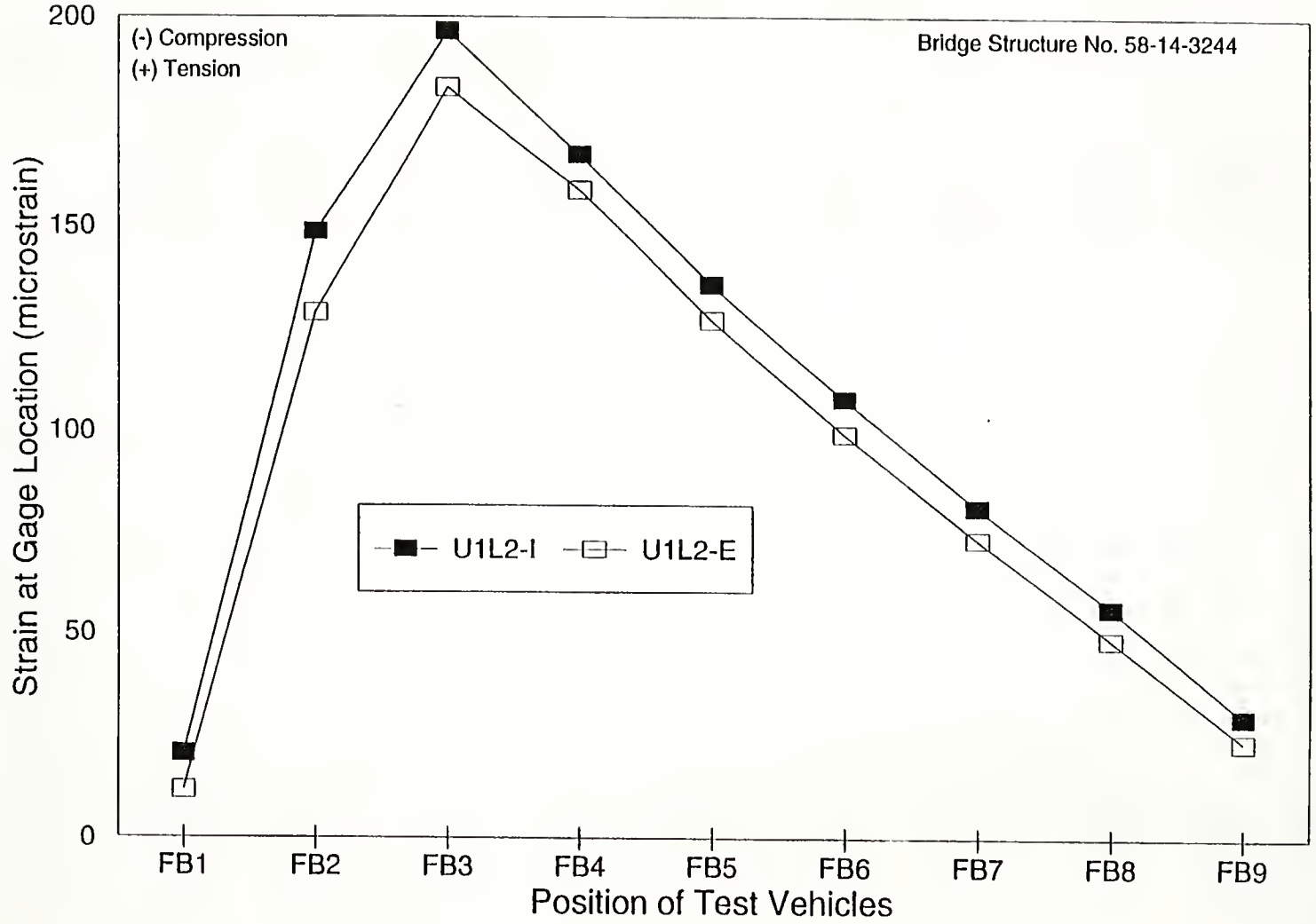

Figure 5.1.2.2.11 Strain measurements in member U1L2 for LC #2 - CENTER

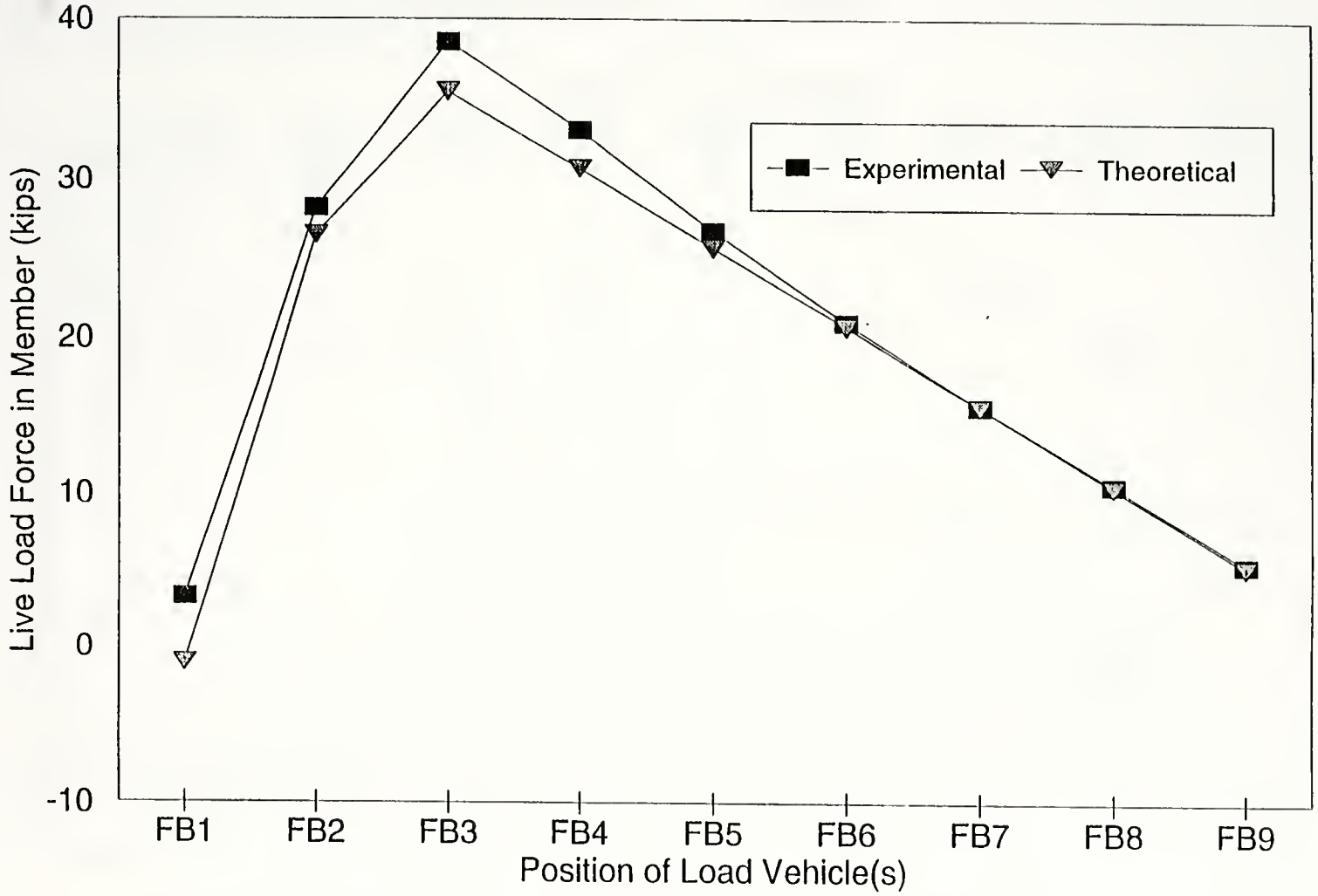

Figure 5.1.2.2.12 Force in member U1L2 for LC #2 - CENTER

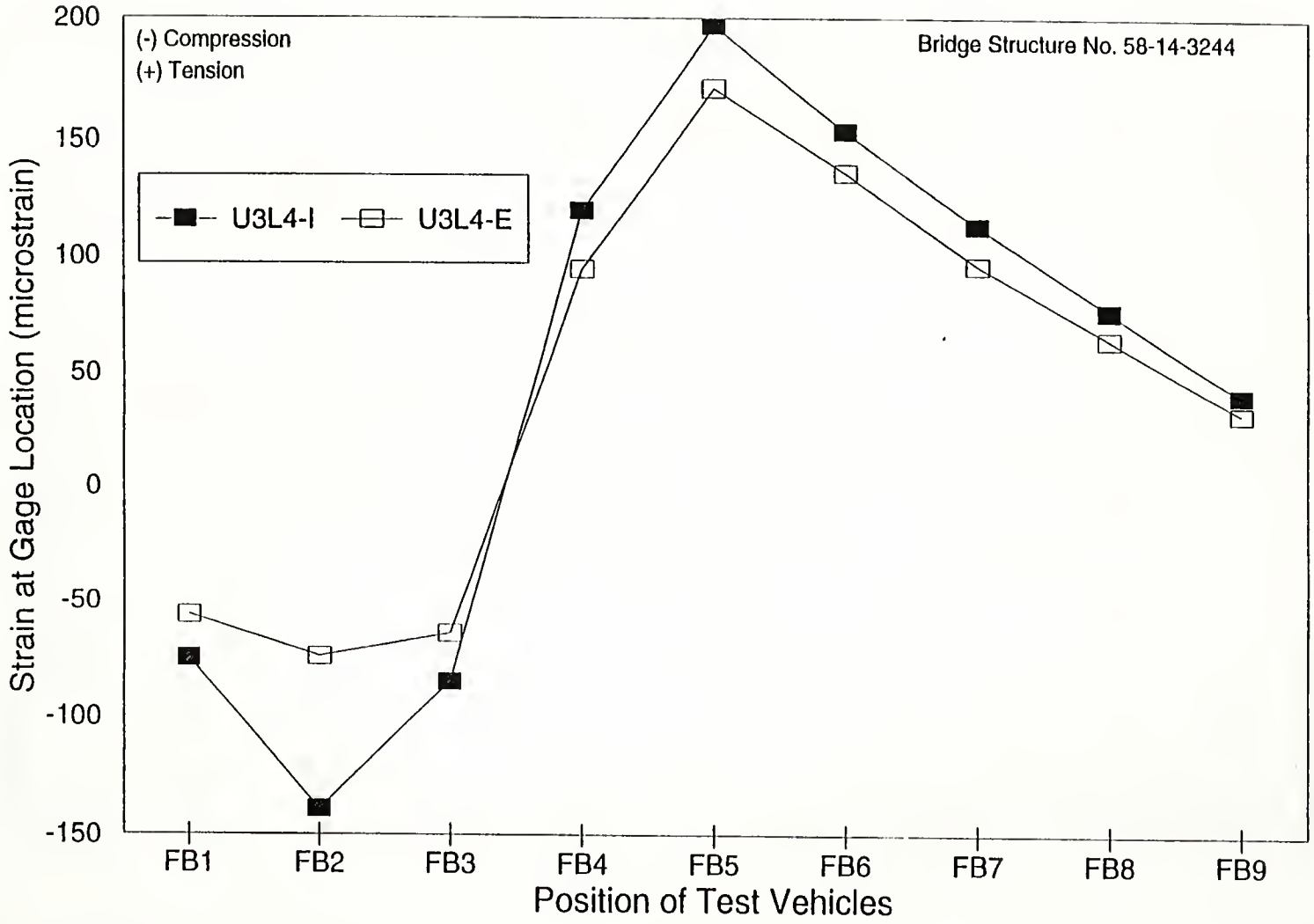

Figure 5.1.2.2.13 Strain measurements in member U3L4 for LC #2 - CENTER

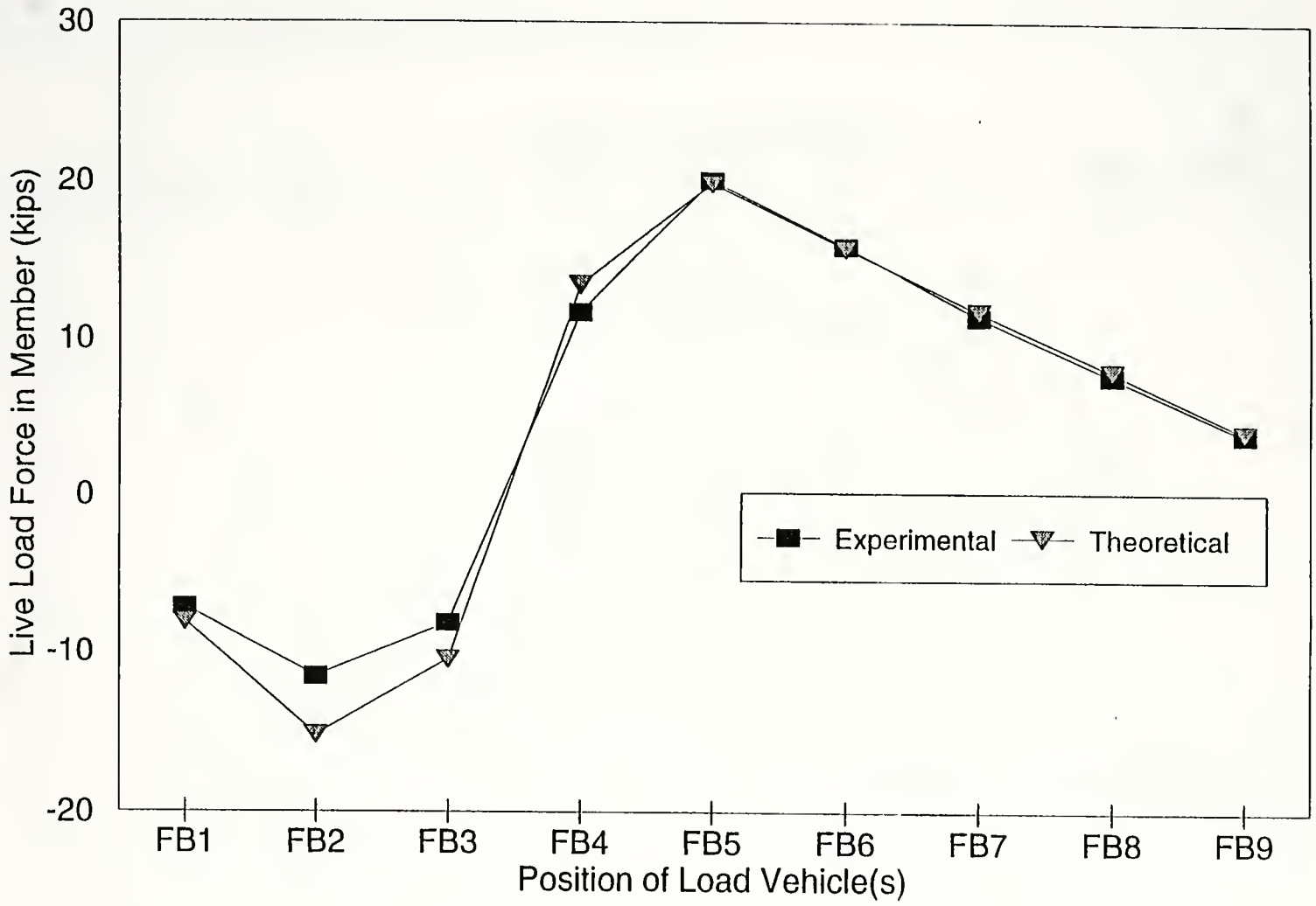

Figure 5.1.2.2.14 Force in member U3L4 for LC #2 - CENTER

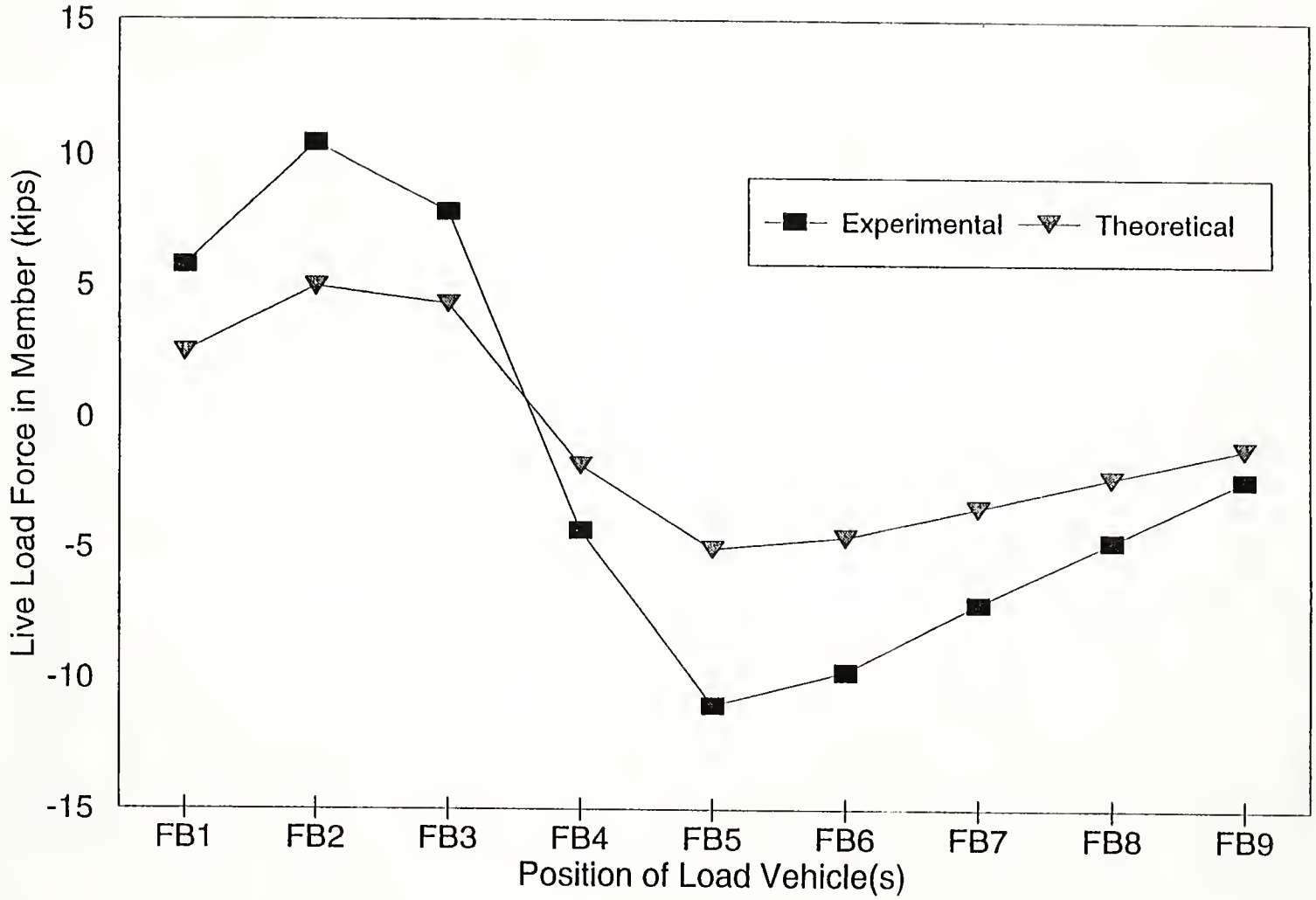

Figure 5.1.2.2.15 Force in member U4L3 for LC #2 - CENTER

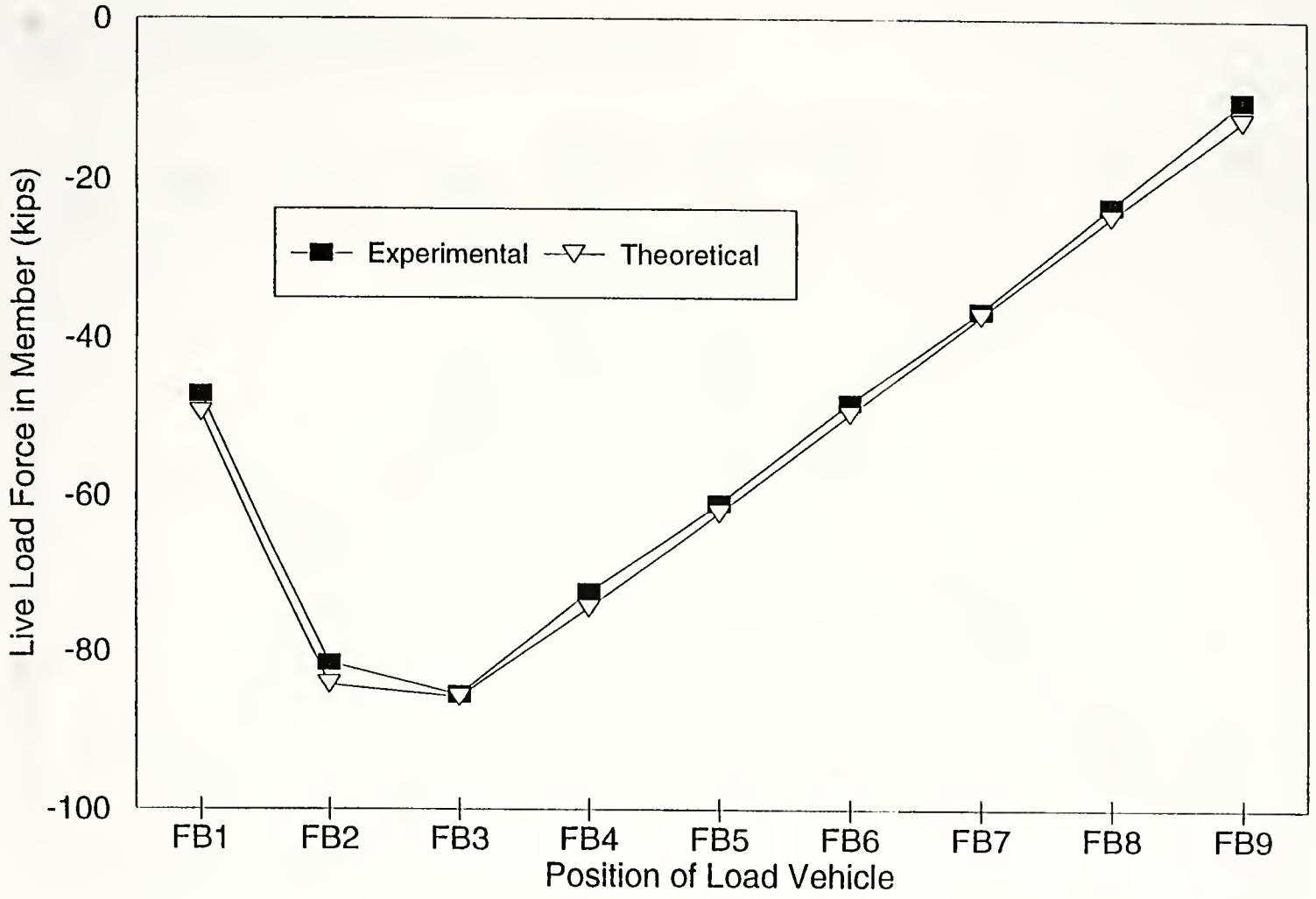

Figure 5.1.2.3.1 Force in member U1U2 for LC #2 - SOUTH

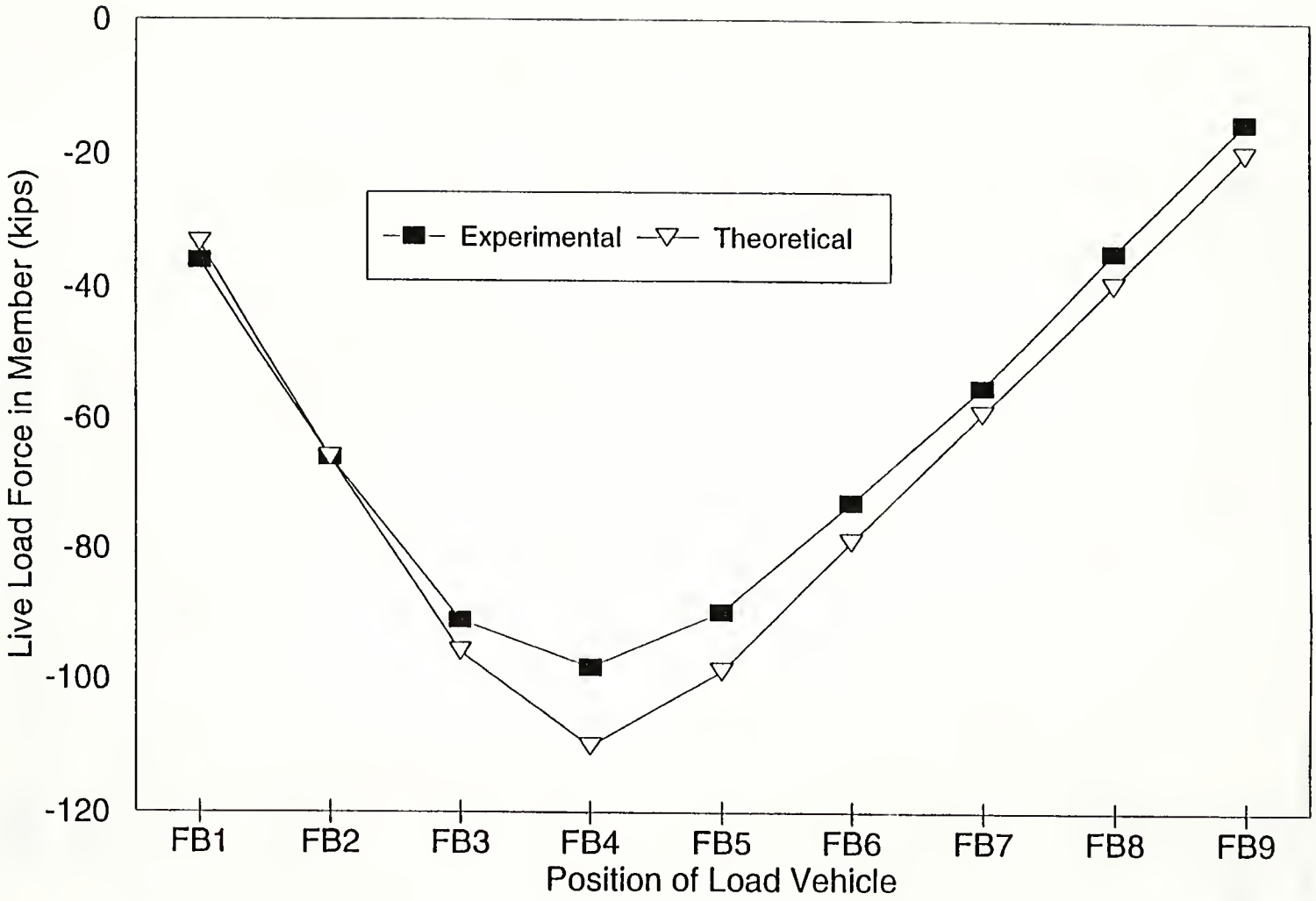

Figure 5.1.2.3.2 Force in member U3U4 for LC #2 - SOUTH

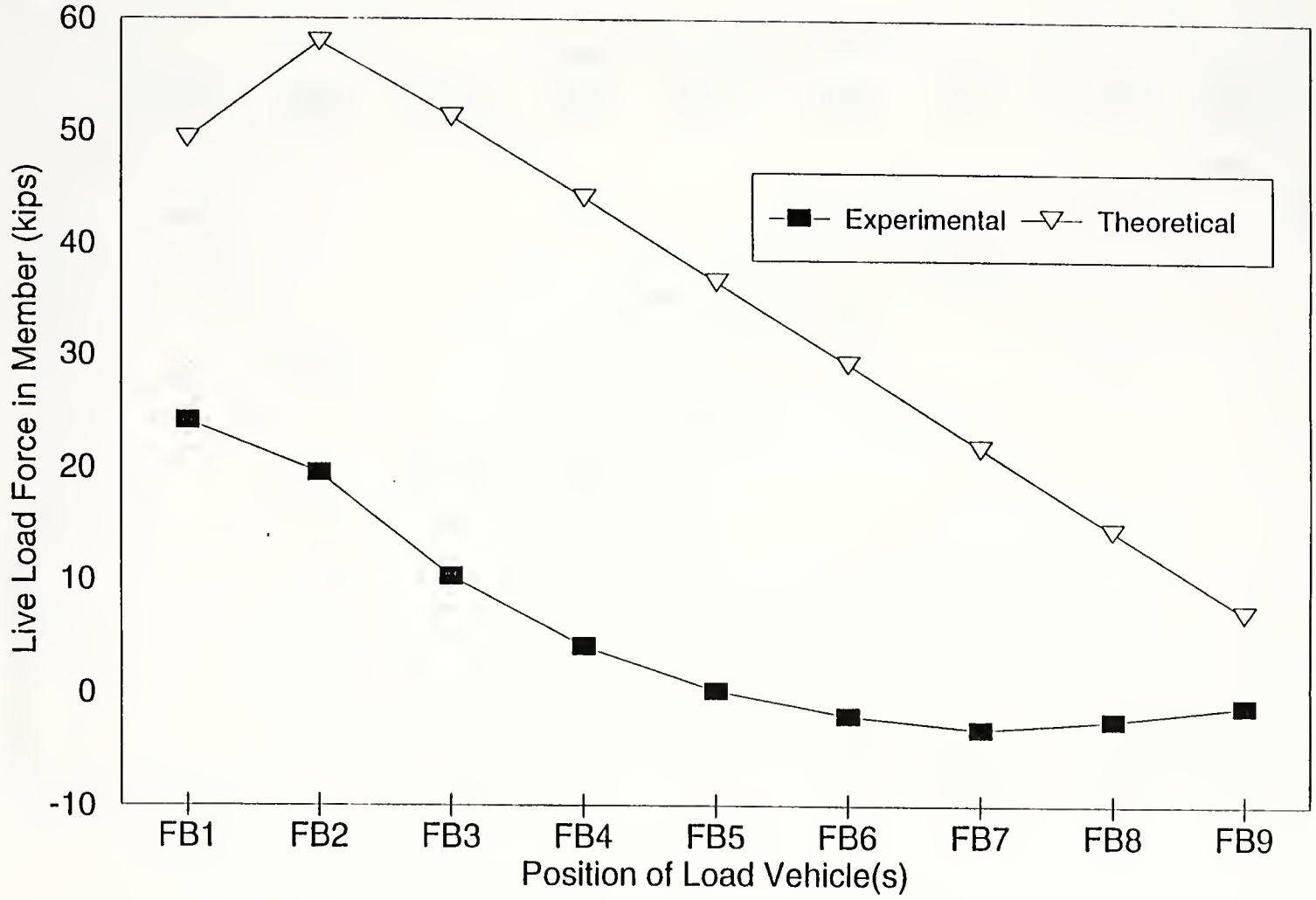

Figure 5.1.2.3.3 Force in member L1L2 for LC #2 - SOUTH

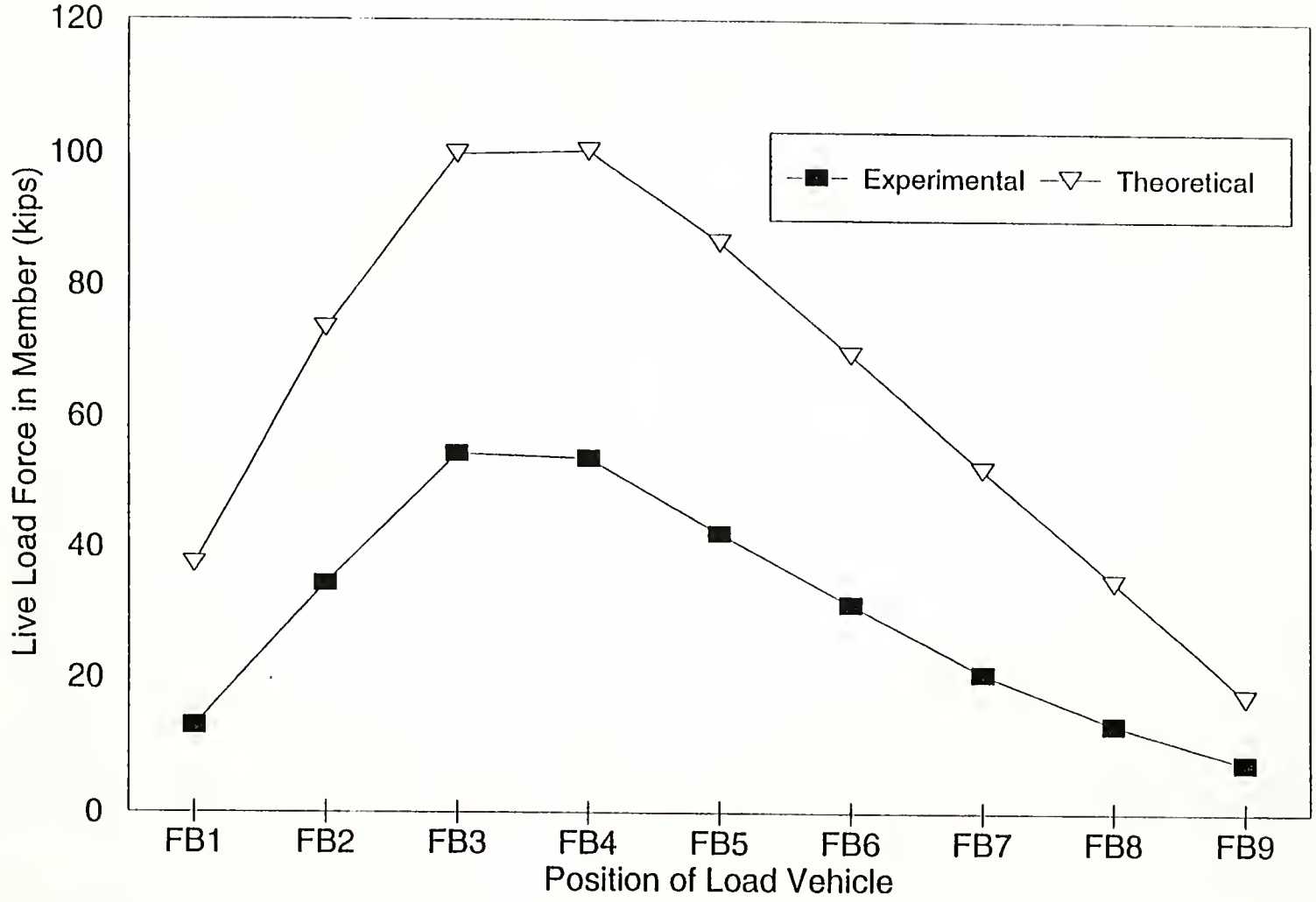

Figure 5.1.2.3.4 Force in member L3L4 for LC #2 - SOUTH

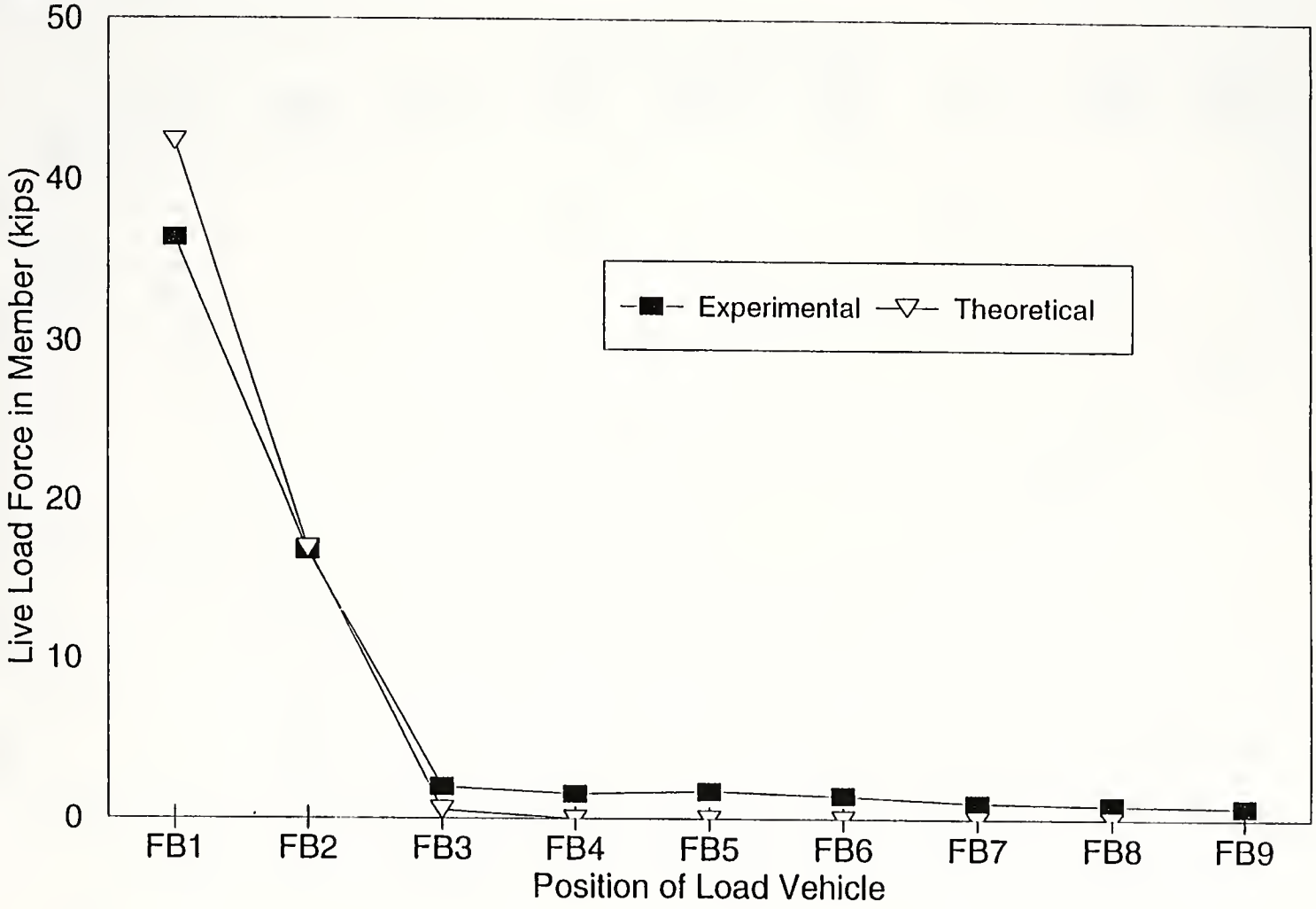

Figure 5.1.2.3.5 Force in member U1L1 for LC #2 - SOUTH

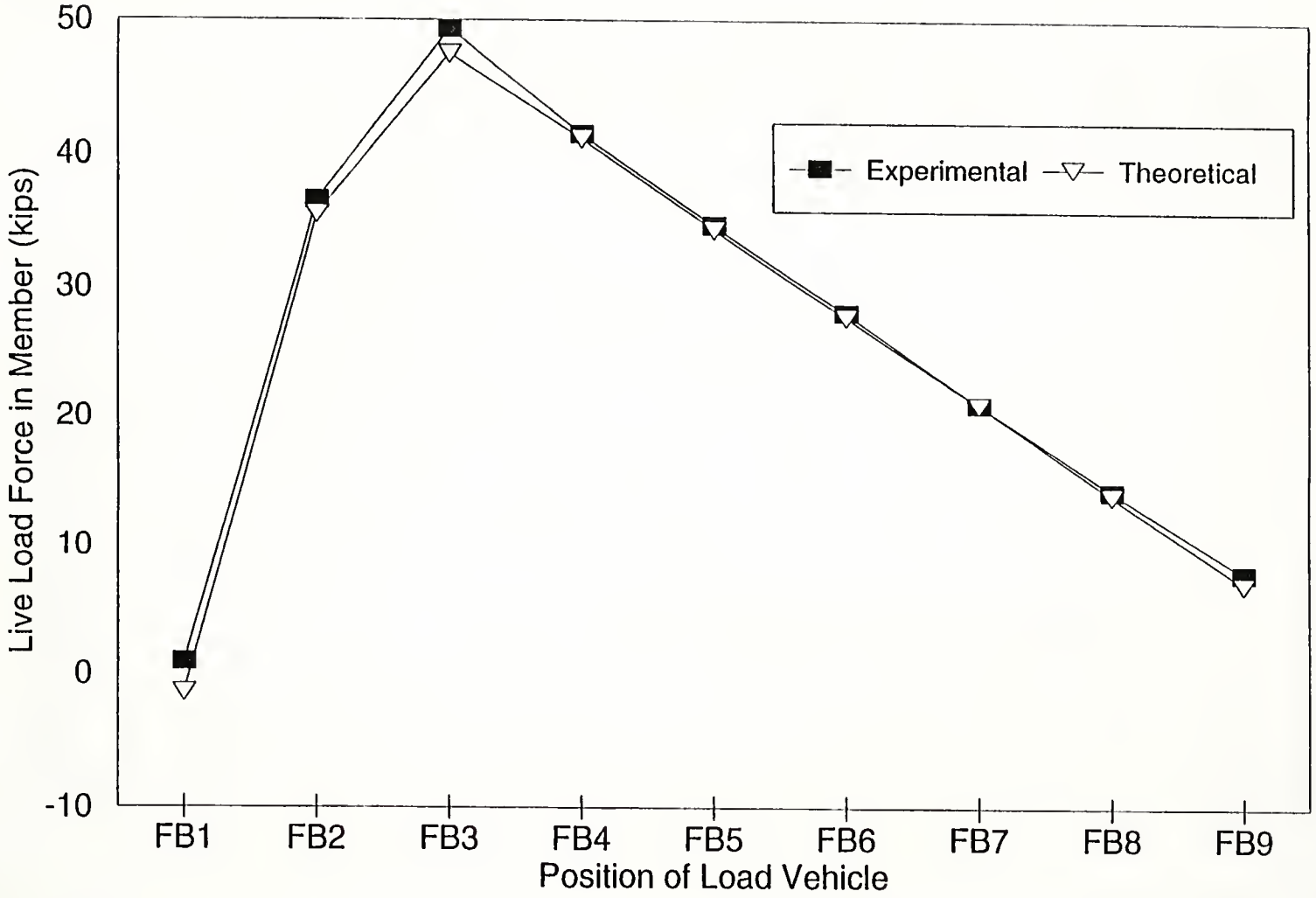

Figure 5.1.2.3.6 Force in member U1L2 for LC #2 - SOUTH

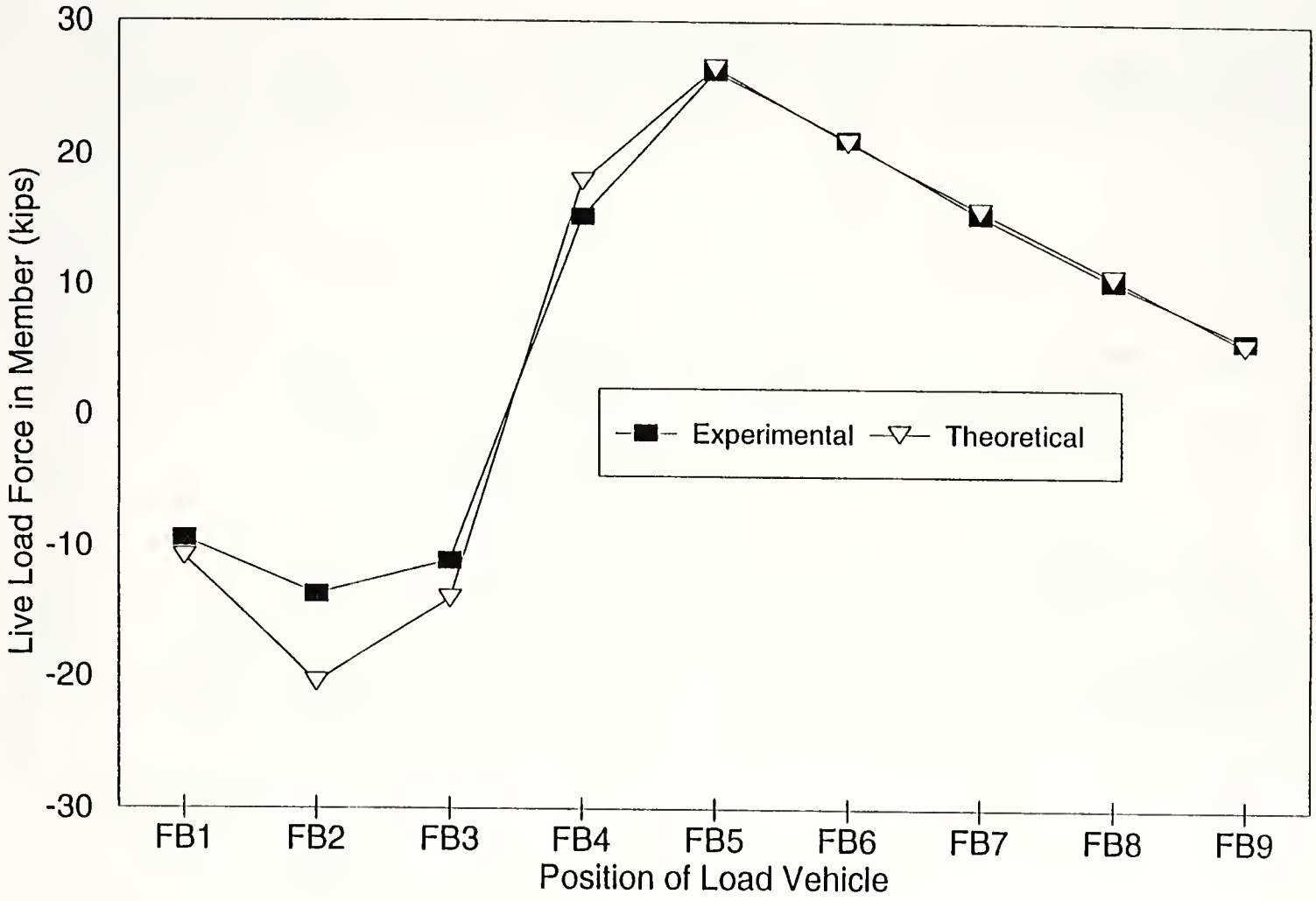

Figure 5.1.2.3.7 Force in member U3L4 for LC #2 - SOUTH

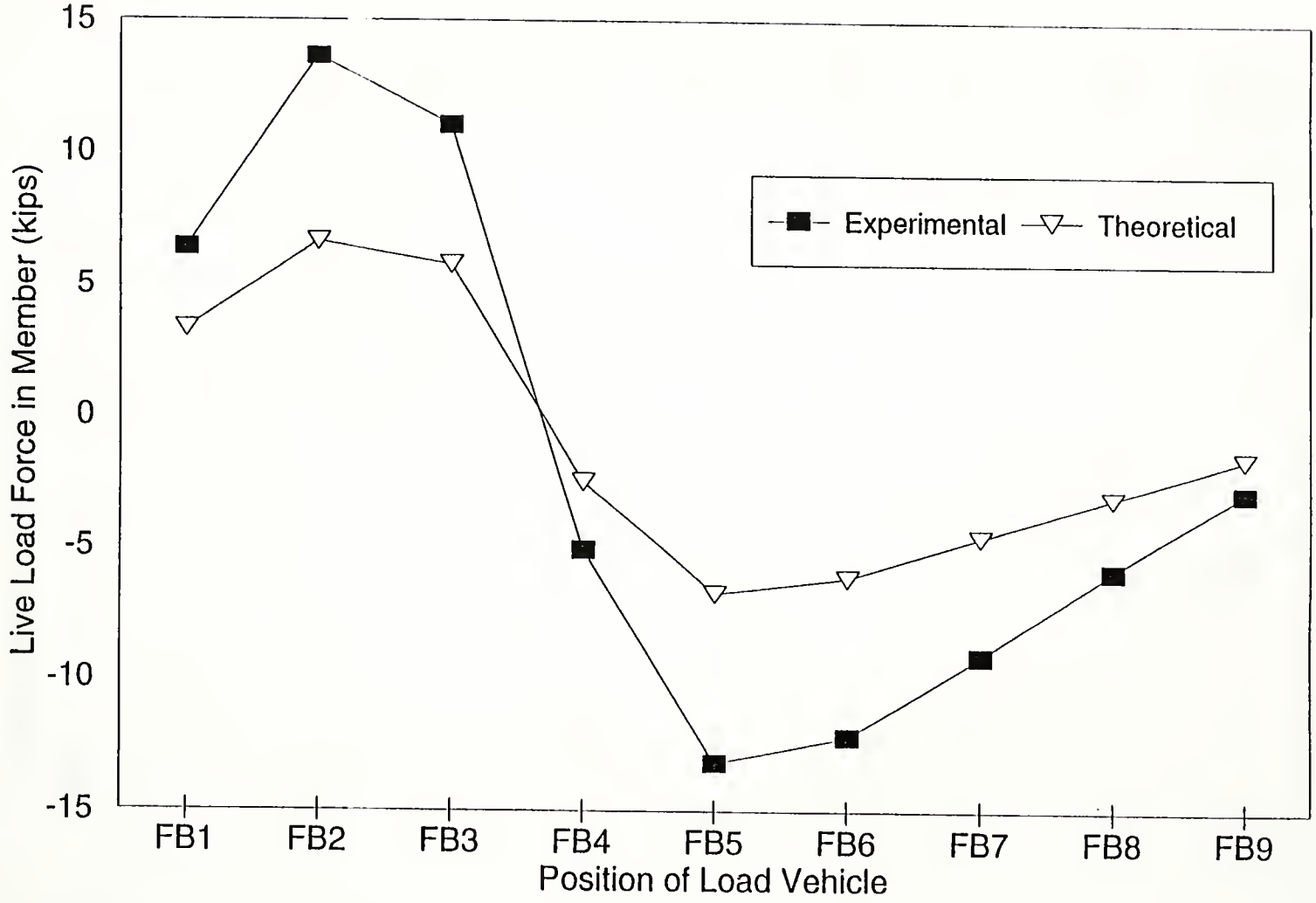

Figure 5.1.2.3.8 Force in member U4L3 for LC #2 - CENTER

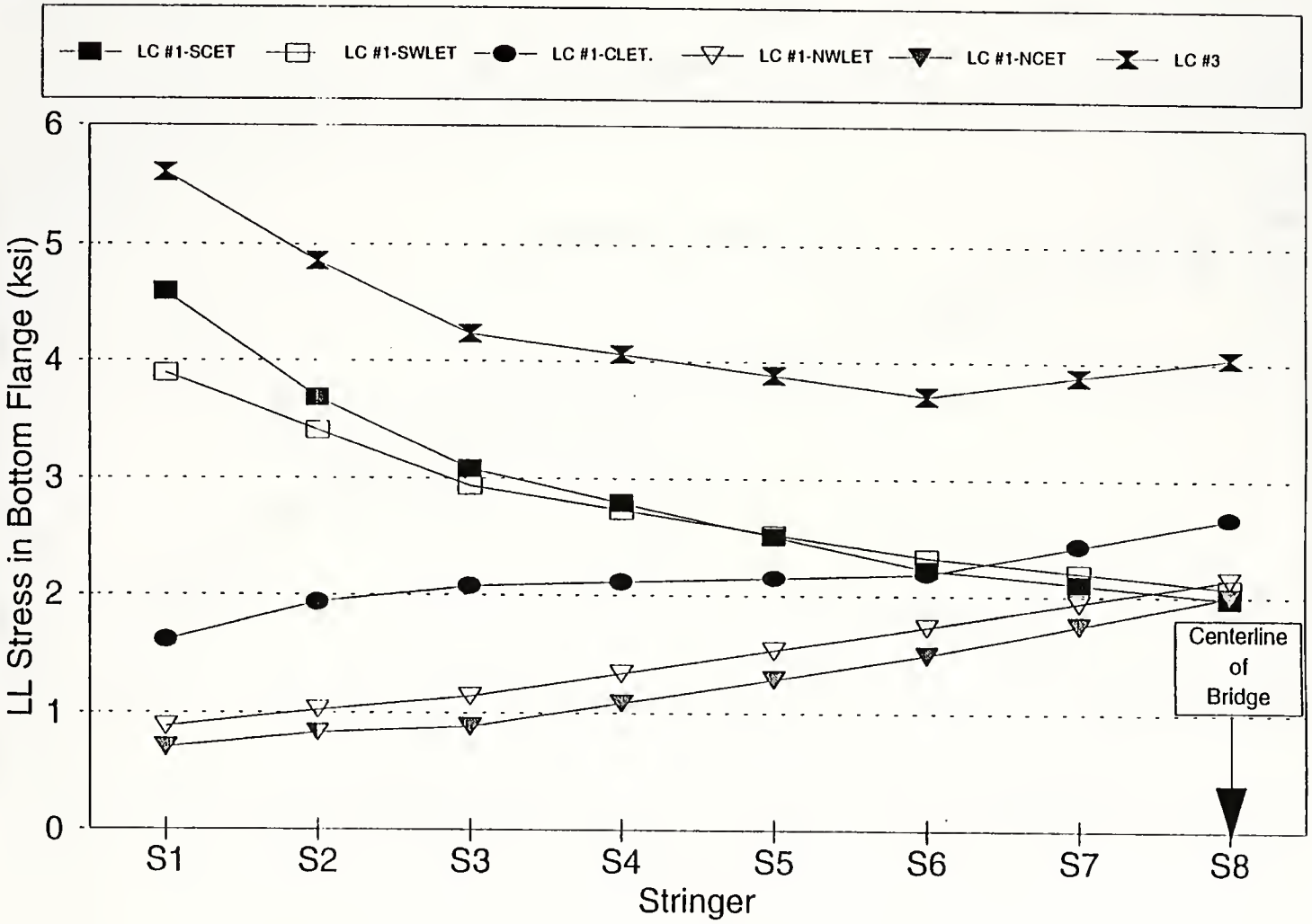

Figure 5.1.3.1.1 Experimental stresses at stringer midspans for transverse position: MS-P3

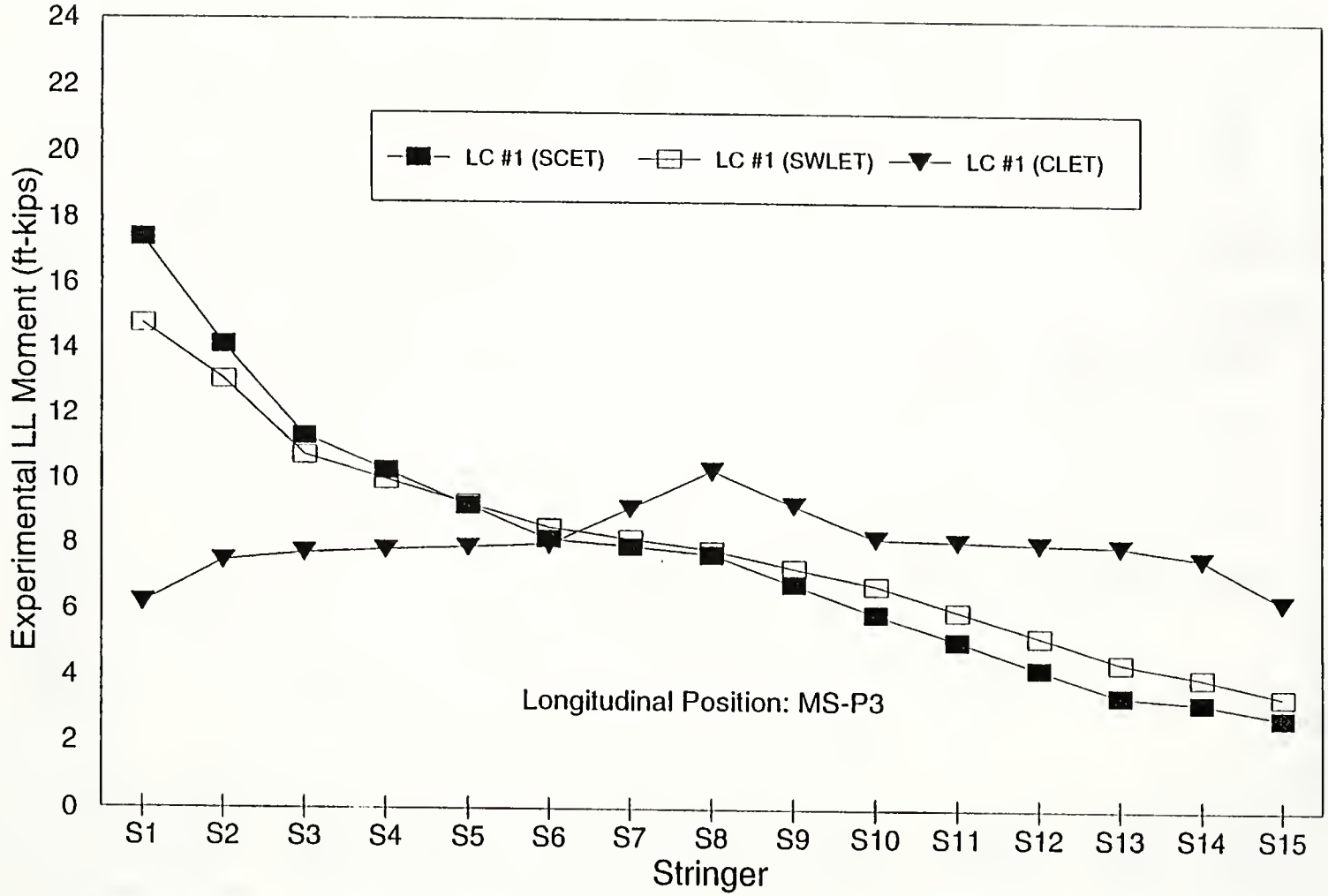

Figure 5.1.3.2.1 Experimental midspan moments in stringers for LC #1 (East facing trucks)

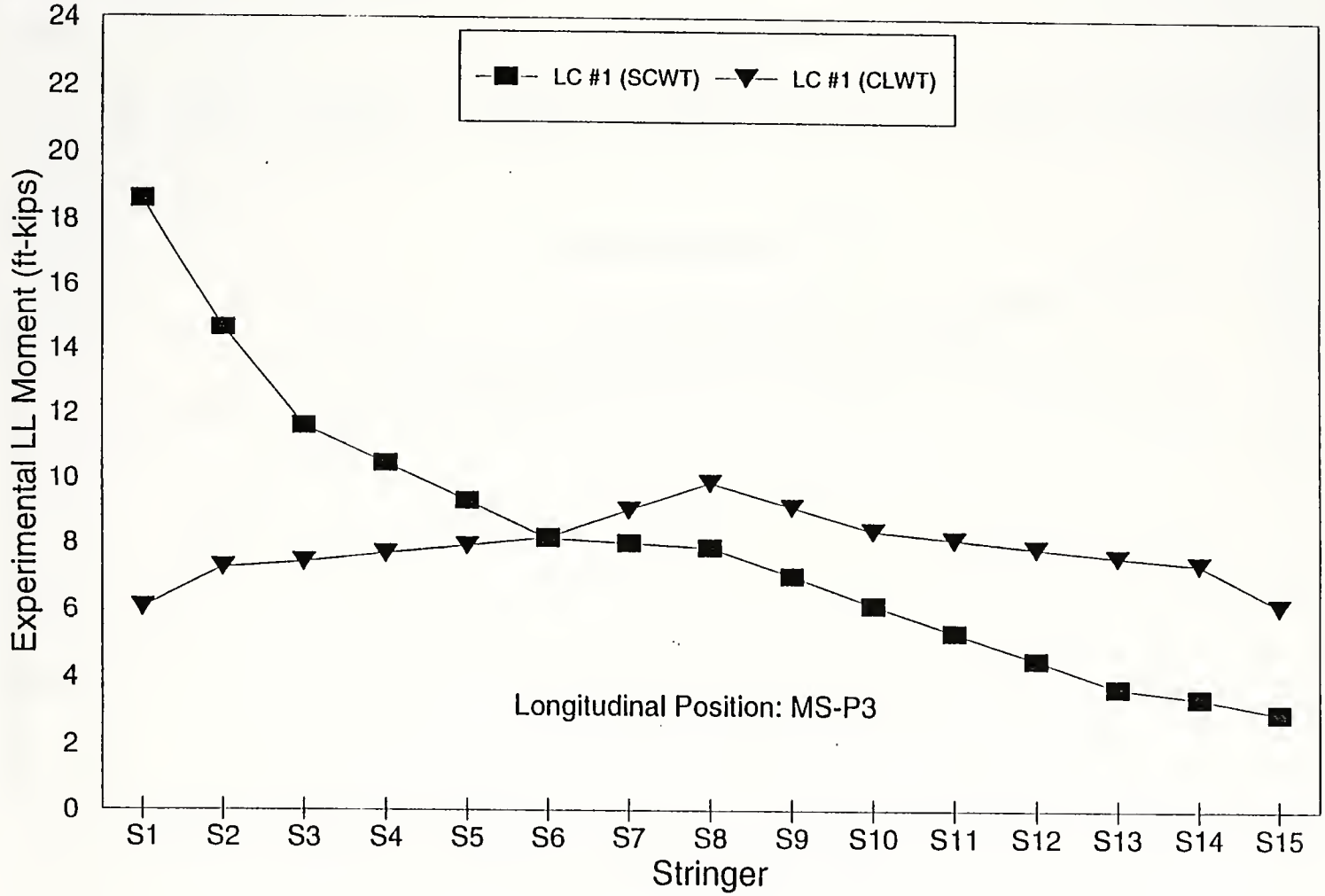

Figure 5.1.3.2.2 Experimental midspan moments in stringers for LC #1 (West facing trucks)

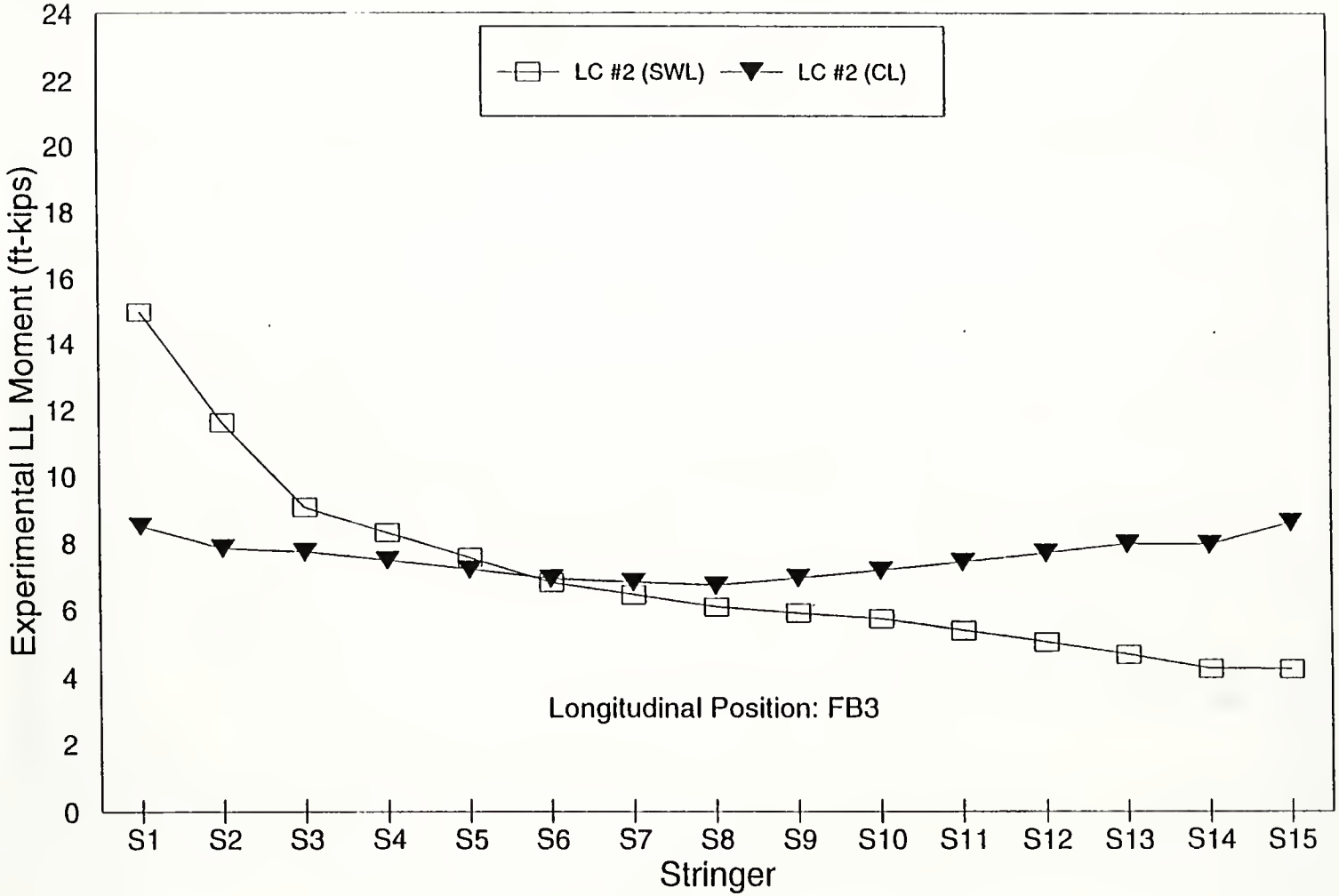

Figure 5.1.3.2.3 Experimental midspan moments in stringers for LC #2

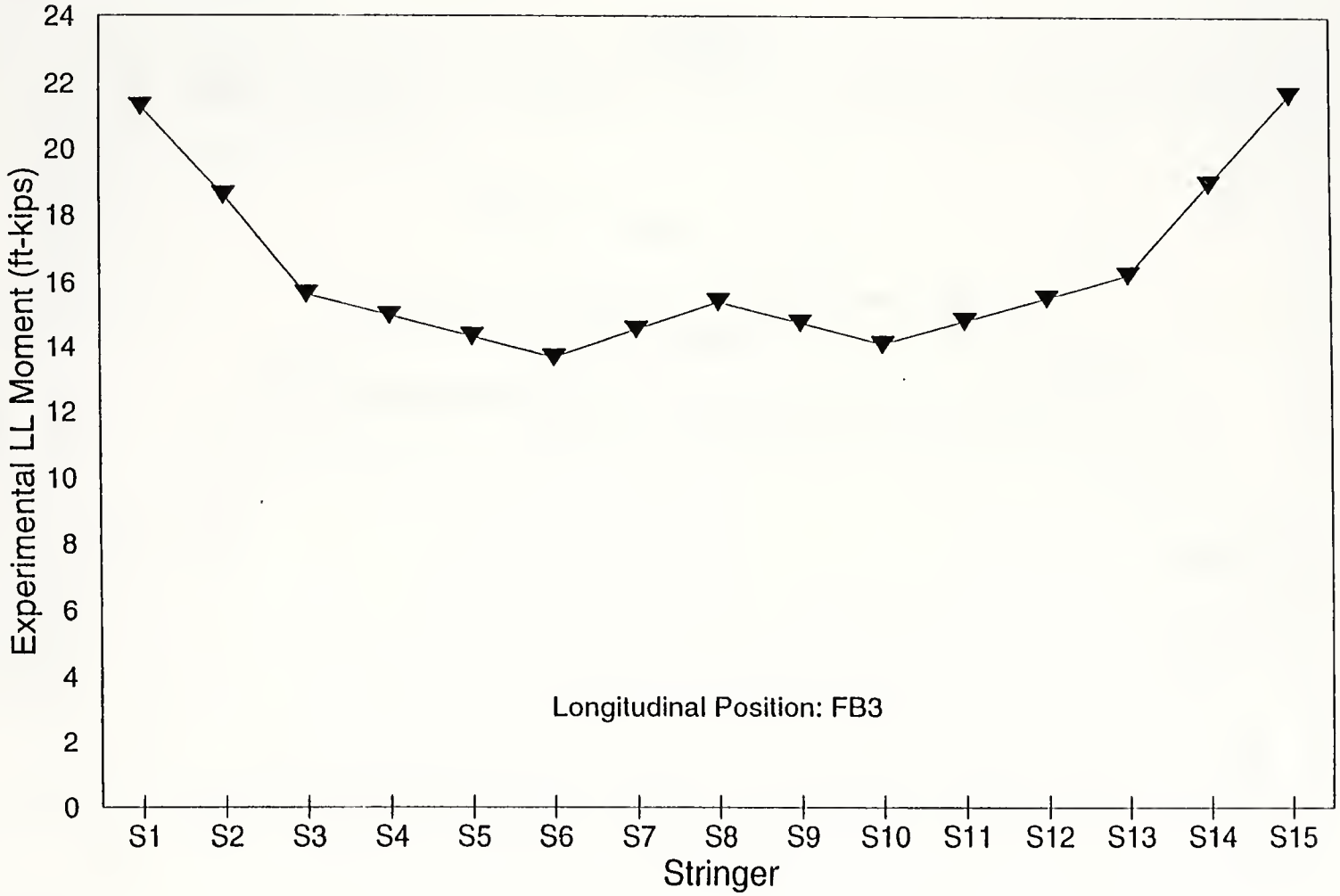

Figure 5.1.3.2.4 Experimental midspan moments in stringers for LC #3

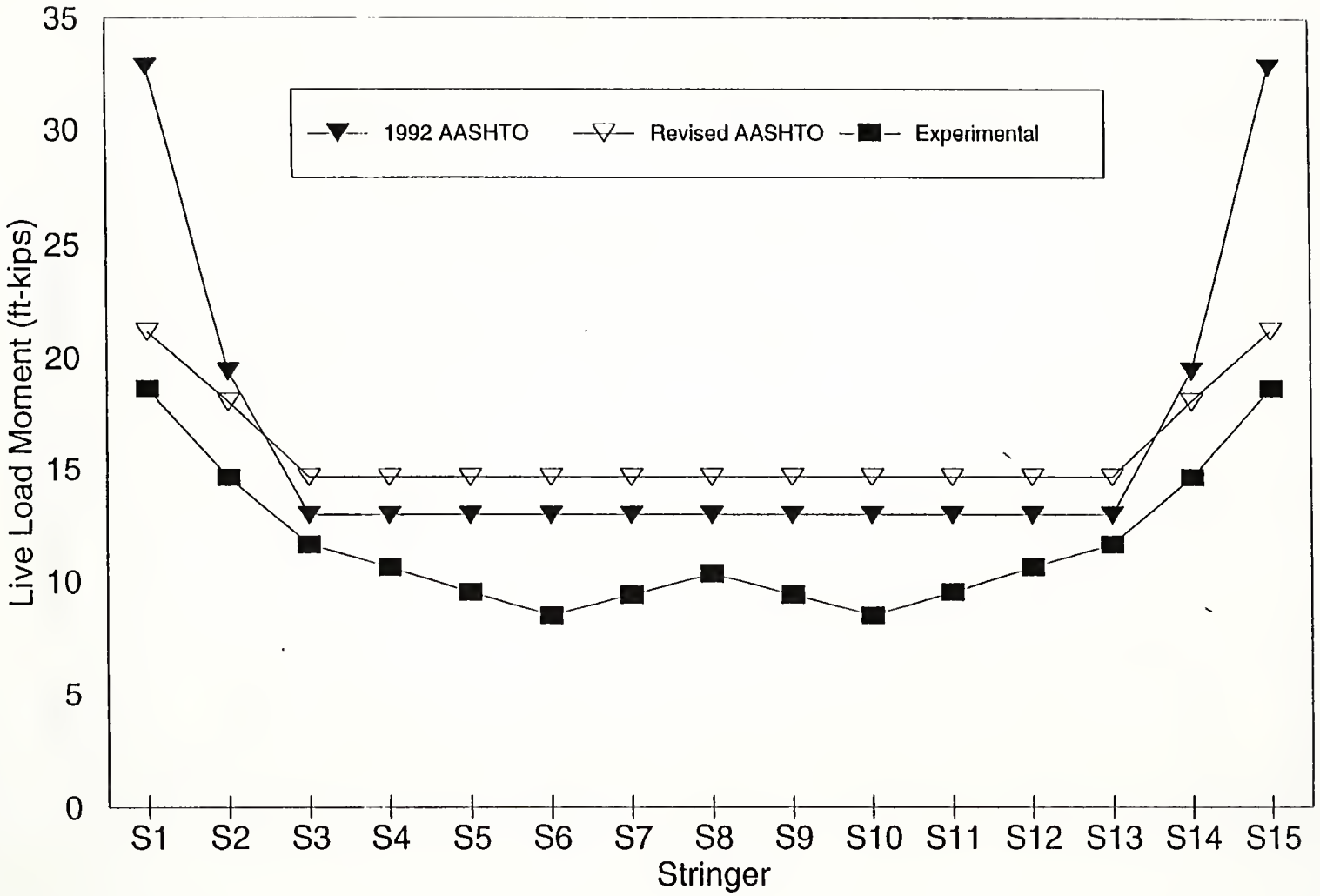

Figure 5.1.3.2.5 Maximum midspan stringer moments

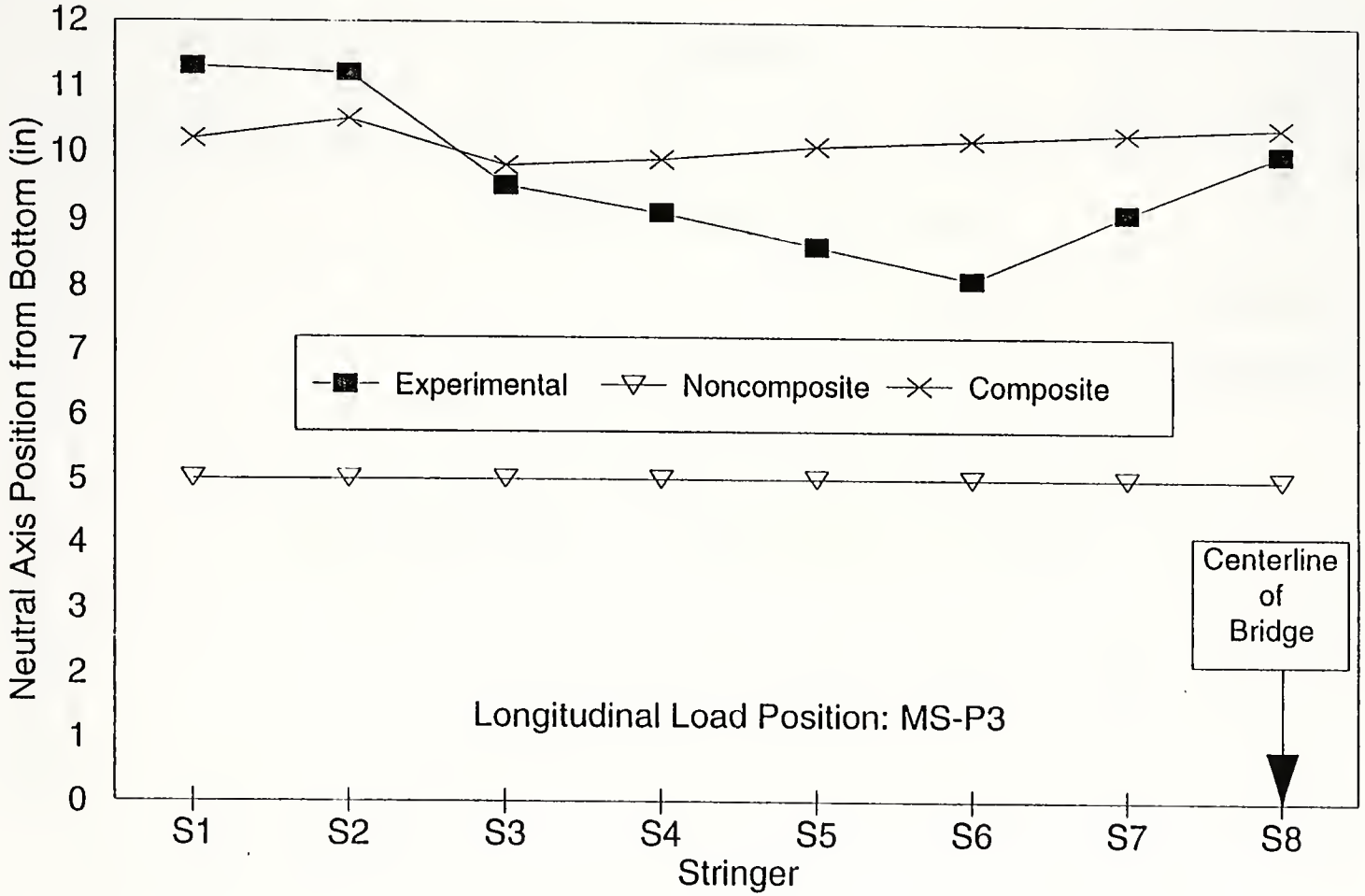

Figure 5.1.3.3.1 Stringer Neutral Axis Positions for LC #1 - SCET

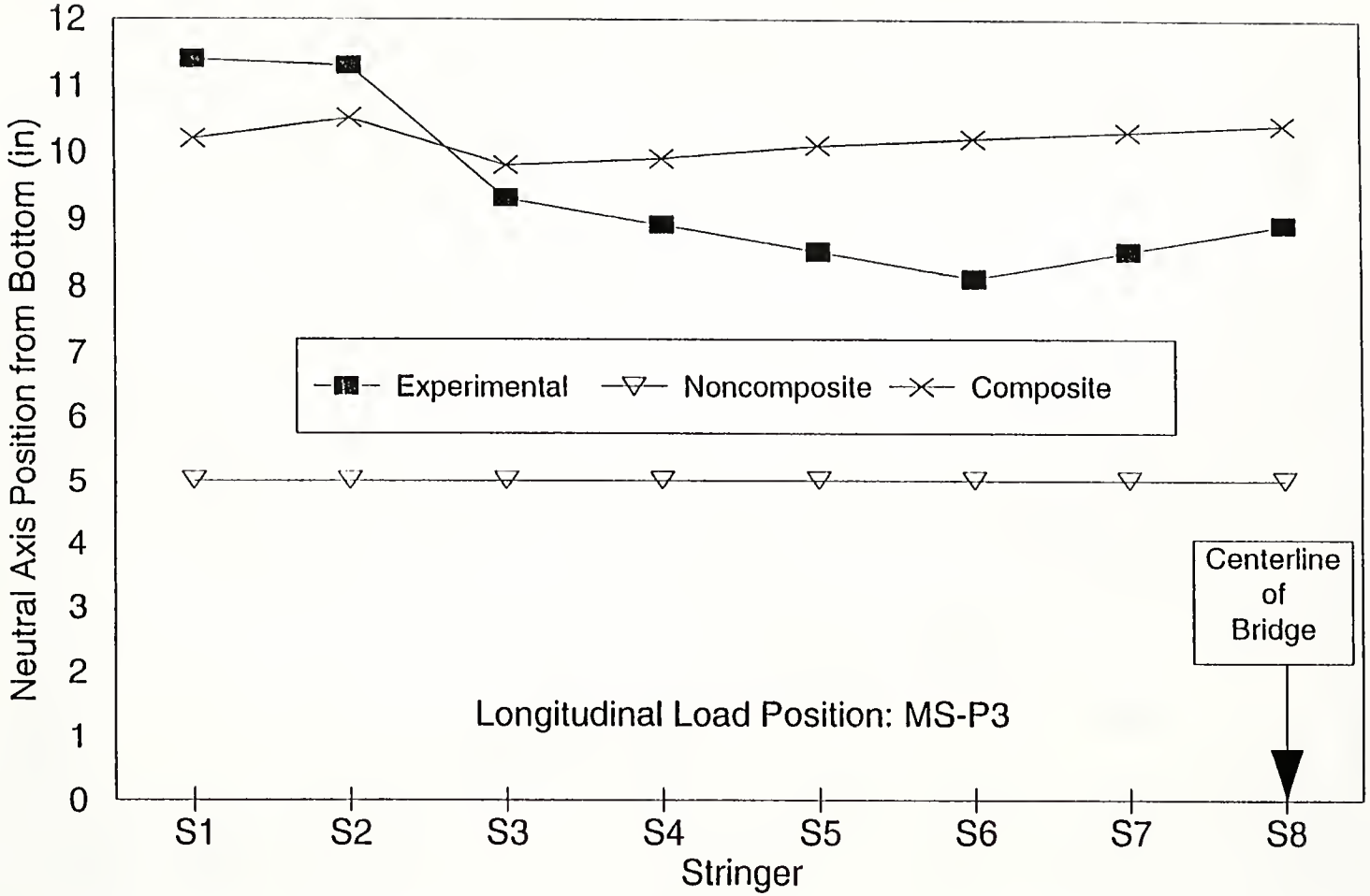

Figure 5.1.3.3.2 Stringer Neutral Axis Positions for LC #1 - SWLET

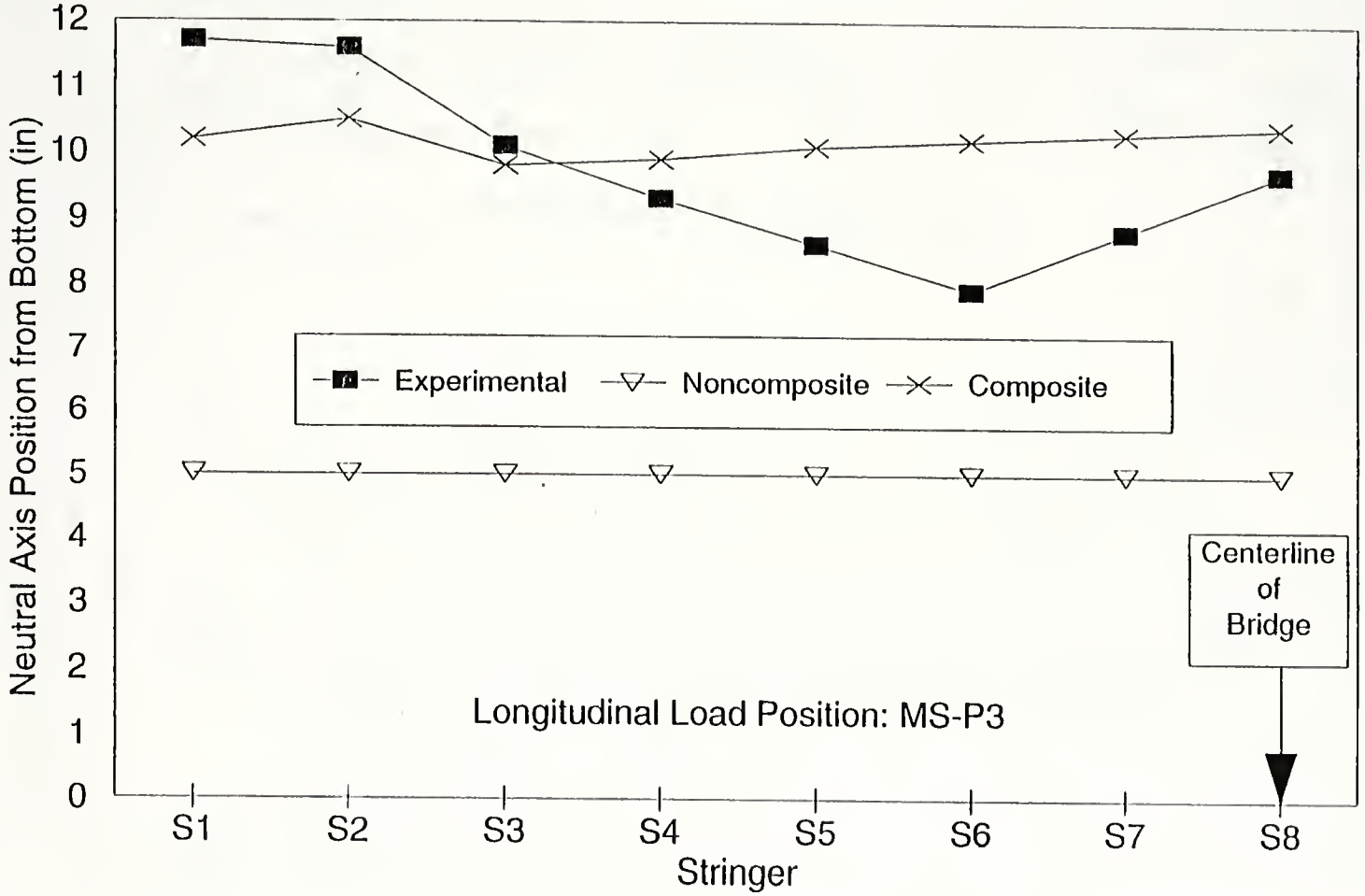

Figure 5.1..3.3.3 Stringer Neutral Axis Positions for LC #1 - CLET

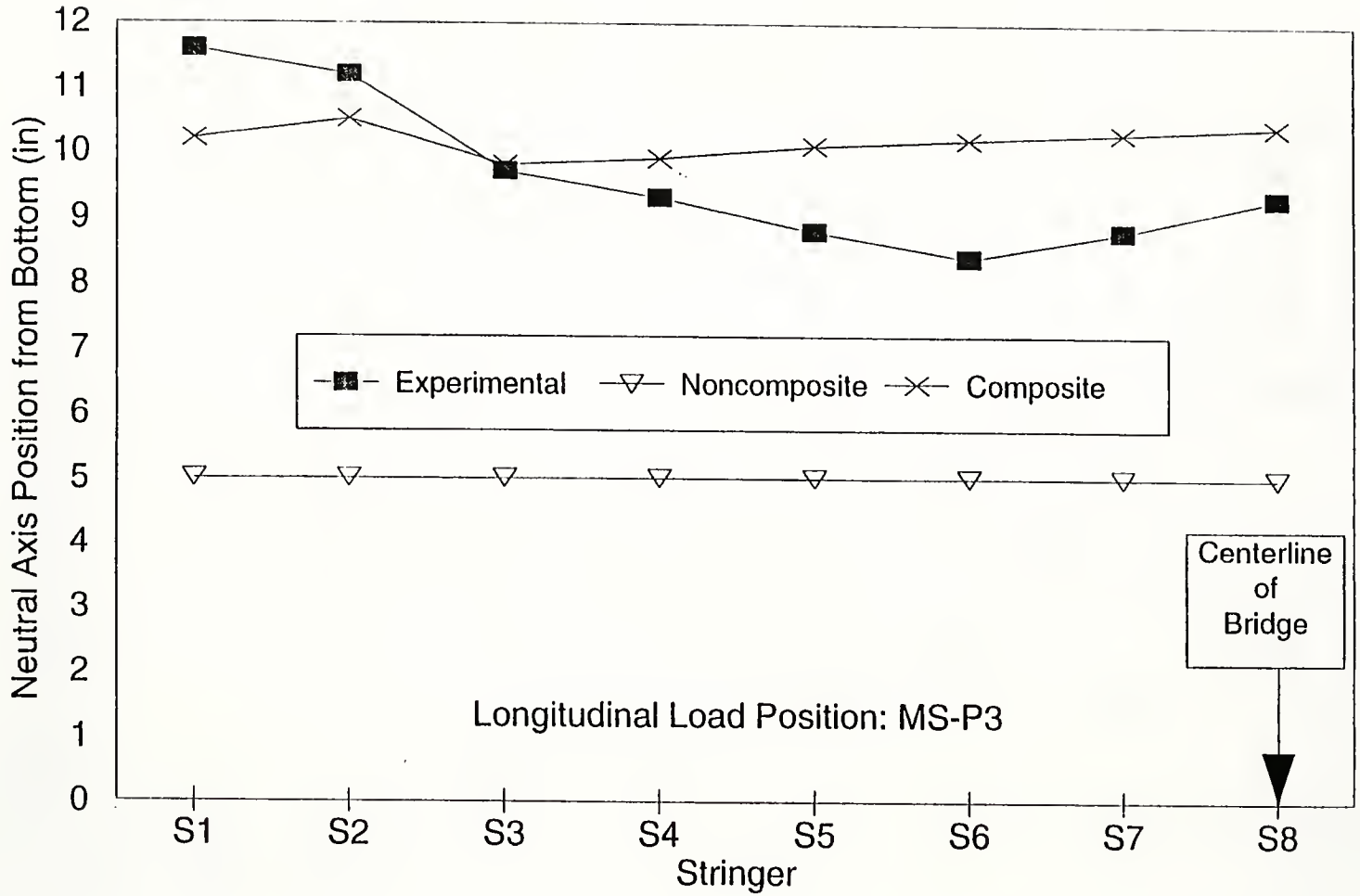

Figure 5.1.3.3.4 Stringer Neutral Axis Positions for LC #3

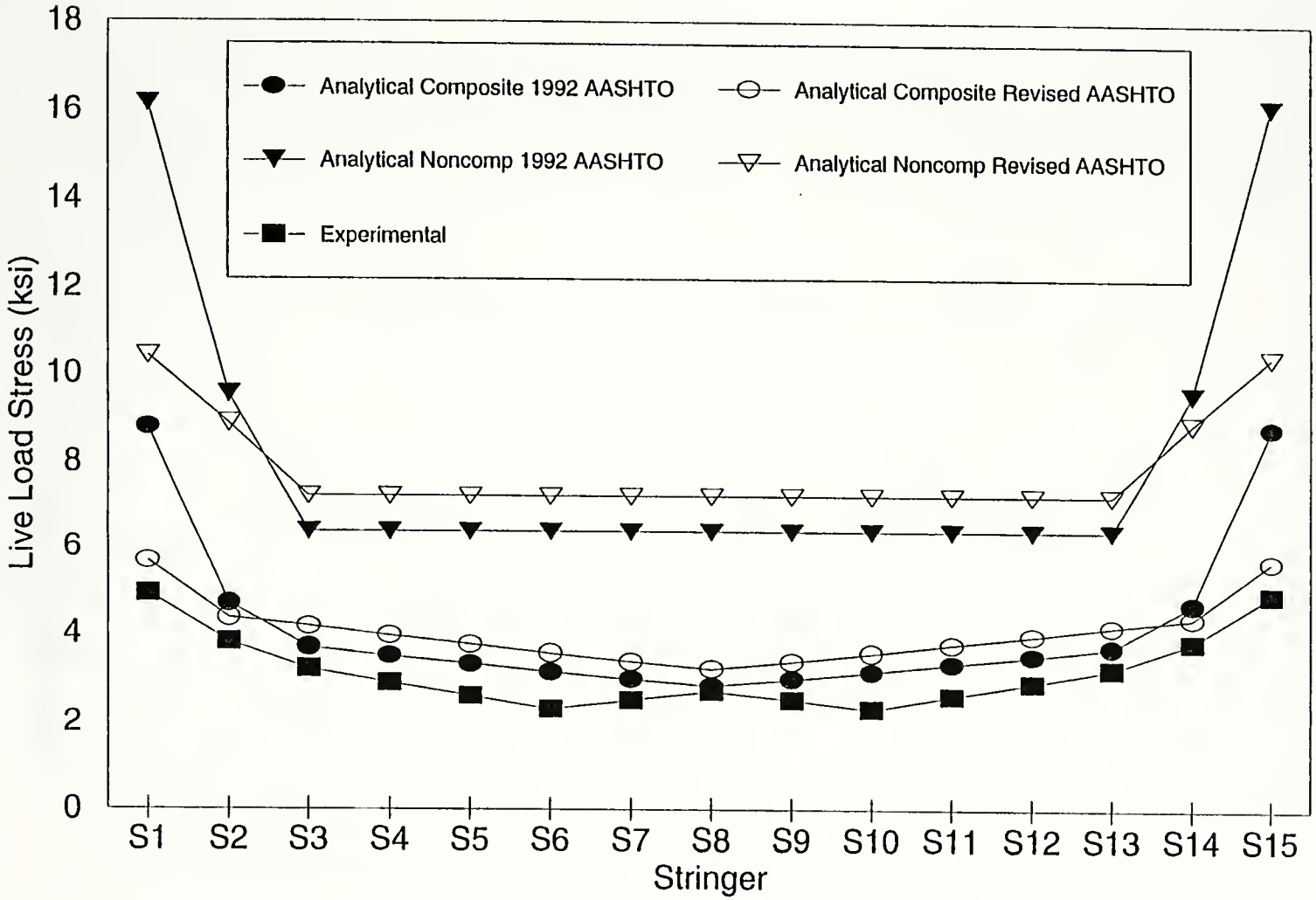

Figure 5.1.3.3.5 Maximum midspan stringer stresses

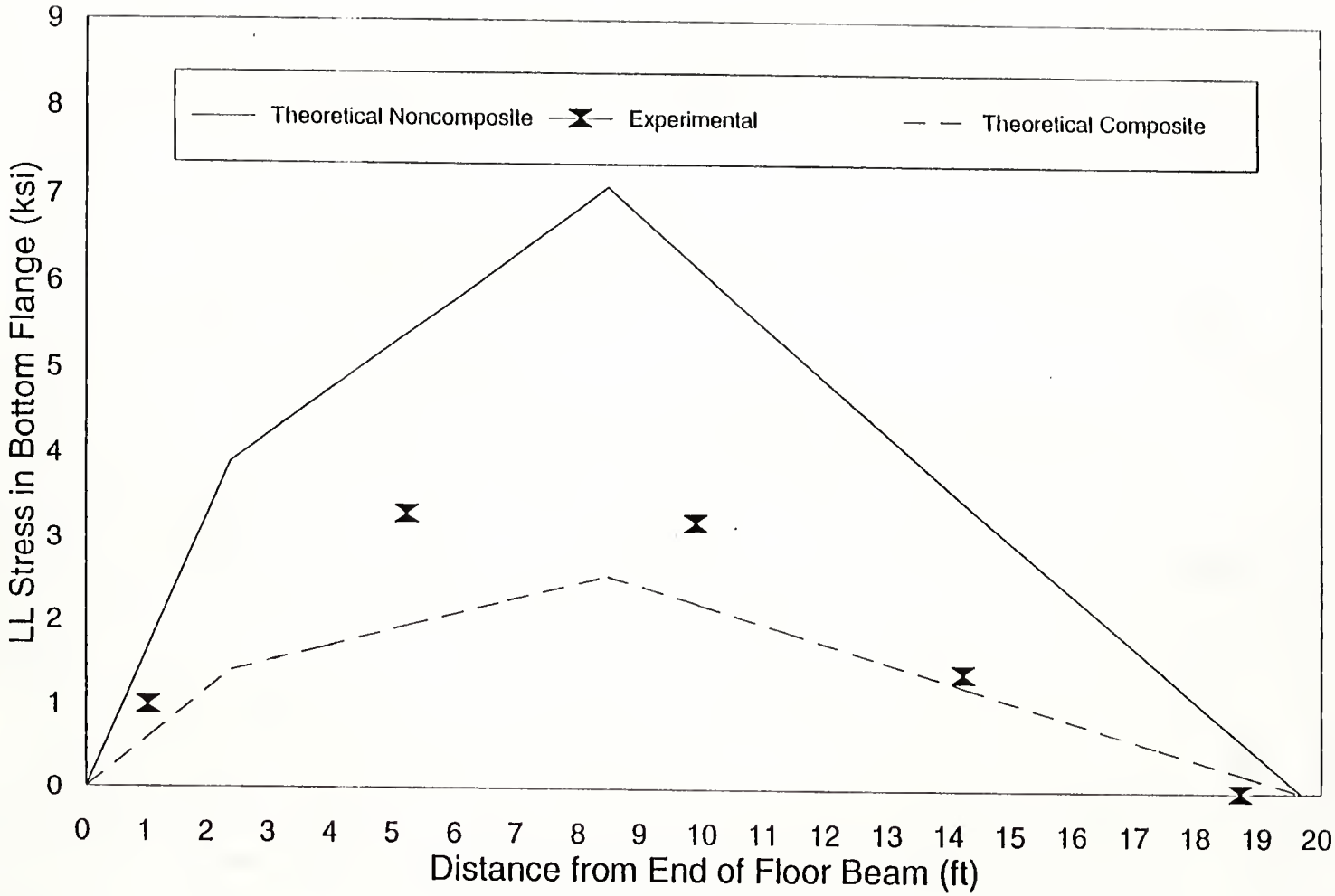

Figure 5.1.4.2.1 Stress in FB2 for LC #1 - SCET - FB2

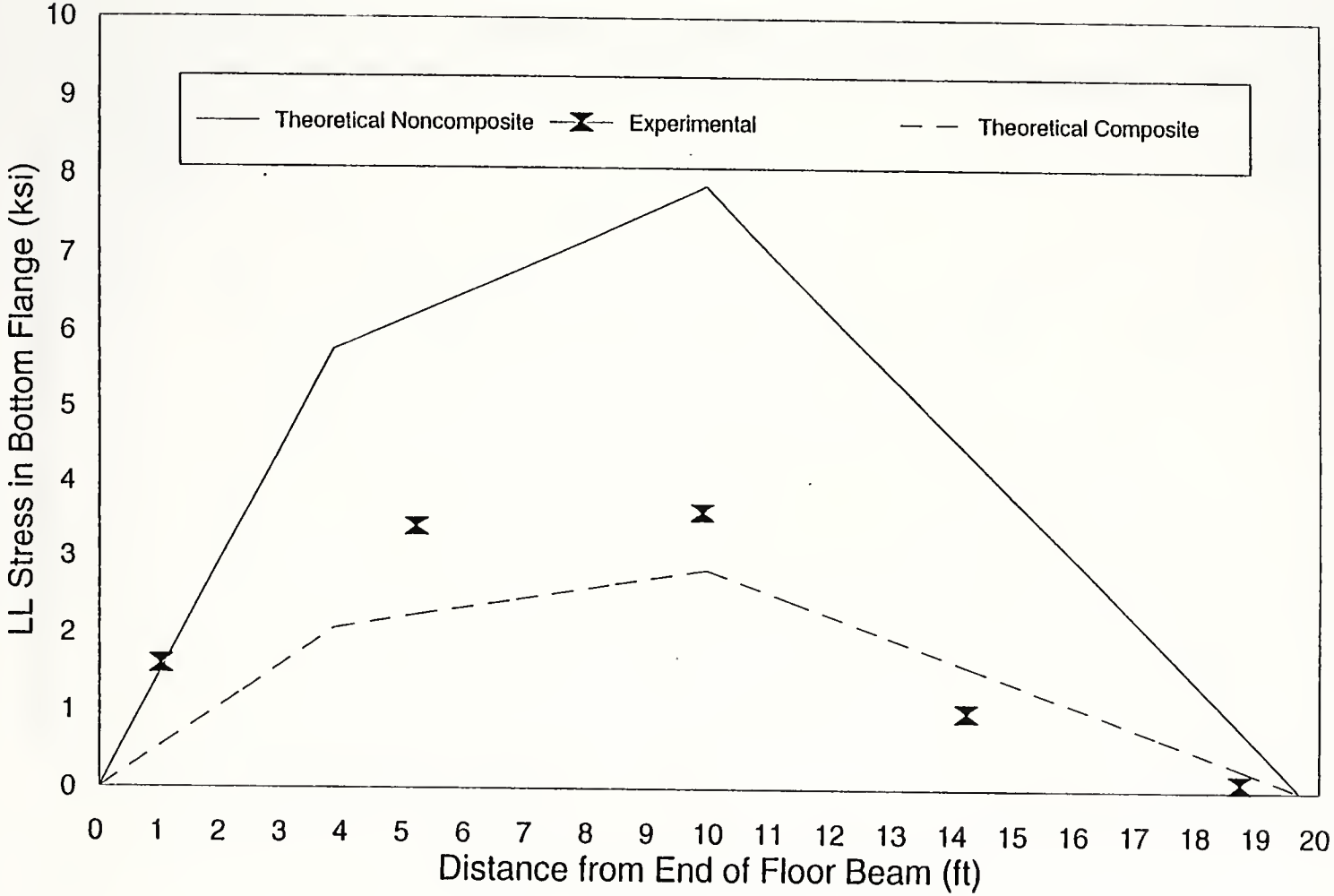

Figure 5.1.4.2.2 Stress in FB2 for LC #1 - SWLET - FB2

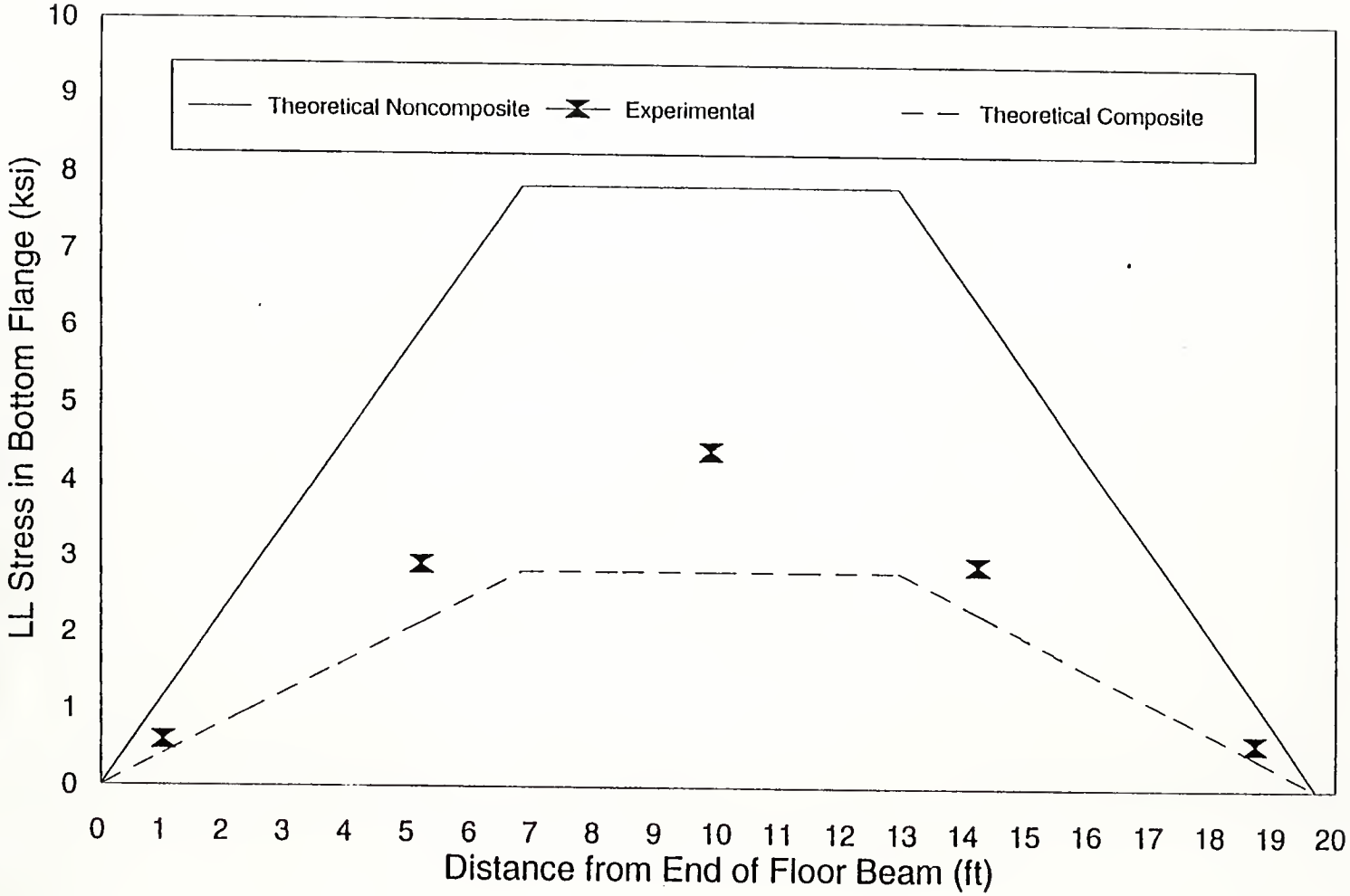

Figure 5.1.4.2.3 Stress in FB2 for LC #1 - CLET - FB2

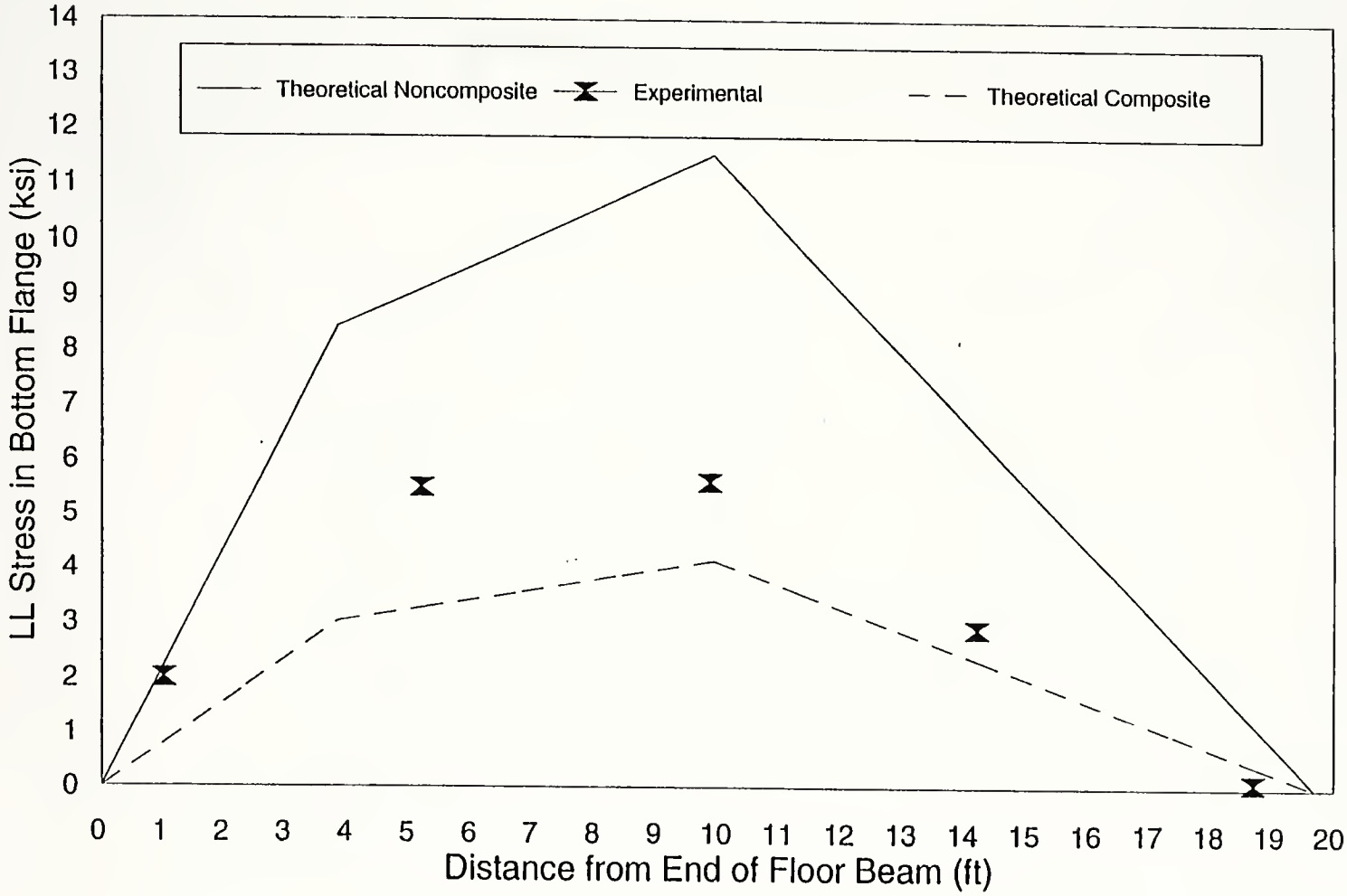

Figure 5.1.4.2.4 Stress in FB2 for LC #2 - SOUTH - FB2

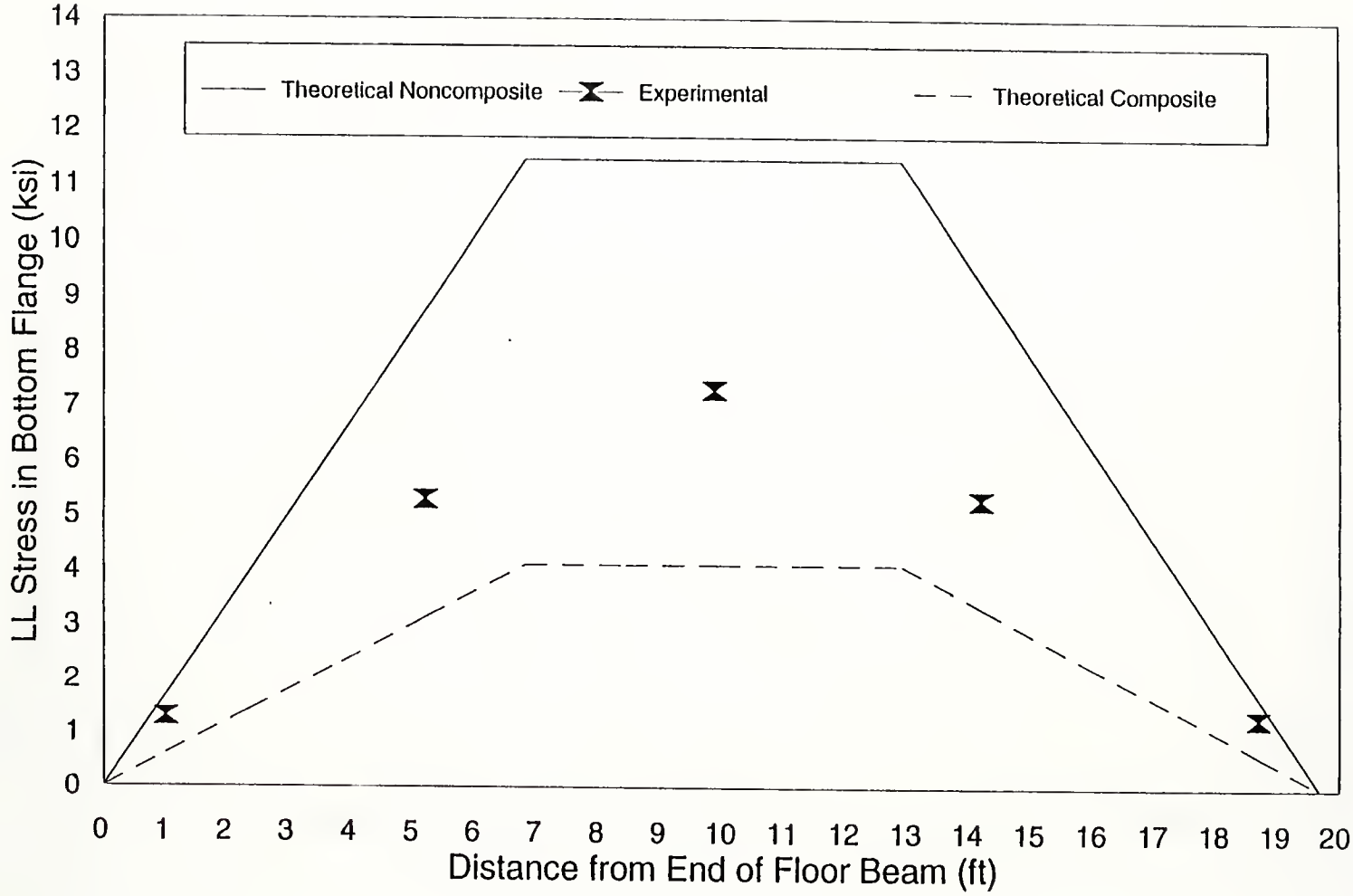

Figure 5.1.4.2.5 Stress in FB2 for LC #2 - CENTER - FB2

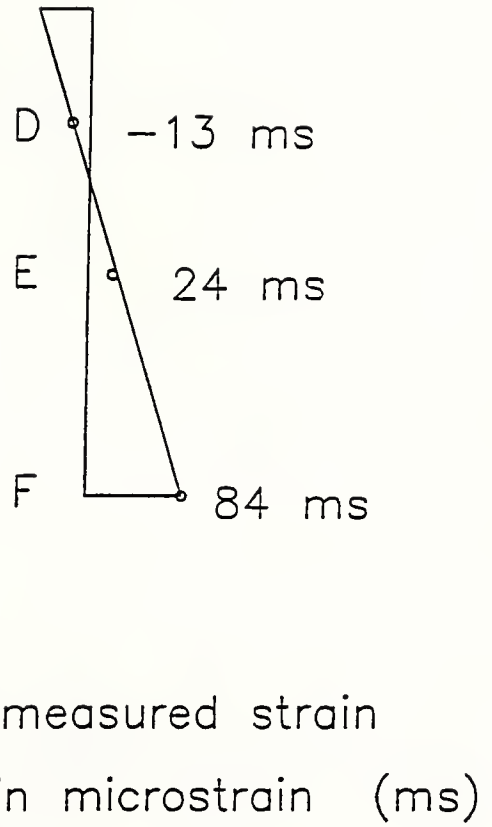

Figure 5.2.1.1 Typical assumed stringer strain distribution

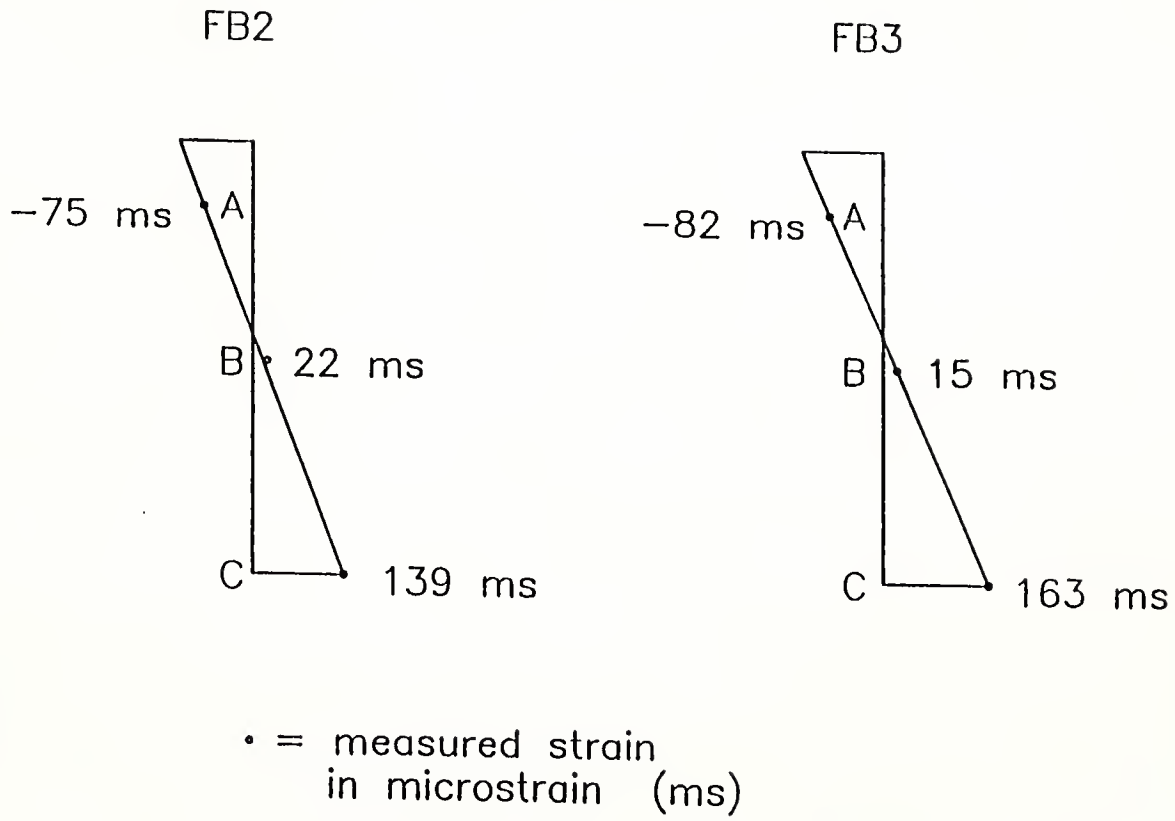

Figure 5.2.1.2 Typical assumed floor beam strain distribution

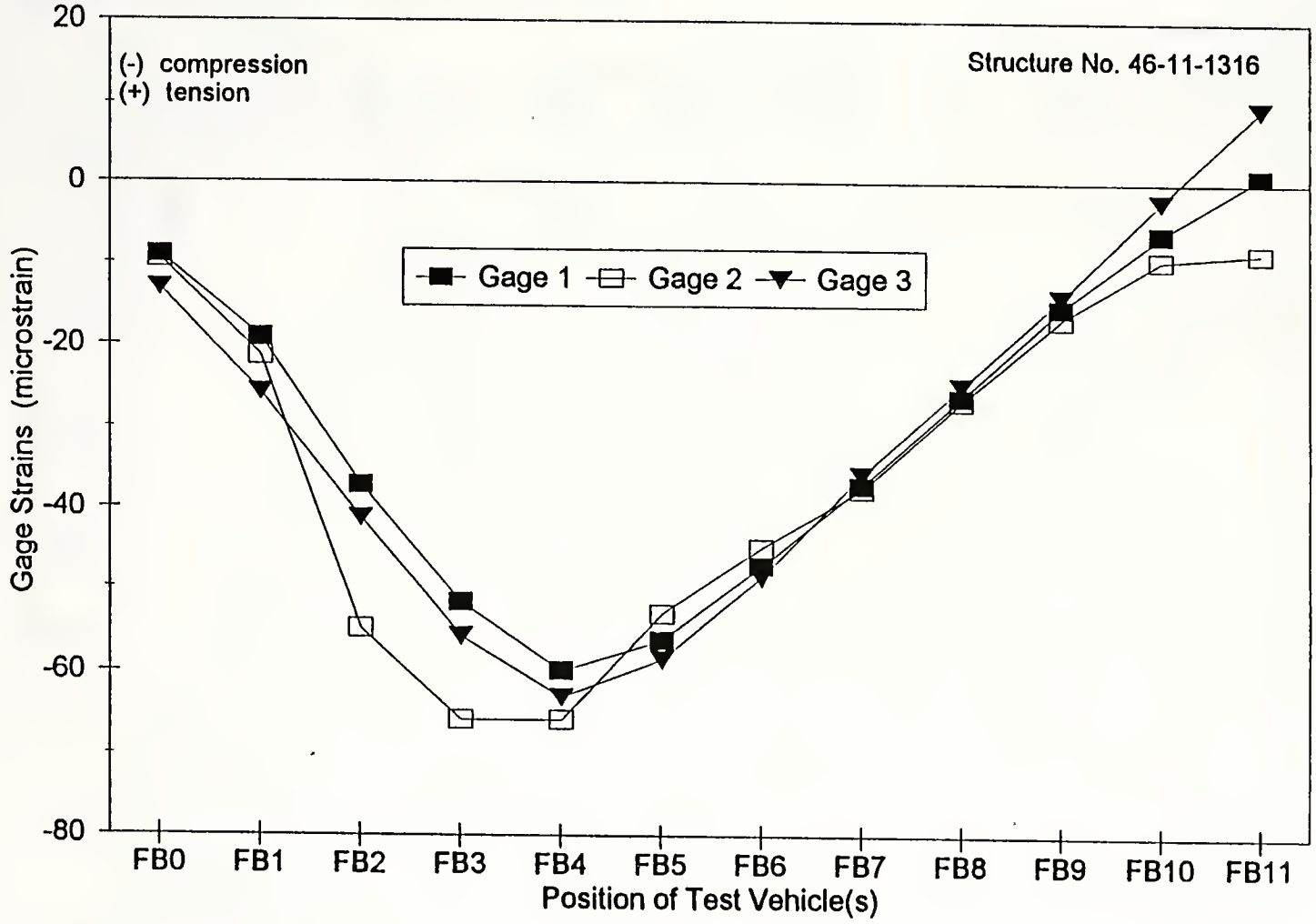

Figure 5.2.2.2.1 Individual gage strains in member U2U3 for LC #2 - Center

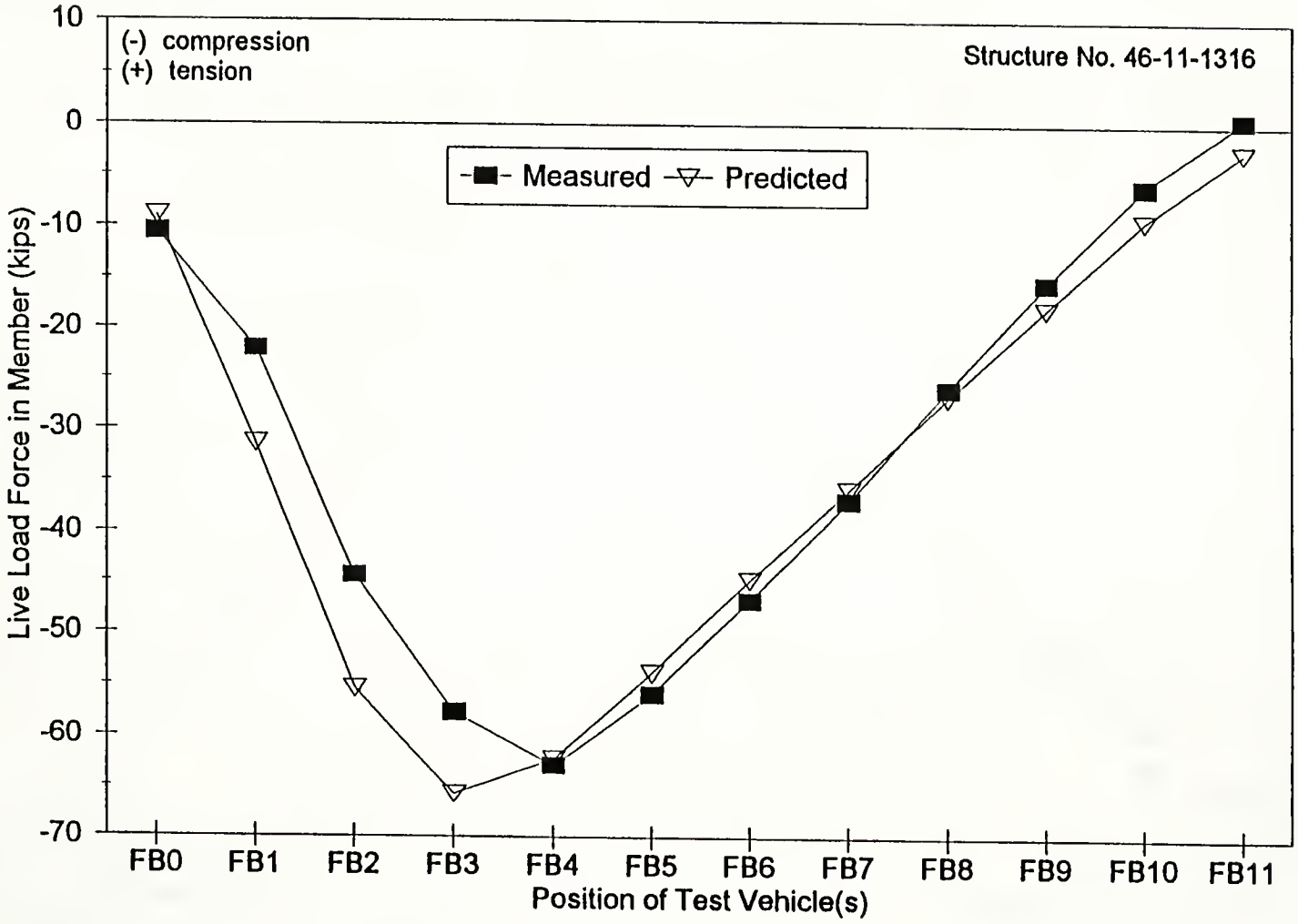

Figure 5.2.2.2.2 Force in member U2U3 for LC #2 - Center

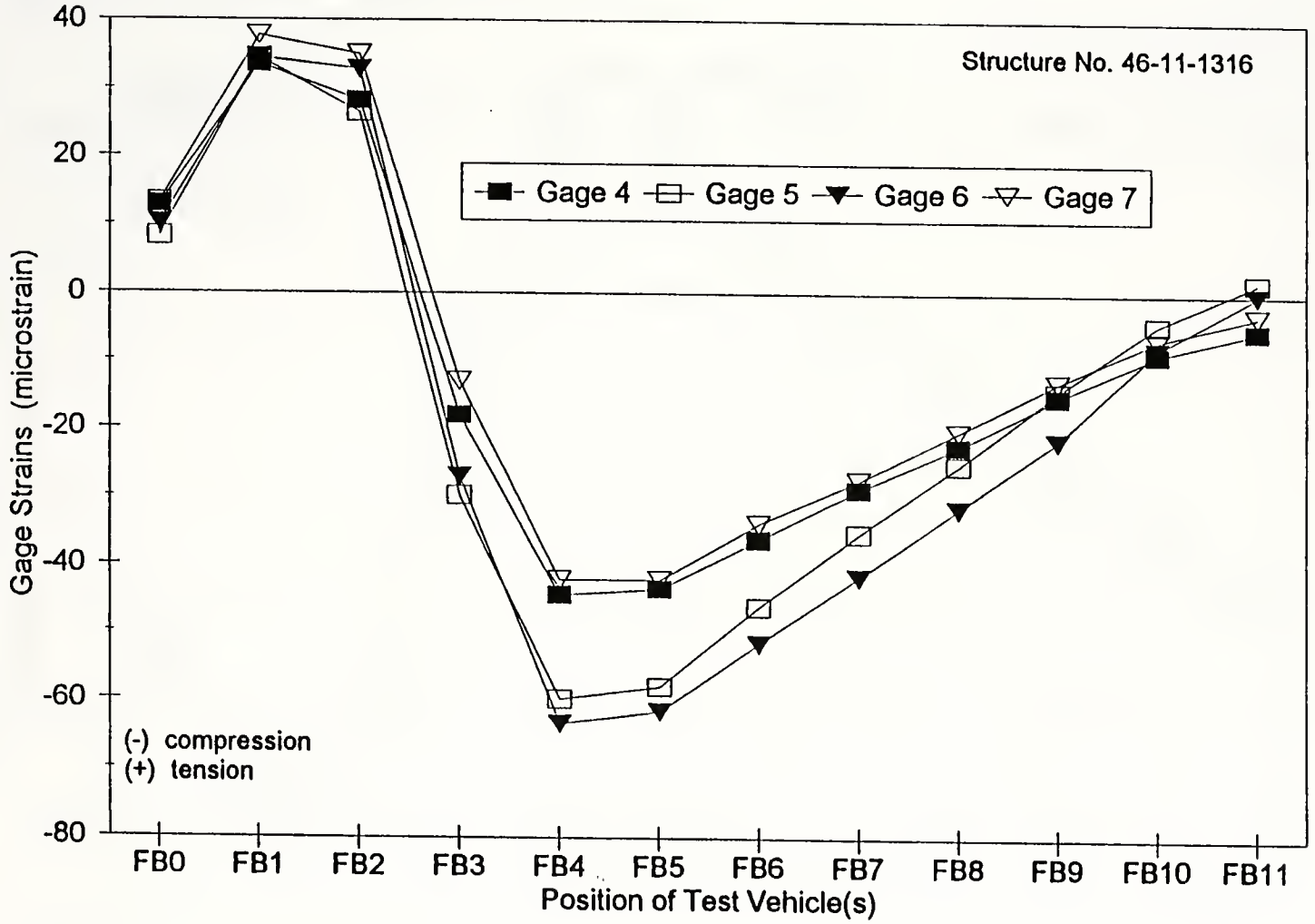

Figure 5.2.2.2.3 Individual gage strains in member L2U2 for LC #2 - Center

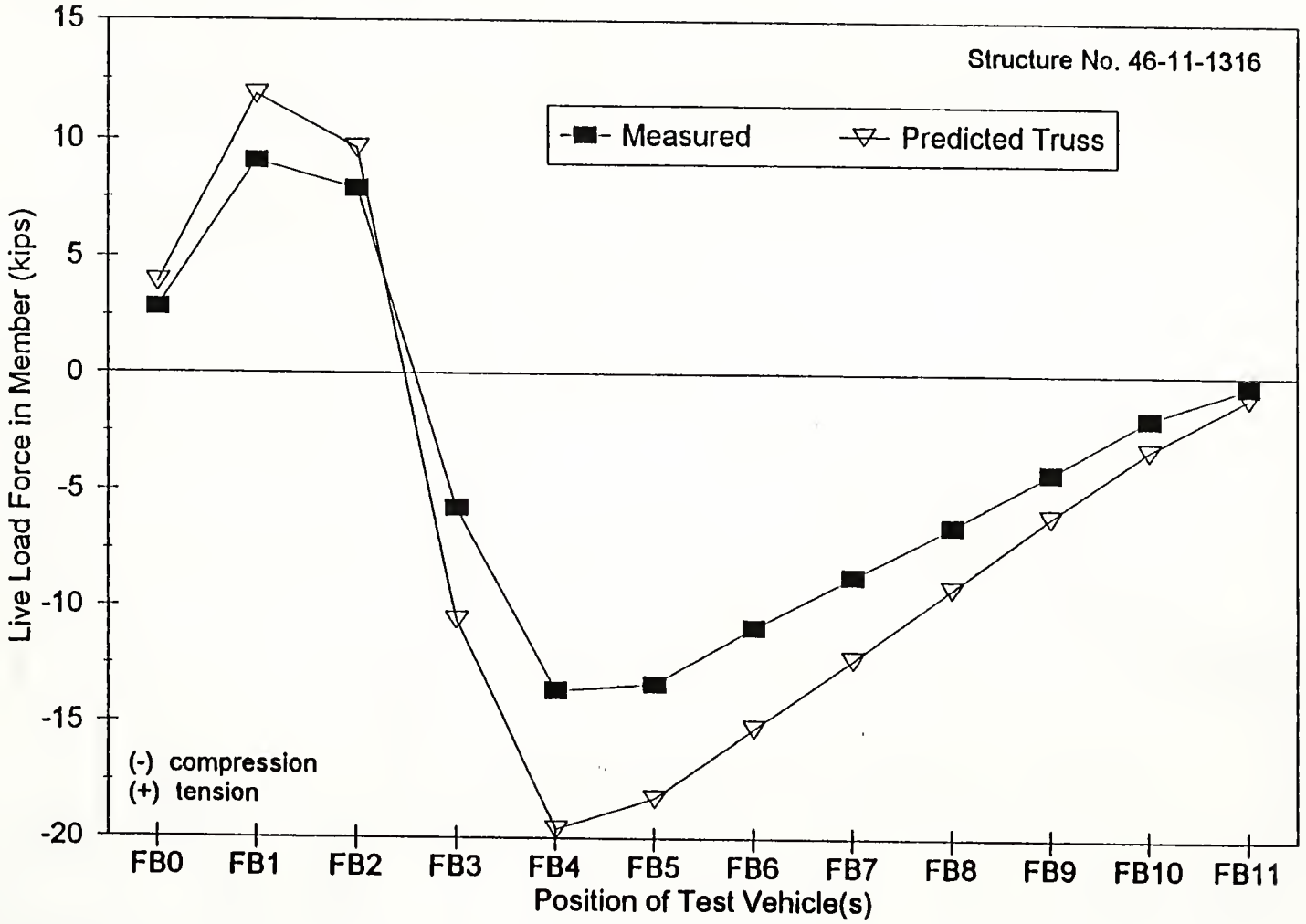

Figure 5.2.2.2.4 Force in member L2U2 for LC #2 - Center

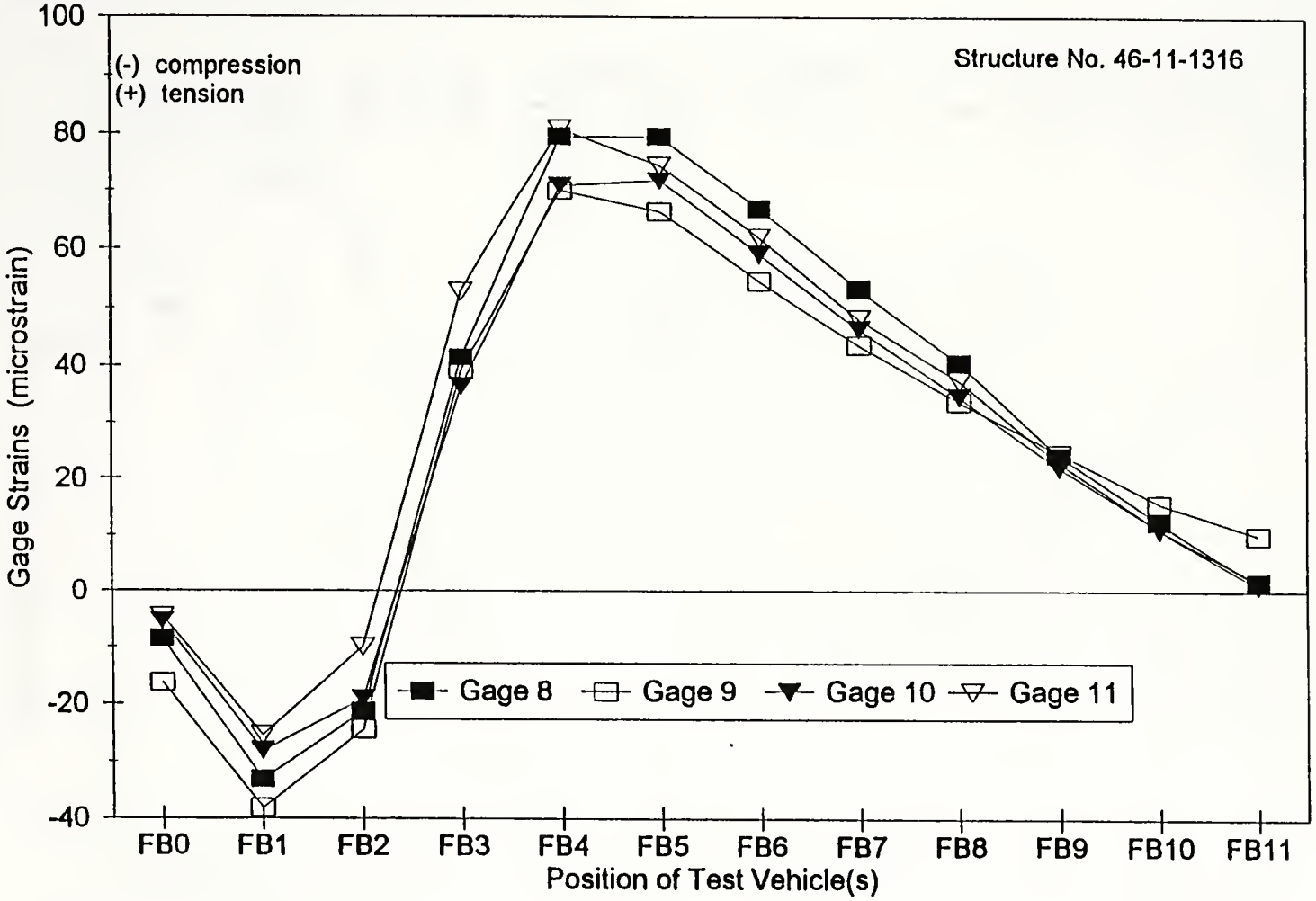

Figure 5.2.2.2.5 Individual gage strains in member U2L3 for LC #2 - Center

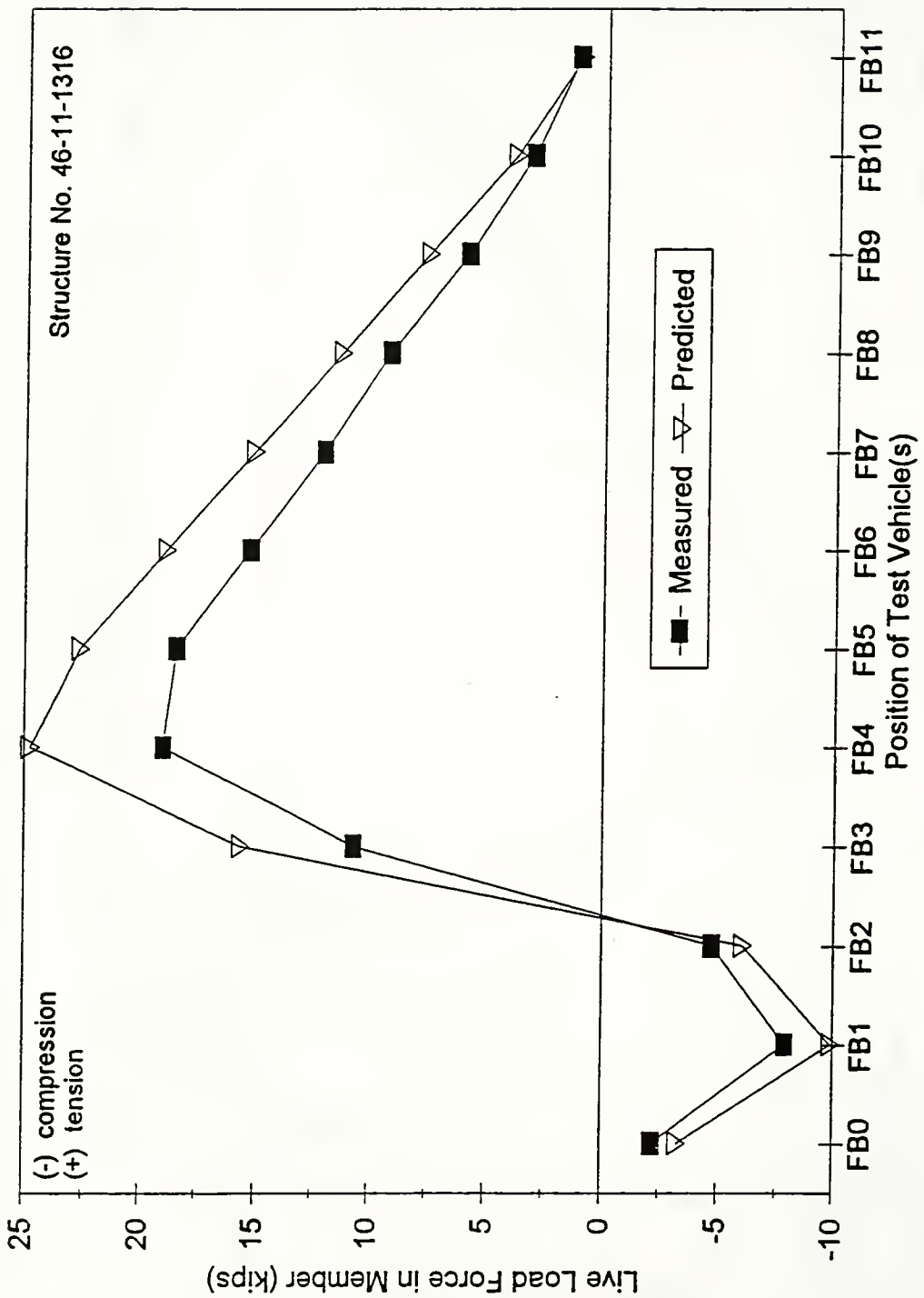

Figure 5.2.2.2.6 Force in member U2L3 for LC #2 - Center

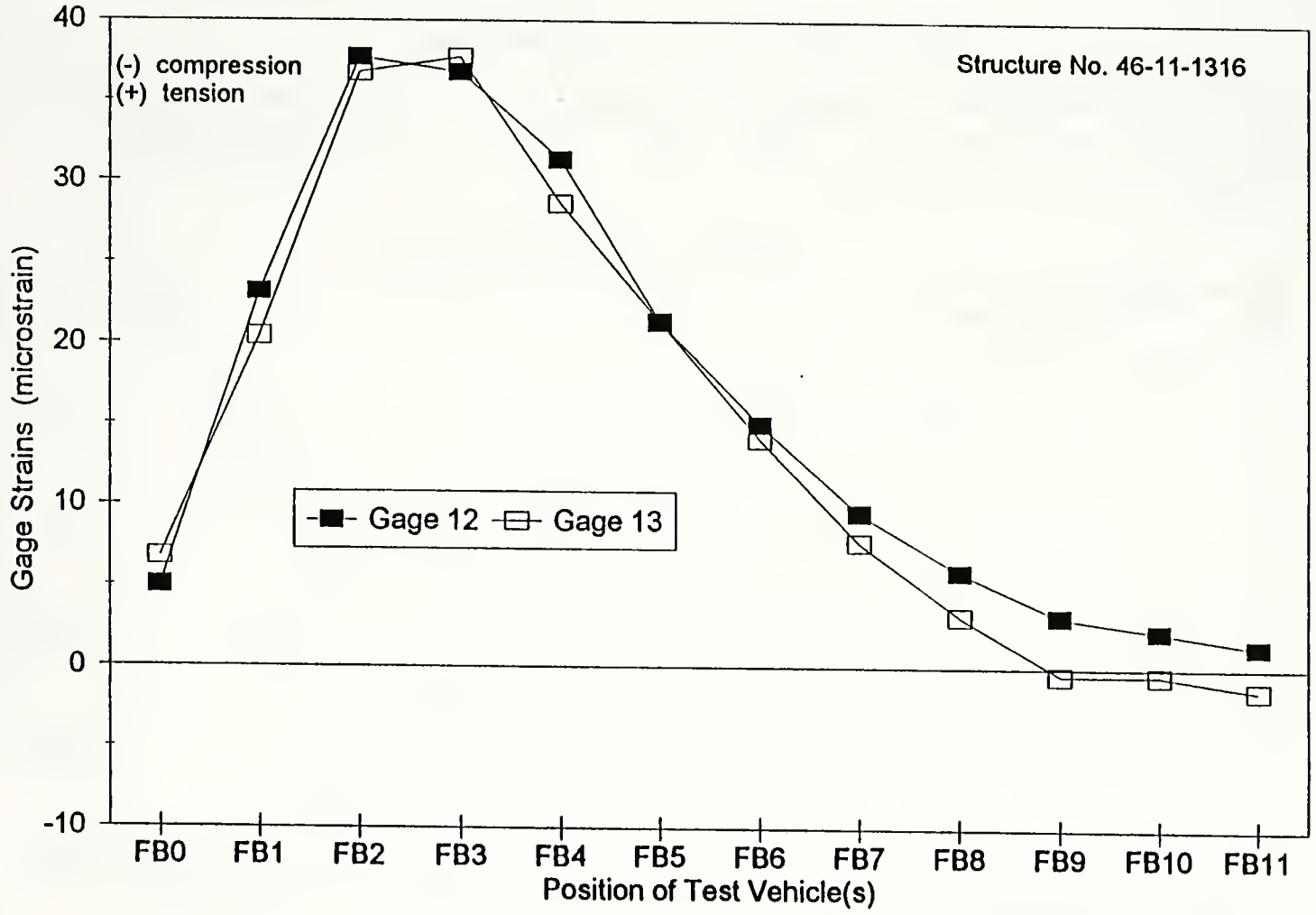

Figure 5.2.2.2.7 Individual gage strains in member L2L3 for LC #2 - Center

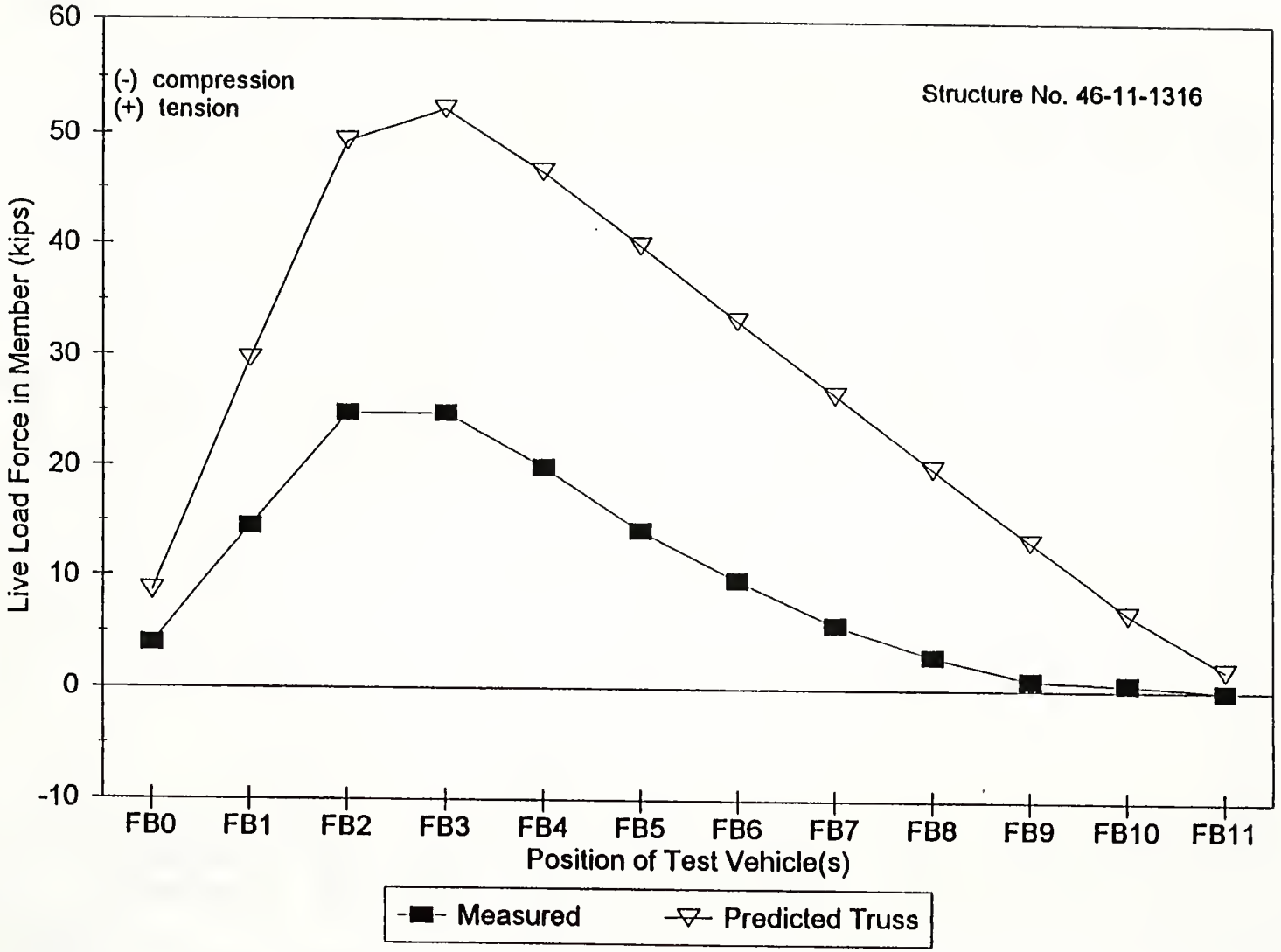

Figure 5.2.2.2.8 Force in member L2L3 for LC #2 - Center

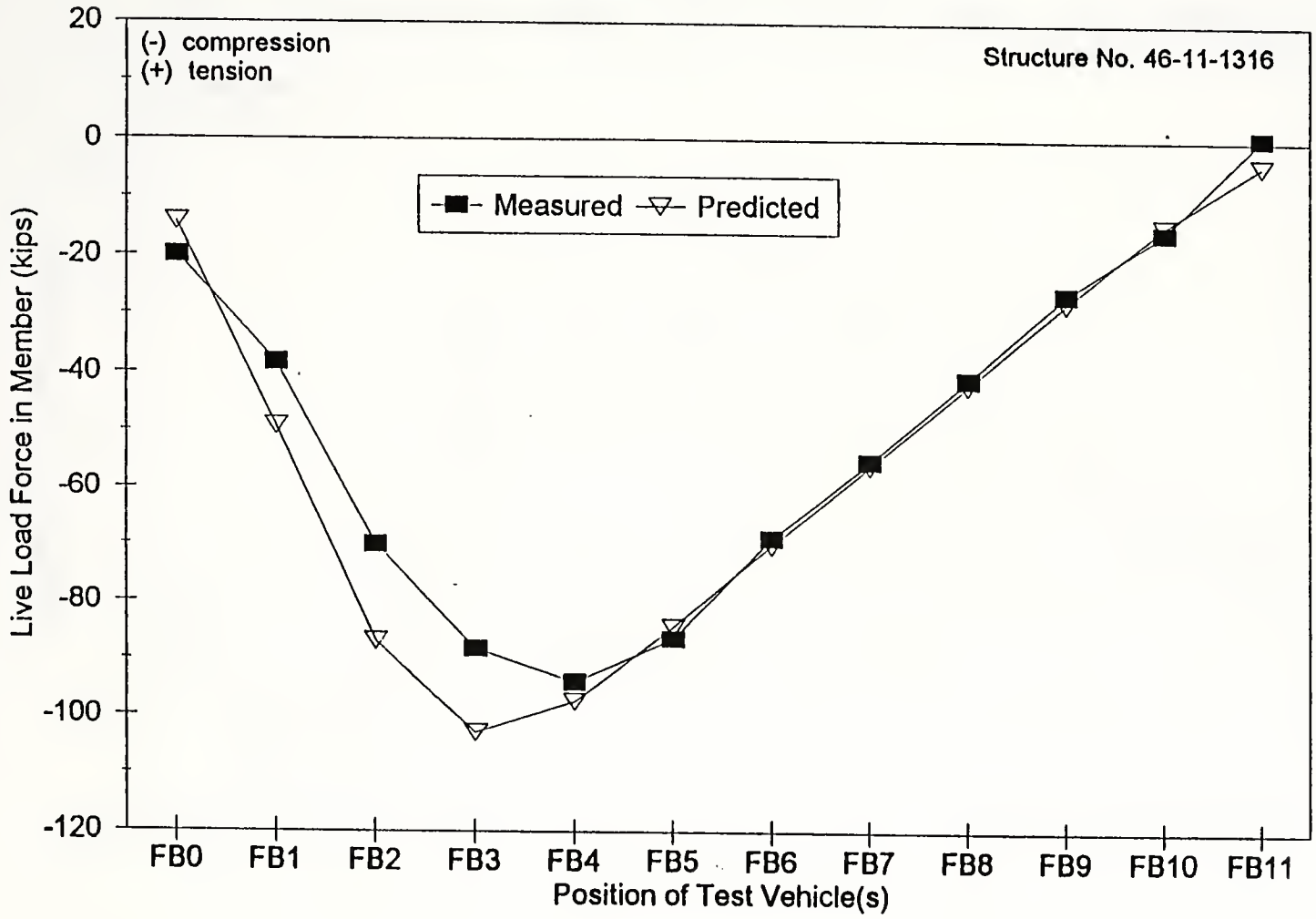

Figure 5.2.2.3.1 Force in member U2U3 for loading Condition #2 - North

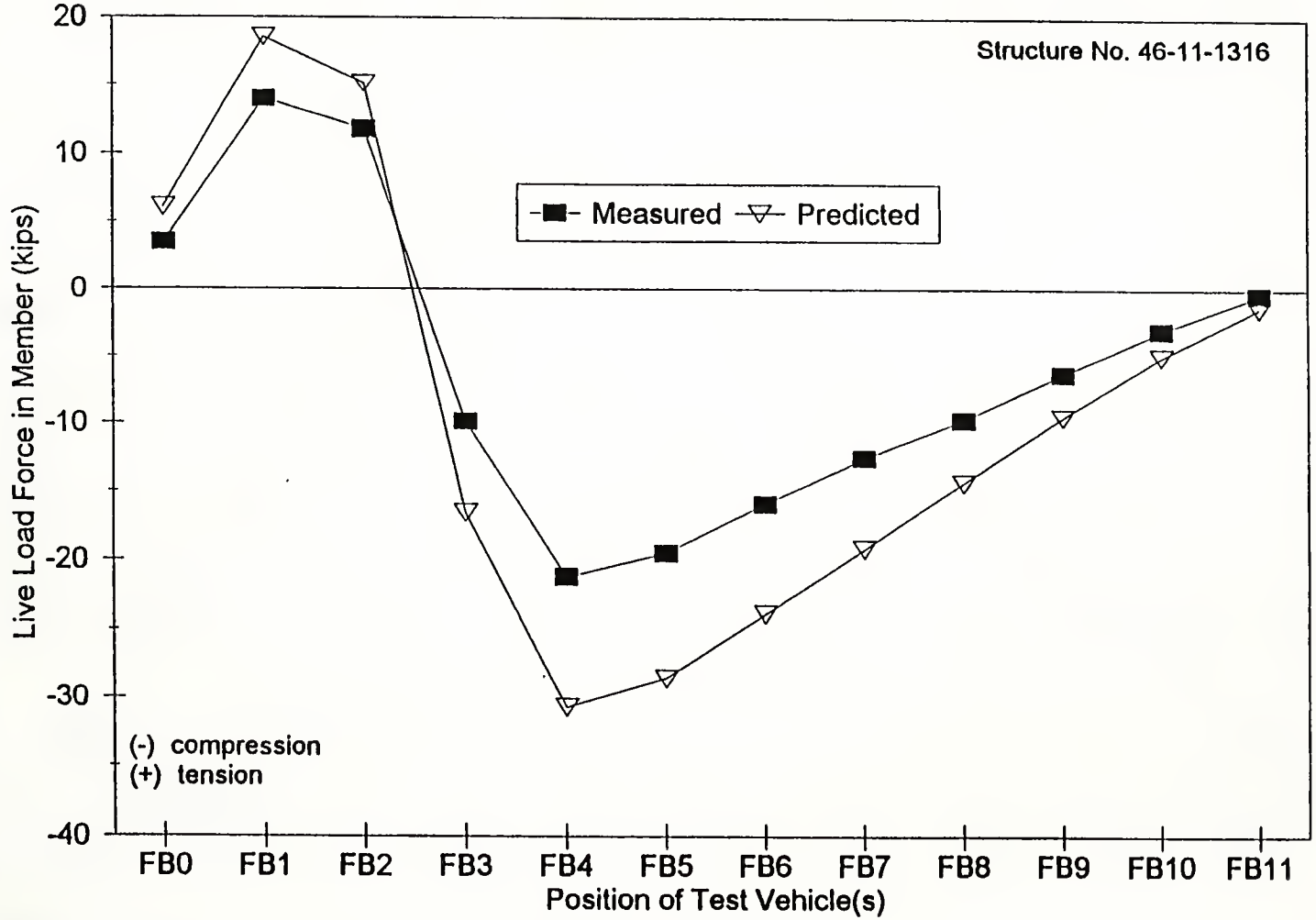

Figure 5.2.2.3.2 Force in member L2U2 for loading Condition #2 - North

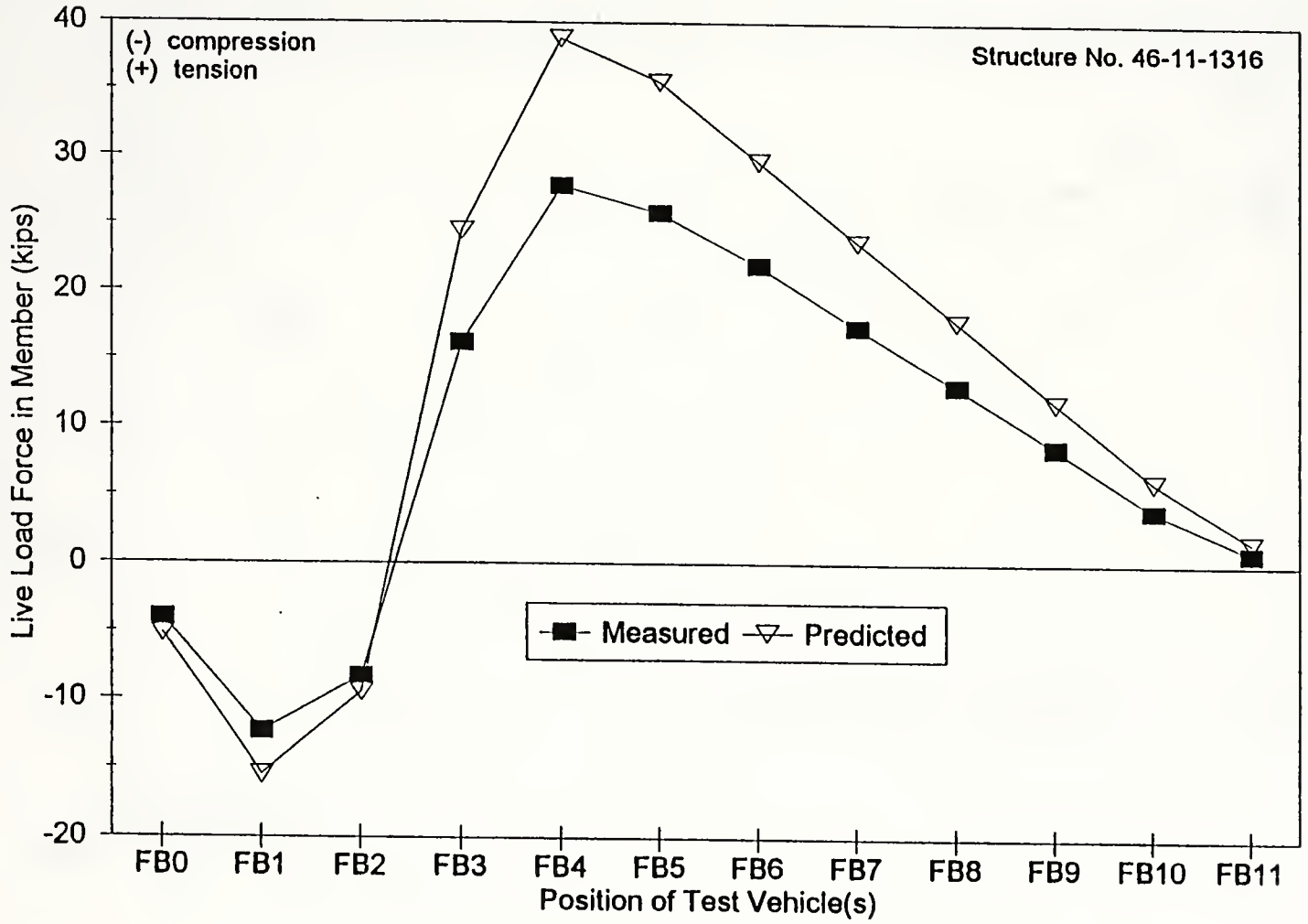

Figure 5.2.2.3.3 Force in member U2L3 for loading Condition #2 - North

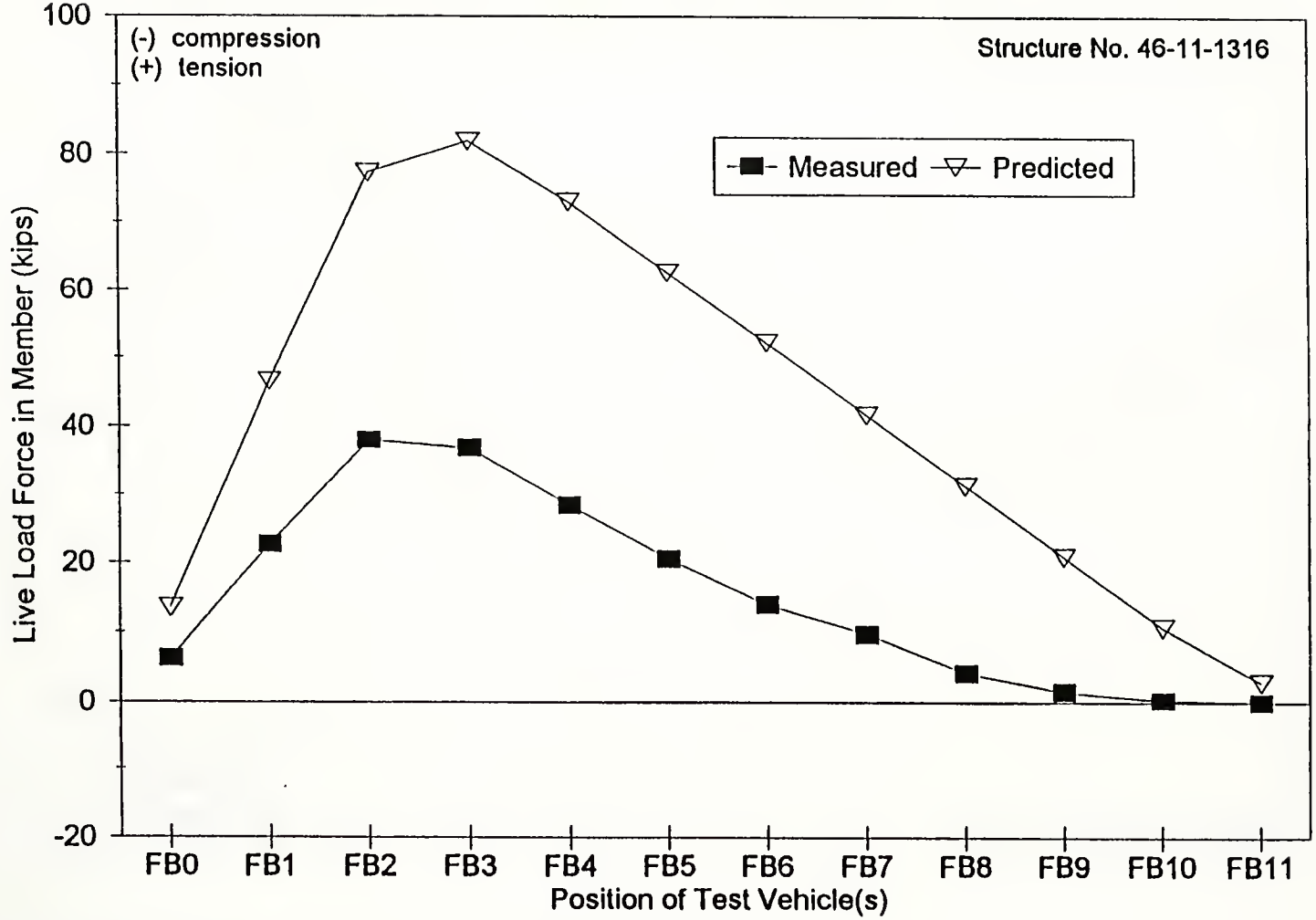

Figure 5.2.2.3.4 Force in member L2L3 for loading Condition #2 - North

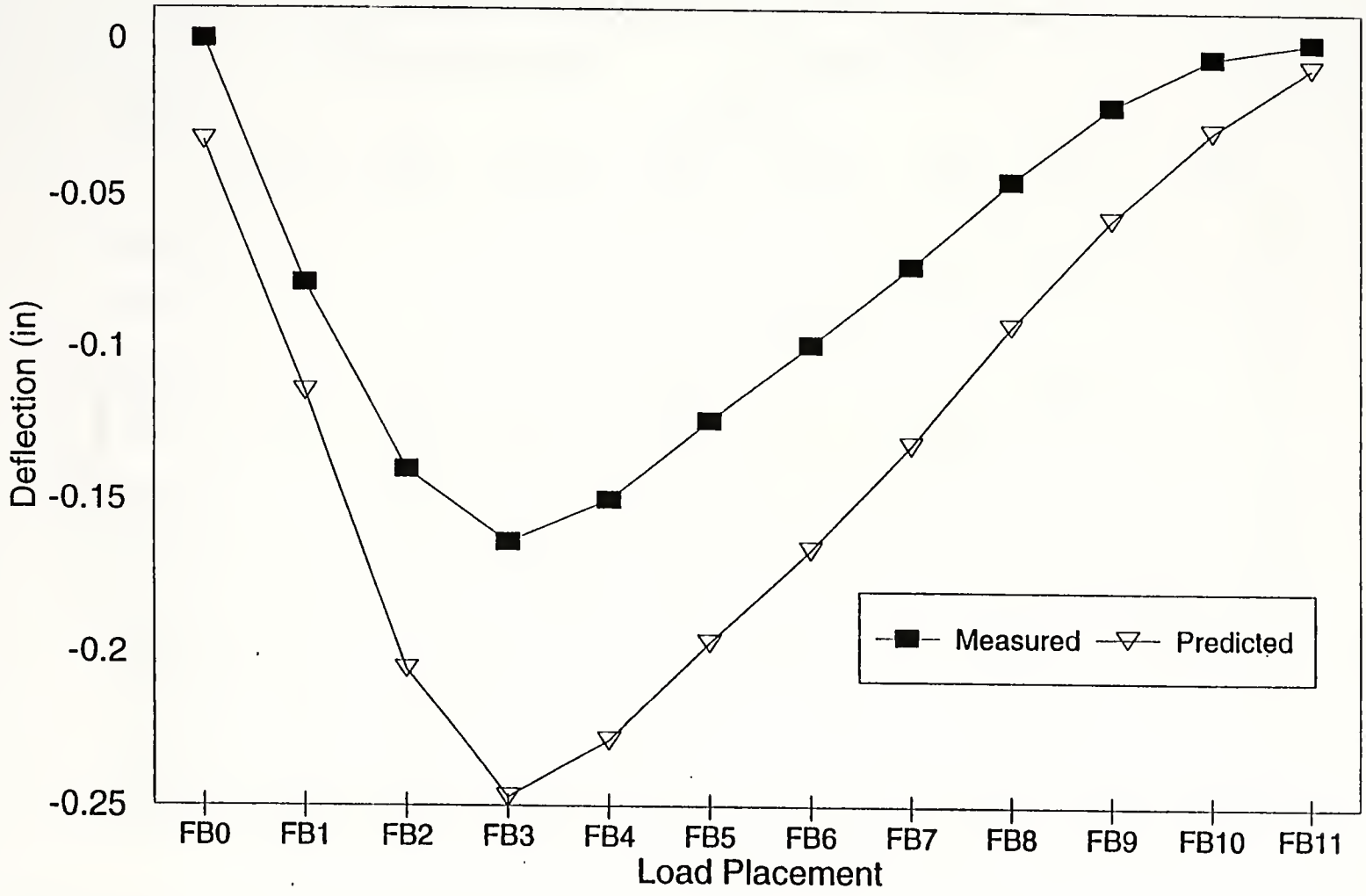

Figure 5.2.2.4.1 Midspan L2L3 deflection

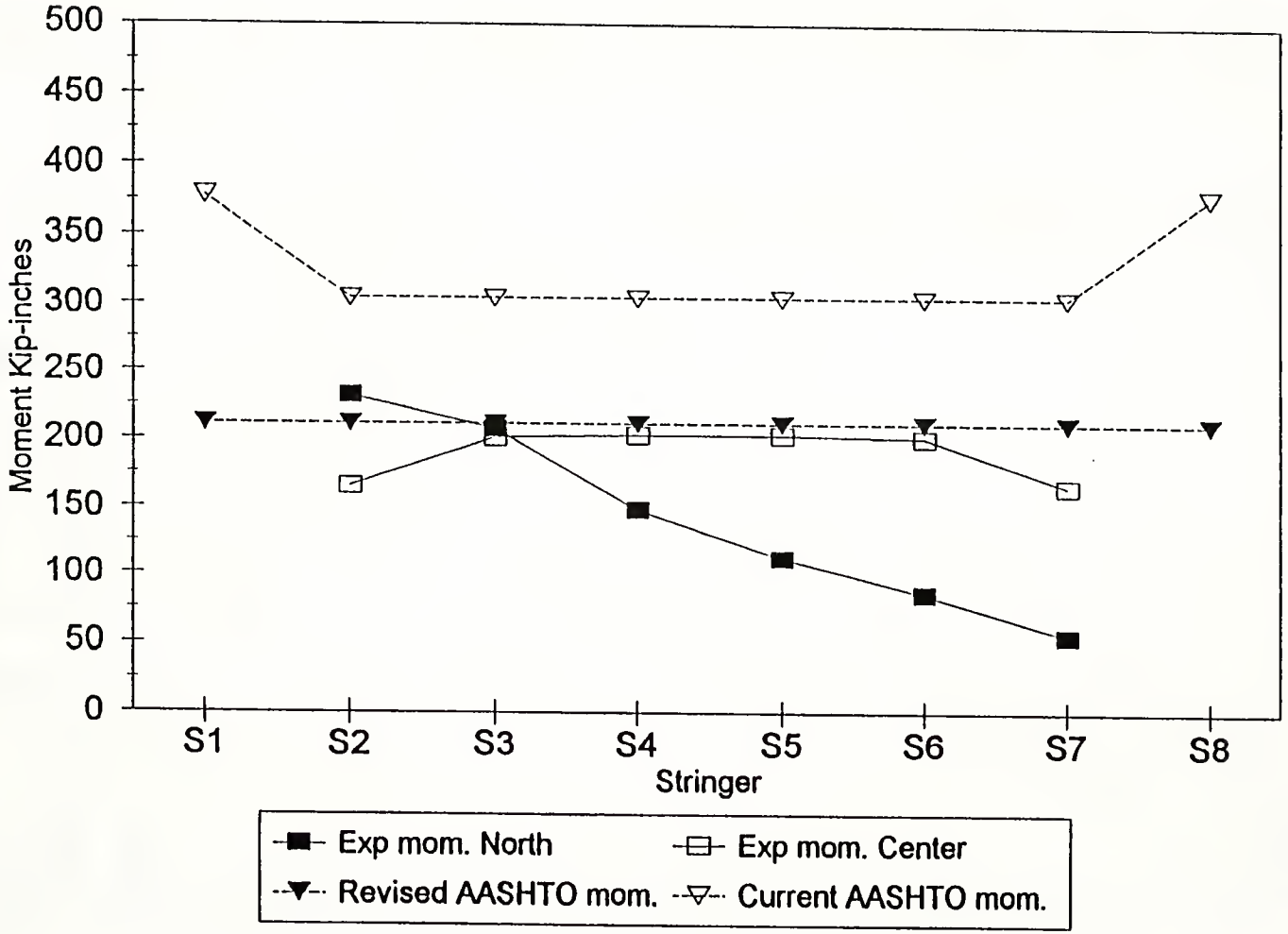

Figure 5.2.3.2.1 Experimental moments for LC#1-P3-North and South

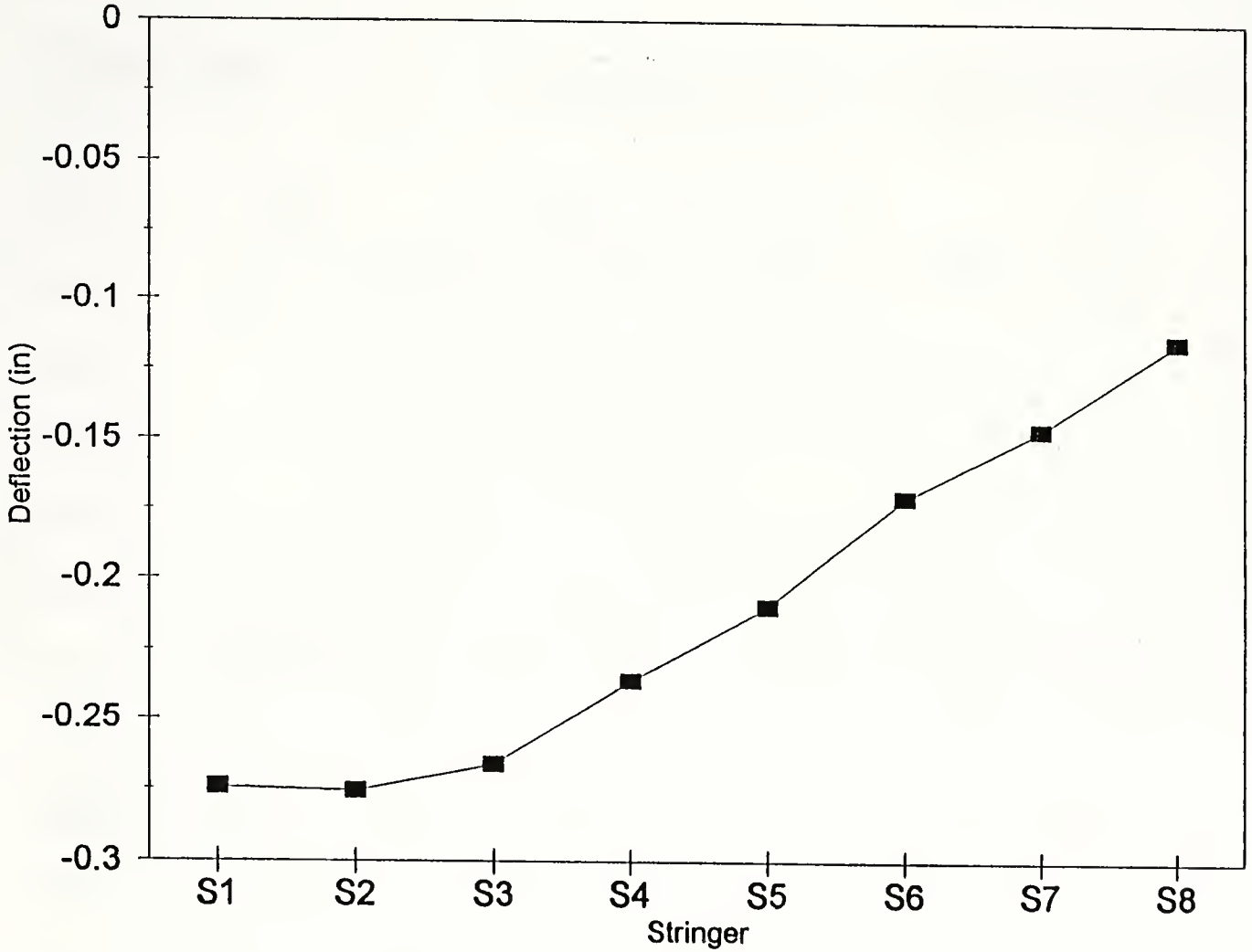

Figure 5.2.3.2.2 Total deck deflection measured at midpan of stringers for LC #1-North

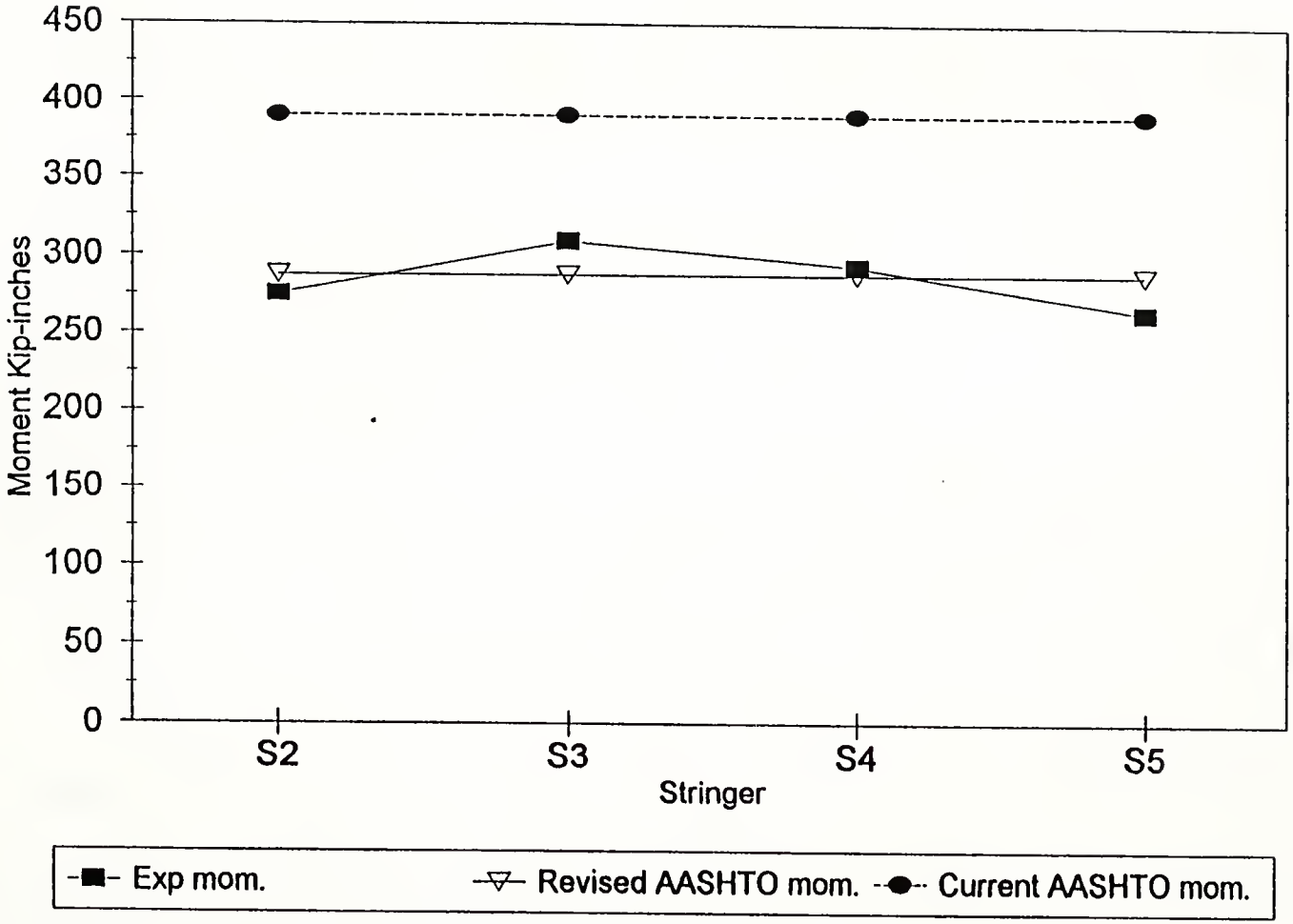

Figure 5.2.3.2.3 Experimental moments for LC#3-1

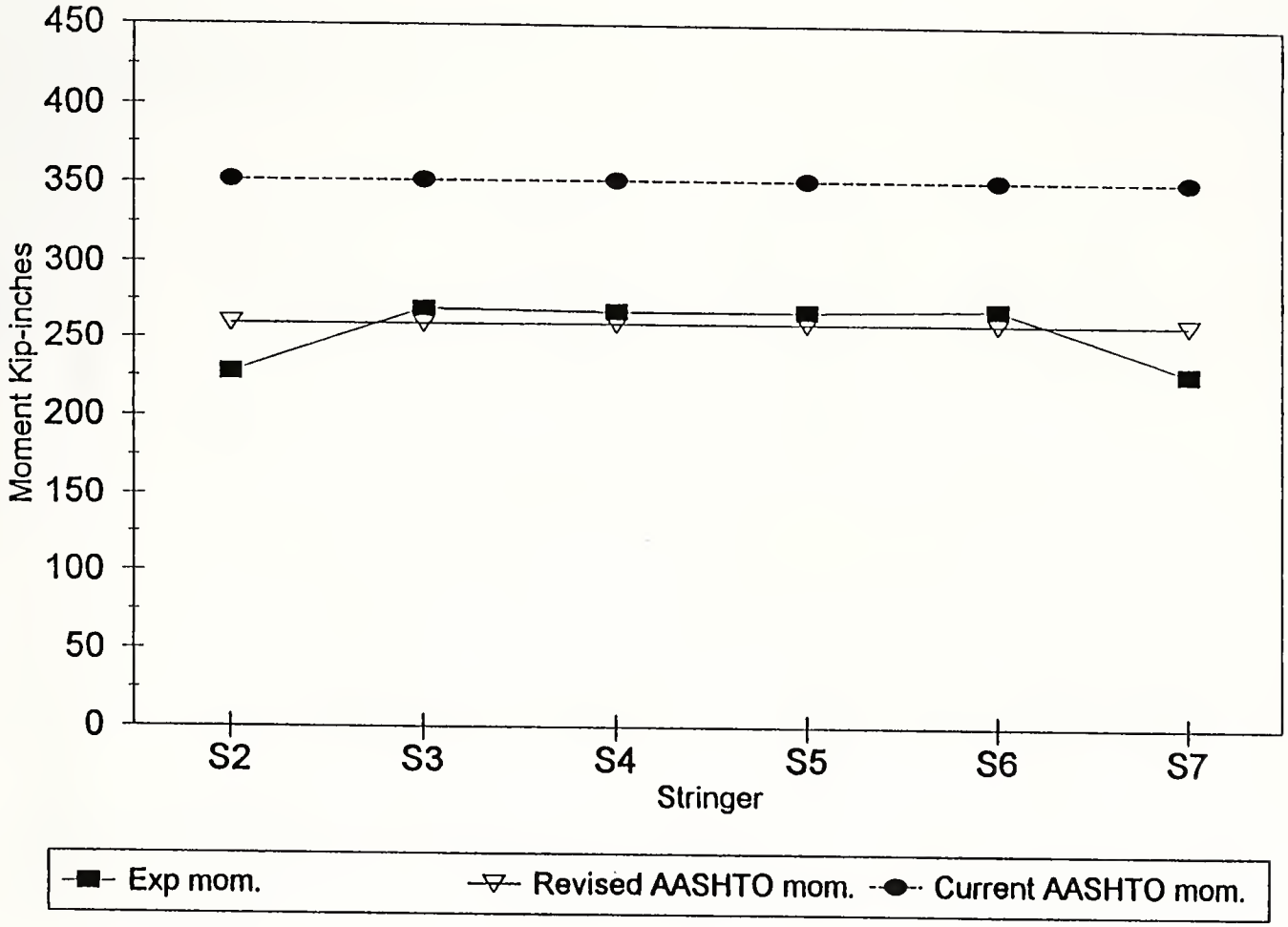

Figure 5.2.3.2.4 Experimental moments for LC#3-3

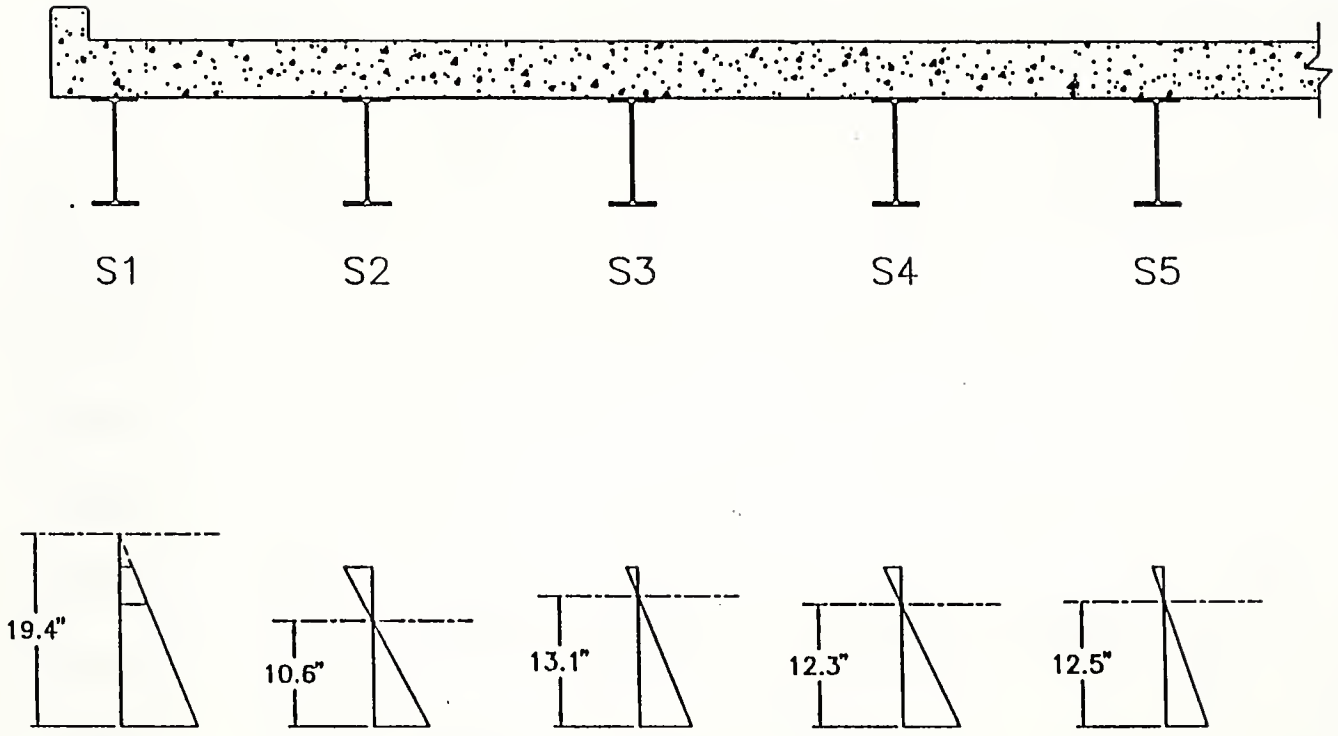

Figure 5.2.3.3.1 Measured strain distribution for LC #1-P3-North

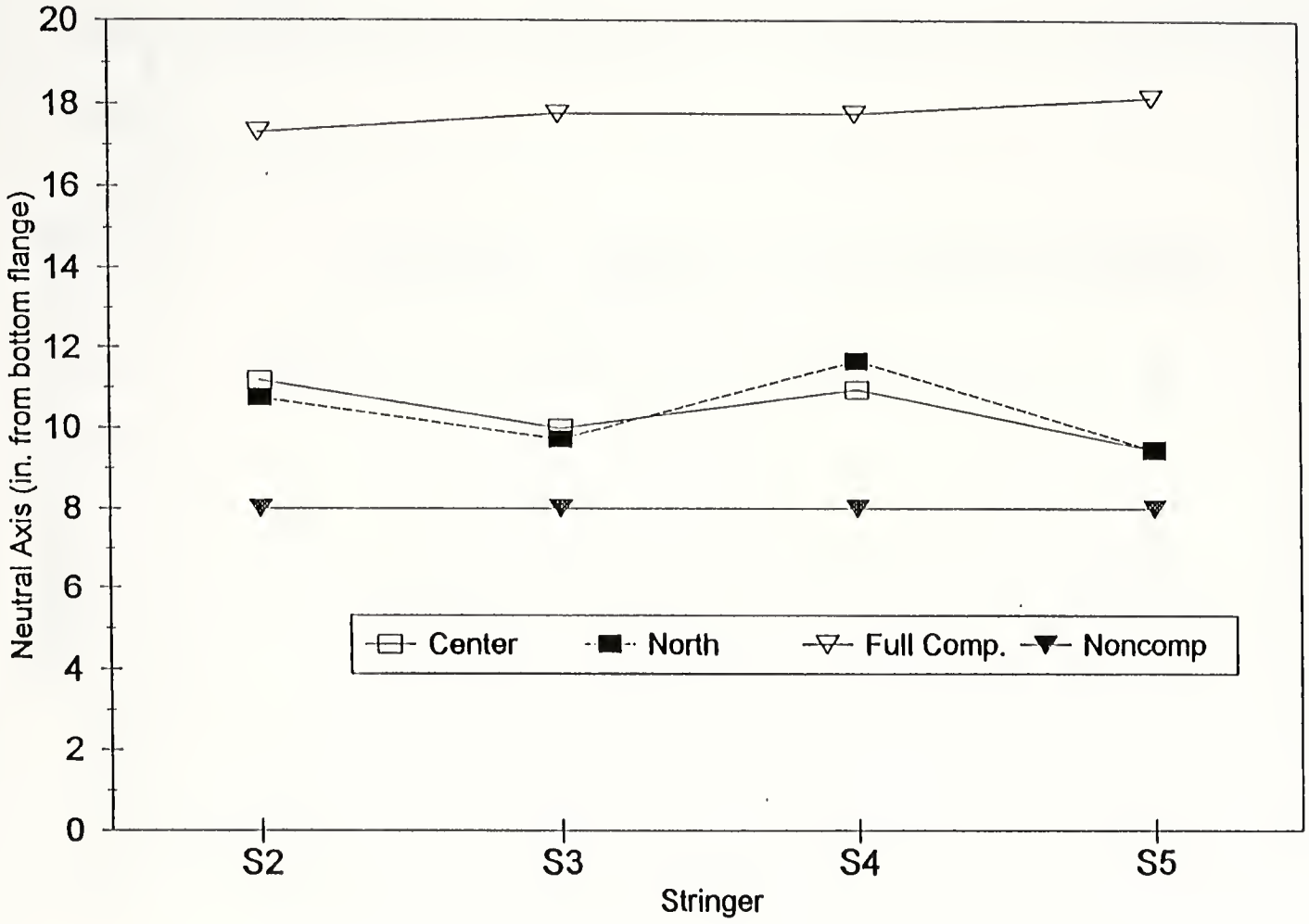

Figure 5.2.3.3.2 Neutral axis positions for LC#4- North and Center

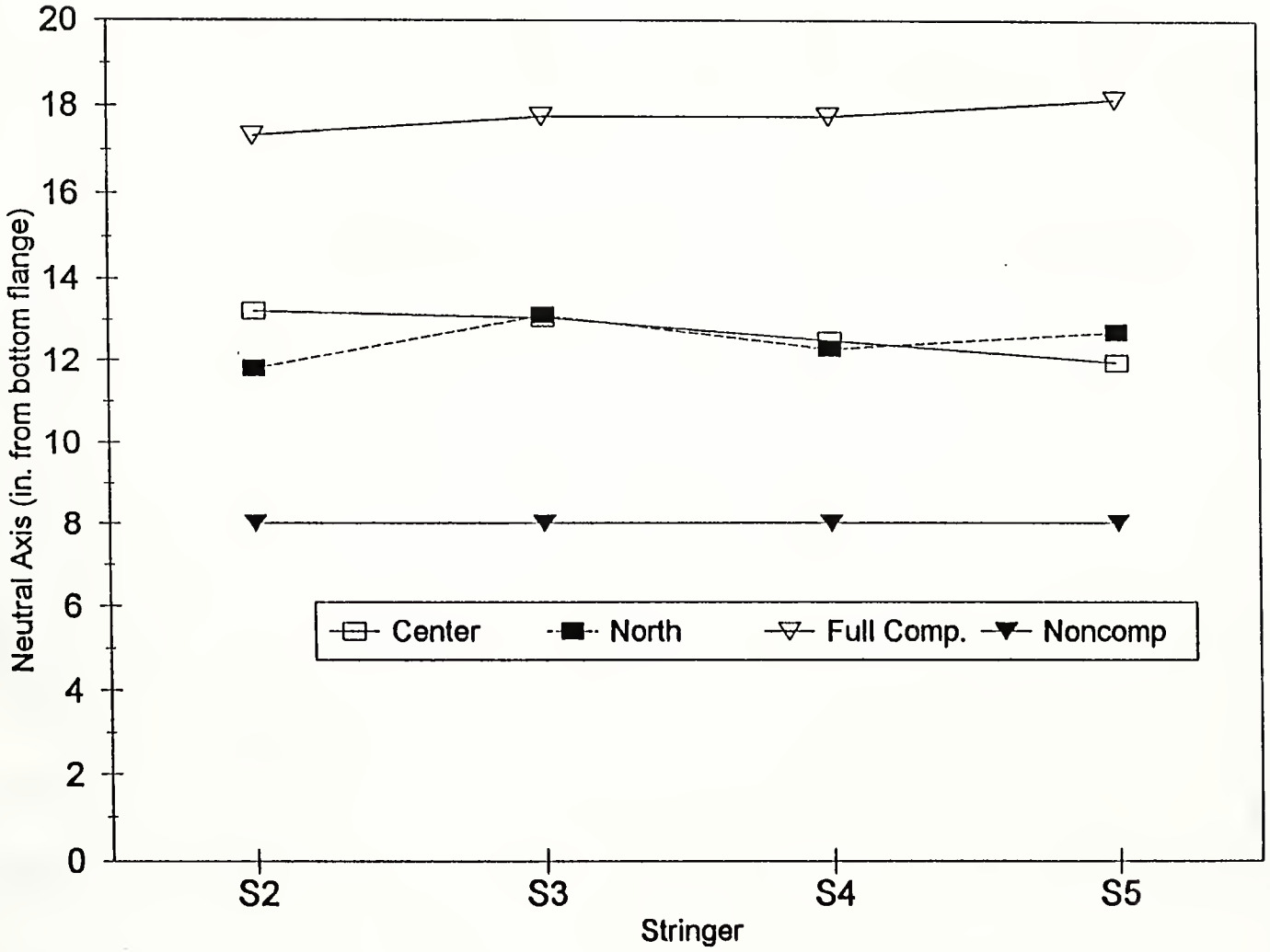

Figure 5.2.3.3.3 Neutral axis positions for LC#1-P3-North and Center

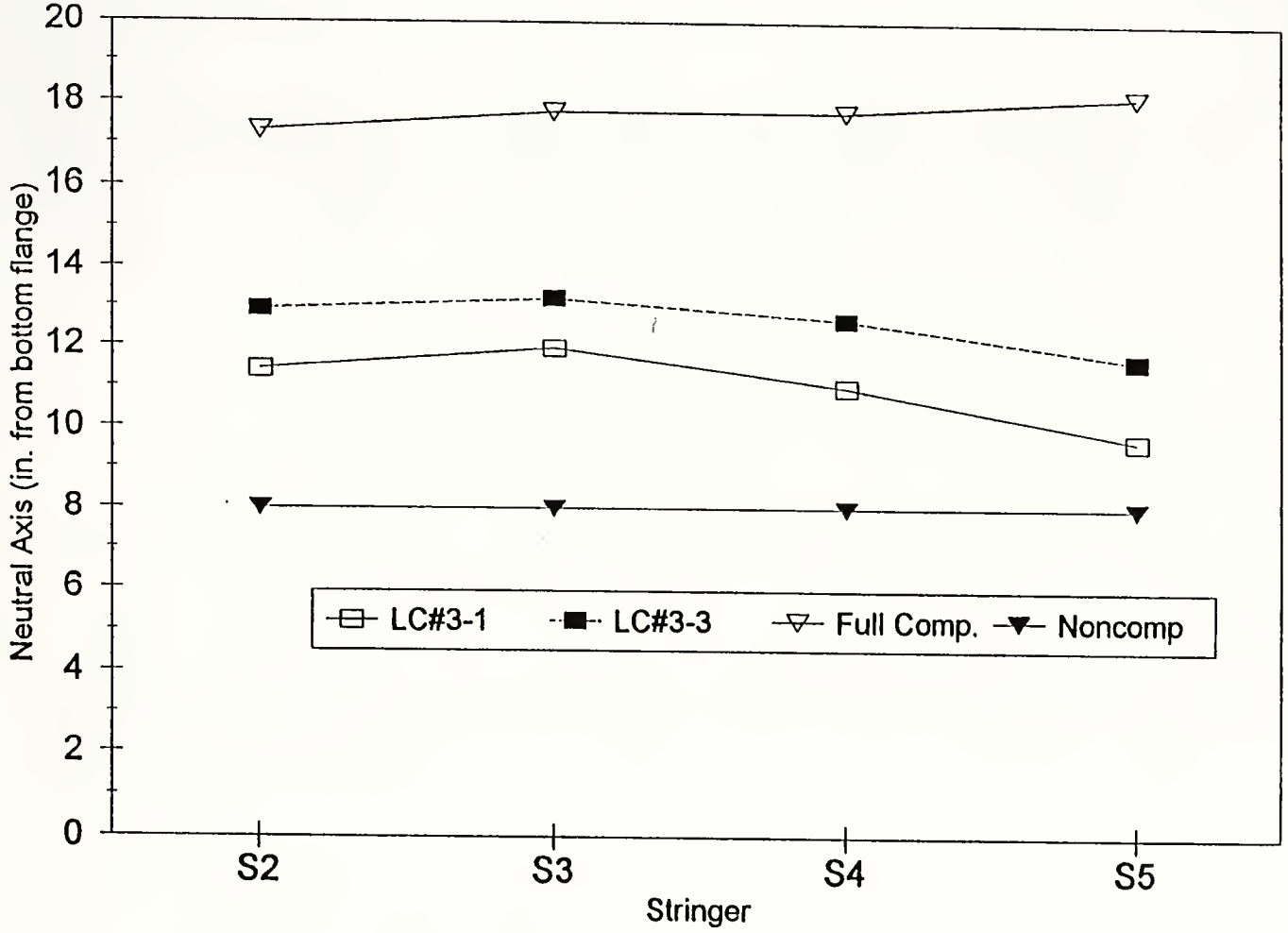

Figure 5.2.3.3.4 Neutral axis positions for LC#3-3-P3

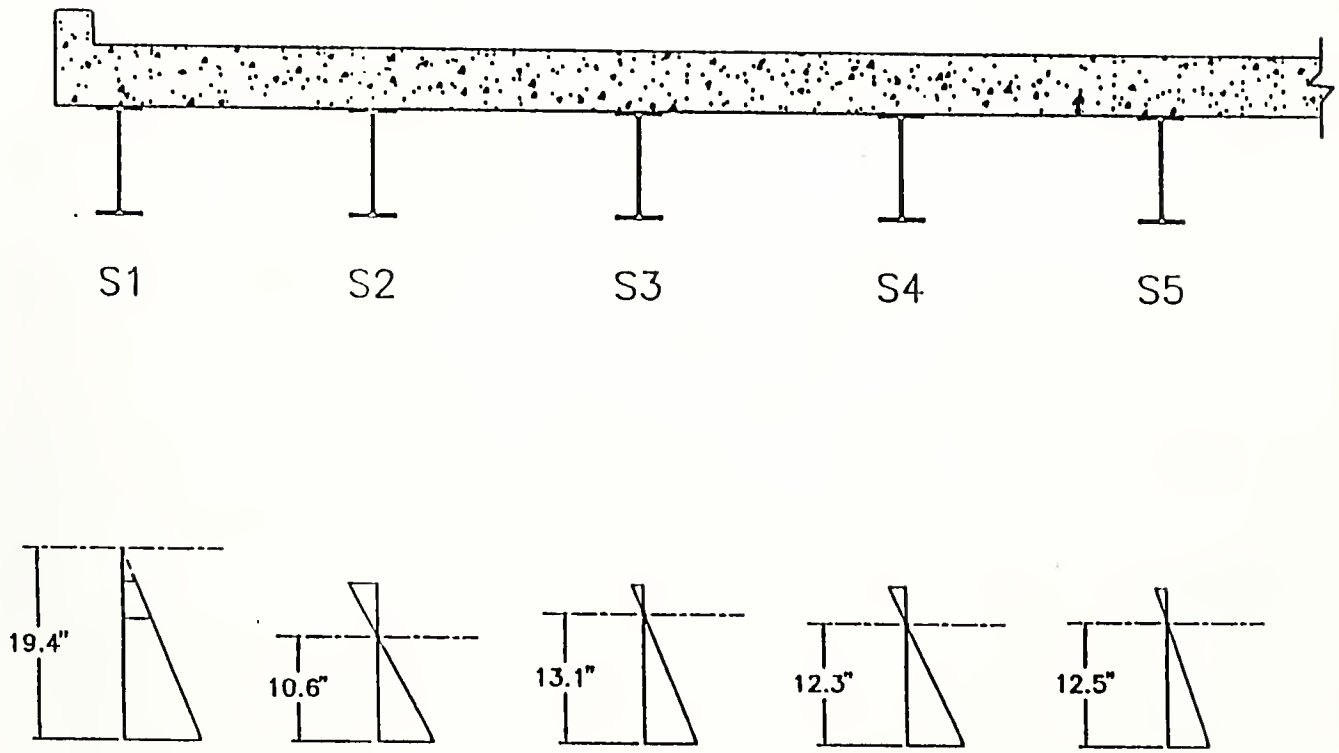

Figure 5.2.3.4.1 Measured strain distribution for LC #1-P3-North

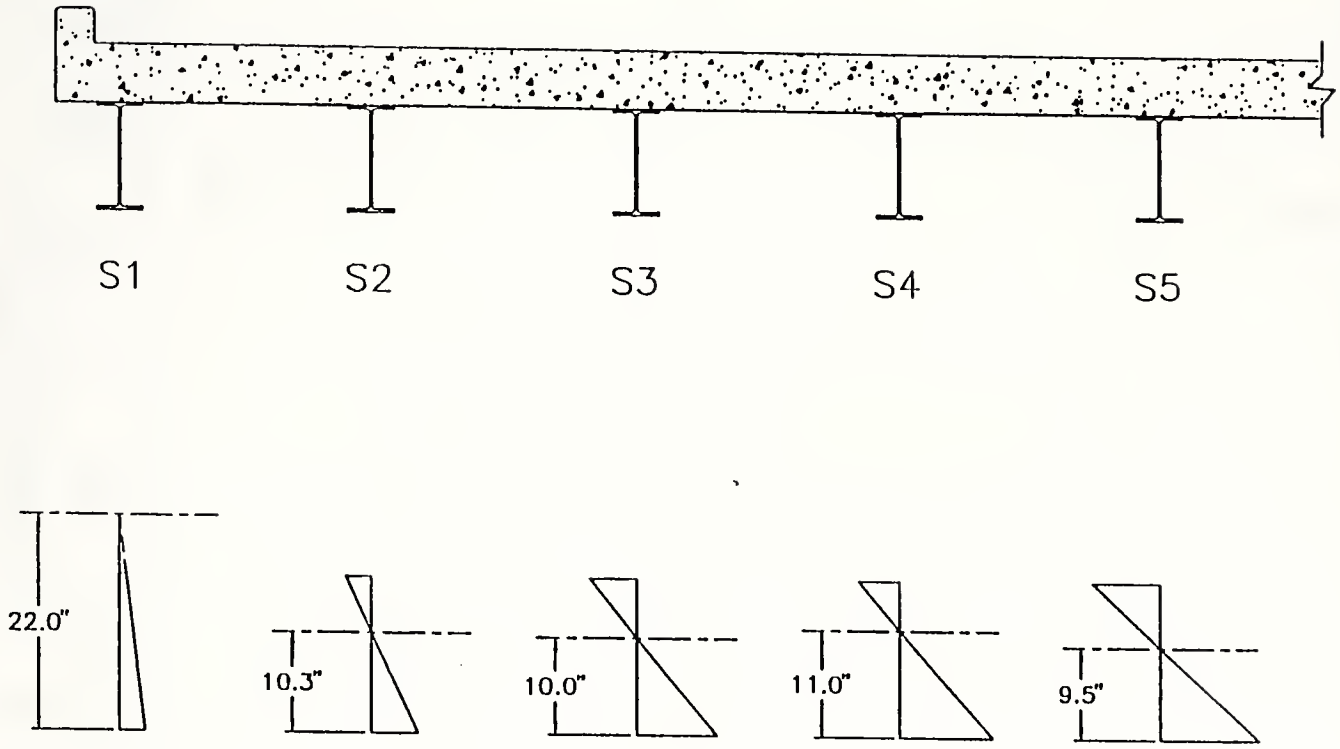

Figure 5.2.3.4.2 Measured strain distribution for LC #4-Center

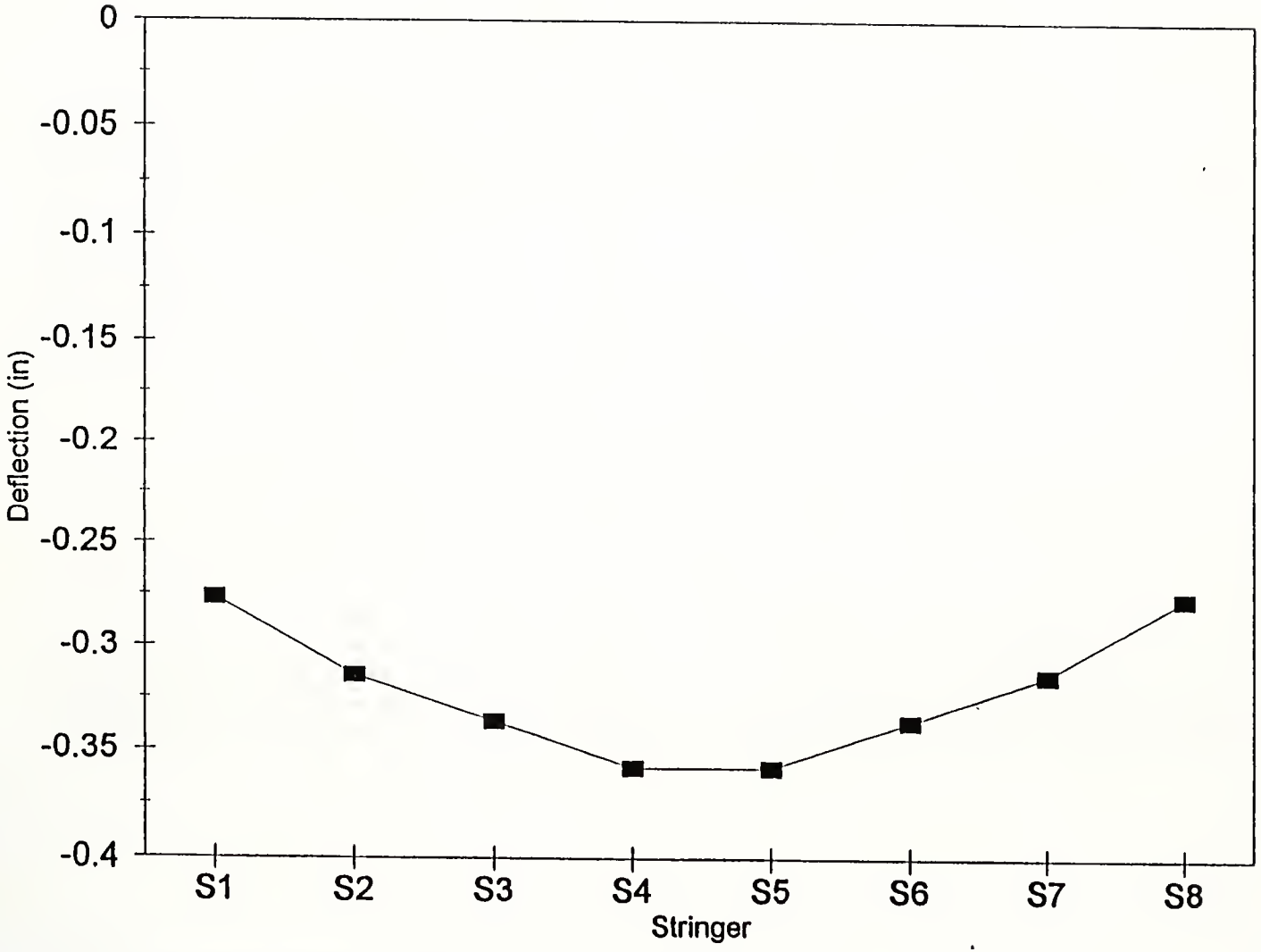

Figure 5.2.3.4.3 Total deck deflection measured at midpan of stringers for LC #3-3

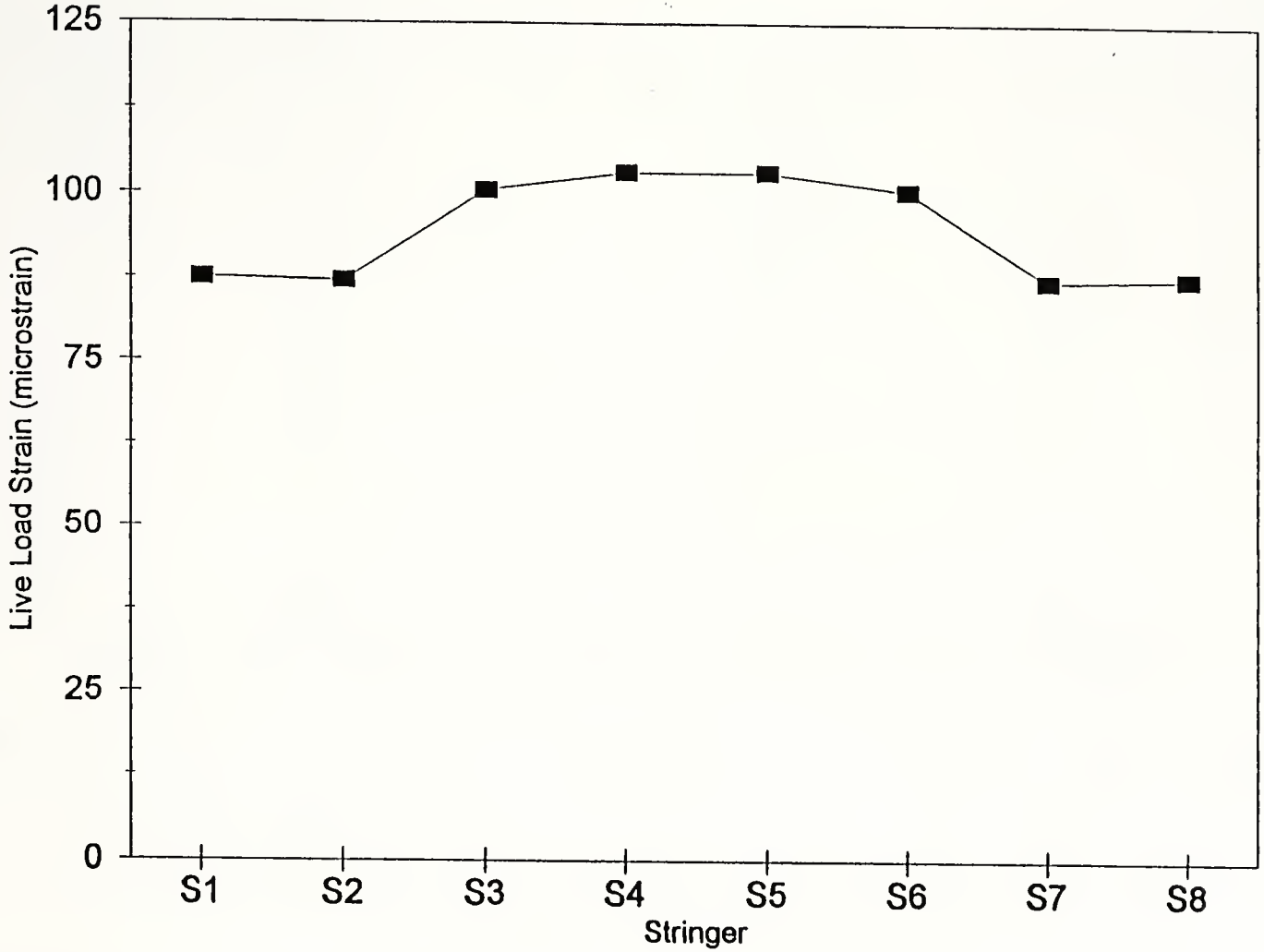

Figure 5.2.3.4.4 Midspan bottom flange strain in stringers for LC#3-3-P3

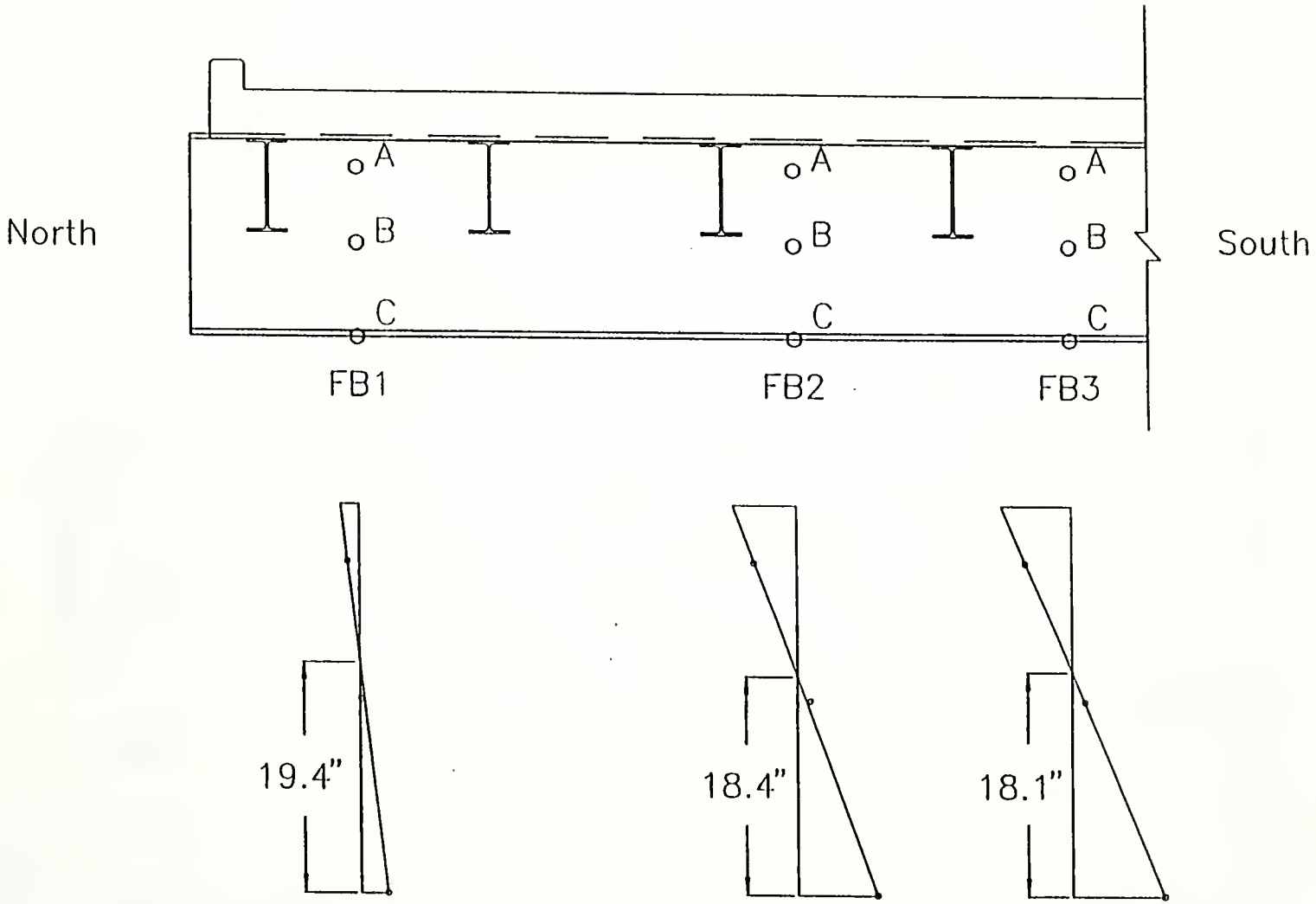

Figure 5.2.4.2.1 Typical measured strain distribution along floor beam three

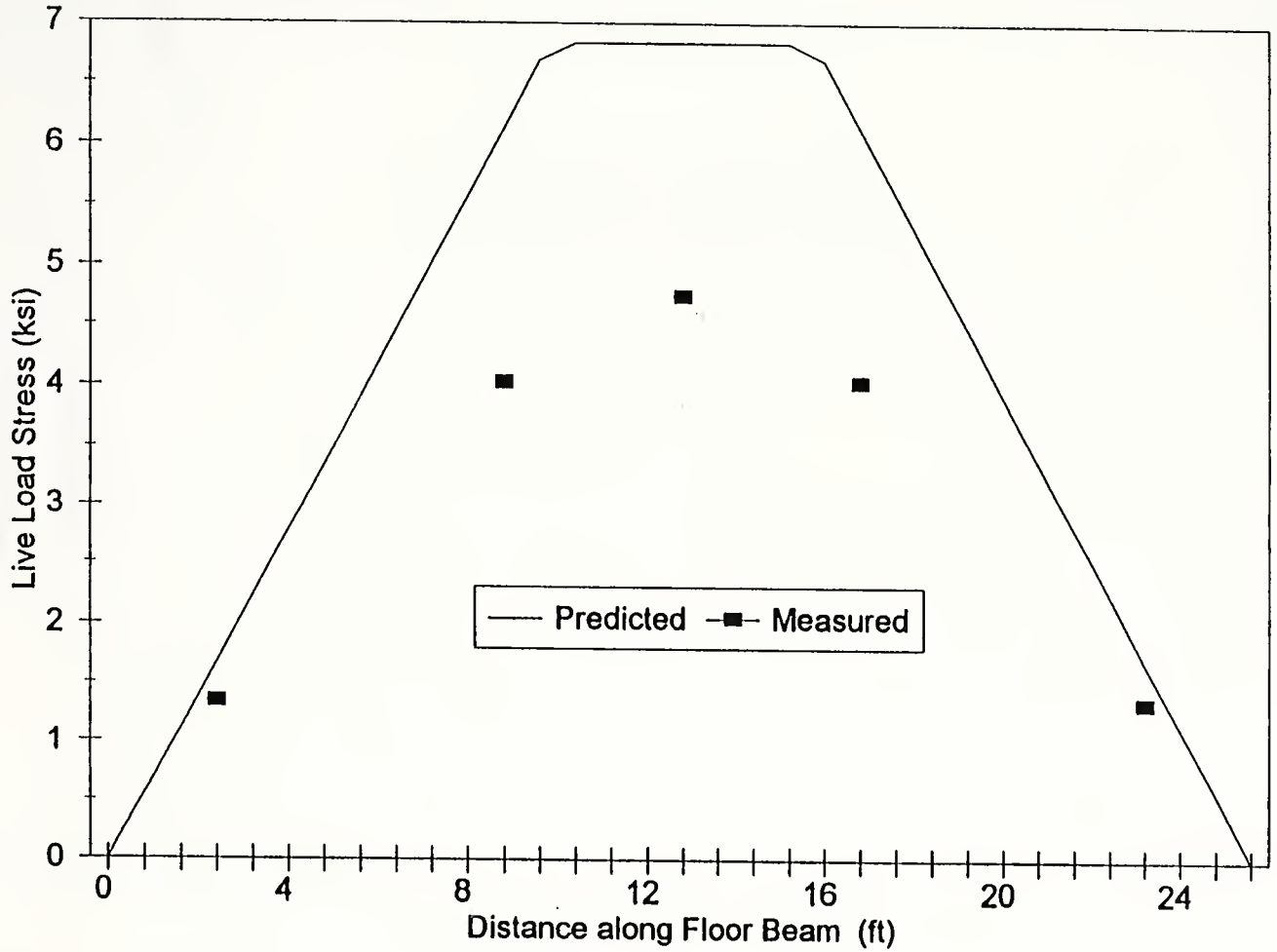

Figure 5.2.4.2.2 Floor beam stress for LC#1-Center

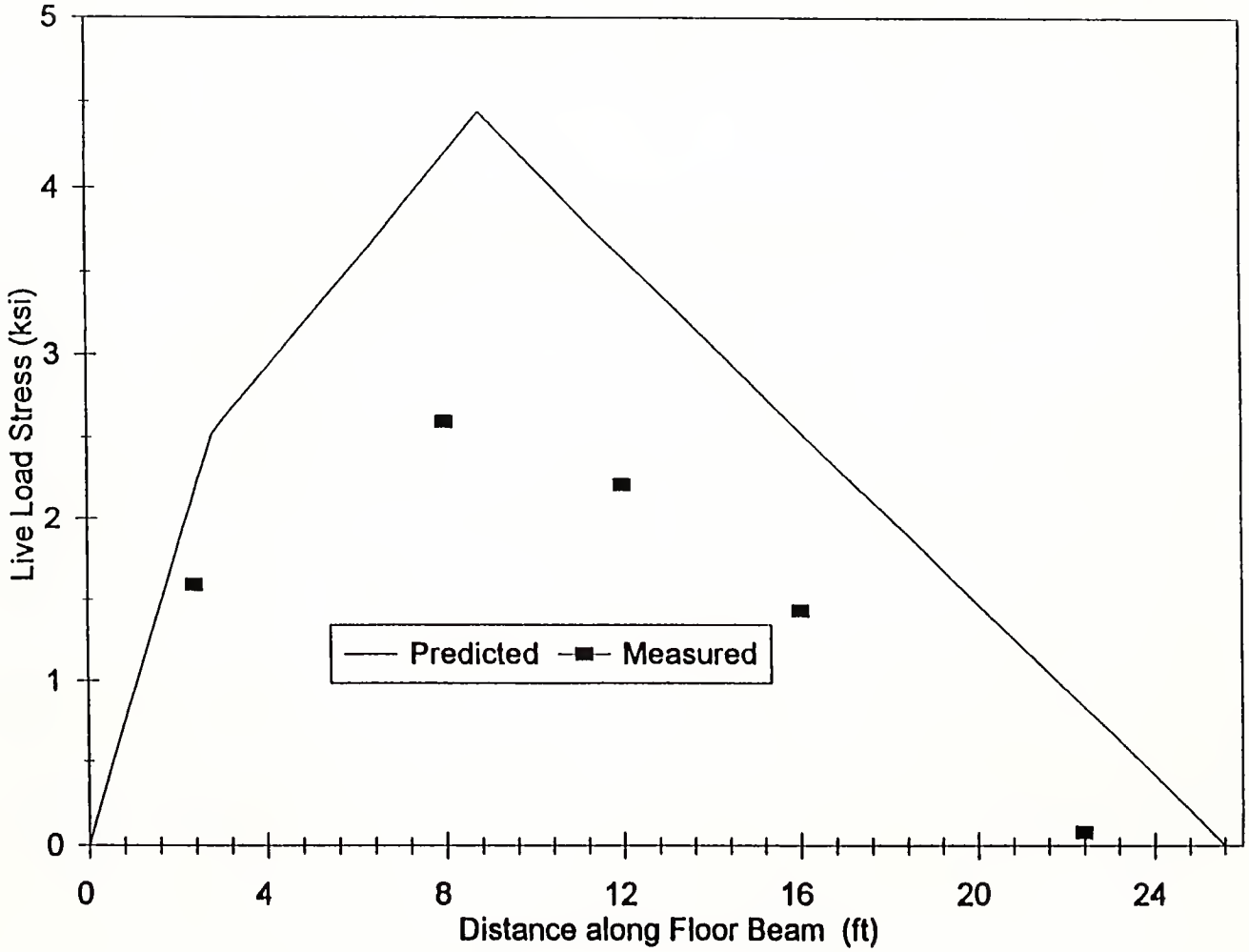

Figure 5.2.4.2.3 Floor beam stress for LC#1-P3-North

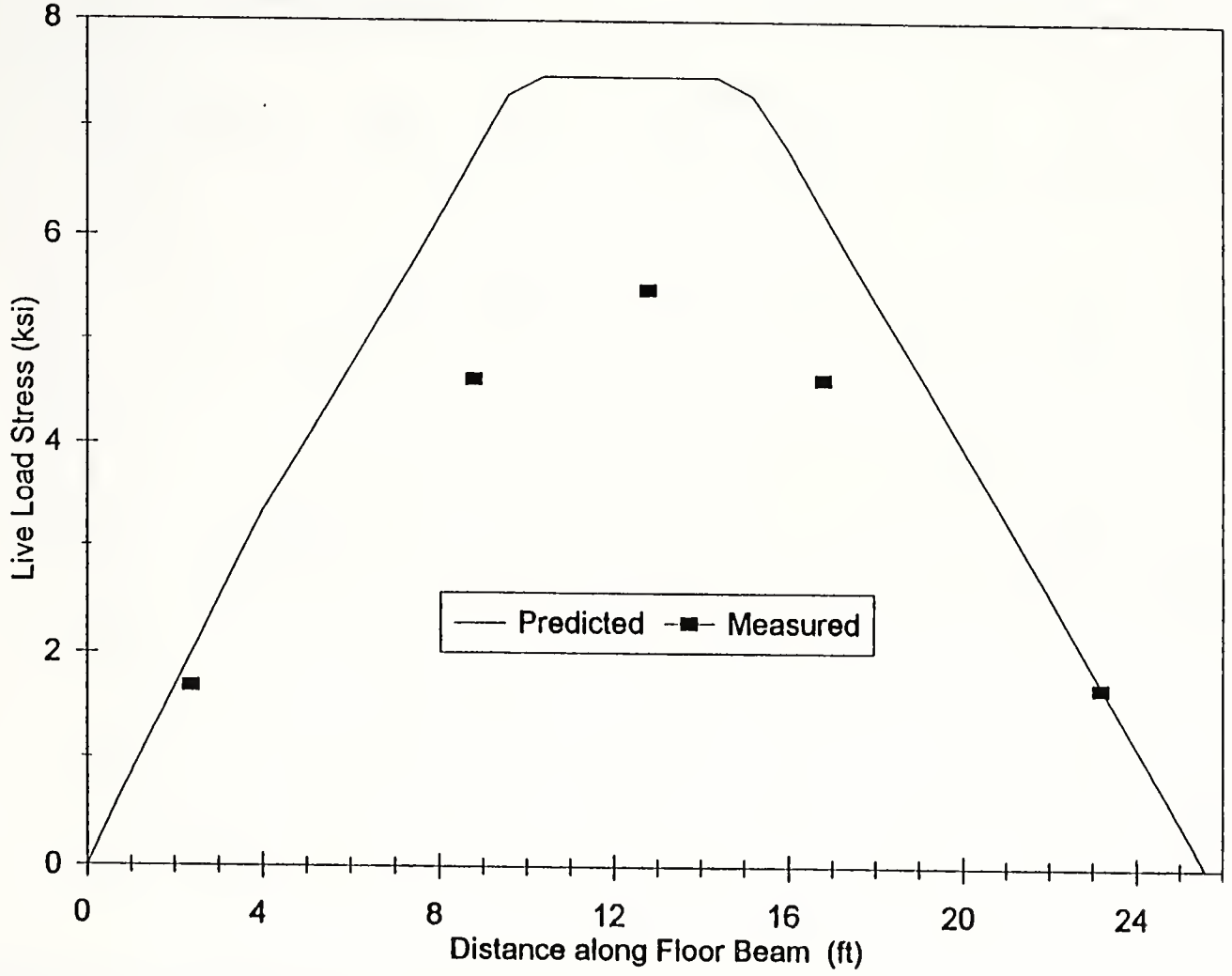

Figure 5.2.4.2.4 Floor beam stress for LC#3-3

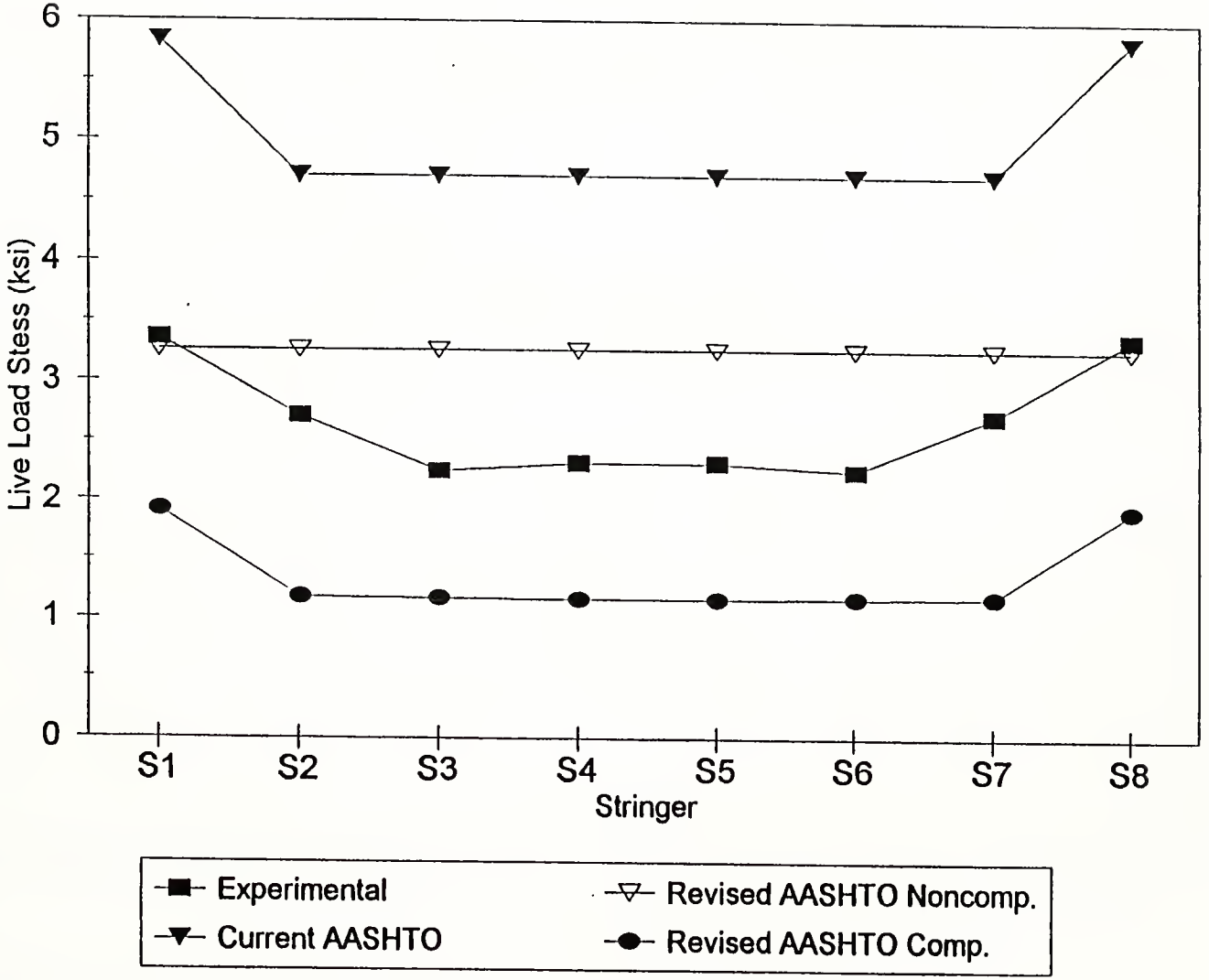

Figure 6.2.2.1 Maximum live load stress in bottom flange of stringers for LC #1-P3

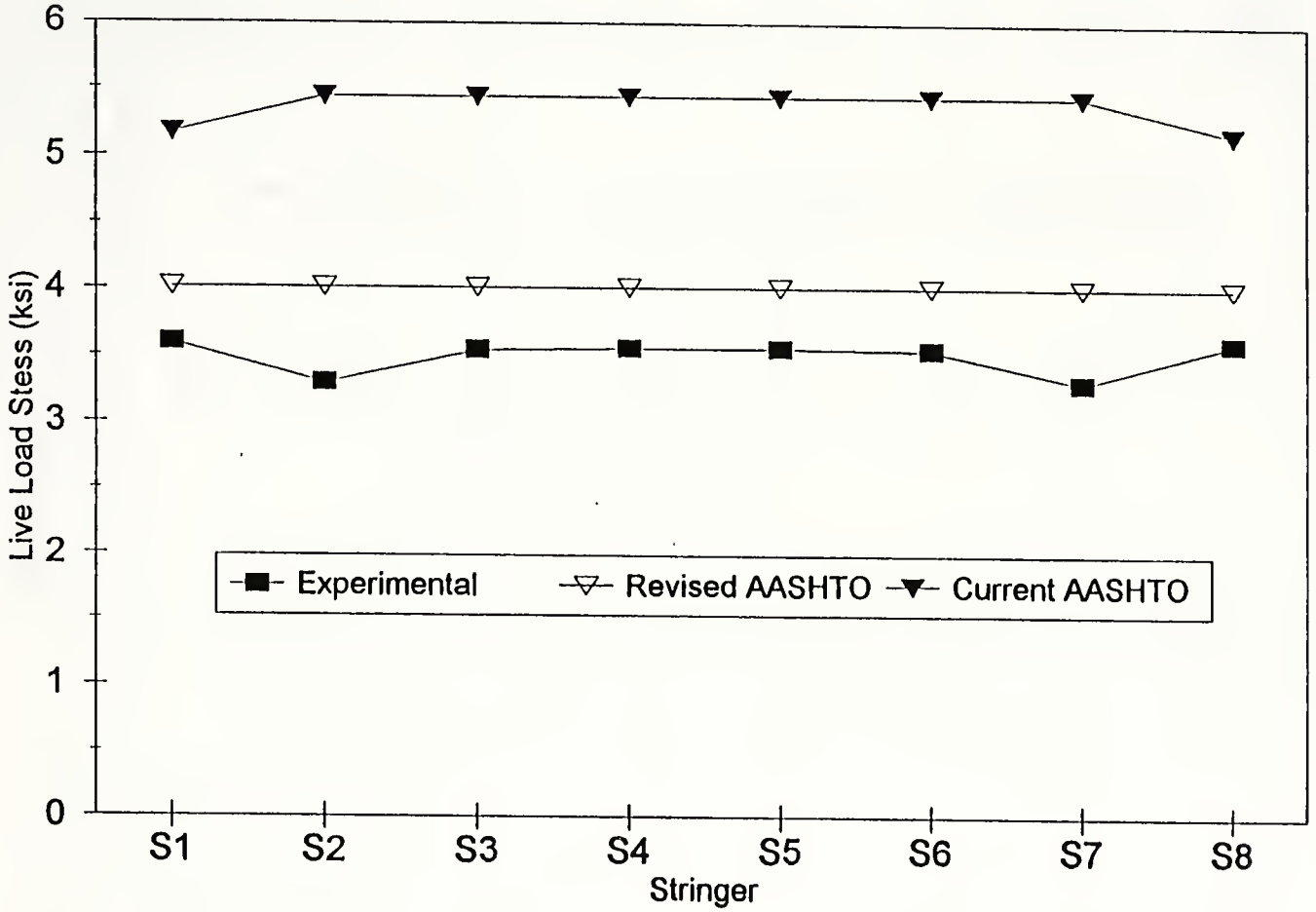

Figure 6.2.2.2 Live load stress in bottom flange of stringers for LC#3-1-P3

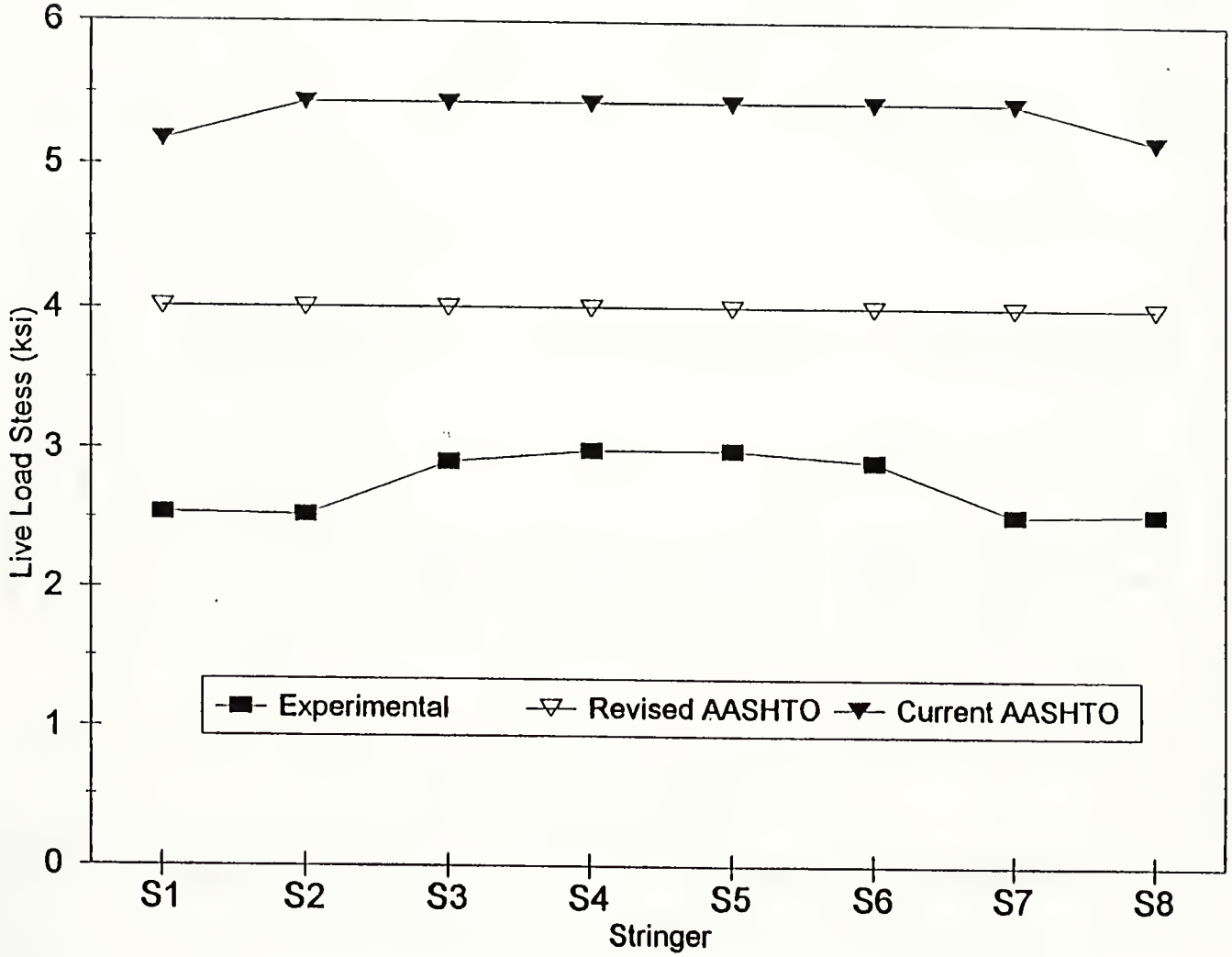

Figure 6.2.2.3 Live load stress in bottom flange of stringers for LC#3-3-P3

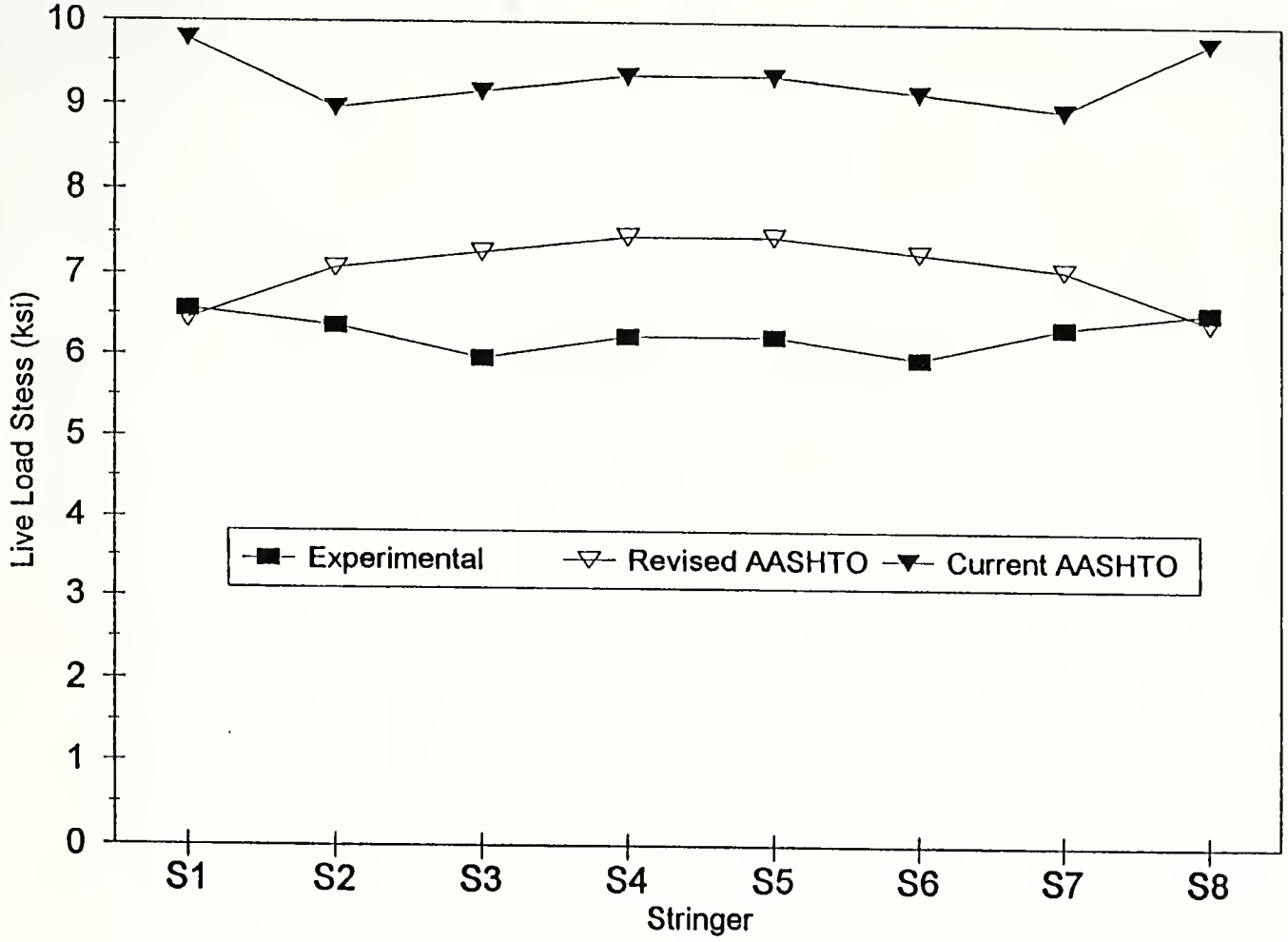

Figure 6.2.2.4 Total stress in bottom flange of stringers for LC#1-P3

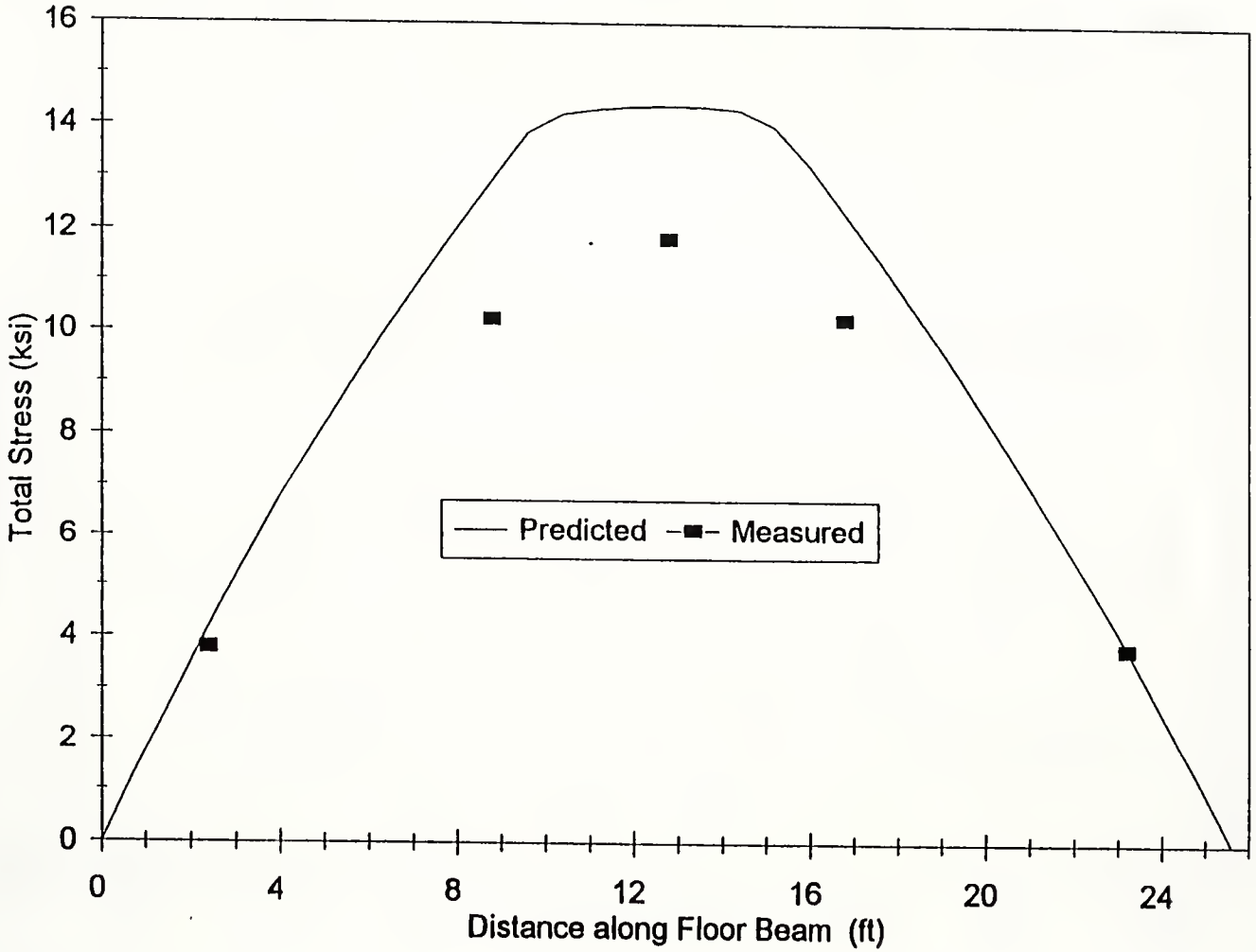

Figure 6.2.3.1 Total stress in bottom flange of floor beam for LC#3-3-FB3

LIST OF REFERENCES

LIST OF REFERENCES

1. AASHTO. Standard Specifications for Highway Bridges. 15th Edition. The American Association of State Highway and Transportation Officials. Washington D. C., 1992.

2. AASHTO. LRFD Standard Specifications for Highway Bridges. First Edition. The American Association of State Highway and Transportation Officials. Washington D. C., 1994.

3. AASHTO. Bridge and Analysis Rating System Manual 1, Structural Analysis Reference, 2nd Edition, March 1986.

4. Bakht, B. and Jaeger, L. G. "Behaviour and Evaluation of Pin-Connected Steel Truss Bridges." Canadian Journal of Civil Engineering, Vol. 14, 1987, pp. 317 - 335.

5. Bakht, B. and Jaeger, L. G. "Bridge Testing - A Surprise Every Time." ASCE Journal of Structural Engineering, Vol. 116, No. 5, May 1990, pp. 1320 - 1383.

6. Bakht, B. and Moses, F. "Lateral Distribution Factors for Highway Bridges." ASCE Journal of Structural Engineering, Vol. 114, No, 8, Aug. 1988, pp. 1785 - 1803.

7. Burdette, E. G. and Goodpasture, D. W. Correlation of Bridge Load Capacity with Test Data." National Cooperative Highway Research Program Report 306, Transportation Research Board, National Research Council, Dec. 1987.

8. Cheung, M. S., Gardner, N. J. and Ng, S. F. "Ultimate Load Distribution Characteristics of a Model Slab-on-Girder Bridge."Canadian Journal of Civil Engineering, Vol 14, 1987, pp. 739 - 752.

9. Dally, J. W. and Riley, W. F. Experimental Stress Analysis. 3rd Edition, McGraw-Hill, Inc., 1991.

10. Duemmel, P. S., Babar, T. T., Barton, F. W. and McKeel, Jr., W. T. "Field Instrumentation and Measured Response of the I-295 Cable-Stayed Bridge Part 1: Field Study of Live Load Responses." Virginia Department of Transportation Research Council, Dec. 1992.

11. Dunker, K. F., Klaiber, F. W. and Sanders, Jr., W. W. "Bridge Strengthening Needs in the United States." Transportation Research Record 1118. Transportation Research Board, National Research Council, pp. 1 - 8.

12. Heins, C. P., Fout, W. S. and Wilkison R. Y. "Replacement or Repair of Old Truss Bridges." pp. 63-65.

13. Holowka, M. "Testing of a Trapezoidal Box Girder Bridge." RR221. Ministry of Transportation and Communications, Research and Development Division, Ontario, Canada.

14. Imbsen, R. A. and Nutt, R. V. "Bridge Weight-Limit Posting Practice in the United States." Transportation Research Record 950, Second Bridge Engineering Conference, Transportation Research Board, Vol. 1, 1984, pp. 70 - 76.

15. Jaeger, L. G. and Bakht, B. "Effect of Poisson's Ratio and Beam Spacing on Grillage Analysis of Slab Bridges." Canadian Journal of Civil Engineering, Vol. 15, 1988, pp. 821 - 827.

16. Jaeger, L. G. and Bakht, B. "The Grillage Analogy in Bridge Analysis." Canadian Journal of Civil Engineering, Vol. 9, 1982, pp. 224 - 235.

17. Klaiber, F. W., Sanders, W. W. and Elleby, H. A. "Ultimate Load Test of a High-Truss Bridge." Engineering Research Institute, Iowa State University, pp. 75 - 80.

18. Koob, M. J. "Instrumentation and Field Testing of the Green River Bridge, I-26 in Henderson County, North Carolina for North Carolina Department of Transportation." Wiss, Janney, Elstner Associates, Inc. Report No. 922229, Jan. 1993.

19. Koob, M. J., Walther, R. A. and Blake, G. T. "Evaluation of Girder to Cross-Girder Connections and Bearing Problems of the Moline Viaduct, Fai Route 74, Moline, Rock Island County, Illinois." Submitted to Illinois Department of Transportation. Wiss, Janney, Elstner Associates, Inc. Report No. 891210, Apr. 1991.

20. Koob, M. J. and Walther, R. A. "Fatigue Evaluation of the Gerald Desmond Bridge, Long Beach, California." Submitted to Moffat & Nichol, Engineers. Wiss, Janney, Elstner Associates, Inc. Report No. 900893, Nov. 1993.

21. Moses, F. and Verma, D. "Load Capacity Evaluation of Existing Bridges." National Cooperative Highway Research Program Report 301, Transportation Research Board, National Research Council, Dec. 1987.

22. Newmark, N. M., Siess, C. P. and Penman, R. R. "Studies of Slab and Beam Highway Bridges: Part I, Tests of Simple-Span Right I-Beam Bridges." University of Illinois Engineering Experiment Station Bulletin Series No. 363, University of Illinois, Vol. 49, No. 45, Feb. 1952.

23. Pinjarkar, S. G., Guedelhoefer, O. C., Smith, B. J. and Kritzler, R. W. "Nondestructive Testing for Bridge Evaluation and Rating, Final Report." Prepared for National Cooperative Highway Research Program, Transportation Research Board, National Research Council, Feb. 1990.

24. Prasad, NBR, and White, D., Ramirez, J., and Kuczek, T. "Statistical Analysis of Overload Vehicle Effects on Indiana Highway Bridges." Final Report No. FHWA/IN/JHRP-92/1, Joint Highway Research Project, Purdue University, 1993.

25. Sanders, W. W. "Distribution of Wheel Loads on Highway Bridges." Synthesis of Highway Practice. National Cooperative Highway Research Program 111, Transportation Research Board, National Research Council, Nov. 1984.

26. Sanders, W. W., Klaiber, F. W., Elleby, H. A. and Timm, L. W. "Ultimate Load Test of Truss Bridge Floor System." Journal of the Structural Division, Proceedings of the American Society of Civil Engineering, Vol. 102, No. ST7, July 1976, pp. 1383 - 1398.

27. Schulz, J. L. "In Search of Better Load Ratings." ASCE Civil Engineering, Sept. 1993, pp. 62 - 65.

28. Siess, C. P., Viest, I. M. and Newmark, N. M. "Studies of Slab and Beam Highway Bridges: Part II, Small-Scale Tests of Shear Connectors and Composite T-Beams." University of Illinois Engineering Experiment Station Bulletin Series No. 396, University of Illinois, Vol. 49, No. 45, Feb. 1952.

29. Silano, L. G. Bridge Inspection and Rehabilitation - A Practical Guide. John Wiley & Sons, Inc. 1983.

30. Smith, K. N. and Mikelsteins, I. "Load Distribution in Edge Stiffened Slab and Slab-on-Girder Bridge Decks." Canadian Journal of Civil Engineering, Vol. 15, 1988, pp. 977 - 983.

31. Stallings, J. M. and Yoo, C. H. "Tests and Ratings of Short-Span Steel Bridges." ASCE Journal of Structural Engineering, Vol. 119, No. 7, July 1993, pp. 2150 - 2168.

32. Tide, R. H. K. and Koob, M. J. "Load Testing of Bridge 1641.0 Over the Columbia River at Rock Island, Washington for the Burlington Northern Railroad." Wiss, Janney, Elstner Associates, Inc. Report No. 880805, Dec.1989.

33. Tonias, D. E. Bridge Engineering - Design, Rehabilitation, and Maintenance of Modern Highway Bridges. McGraw-Hill, Inc. 1995.

34. Viest, I. M., Siess, C. P., Appleton, J. H. and Newmark, N. M. "Studies of Slab and Beam Highway Bridges: Part IV, Full-Scale Tests of Channel Shear Connectors and Composite T-Beams." University of Illinois Engineering Experiment Station Bulletin Series No. 405, University of Illinois, Vol. 50, No. 29, Dec. 1952.

35. Walther, R. A. and Koob, M. J. "Instrumentation and Field Testing of the Elevated Loop Structures, Chicago, Illinois." Submitted to ICF Kaiser Engineers/ Bascor, Inc. for the Chicago Transit Authority, Wiss, Janney, Elstner Associates, Inc. Report No. 901210, Dec. 1991.

36. Xanthakos, P. P. Theory and Design of Bridges. John Wiley & Sons, Inc. 1994.

COVER DESIGN BY ALDO GIORGINI